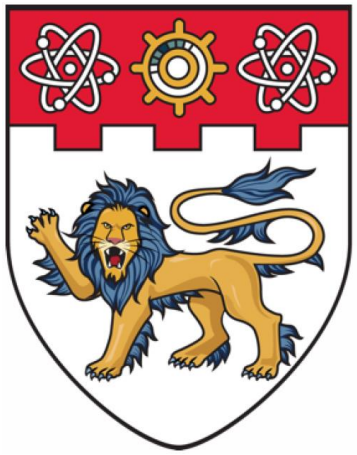

NANYANG TECHNOLOGICAL UNIVERSITY
SINGAPORE

NOVEL PLANT-DERIVED MACROPOROUS SCAFFOLDS

MOHAMMED SHAHRUDIN BIN IBRAHIM

INTERDISCIPLINARY GRADUATE SCHOOL/
INTERDISCIPLINARY GRADUATE PROGRAMME-NTU
INSTITUTE FOR HEALTH TECHNOLOGIES (HEALTHTECH NTU)

SCHOOL OF MATERIALS SCIENCE AND ENGINEERING

2021

NOVEL PLANT-DERIVED MACROPOROUS SCAFFOLDS

MOHAMMED SHAHRUDIN BIN IBRAHIM
(M.Eng, NTU)

INTERDISCIPLINARY GRADUATE SCHOOL/
INTERDISCIPLINARY GRADUATE PROGRAMME-NTU
INSTITUTE FOR HEALTH TECHNOLOGIES (HEALTHTECH NTU)

SCHOOL OF MATERIALS SCIENCE AND ENGINEERING

A thesis submitted to the Nanyang Technological University
in partial fulfilment of the requirement for the degree of
Doctor of Philosophy

2021

Statement of Originality

I hereby certify that the work embodied in this thesis is the result of original research, is free of plagiarized materials, and has not been submitted for a higher degree to any other University or Institution.

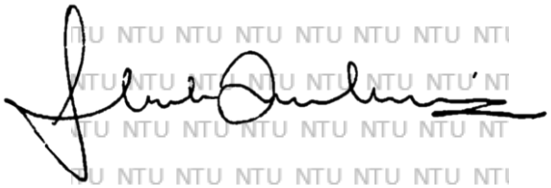

July 27, 2021

.....

Date

.....

Mohammed Shahrudin Bin Ibrahim

Supervisor Declaration Statement

I have reviewed the content and presentation style of this thesis and declare it is free of plagiarism and of sufficient grammatical clarity to be examined. To the best of my knowledge, the research and writing are those of the candidate except as acknowledged in the Author Attribution Statement. I confirm that the investigations were conducted in accord with the ethics policies and integrity standards of Nanyang Technological University and that the research data are presented honestly and without prejudice.

July 27, 2021

.....

Date

.....

Professor Nam-Joon Cho

Authorship Attribution Statement

This thesis contains material from 3 papers published in the following peer-reviewed journals in which I am listed as an author.

Substantial amount of Chapter 3 is published as Fan TF*, Park S*, Shi Q, Zhang X, Liu Q, Song Y, Chin H, Ibrahim MS, Mokrzecka N, Yang Y, Li H, Song J, Suresh S. & Cho NJ. *Transformation of hard pollen into soft matter*. Nature Communications 11, 1449 (2020). https://doi.org/10.1038/s41467-020-15294-w

The contributions of the co-authors are as follows:

- Dr Fan Teng-Fei and I evaluated the variables and proposed the thermal heating treatment to accelerate and optimize the microgel synthesis.
- Dr Fan Teng-Fei and I prepared all the microgels utilized in this study.
- Dr Fan Teng-Fei, Natalia Mokrzecka and I performed and analyzed immunofluorescence studies.
- Dr Chin Hokyun performed AFM force-distance measurements.
- Dr Park Soohyun and Song Yoohyun designed, assembled and performed studies on swelling of discrete pollen microgels via cations.
- Yang Yun designed the graphics.
- Shi Qian, Zhang Xingyu, Liu Qimin & Li Hua contributed to numerical modeling and theoretical analysis (not included in this thesis)

- Dr Fan Teng-Fei, Dr Park Soohyun, Asst Prof Song Juha, Prof Cho Nam-Joon and I prepared the early drafts.
- All authors contributed to final data analysis and editing of the manuscript.
- Asst Prof Song Juha, Prof Subra Suresh and Prof Cho Nam-Joon designed and oversaw the whole project.

Partial amount of Chapter 3 and partial amount of Chapter 4 is published as Fan TF*, Hwang Y*, Ibrahim MS, Ferracci G, Cho NJ. *Influence of Chemical and Physical Change of Pollen Microgels on Swelling/De-swelling Behavior.* Macromolecular Rapid Communications (2020) 41, 2000155. https://doi.org/10.1002/marc.202000155

The contributions of the co-authors are as follows:

- Dr Fan Teng-Fei and I evaluated the variables and proposed the thermal heating treatment to accelerate and optimize the microgel synthesis.
- Dr Fan Teng-Fei and I prepared all the microgels utilized in this study.
- I performed and analyzed the rheological studies and microgel size characterizations.
- Dr Fan Teng-Fei and Dr Hwang Youngkyu prepared the early drafts of the manuscript.
- All authors contributed to final data analysis and editing of the manuscript.
- Prof Cho Nam-Joon designed and oversaw the whole project.

Partial amount of Chapter 4 and whole of Chapter 5 was published as Hwang Y*, Ibrahim MSB*, Deng J, Jackman JA**, Cho NJ**. *Colloid-Mediated Fabrication of a Three-Dimensional Pollen Sponge for Oil Remediation Applications*. Advanced Functional Materials (2021) 31, 2101091. https://doi.org/10.1002/adfm.202101091

The contributions of the co-authors are as follows:

- Dr Hwang Youngkyu and I evaluated the optimal pollen scaffold conditions and co-wrote the manuscript.
- Deng Jingyu and I prepared all the microgels utilized in this study.
- I fabricated all the sponges with all the variables in this study.
- Dr Hwang Youngkyu and Deng Jingyu coated and performed solvent absorption experiments.
- Dr Hwang Youngkyu and I performed all heating and mechanical characterizations.
- All authors contributed to final data analysis and editing of the manuscript.
- Asst Prof Jackman Joshua and Prof Cho Nam-Joon designed and oversaw the whole project.

July 27, 2021

.....

Date

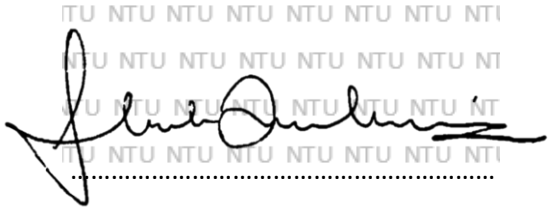

.....

Mohammed Shahrudin Bin Ibrahim

Acknowledgements

بِسْمِ اللَّهِ الرَّحْمَنِ الرَّحِيم

In the name of Allah, The Most Gracious and The Most Merciful. My PhD journey could never have begun without the opportunities bestowed by Him unto me, in providing me with abilities that define me, the love of all the people around me, and the opportunities in the world that surround me.

A big appreciation to my supervisor, Professor Cho Nam-Joon for supporting and guiding me in my journey since my pre-PhD days. I have benefitted tremendously under his tutelage in terms of academic proficiency, technical capabilities and project management, and would be more than happy to continue to work alongside him. To my thesis advisory committee, Prof Song Juha and Prof Jeffery Glenn, thank you for having me under your mentorship. Although our time was sporadic, I have learnt much during those discussion sessions.

To the lab family in ETS/TMIG and other friends in RTP, thank you for making the lab and office a conducive yet enjoyable environment for work and fruitful discussions. I enjoyed every single day that I came in. I will miss our group meetings, formal or otherwise. Special mentions to Soo, Elba, Gaia, Tengfei, Shu Hui and Youngkyu who are always providing much needed discussions about anything under the sun and inspiring me. I hope we continue to keep in touch! My students whom I have mentored, it has been an honor to be given the opportunity to be an influence. I hope I had made a positive one.

My appreciation to my external family. Denise for always seeing me in a positive light and spurring me on, my biker bros for encouraging me in your own unconventional ways, ex-

colleagues from IBN who have always believed in me, and Team 7 members for always reminding me that I got this.

A special thank you to my longtime friend Ferhan, for always looking out for my best interests. The many discussions over a multitude of topics over countless lunch and lab sessions have always made me a greater person. May your good deeds bring great rewards to you and your family.

I reserve my deepest heartfelt gratitude to my dearest family, who has always been very patient and gave me their full trust in every decision I have made, I love you all. All my brothers and sisters, especially Liza and Fuddin, thank you for supporting my pursuit and covering my duties as a child where I have fallen short. My lovely wife, Yanni, thank you for supporting me in my chosen path and looking out for our family's interest during my periods of absence. May He reward you for it. My son, Mikhail, may you read this one day and be inspired to pursue your passion, regardless how challenging and winding the journey may be. Nael and Hannan, thank you for the laughs every weekend!

Mak and Abah, thank you for keeping me in your prayers. I hope I have embodied all that you have envisioned in me. I love you both. My achievements are dedicated to the both of you.

Table of Contents

Summary

Pollen is generated in large amounts in flowering plants, but a majority of these end up as biological waste. Harvesting and modulating the properties of pollen could potentially turn pollen into a sustainable source of materials with specialized purposes. However, the understanding of how the mechanical and chemical properties of pollen are biologically controlled are limited, and strategies to manipulate pollen's robust shell beyond its natural performance limits would have tremendous advantages.

A facile method to transform pollen grains into soft microgel by remodeling pollen shells was optimized. Utilizing a range of characterization techniques, marked increase in the level of carboxyl groups present in the intine and reduced Young's modulus of the exine gave rise to pollen with tunable mechanical characteristics resembling microgels, while exhibiting physical properties that rapidly respond to stimuli, reminiscent of smart polymers.

The ability of pollen microgels to form 3D porous sponges via freeze-drying and the various factors that influence the sponge characteristics were investigated. Regulation of stiffness of pollen microgels, the swell state of the microgels and the freezing rate of the microgel slurry greatly influences the morphology, porosity, hydrophilicity and compression modulus of the fabricated 3D sponges. The interparticle bonding mechanism during the sponge formation process was also investigated. Observations in this study suggests that pressure from the ice crystals and removal of "bound water" were essential to form strong chemical bonds that conjugates adjacent pollen particles. A 'zipping' mechanism of the interface of pollen microgel was proposed.

The pollen sponge fabrication process was optimized by tuning the processing conditions during freeze-drying and thermal annealing steps. Stearic acid functionalization transforms the

pollen sponge into a hydrophobic scaffold that can readily and repeatedly absorb oil and other organic solvents from contaminated water sources. Optimized and coated pollen scaffolds show good absorption to a variety of known organic solvent contaminants of water such as chloroform, dichloromethane, hexane, gasoline, silicone oil, pump oil, motor oil and coconut oil, with good absorption and desorption repeatability, with similar performance levels to commercial, synthetic polymer-based absorbents and an improved environmental footprint.

Figure Captions

Table Captions

Abbreviations

µL	Microlitre
% v/v	Percentage in volume per volume
% w/v	Percentage in weight per volume
µm	Micrometre
3D	Three dimensional
AFM	Atomic force microscopy
ANOVA	Analysis of variance
APTES	(3-Aminopropyl) triethoxysilane
ASR	Alkali-silica reactions
ATR	Attenuated total reflection
AUC	Area under curve
BSA	Bovine serum albumin
CLSM	Confocal laser scanning microscopy
cm	Centimetres
DAPI	4',6-diamidino-2-phenylindole
dI	Deionized
DIPA	Dynamic image particle analysis
DLS	Dynamic light scattering
ECM	Extracellular matrices
EDC	1-ethyl-3-(3-dimethylaminopropyl) carbodiimide hydrochloride
EDTA	Ethylenediaminetetraacetic acid

EMCCD	Electron Multiplying Charge-Coupled Device
FE-SEM	Field emission- scanning electron microscope
FTIR	Fourier-transform infrared
h	Hour
HCl	Hydrochloric acid
IF	Immunofluorescence
KOH	Potassium hydroxide
kV	Kilovolts
mA	Milli-Ampere
mbar	Millibar
MES	2-(N-morpholino) ethanesulfonic acid
mg	Milli-gram
min	Minute
mL	Milli-Litre
mM	Milli-Molar
mV	Milli-volts
NHS	N-hydroxysuccinimide
nm	Nanometres
PBS	Phosphate-buffered saline
PDMS	Polydimethylsiloxane
PEDOT	Poly(3,4-ethylenedioxythiophene
pH	Power of hydrogen
PME	Pectin methylesterase

PTFE	Polytetrafluoroethylene
PU	Polyurethane
rpm	Rounds per minute
sd	Standard deviation
SEM	Scanning electron microscopy
UV	Ultra-violet
μN	Micro-Newton
μs	Micro-second

List of Publications

Directly Relevant to Thesis

Hwang Youngkyu*, Mohammed Shahrudin Bin Ibrahim*, Jingyu Deng, Joshua A. Jackman, and Nam-Joon Cho.

"Colloid-Mediated Fabrication of a 3D Pollen Sponge for Oil Remediation Applications."

Advanced Functional Materials (2021): 2101091.

Publication highlighted in NTU media, national media (Channel NewsAsia, The Straits Times, Berita Harian, Lianhe Zaobao, Today) and other related social media news outlets (Mothership).

Teng-Fei Fan, Youngkyu Hwang, Mohammed Shahrudin Ibrahim, Gaia Ferracci, and Nam-Joon Cho.

"Influence of Chemical and Physical Change of Pollen Microgels on Swelling/De-Swelling Behavior."

Macromolecular Rapid Communications 41, no. 21 (2020): 2000155.

Teng-Fei Fan, Soohyun Park, Qian Shi, Xingyu Zhang, Qimin Liu, Yoohyun Song, Hokyun Chin, Mohammed Shahrudin Bin Ibrahim, Natalia Mokrzecka, Yun Yang, Hua Li, Juha Song, Subra Suresh & Nam-Joon Cho.

"Transformation of hard pollen into soft matter."

Nature Communications 11, no. 1 (2020): 1-10.

Publication highlighted in NTU media, national media (Channel NewsAsia, The Straits Times, Lianhe Zaobao).

Others

Zhao Ze, Jatin Kumar, Youngkyu Hwang, Jingyu Deng, Mohammed Shahrudin Bin Ibrahim, Changjin Huang, Subra Suresh, and Nam-Joon Cho.

"Digital printing of shape-morphing natural materials."

Proceedings of the National Academy of Sciences 118, no. 43 (2021).

Chen Shengyang, Qian Shi, Taesik Jang, Mohammed Shahrudin Bin Ibrahim, Jingyu Deng, Gaia Ferracci, Wen See Tan, Nam-Joon Cho, and Juha Song.

"Engineering Natural Pollen Grains as Multifunctional 3D Printing Materials."

Advanced Functional Materials 31, no. 49 (2021): 2106276.

Ferhan Abdul Rahim, Youngkyu Hwang, Mohammed Shahrudin Bin Ibrahim, Shikhar Anand, Ahram Kim, Joshua A. Jackman, and Nam-Joon Cho.

"Ultrahigh surface sensitivity of deposited gold nanorod arrays for nanoplasmonic biosensing."

Applied Materials Today 23 (2021): 101046.

Ferracci Gaia, Mengxiang Zhu, Mohammed Shahrudin Ibrahim, Gamaliel Ma, Teng Fei Fan, Bae Hoon Lee, and Nam-Joon Cho.

"Photocurable Albumin Methacryloyl Hydrogels as a Versatile Platform for Tissue Engineering."

ACS Applied Bio Materials 3, no. 2 (2020): 920-934.

Teng-Fei Fan, Youngkyu Hwang, Michael G. Potroz, Kai-Lin Lau, Ee-Lin Tan, Mohammed Shahrudin Ibrahim, Eijiro Miyako, and Nam-Joon Cho.

"Degradation of the sporopollenin exine capsules (SECs) in human plasma."

Applied Materials Today 19 (2020): 100594.

Teng-Fei Fan, Michael G. Potroz, Ee-Lin Tan, Mohammed Shahrudin Ibrahim, Eijiro Miyako, and Nam-Joon Cho.

"Species-Specific Biodegradation of Sporopollenin-Based Microcapsules."

Scientific Reports 9, no. 1 (2019): 1-13.

Chapter 1 Introduction

1.1 Pollen, a tough sustainable natural material

Pollen is a remarkable natural material that plays a critical role in plant reproduction and transfers viable cellular material between different reproductive parts of plants.[1,2] While pollen grains are units of gametes derived from flowering and seeding plants for reproduction, spores are utilized by non-flowering plants and fungi for the same purpose. However, they share similar characteristics and are collectively referred to as pollen in this thesis.

Pollen grains have a hollow microcapsule structure, function-driven shape, and ornamental architecture.[3] The outermost exine layer is made up of sporopollenin, which is a strong, cross-linked biopolymer,[4] while the inner intine layer is composed of elastic, load-bearing cellulose/hemicellulose and pectin microfibril network structures.[5,6]

Given that the pollen's biological function is to protect sensitive genetic materials from the harsh environments, it is hardly surprising that pollen are robust and practically indestructible.[7,8] Many literatures have reported on the pollen's ability to remain unchanged even when subjected to harsh environmental and biological conditions for prolonged periods, such as in fossilized feces.[9] Despite that, pollen are highly dynamic microscale structures and are ductile enough to undergo transformation upon receipt of appropriate cues.[4,10] Upon release from the parent plants, pollen become dehydrated and the individual grains fold onto themselves – a structurally intricate process termed "harmomegathy".[11,12] Conversely, pollen are able to undergo architectural remodeling during pollen tube growth, initiated by an organized sequence of enzymatically-controlled reactions,[13,14] which leads to the opening up of the pollen aperture. Biologically, this

process is spatially-controlled within the structure of the pollen wall[15,16] by converting as-synthesized esterified pectin molecules into a de-esterified form.[17]

1.2 Problem statement: Cracking the pollen, opening up fields.

Both synthetic polymers and natural materials, including but not limited to proteins, polysaccharides and polyesters, have been extensively explored as scaffolds for mechanical or biological engineering applications. However, there exist persistent drawbacks which limit the application of natural materials, namely its frail mechanical properties, low chemical stability, batch-to-batch variability and susceptibility to enzymatic degradation.[18] Nevertheless, recent studies have demonstrated other novel natural materials that exhibit desirable robustness. Silk, a naturally-occurring protein polymer known for its strength and elasticity while remaining lightweight,[19-21] had been extensively explored to be promising alternative biomaterial for scaffold fabrication.[21,22] Simultaneously, there are growing concerns about the environmental impact of synthetic polymer-based scaffolds and a desire to instead use natural materials such as cellulose, collagen, and silk that are affordable, plentiful, renewable, and biodegradable.[23-26] Attention to this topic falls in line with current trends to view renewable biomass as a promising source for developing advanced materials.[27-29] To date, most natural materials that are used to make 3D scaffolds consist of fibril structures, and it would thus be advantageous to explore the development of scaffolds from natural materials that self-assemble into other types of supramolecular structures.

Scaffolds may be fabricated via various methods such as electrospinning, freeze casting, or *in situ* gelling. While the method of fabrication is dependent largely upon the application (Figure 1.1), each has its own merits. For the field of tissue engineering, scaffolds would need to mimic

cues of tissue-specific extracellular matrices (ECM) such as stiffness and elasticity of the cellular niche, which have been unanimously accepted to influence cellular behavior.[30,31] These scaffolds also need to have proper functionalizations that allow it to be utilized as depots to encapsulate and release chemical compounds, drugs, or biological factors.[32-34] On the other end of the spectrum, scaffolds for the purpose of membranes in forward osmosis water filtration need to be highly robust, with nanopores to filter out impurities and increase efficient surface area of contact for adsorption of impurities, while maintaining a high flux via heightened hydrophilicity to reduce the internal concentration polarization (ICP) phenomenon.[35-37] In industrial application such as oil absorbents, scaffolds would need to be designed to adopt physical and chemical traits that effectively promote high absorption selectivity and capacity of organic pollutants while exhibiting mechanical robustness and good recyclability with environmental friendliness. Simultaneously, the scaffold has to be flexible and lightweight while keeping cost low in order to allow translation to large scale applications.[38-42]

Fabrication and design of these scaffolds is very much dependent on the raw materials being utilized. The flexibility and ease of altering the physicochemical properties of the starting materials, from imbuing the polymer backbone with chemical moieties to modulating the modulus of the modular components, is a crucial factor in the choice of materials. One excellent candidate for materials is natural pollen grains, which are renewably produced in abundant supply by plants and possess many attractive material properties, including hollow microcapsule structure, chemical stability, mechanical strength, species-specific architectural details, and high monodispersity among each species of pollen grains.[11,43-47] Several groups have begun exploring pollen as a novel material for a diverse range of applications, ranging from biological

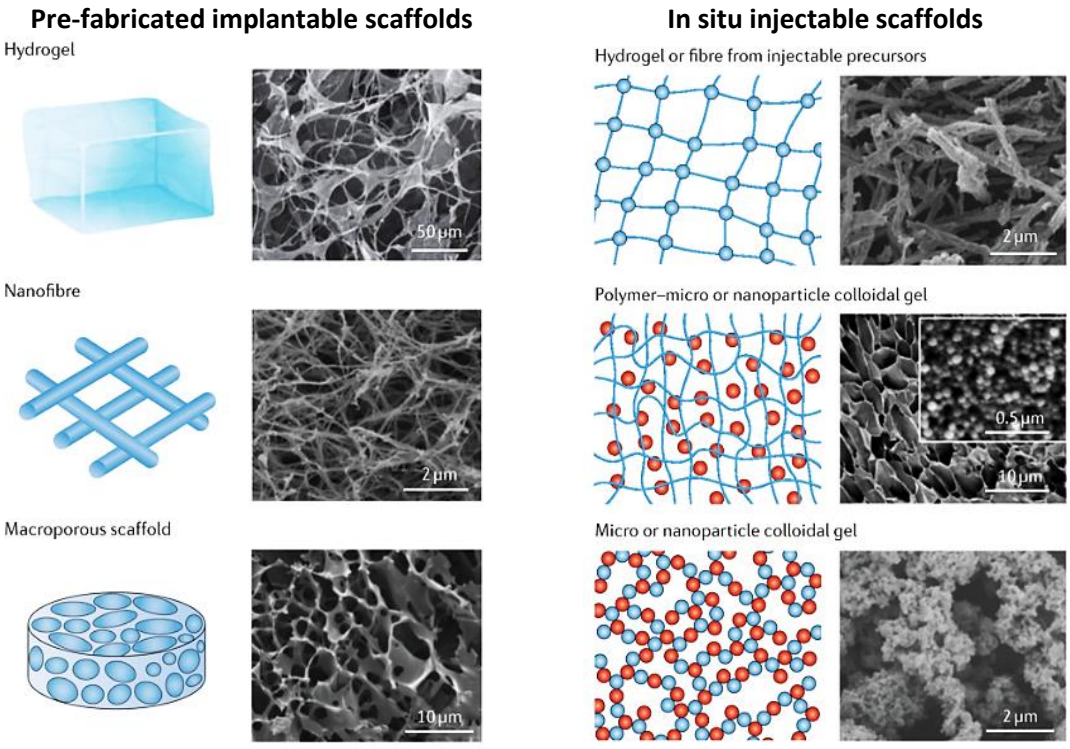

Figure 1.1. Various types of pre- fabricated and *in situ* scaffolds utilized for tissue engineering applications. Figure adapted from Xia *et al.* (2018).[48]

applications such as drug delivery to industrial applications as possible alternatives to plastics. The resilience of pollen to remain robust in the face of extreme external conditions means pollen manipulation and their subsequent applications have been very limited.

In accordance, several key questions are posed:

1. Can pollen be manipulated to allow it to attain properties that would finally allow it to be utilized as building blocks of scaffolds?
2. What are the properties that need to be attained for pollen to form robust interparticle interaction and thus allow successful scaffold fabrication?
3. Are these scaffolds tunable and robust enough to be used in industrial applications where most natural polymers are usually unsuitable?

Being a tough and natural material, pollen holds the potential to be used as a biomaterial in the fabrication of scaffolds for tissue engineering applications. While the immediate application of pollen has always been as a vehicle for cargo delivery due to its hollow macrostructure, few research, if any, have been successful in employing pollen as building blocks for scaffold fabrication, and this field remain a largely unchartered territory worthy of exploration.

1.3 Objectives & Scope

The major challenge of manipulating pollen into macroscaffolds lies in cohesion of the pollen grains to allow it to form the walls of the scaffold itself. Being discrete, stiff, and virtually inert, pollen grains do not aggregate together (except in the presence of the outer lipid cement), and thus interlinking pollen grains require synthetic adhesive forces, in the form of either chemical or physical bonds.

As the chemical makeup of sporopollenin which makes up the major composition of pollen exine has not been well-characterized,[49] grafting of functional groups to allow aggregation via chemical bonds would not be feasible. Given that the component of the pollen exine differs between different species, this strategy would hence be limited to a narrow variety of pollen sources, and the difficulty in portability of the method to other pollen species makes it less than ideal.

Recently, a novel 28-day hydrolysis process of softening pollen grains. Sunflower pollen grains subjected to this process were very much softer than its naïve counterparts. This is evident from their Young's modulus measured via atomic force microscopy (AFM) showing a significant decrease to approximately 24 % of its original value after a 28-day hydrolysis process (17 ± 2 GPa vs 4 ± 1 GPa) (Figure 1.2b), This process effectively converts the pollen grains into discrete, pliable microgels (Figure 1.2a), which are defined as a network of solvent and swollen colloidal particles with diameters ranging from tens of nanometers to several micrometers in size.[50] The resultant pollen suspension transitions from a wet sand consistency to an increasingly translucent gel-like slurry with increased incubation time (Figure 1.2c).

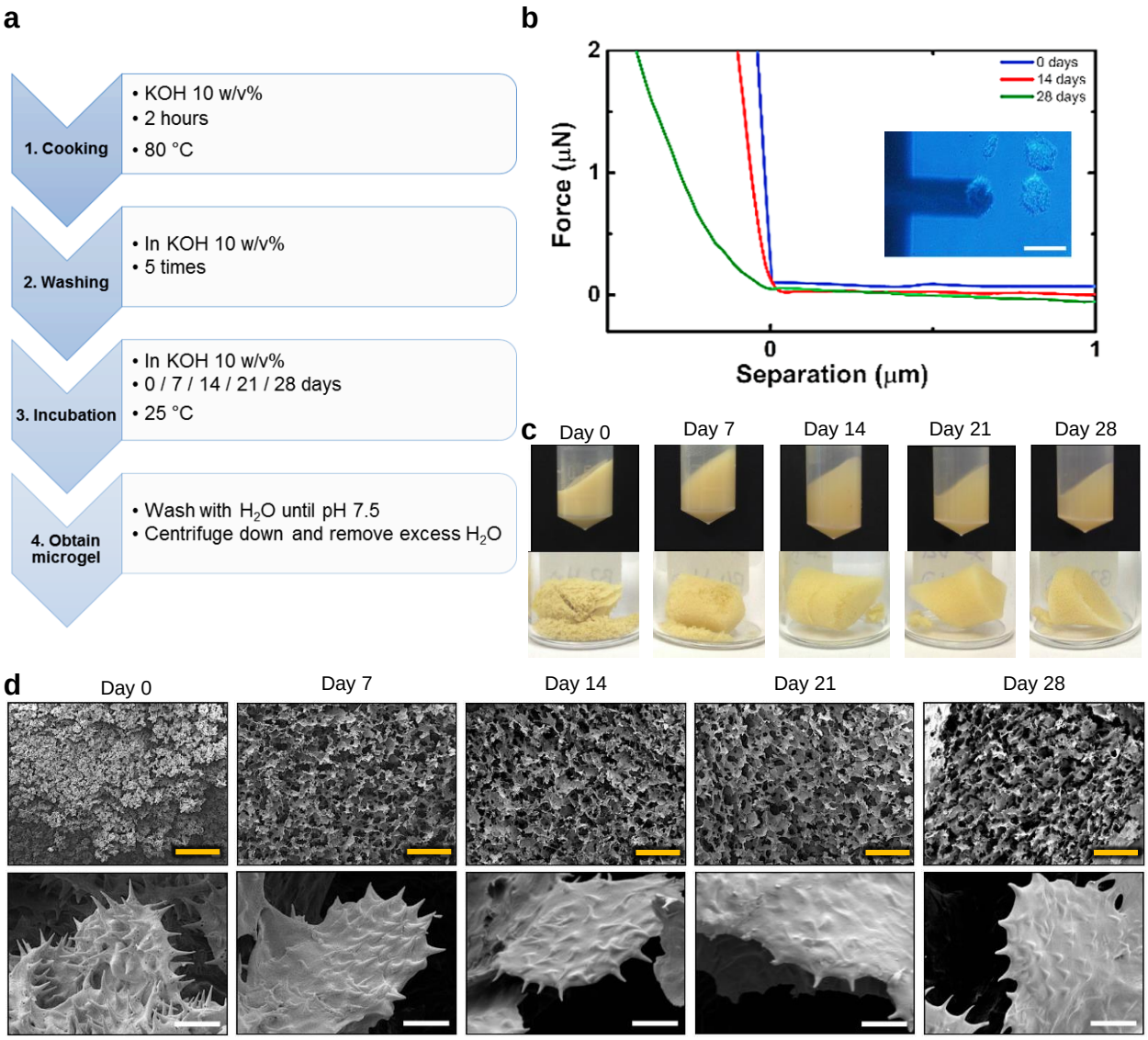

Figure 1.2. a) Hydrolysis process of defatted pollen to obtain pollen microgel. b) Representative force-distance measurement curves of sunflower pollen incubated in KOH for 0, 14 and 28 days. Young's modulus reading obtained from dried pollen were 17 ± 2 GPa, 14 ± 5 GPa and 4 ± 1 GPa for Day 0, 14 and 28 pollen. Inset shows representative microimage of measurement of Young's modulus for individual sunflower pollen grain. c) Resultant sunflower pollen microgel post-hydrolyzed for 0, 7, 14, 21 and 28 days and the resultant respective sponge scaffolds. d) SEM microimages of the respective sunflower pollen sponge scaffolds and the high magnification image showing the scaffold wall made up of pollen particles. Yellow and white scale bars represent 500 μm and 10 μm, respectively.

Subsequently, utilizing freeze-drying process, these pollen particles within the pollen microgel slurry can be sintered to form integrated structures which make up the scaffold walls, a process known as freeze-casting, and followed by lyophilization, these pollen microgel slurry could be processed to give rise to macroporous sponge scaffolds. The resultant scaffolds display an increasing stability and robustness correlating positively with the increased incubation time (Figure 1.2c), in which Day 0 scaffolds were the most fragile. This casting technique led to the formation of scaffolds with interconnected pores and tunable pore geometries and complexities.

As the scaffold porosity is determined by the void left by the sublimed ice crystal grain,[51] regulation of the ice crystal formation process would greatly influence the morphology of the scaffold.[51] However, given the same freezing-drying conditions, morphology of the resultant scaffolds differed significantly between Day 0 and Day 7 scaffolds, with Day 0 scaffold showing poor homogeneity in porosity. Scaffolds formed from Day 7 onwards showed pore morphologies that closely resemble the boundaries of ice grain crystals of freezing water (Figure 1.3),[52] with pores being most well-defined for Day 21 and 28 scaffolds. Clearly, the characteristics of the pollen particles contribute significantly to the topographical features of the scaffold. Higher magnification images reveal that pollen particles in Day 0 scaffolds showed prominent spiky appendages, more pronounced than those of the naïve sunflower pollen. Furthermore, the pollen particles in this scaffold still appeared to have rather distinct boundaries, indicating that that the particles were not fused well, which may explain the scaffold's fragility. In comparison, pollen particles from the other scaffolds have spikes that are flattened against the walls of the particles themselves, with the spikes getting less pronounced or pressed further with increasing incubation time. In addition, the inter-particle boundary also became less distinct as the incubation time was

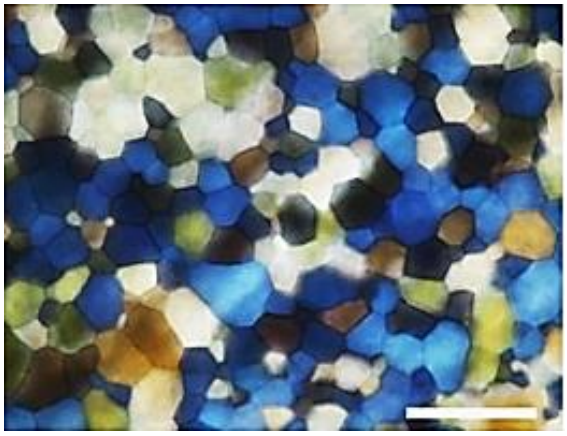

Figure 1.3. Ice crystals of pure water frozen at -6 ˚C. Scale bar: 200 μm. Figure adapted from Wu *et al.* (2017).[52]

increased, pointing to improved sintering of the pollen particles, contributing to the increasing robustness of the sponge scaffolds.

Through high-throughput dynamic imaging particle analysis (DIPA) characterization, base-hydrolyzed sunflower pollen also displayed pH-responsive swelling at basic conditions and shrinking at acidic conditions. This shrink/swell phenomenon was observed on Day 0 pollen and was most dramatic for Day 28 pollen, whereas naive defatted pollen showed negligible size changes across the pH range (Figure 1.4a). This pH-dependent swelling behavior was also seen in base hydrolyzed camellia, ragweed and baccharis pollen (Figure 1.4b, e, f). Similarly, these pollen also successfully formed sponge scaffolds after freeze-drying their respective 28-day incubated pollen microgel slurry, with the scaffold wall showing inconspicuous pollen grain boundary, indicating a degree of interparticle interaction.

Conversely, base-hydrolyzed dandelion and lycopodium pollen did not display any significant size changes across the pH range and were not able to form intact sponge scaffolds successfully

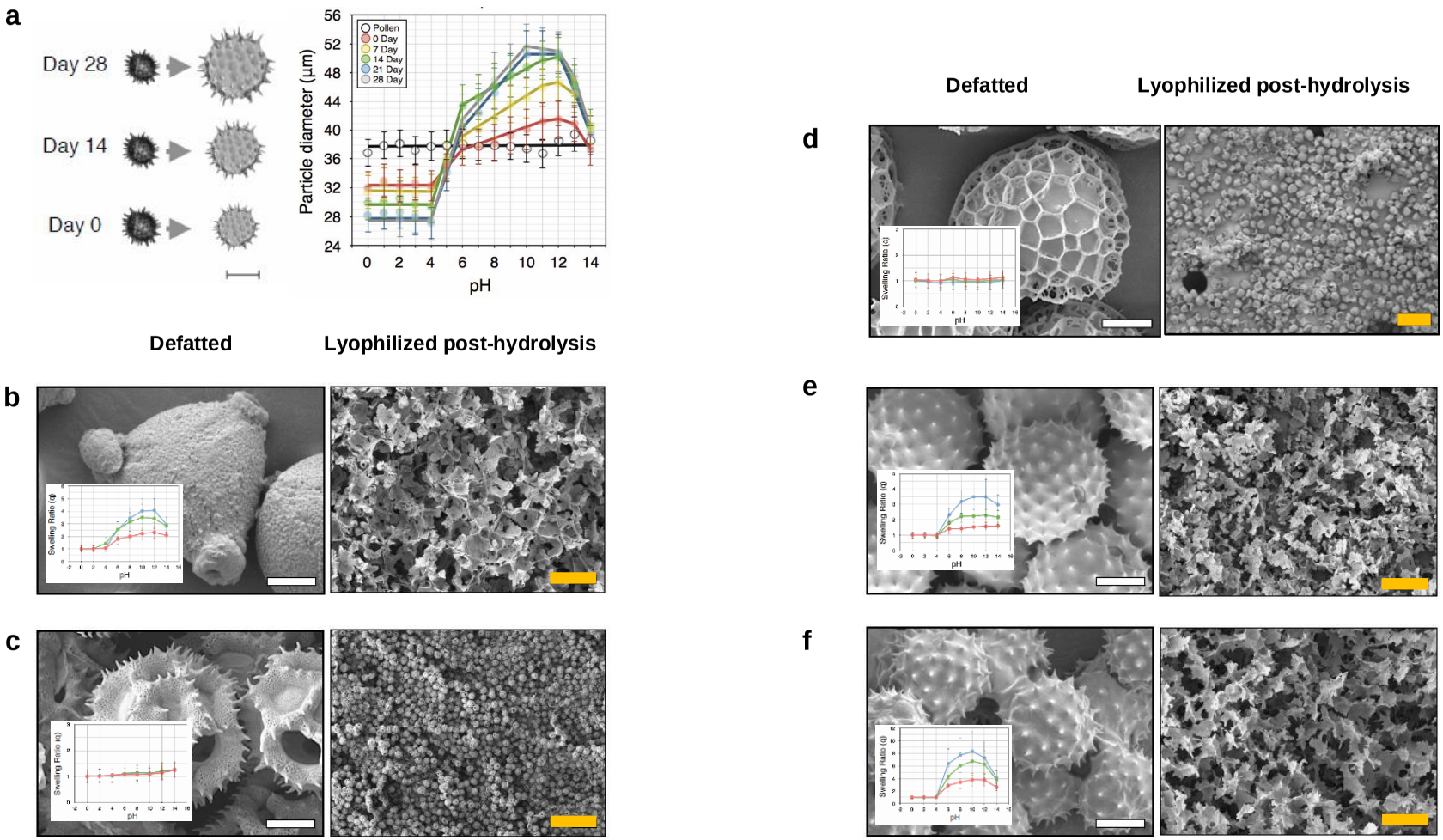

Figure 1.4. a) DIPA representative images of sunflower pollen from pH 2 to pH 14 and plot of sunflower pollen diameter against pH. Scale bar represents 30 µm. SEM micrographs of naïve defatted pollen and lyophilized 28-day post-hydrolyzed pollen of b) camellia, c) dandelion, d) lycopodium, e) ragweed, f) baccharis. Inset graphs show the normalized diameter of the pollen grains across the pH range. Red, green and blue lines indicate 0-, 14- and 28- day incubated pollen respectively. White scale bars:10 µm. yellow scale bars: 200 µm.

(Figure 1.4c, d). Clearly, there exists a relationship between the ability of a post-processed pollen grain to undergo swelling and its propensity to be manipulated to form macroporous sponge scaffolds upon freeze-drying. This novel pH-dependent size change and the ability to form robust scaffolds upon freeze- drying could partially be attributed to the softening of the pollen walls upon subjected to the hydrolysis process, allowing the pollen particles flexibility to swell and shrink, or be pressed and fused to each other.

The scope of this research project was to fabricate robust pollen sponge scaffolds that will be suitable for the purpose of oil-absorbing water treatment applications. Multiple factors influencing the fabrication of these pollen scaffolds via molding and bonding of processed pollen microgel slurry were thoroughly analyzed. Elucidation of factors that govern the performance of the resultant scaffolds, especially those that allow manipulation of the pollen grain properties, would be the most important aspect of this thesis. To accomplish the scope and answer the key questions from the hypothesis, the following specific objectives were achieved:

Objective 1: Significantly reduce the pollen microgel synthesis process via careful analysis of variables involved in the pollen hydrolysis process to obtain stable pollen microgel slurries. In alignment with the hypothesis, deep analytical experiments were designed and performed to optimize the pollen microgel synthesis process, analyze the mechanism of pollen softening, and systematic physical, chemical, and mechanical characterizations.

Objective 2: Fabrication of macroporous pollen sponge scaffold with tunable properties via rigorous experimental design and analysis of resultant properties to correlate with various variables, especially properties of the pollen microgel itself. The variables studied include

microgel stiffness, pH and swell state, and freezing rate. A series of careful yet simple experiments was also performed to elucidate the mechanism of pollen interaction for scaffold formation.

Objective 3: Optimization of fabrication and functionalization of pollen sponge scaffolds for oil-absorbing water treatment applications via post-fabrication treatments to improve robustness and recyclability of scaffolds, and improved selectivity and capacity for organic pollutants. The improved performance of these pollen scaffolds was demonstrated via experiments that effectively analyzed the physical aspects of the scaffold over multiple cycles of use through cyclic compression tests, as well as quantification of absorption of a range of known organic solvent contaminants present in water.

1.4 Organization of thesis

This thesis is organized in the following sequence

Chapter 1: Introduction. This chapter gives the problem statement and contextualizes the thesis. Motivations, hypothesis, proposed solutions and methods, including the scope and key questions are stated. The objectives achieved throughout the entire thesis is also stated.

Chapter 2: Evolution of Natural and Nature-derived Polymers in Fabrication of Porous Scaffolds: A Literature Review. This chapter provides up to date knowledge on biopolymers widely utilized in engineering, their use in fabrication of porous scaffolds, as well as applications of porous scaffolds in extensive fields spanning biomedical, such as wound healing, to industrial, such as water treatment and battery applications. This chapter further emphasizes on the need for diversity in natural polymers, especially those that are robust enough to be used in more vigorous applications.

Chapter 3: Hard Pollen to Stimuli-Responsive Soft Microgels. This chapter focuses on the improvement and optimization of the pollen microgel synthesis process down from 28 days to 24 h via incorporation of a thermal-treatment step to accelerate the de-esterification process of pectin. The chapter provides insights to the factors that govern the resultant stimuli-responsive property of the soft microgels

Chapter 4: Influence of Variables and Mechanism of Formation of 3-Dimensional Pollen Microgel-derived Sponge Scaffold. This chapter exploits the properties of the microgel derived from the previous chapter and employs freeze-casting as a facile strategy to evaluate the possibility of using pollen microgels to fabricate three dimensional scaffolds. Variables that influence the

scaffold topography and properties were studied and the mechanism of interparticle interaction between pollen microgel was analyzed.

Chapter 5: Optimization and Functionalization of Pollen Sponge for Oil Remediation Applications. In this chapter, the optimal condition for fabrication of pollen scaffold for the purpose of oil-absorbing applications was employed, and this scaffold was further functionalized for greater mechanical properties for the purpose of recyclability and as a method to allow wet-functionalization via thermal treatment. The scaffold was then further coated with a naturally-abundant fatty acid, stearic acid to imbue the former with improved hydrophobicity and selectivity for organic solvents. Absorption of a variety of known organic solvent contaminants were quantified to evaluate the performance and possibility of utilizing these functionalized pollen scaffold for oil cleanup applications.

Chapter 6: Conclusion and Future Work. This chapter further summarizes the key findings and surmises future implications and applications of pollen as modular building blocks in diverse fields of engineering. Particular attention is placed on how the key findings from the preceding chapters accomplishes the objectives set out in the thesis. Preliminary results of pollen microgel applications that is worthy of further explorations are also included.

1.5 Findings and Outcomes

The findings disclosed in this research led to several novel discoveries in the ground of novel material research. The never-before reported softening of pollen was achieved and the mechanism of softening was elucidated. Following that, the first modular scaffold derived from pollen particles was achieved and the mechanism of interaction was explored and theorized. Pollen-derived scaffolds were also shown to be robust enough for use in industrial applications. All these findings are summarized below.

1. Pollen microgel was synthesized via a facile base hydrolysis process. This process was accelerated from 28-days to as little as 24 h via incorporation of a thermal incubation step in an 80 °C oven. The physical and mechanical properties of the resultant pollen microgel showed a positive correlation to the duration of incubation, with increasing incubation duration in 10 % w/v KOH giving rise to microgels that were progressively softer and exhibiting more dramatic pH-induced swelling characteristics.
2. The pollen microgel underwent swelling as pH of its environment was steadily increased up to pH of approximately 10, where the maximum swollen state was regardless of the conditions of microgel synthesis. Beyond pH 10, the pollen microgel started to shrink again, also in a pH-dependent manner. This stimuli-responsive swelling/deswelling phenomenon was also observed upon subjecting the pollen microgel to cations such as Fe^{3+}, Mg^{2+}, Ca^{2+}, and Sr^{2+}, and reversed via addition of cation chelator EDTA.
3. Pollen microgel was achieved due to alkali-induced de-esterification of the pectin that makes up the major composition of intine layer of pollen. This led to the increased presence of free carboxyl and hydroxyl groups, which are susceptible to changes in concentration of free ions in the immediate vicinity. The base hydrolysis process also led to a reduction in

the Young's modulus of the outer exine shell. An interplay of the swelling of the de-esterified intine and the stiffness of the exine determines the maximum and minimum swelling limit of the microgels.

4. Synthesized pollen microgels could form 3D scaffolds via freeze-drying method, with properties that are modulated by the pollen microgel duration of incubation, the pH-influenced swell state of the microgel, and the freezing rate of the slurry. Optimal scaffold fabrication parameters were narrowed to pollen microgels with 48 h incubation duration, swell state at pH 7 (due to ease of processing), and freezing rate brought about by freezing at -20 °C.
5. Robust interparticle bonding is dependent on a combination of factors, microgel synthesized having a modulus that can be overcome by the forces generated by ice crystals during freezing, swollen microgels that exhibit low stiffness, slow freezing rate to allow generation of large ice crystals to generate enough forces to overcome microgel modulus, and the removal of bound water while adjacent pollen microgels are immobilized.
6. Thawing of frozen pollen microgel slurries in 100 % ethanol was able to preserve the structure of the scaffold. This was due to the reduced distance of interaction brought about by the lower surface tension of ethanol following its displacement of bound water. This thawing followed by heating step was able to replace the lyophilization step of scaffold fabrication, thus opening up possibilities of scaling up pollen scaffold production.
7. Post-fabrication thermal treatment of pollen scaffold at 200 °C led to an increasd mechanical property of the scaffold, that allowed wetted scaffolds to remain uncollapsed even upon ambient drying. This thermal sintering process allows the possibility of post-fabrication functionalization of the pollen scaffold via wet-immersion methods.

Furthermore, this thermal treatment allowed improved recyclability of the pollen sponges as determined by the recovery of the scaffold height after cyclical compressions.

8. Coating of pollen scaffolds with naturally derived and abundant fatty acids imbues the scaffold with hydrophobic properties. Pollen scaffolds coated with 2 mmol/L stearic acid allows the scaffold to have high selectivity and high absorption capability towards organic solvents in water.
9. Optimized and coated pollen scaffolds show good absorption to a variety of known organic solvent contaminants of water such as chloroform, dichloromethane, hexane, gasoline, silicone oil, pump oil, motor oil and coconut oil, with good absorption and desorption repeatability.

1.6 References

1 Faegri & Van Der Pijl. *Principles of pollination ecology*. (Elsevier, 2013).

2 Tylianakis. The global plight of pollinators. *Science* **339**, 1532-1533 (2013).

3 Erdtman. *Pollen morphology and plant taxonomy: angiosperms*. Vol. 1 (Brill Archive, 1986).

4 Mackenzie, Boa, Diego-Taboada, Atkin & Sathyapalan. Sporopollenin, the least known yet toughest natural biopolymer. *Frontiers in Materials* **2**, 66 (2015).

5 Rojas, Hotton & Dumais. Chemically mediated mechanical expansion of the pollen tube cell wall. *Biophysical journal* **101**, 1844-1853 (2011).

6 Heslop-Harrison & Heslop-Harrison. The microfibrillar component of the pollen intine some structural features. *Annals of Botany* **50**, 831-842 (1982).

7 Birks, Birks & Ammann. The fourth dimension of vegetation. *Science* **354**, 412-413 (2016).

8 de Miranda Chaves. Pollen Grains, Landscapes, and Paleoenvironments. *Foundations of Paleoparasitology*, 205.

9 Martin & Sharrock. Pollen analysis of prehistoric human feces: a new approach to ethnobotany. *American Antiquity* **30**, 168-180 (1964).

10 Blackmore, Wortley, Skvarla & Rowley. Pollen wall development in flowering plants. *New Phytologist* **174**, 483-498 (2007).

11 Katifori, Alben, Cerda, Nelson & Dumais. Foldable structures and the natural design of pollen grains. *Proceedings of the National Academy of Sciences* **107**, 7635-7639 (2010).

12 Couturier, Dumais, Cerda & Katifori. Folding of an opened spherical shell. *Soft Matter* **9**, 8359-8367 (2013).

13 Heslop-Harrison. in *International review of cytology* Vol. 107 1-78 (Elsevier, 1987).

14 Bosch & Hepler. Pectin methylesterases and pectin dynamics in pollen tubes. *The Plant Cell* **17**, 3219-3226 (2005).

15 Wolf, Hématy & Höfte. Growth control and cell wall signaling in plants. *Annual review of plant biology* **63**, 381-407 (2012).

16 Vieira & Feijó. Hydrogel control of water uptake by pectins during in vitro pollen hydration of Eucalyptus globulus. *American Journal of Botany* **103**, 437-451 (2016).

17 Bosch, Cheung & Hepler. Pectin methylesterase, a regulator of pollen tube growth. *Plant physiology* **138**, 1334-1346 (2005).

18 Place, Evans & Stevens. Complexity in biomaterials for tissue engineering. *Nature materials* **8**, 457 (2009).

19 Wang, Kim, Vunjak-Novakovic & Kaplan. Stem cell-based tissue engineering with silk biomaterials. *Biomaterials* **27**, 6064-6082 (2006).

20 Ebrahimi, Tokareva, Rim, Wong, Kaplan & Buehler. Silk–its mysteries, how it is made, and how it is used. *ACS biomaterials science & engineering* **1**, 864-876 (2015).

21 Gupta, Lorentz, Haskett, Cunnane, Ramaswamy, Weinbaum, Vorp & Mandal. Bioresorbable silk grafts for small diameter vascular tissue engineering applications: In vitro and in vivo functional analysis. *Acta Biomaterialia* (2020).

22 Li, Li, Chen, He, Han, Wang & Kaplan. Silk-based biomaterials in biomedical textiles and fiber-based implants. *Advanced healthcare materials* **4**, 1134-1151 (2015).

23 Li, Xu, Xu, Mao, Xu, Zhong, Zhang, Wang & Sui. Cellulose sponge supported palladium nanoparticles as recyclable cross-coupling catalysts. *ACS applied materials & interfaces* **9**, 17155-17162 (2017).

24 Wang, He, Wang, Zhang, Yu, Peng, Wu, Ren, Zeng & Xue. A cellulose sponge with robust superhydrophilicity and under-water superoleophobicity for highly effective oil/water separation. *Green Chemistry* **17**, 3093-3099 (2015).

25 Wang, Gunasekara, Reed, DiSalvo, Bultman, Sims, Magness & Allbritton. A microengineered collagen scaffold for generating a polarized crypt-villus architecture of human small intestinal epithelium. *Biomaterials* **128**, 44-55 (2017).

26 Tozzi, Laurent, Di Buduo, Mu, Massaro, Bretherton, Stoppel, Kaplan & Balduini. Multi-channel silk sponge mimicking bone marrow vascular niche for platelet production. *Biomaterials* **178**, 122-133 (2018).

27 Somsesta, Sricharoenchaikul & Aht-Ong. Adsorption removal of methylene blue onto activated carbon/cellulose biocomposite films: equilibrium and kinetic studies. *Materials Chemistry and Physics* **240**, 122221 (2020).

28 Lu, Xu, Zhang, Pan, Wang, Alshehri, Ahamad, Kim, Na & Hossain. High-Performance Capacitive Deionization by Lignocellulose-Derived Eco-Friendly Porous Carbon Materials. *Bulletin of the Chemical Society of Japan* **93**, 1014-1019 (2020).

29 Guo, Lu, Zhao, Zhou, Shi & Yu. Biomass-Derived Hybrid Hydrogel Evaporators for Cost-Effective Solar Water Purification. *Advanced Materials* **32**, 1907061 (2020).

30 Vining & Mooney. Mechanical forces direct stem cell behaviour in development and regeneration. *Nature Reviews Molecular Cell Biology* **18**, 728 (2017).

31 Ladoux & Mège. Mechanobiology of collective cell behaviours. *Nature Reviews Molecular Cell Biology* **18**, 743 (2017).

32 Sheridan, Shea, Peters & Mooney. Bioabsorbable polymer scaffolds for tissue engineering capable of sustained growth factor delivery. *Journal of controlled release* **64**, 91-102 (2000).

33 Sill & von Recum. Electrospinning: applications in drug delivery and tissue engineering. *Biomaterials* **29**, 1989-2006 (2008).

34 Biondi, Ungaro, Quaglia & Netti. Controlled drug delivery in tissue engineering. *Advanced drug delivery reviews* **60**, 229-242 (2008).

35 Zhao, Zou, Tang & Mulcahy. Recent developments in forward osmosis: opportunities and challenges. *Journal of membrane science* **396**, 1-21 (2012).

36 Klaysom, Cath, Depuydt & Vankelecom. Forward and pressure retarded osmosis: potential solutions for global challenges in energy and water supply. *Chemical society reviews* **42**, 6959-6989 (2013).

37 Gray, McCutcheon & Elimelech. Internal concentration polarization in forward osmosis: role of membrane orientation. *Desalination* **197**, 1-8, doi:https://doi.org/10.1016/j.desal.2006.02.003 (2006).

38 Pham & Dickerson. Superhydrophobic Silanized Melamine Sponges as High Efficiency Oil Absorbent Materials. *ACS Applied Materials & Interfaces* **6**, 14181-14188, doi:10.1021/am503503m (2014).

39 Zhu, Chu, Wang, Chen, Lin, Liu & Pan. Robust superhydrophobic polyurethane sponge as a highly reusable oil-absorption material. *Journal of Materials Chemistry A* **1**, 5386-5393, doi:10.1039/C3TA00125C (2013).

40 Chu & Pan. Three-Dimensionally Macroporous Fe/C Nanocomposites As Highly Selective Oil-Absorption Materials. *ACS Applied Materials & Interfaces* **4**, 2420-2425, doi:10.1021/am3000825 (2012).

41 Lim & Huang. Evaluation of kapok (Ceiba pentandra (L.) Gaertn.) as a natural hollow hydrophobic–oleophilic fibrous sorbent for oil spill cleanup. *Chemosphere* **66**, 955-963 (2007).

42 Zhang, Sèbe, Rentsch, Zimmermann & Tingaut. Ultralightweight and Flexible Silylated Nanocellulose Sponges for the Selective Removal of Oil from Water. *Chemistry of Materials* **26**, 2659-2668, doi:10.1021/cm5004164 (2014).

43 Quilichini, Grienenberger & Douglas. The biosynthesis, composition and assembly of the outer pollen wall: A tough case to crack. *Phytochemistry* **113**, 170-182 (2015).

44 Gonzalez-Cruz, Uddin, Atwe, Abidi & Gill. Chemical treatment method for obtaining clean and intact pollen shells of different species. *ACS biomaterials science & engineering* **4**, 2319-2329 (2018).

45 Bernard, Benzerara, Beyssac, Balan & Brown Jr. Evolution of the macromolecular structure of sporopollenin during thermal degradation. *Heliyon* **1**, e00034 (2015).

46 Bağcıoğlu, Zimmermann & Kohler. A multiscale vibrational spectroscopic approach for identification and biochemical characterization of pollen. *PLoS One* **10**, e0137899 (2015).

47 Liu & Zhang. Mechanical properties of desiccated ragweed pollen grains determined by micromanipulation and theoretical modelling. *Biotechnology and bioengineering* **85**, 770-775 (2004).

48 Xia, Li, Gao, Fu, Fang, Zhang & Zhang. Tissue repair and regeneration with endogenous stem cells. *Nature Reviews Materials* **3**, 174 (2018).

49 Mikhael, Jurcic, Schneider, Karr, Fisher, Fridgen, Diego-Taboada, Georghiou, Mackenzie & Banoub. Demystifying and Unravelling the Molecular Structure of the Biopolymer Sporopollenin. *Rapid Communications in Mass Spectrometry* (2020).

50 Saxena, Hansen & Lyon. Microgel mechanics in biomaterial design. *Accounts of chemical research* **47**, 2426-2434 (2014).

51 Li, Lu & Walz. Freeze casting of porous materials: review of critical factors in microstructure evolution. *International materials reviews* **57**, 37-60 (2012).

52 Wu, Zhu, He, Xue, Fan, Song, Francisco, Zeng & Wang. Ion-specific ice recrystallization provides a facile approach for the fabrication of porous materials. *Nature communications* **8**, 15154 (2017).

Chapter 2 Evolution of Natural and Nature-derived Polymers in Fabrication of Porous Scaffolds: A Literature Review

Chapter Abstract

Natural and nature-derived polymers belong to a special class of versatile materials with wide application in a variety of fields. Their hierarchical architectures display significant evolutions of their bioactive and structural properties over millions of years which have ultimately given them critical functions including biocompatibility,[53,54] bioactivity,[55] electromagnetic properties,[56] and mechanical toughness.[57,58] The impressive palette of functions and properties possessed by this class of biopolymers make them a target material for a variety of engineering applications. Natural polymers including resins, starch, cellulose, and proteins have a long history in the fabrication of porous scaffolds. Multiple paradigm shifts in the development of engineering fields have been critical in the evolution of natural and nature-derived polymers in scaffold fabrication due to increased demand for biosubstitutes with structural and functional qualities with the capacity to restore, maintain, and/or improve pristine structures. The efficacy of natural polymers in the fabrication porous scaffolds is attributable to their ease of workability,[59-61] versatility[62,63] and amenability,[64-66] which are a function of their fundamental building blocks characterized by covalent bonding of monomers to form macromolecules.[67,68] This review explores and analyzes the evolution of the natural and nature-derived polymers' applications in the fabrication of porous scaffolds in diverse engineering fields.

Keywords : Natural polymers, 3D scaffolds, porous scaffolds, tissue engineering, batteries, catalyst support, piezoresistive sensors, water treatment

2.1 Natural vs. Synthetic Polymers

Natural and synthetic polymers represent a special category of excipient materials within the taxonomical category of polymers. The two materials are fundamentally made of organic bases and phosphates composed of long chains of hydrogen and carbon atoms covalently bonded together.[69,70] Natural and synthetic polymers differ significantly on a wide range of parameters-physical-chemical properties and thermodynamic characteristics - despite their foundational structural and functional similarities. Natural polymers are derived from a wide spectrum of biological systems in microorganism, plants, and animals.[71] Generally, the polymerization of natural polymers is necessitated by complex cell metabolic processes that leads to concatenation of multiple monomeric substrate units to form branched or linear polymers structurally composed of lipids, proteins, and carbohydrates. Natural polymers are categorized into three major classes that include polynucleotides, proteins, and polysaccharides. They are characteristically hydrophilic,[72,73] biocompatible,[74] chemically stable, mechanically tunable,[75] thermally stable,[76] and can exhibit good optical properties.[77] They also possess several advantages including biodegradability,[78] biocompatibility,[79-81] non-toxicity,[82,83] economical,[84] and broad availability,[85,86] which make them useful in a wide range of applications. On the down side, natural polymers have low tensile strength, which necessitates reinforcement to improve their applicability.[87] Furthermore, natural polymers are structurally complex, which complicates the identification of the best manufacturing techniques.

Synthetic polymers including nylon, Teflon, and polythene are polymerized artificially using hydrocarbons. They are broadly categorized into thermoplastics, thermosets, elastomers, and synthetic fibers. Thermoplastics describe a special category of synthetic polymers that are malleable to thermal forces. On the other hand, thermosets cannot be remolded once set, and this

property makes them suitable to be used in adhesives.[88] An elastomer is considered a flexible polymer. Their leading chains and side chains are used to make various types of synthetic polymers. Their backbones are usually made of carbon-carbon bonds. Synthetic polymers are usually created with the aim of improving the properties of natural plant and animal fibers to make a massive category of polymers. Generally, they are strong, flexible, and chemically inert.[89] However, drawbacks of synthetic polymers are associated with their toxicity, pollution-generating methods of synthesis, and generally non-degradable characteristic, which make them a less-than ideal candidate in the search for sustainable materials.

2.2 Natural and Nature-Derived Biopolymers

2.2.1 Gelatin

Gelatin is a natural, non-toxic biomacromolecule comprised of bioactive polypeptides obtained from collagen in skins, bones, and connective tissues of animals such as fish, cow and pigs and poultry.[90-94] It is synthesized by thermally denaturalizing collagen, usually contained in the animal skin, bones, and bones using via thermal hydrolysis.[95,96] The major composition of amino acids that make up the gelatin polymer is composed of repeating motifs of glycine, proline, and hydroxy-proline residues.[97] Gelatin finds ready application in food, pharmaceutical, and cosmetic industries.[98,99] It is hydrophilic and has been utilized in gas barrier applications.[100] Gelatin is considered an essential polymer in scaffold engineering but its mechanical properties limit it to low load applications such as soft scaffolds for tissue engineering applications.[101-104]

2.2.2 Cellulose

Arguably the most widely utilized natural polymer, cellulose is a linear polysaccharide that comprises many glucose monosaccharide units linked in unbranched chains by β 1-4 glycosidic linkages.[105-107] Cellulose is a naturally abundant and renewable polymer because it is makes up the main component of the cell walls of plants, although more recently, bacteria has been utilized as an alternative source.[108,109] Cellulose therefore presents an easily available and an inexpensive source for applications in various fields of materials engineering. Similarly, use of cellulose as a bulk constituent of scaffolds limits it to soft applications, most notably in tissue engineering films and photonics.[108,110-112] Although crystalline cellulose nanowhiskers and nanocellulose obtained via bacteria or acidic hydrolysis of cellulose show enhanced modulus and stiffness, mainly due to the significant reduction of the amorphous region of the cellulose polymer backbone,[113] their use

in industrial engineering applications are limited to doping as reinforcement to the primary matrix.[114-117] Recently however, delignification of wood and subsequent densification of the remaining cellulose network has yielded bulk materials that display exceptional strength that was sufficient for applications such as water filtration and oil separation.[118] The high strength could be theorized to be primarily due to the top-down process, which retains the optimized linear and branched cellulose network inherent in wood.

2.2.3 Collagen

Collagen is the predominant extracellular matrix (ECM) in the body's tissues, consisting one-third of all proteins simultaneously making it the abundant protein found in animals,[119] of which the majority are of Type I. It comprises of three chains that are bound together to form a triple helical structure.[120,121] Collagen is made up of a unique composition of amino acids, with glycine at almost every third residue, with the subsequent 17% of its composition being composed of proline.[122] Collagen-derived materials are susceptible to mechanical failure.[123] Although modifications by means of physical or chemical processing can improve the strength of collagen, these processes also lead to denaturation of the native structure.[123] Capitalizing on the source of collagen as an ECM, almost every application of collagen has been focused on cellular growth and support, be it as cosmetic formulations or 3D scaffolds, where they are utilized as ECMs.[124-128]

2.2.4 Silk fibroin

Silk fibroin are natural polymers derived from various insect and spider species. They are majorly used in the textile industries, biomedicine, and catalysis[129,130] and is considered a versatile material in micro, macro, and nanoscale engineering applications.[130] Silk fibroin's relatively high

mechanical strength and low degradation rate have made it essential in the generation of scaffolds, electrospun mats, and hydrogels.[131,132] Silk obtained from spiders display an incredibly strong mechanical property in weight of up to five times stronger when compared to steel.[133] The biocompatibility of silk coupled with its resilient mechanical properties make silk an apt choice of natural polymer for applications in 3D printing and bioprinting for tissue engineering applications.[134-136] Silk's high tensile properties with modifications in processing conditions to regulate its degradation propensity have also seen it being fabricated into robust scaffolds for high flux applications such as water treatments, toxin sequestrations and oil-water separations, as well as electronic sensors.[137-139]

2.2.5 Chitin and chitosan

In nature, chitin is the most common natural aminopolysaccharide, and the second polysaccharide to cellulose.[140] Chitin is derived from the exoskeleton of the crustaceans or the fungus *Aspergillus niger* and consists of β 1-4 linkage of 2-acetamido-2-deoxy-β-d-glucose.[141] N-deacetylation of chitin by means of chemical or enzymatic process yields chitosan.[141] The high nitrogen content of chitin makes them useful in metal chelating applications.[140]

Being a bioactive polymer with attractive traits such as non-toxicity, antibacterial activity, and biodegradability,[142] chitin and chitosan-derived 3D materials in the form of hydrogels, fibers and films are heavily geared towards tissue engineering and soft scaffold applications such as wound dressings.[143-146] Nevertheless, chitin and chitosan has been applied as a coating in water filtration membranes where their chelating properties can be positively exploited.[147-149]

Biopolymer	Origin	Properties
Gelatin	Partial hydrolysis of primarily Type I collagen from animal connective tissue, skin, bones.	Linear polypeptides, largely composed of repeating motifs of Gly-X-Y, where X is frequently Pro, and Y is frequently Hyp.[97,150] Property is dependent heavily on health of animal source.[151] Biodegradable and biocompatible.[152] Low mechanical strength, low thermal stability, rapid degradation rates.[152,153] Limited scaffold applications in tissue engineering and as gas barriers in food packaging.[100-104]
Cellulose	Plant cell walls and bacteria (for nanocellulose).[108,109]	Linear polysaccharide composed of glucose units linked by β 1-4 glycosidic linkages.[105-107] Inexpensive and readily available. Scaffolds are limited to soft applications e.g. tissue engineering, photonics.[108,110-112] Crystalline nanocellulose mainly used as reinforcements via doping.[114-117] Delignification of wood, preserving inherent cellulose network able to support high load applications e.g. water filtration, oil separation. [118]
Collagen	Animal connective tissue, skin, bones, muscles.	Most abundant protein, largely composed of glycine at every third residue.[122,152] Right-handed helical structure, composed of three left-handed helices.[154] Low mechanical stability.[123] Due to presence of cell-adhesive RGD motifs, scaffold applications are focused on tissue engineering.[124-128]
Silk fibroin	Insects and spiders.	Consists of heavy and light polypeptide chain linked by disulfide bridge, and a hydrophobically-linked P25 glycoprotein.[155] Gly-X dipeptide motifs on heavy chain accounts for 60-75% of amino acid and forms stable antiparallel β-sheet crystalline regions. [156-159] Lightweight, flexible, relatively high mechanical strength and low degradation rate, suitable for scaffolds, mats and hydrogels.[131,132,160] Scaffold applications range from soft bioinks in 3D printing for tissue engineering, as well as robust applications such as water treatments and electronic sensors.[134-139]

Chitin and chitosan	Chitin derived from shells of crustaceans and *Aspergillus niger*. Chitosan derived from deacetylation of chitin.	Second most common polysaccharide after cellulose.[140] Consists of β 1-4 linkage of 2-acetamido-2-deoxy-β-d-glucose.[141] High nitrogen content exploited as metal chelating coat in water filtration membranes.[147-149] Being bioactive and biodegradable, scaffold applications are focused towards tissue engineering and wound healing.[143-146]

Table 2.1. Common natural polymers and their properties

2.3 Fabrication Methods of Porous Scaffolds

Scaffold architecture is essential for modulation of mechanical properties in engineered porous scaffolds.[161] While high porosities provide an exponentially large surface area per volume, it usually comes at the compromise of mechanical properties. Various techniques of fabrication have been successfully employed to obtain porous scaffolds, with each techniques having its own distinct advantages and limitations with regards to ease of implementation, scale of application, reproducibility, post-processing steps, and environmental friendliness.

2.3.1 Ice-templating and freeze-drying

The freeze-drying process begins with the freeze-casting or ice-templating stage, where the scaffold pores are shaped by ice crystal grains during the freezing process. Removal of the ice crystals during lyophilization or freeze-drying gives rise to an interconnected scaffold that mirrors the ice crystal structure. This makes the scaffold fabrication process with slurry to be heavily reliant on the ice crystallization process. The crystallization of the ice usually incorporates nucleation and the growth of the crystal. Regulating the nucleation initiation when the ice structures start to form can determine whether the resultant scaffolds are isotropic or anisotropic.

While isotropic scaffolds are favored for its homogeneity, especially in turn of scaling up, anisotropic scaffolds can be applied to resemble complex biological tissues. Modulation of the nucleation process thus heavily influences final the size, shape, and density of porosity of a scaffold.

The particles contained in the slurry are ejected using the moving freezing front and pile themselves at the growing ice interface.[162] During the process, pore anisotropy can be altered by freezing rates. Changing the freezing rate would thus influence the sizes of pores to tailor the scaffold for different applications.[163] Freezing rate also influences the thickness of the wall that form the pores of the scaffold. A high freezing rate brought about by extreme low temperatures leads to rapid nucleation, small ice crystal grains, and thus results in small pores and thin scaffold walls,[164] as a result of the distribution of material over a larger surface area of many growing crystals.

Nucleation and the development of the crystal are in turn determined by the components of the liquid phase.[165] Varying the solvent used can give rise to different crystal and pore morphology. water gives lamellar crystals, camphene gives cellular, camphor-naphthalene gives dendritic crystals, and tert-butyl alcohol results in prismatic crystals. Furthermore, presence of alcohols and salts during freezing would also lead to variations in crystallization of ice and the imparted pore morphology.[166-169]

Sublimation of the ice is necessary to preserve the pore structure by preventing collapse of the structure due to surface tension and capillary action of the withdrawing liquid from the pores. Freeze-drying is a commonly employed method of sublimation of the ice crystals. In this process, the freeze-casted slurry is placed under extreme vacuum condition well below the triple point of the solvent. Raising of the temperature under these conditions leads to bypassing of the liquid state,

and thus avoiding the collapse of formed pores (Figure 2.1).[170] It is widely believed that freeze-drying process does not influence the final microstructure of the scaffolds.[164]

Regular patterns with high level of reproducibility can be obtained via the ice templating method.[165] Generally, in this method, freezing is usually regulated using both intrinsic and extrinsic processes, which ensures that desirable outcomes are generated regularly. Reliance on freezing rates that can be obtained by commercial freezers also make the ice templating process to be an economically viable option of obtaining porosity. However, freezing can be a time-consuming process. The reliance on the freeze-dryer also limits the potential of scaling up due to limitations of vessel size that can be fitted onto the freeze-dryer. Furthermore, the slurry needs to be stable in a homogenous dispersion throughout the solvent, and this may require the use of surfactants to achieve a stable emulsion.[171]

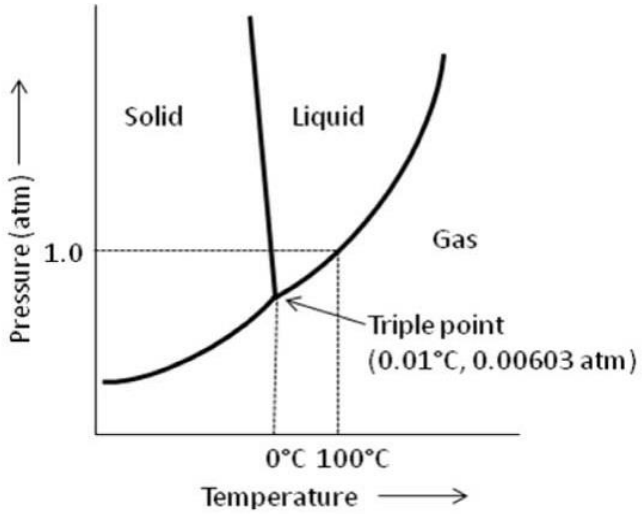

Figure 2.1. Phase diagram showing the triple point of water at 0.01°C, 0.00603 atm. Lyophilization is carried out below the triple point to enable conversion of ice into vapor, without entering the liquid phase (known as sublimation).[170]

2.3.2 Porogen Leaching

Porogen leaching involves incorporating a chemically or physically incompatible porogen such as sodium chloride, paraffin spheres, gelatin, or polymers as a template and the subsequent removal via aqueous methods to fabricate porous structures (Figure 2.2).[172] In this method, casting of the polymer solution mixed with the relevant porogen particles into the required molds can be done.[173] Otherwise, casting of the polymer solution onto a pre-fabricated scaffold containing the porogen can be performed.[104] Solidification of the polymer is then performed via polymerization or removal of solvent via the evaporation or lyophilization. On the other hand, crystallization is an alternative method based on the change in phases of the materials from the solvated state into crystal structures generated by the reduction of free energy from the solution. As the process continues, the solute molecules nucleate and rearrange into crystal structures[174] to achieve distinctly-shaped pores. The remaining composites are then washed with a solvent capable of solubilizing the porogen, leaving voids in place of the porogen particles.

The porogen leaching method provides a direct route of modulating resultant scaffold pore topography. Using monodispersed porogen of predefined size allows convenient regulation of the porogen size and density to acquire desired scaffold porosity and pore sizes. However, interconnectivity of the pores require a high density and close packing of the porogen, or requires the porogen to be fused prior to casting.[175] Furthermore, porogen leaching is a cost-effective method, entailing the use of inexpensive materials and no reliance on complex apparatus. However, a thorough post-leach wash should be performed as incomplete solvent removal may negatively impact its final application, such as loss of cell viability.[174] Post-leaching of porogen also limits the use of this process in the loading of additional constituents such as biologics into the materials in a single step. Scaffolds fabricated via porogen leaching usually have limitations in

terms of fabricating anisotropic scaffolds. Furthermore, crystallization method of forming porogen produces wide variations of pore sizes, creates irregular pore geometry, and cannot generate submicron pore sizes.[176]

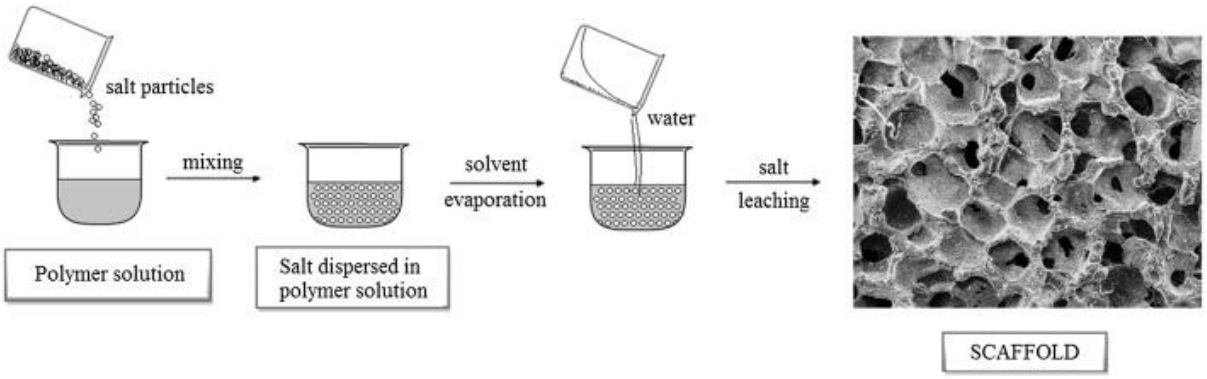

Figure 2.2. Schematic of porogen leaching process. Casting of polymer solution with salt porogen, followed by solidification of polymer and dissolution of porogen particles by water, resulting in a porous polymer scaffold. Figure adapted from Janik and Marzec, (2015).[177]

2.3.3 3D Printing

3D printing is also referred to as additive manufacturing and is an advanced scaffold fabrication technique. It entails processes that are managed by a computer model that incorporates cross-sectional information acquired by a digital image of the defective areas.[178] 3D printing uses solid polymers to form products through selective sintering and stereolithography. The materials that are used in 3D printing include fibrous materials, powder materials, and bio-inks. Techniques used in 3D printing include the fused deposition modeling technique. This technique is mainly based on the heating of thermostatic polymers that are introduced into the gadget then into the heating chamber, where they are converted into a molten form and then forced out through a nozzle onto a set platform where it is deposited layer for more straightforward construction of a 3D model.[179] The nozzle that is used in the process is controlled by a relevant computer program that makes the nozzle move in an x-y plane to facilitate easier creation of the required pattern.[180] The process is usually repeated layer by layer in a z direction until the required and the desired model is created. The diameter of the nozzle, the printer's speed, and the angle usually determine the resolution of the product.

Variation in 3D printing include selective laser sintering. In this method, the use of a laser beam is incorporated. The laser beam is used as a source of energy used to melt some thin layers of powder materials spread in the form of a powder bed. The material is then heated by the laser beam using a computer program, which later fuses them in drawing a 2D shape. After a complete fabrication, the process is repeated subsequently until the final and required structure is formed.[181] Another technique of 3D printing is stereolithography. This technique prints complex tissues and generate transferable soft tissues. Additionally, scaffolds manufactured using this technique

exhibit property such as controllable porosity and a fully interconnected network. This technique incorporates inkjet, extrusion, and laser-assisted bioprinting.

3D printing is able to yield scaffolds with very high resolution, especially via laser-assisted method,[182] thus scaffolds with defined geometries can be fabricated. Another advantage is its flexibility in printing cell-loaded bioinks via the deposition method. Using inks that solidifies via polymerization post-ejection from the nozzle, cells mixed with the polymeric solutions are able to retain their viabilities and the resultant scaffolds were able to support cell proliferation and high cell viability.[180] Furthermore, using 3D printing method, high levels of accuracy of scaffold dimensions can be achieved by computer programs that make ensure no errors are made. This in turn allows #D printing to achieve different level of porosities and pore sizes in the fabricated scaffolds.[178]

3D printing can consume be a time-consuming method of scaffold fabrication, especially if large numbers are required. Furthermore, laborious post-processing procedures need to be employed if machines with low tolerance are used.[181] 3D printing is an advanced scaffold fabrication method with low throughput and requires the use costly machines, although its popularity is bringing its cost down. While 3D printing has obvious benefits in fabrication of unique scaffolds for exotic applications, scaling up of scaffold fabrication via 3D printing limits the application of this method especially in industrial applications.

2.3.4 Gas Foaming

Gas foaming is a technique for creating porous scaffolds that do not incorporate solvents.[183] Instead, the release of gas as a product of degradation of the gas foaming agent creates pores within the polymer.[177] It is considered the most preferred method for converting sensitive molecules into

matrices while avoiding loss their bioactivity. In this method, scaffolds are generated through the use of high-pressure carbon dioxide (CO_2) at low temperatures. CO_2 is used as a foaming agent to create porous structures because the method perfectly blends with other polymers.

During the process, a shift in thermodynamics is usually provoked by reducing the pressure caused by the polymer matrix's saturation with CO_2.[184] The pore formation does not occur below the glass transition temperatures as the polymer matrix would still be in its glassy rigid state. The separation of phases and nucleation is enhanced when the saturated sample is heated above the glass transition temperatures.[185] Generally, foaming occurs instantly if the conditions are kept above the glass transition temperature. The formation of scaffolds is mainly affected by the concentration of carbon dioxide concentration and temperature. Generally, a decrease in temperature or CO_2 concentration within the matrix terminates the pore formation.

Being free of organic solvents, gas foaming process minimizes the possibility of post-fabrication solvent retention, which favors its use for biological applications.[186,187] However, due to relatively large pore sizes between 500 to 2000 µm, scaffolds fabricated by this technique are not suitable for cell encapsulation and proliferation due to the large size disparity which does not favor cell support.[188] Furthermore, the scaffolds generated from this method are normally used for mechanical support applications due to its lack of pore interconnectivity.[189]

2.3.5 Electrospinning

Electrospinning is a relatively facile method that involves the use of electrical fields to cause the formation of a solid fiber comprised of the viscous polymer solution. Generally, in this method, fibers of nano to sub-micrometer diameters are generated[190,191] when continuous stretching is caused by the electrostatic repulsion between charged nanofibers and the solvent

evaporation. The technique involves high voltage applications to a capillary filled with a polymer solution to be spun, causing the hemispherical surface of the liquid to elongates and form a Taylor cone to be generated between the capillary tip and the collector when the electrical intensity is increased. A mutual charge of repulsion caused by the electrical fields usually causes a force directed to the opposite surface tension of the polymer fluid.[192]. As the electrostatic field increases, the critical value of surface tension is overcome and results in a polymer jet that is spooled at the collector mandrel (Figure 2.3). The stretching of the solvent molecules usually causes the diameter of the plane to decrease.[193] Electrospinning thus allows long continuous fibers to be generated. Applications that have utilized scaffolds generated from electrospinning include pressure sensors, reverse osmosis filter membranes, and oil-water separating scaffolds.[194-197]

Electrospinning is a simple method of generating porous scaffolds. This versatile technique yields fibers for high output of the non-woven scaffold. Furthermore, electrospinning is an economically viable fabrication process utilizing simple components that are considered to be less costly and readily available.[198] More importantly, electrospun scaffolds have highly interconnected pores,[199] which is a crucial factor in certain application aspects. Most notable limitation to electrospinning would be the generation of flat, almost two-dimensional scaffolds. Also, electrospinning process may result in scaffolds with residual solvent, which are usually highly toxic and may impact cellular viability is cell encapsulation application was intended.[200,201]

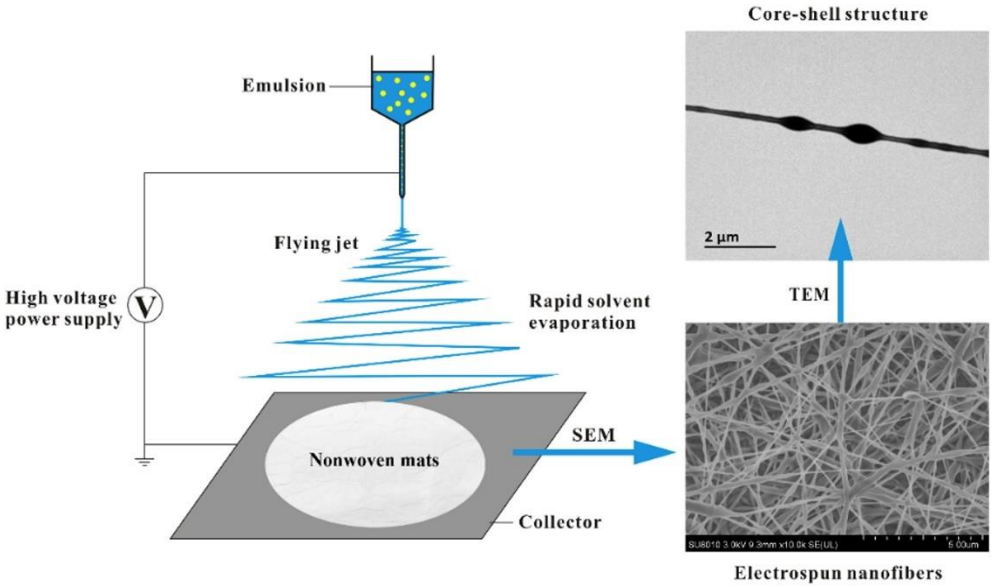

Figure 2.3. Schematic overview of electrospinning scaffold fabrication process. Polymer emulsion is ejected out of the capillary via increment in electric field, generating elongated polymer fibers in a Taylor cone. Fibers deposited on the collector forms a non-woven mat containing pores with high degree of interconnectivity. Figure adapted from Zhang *et al.* (2018).[202]

2.4 Applications of Porous Sponge Materials

The porous scaffold sponge structure plays a crucial role in increasing the infiltration capability in scaffolds. The pore spaces usually determine the permeability of the scaffold, the larger the pore space, the high the levels of permeation. Additionally, the interconnectivity of pores exhibited by the scaffold sponge structure enhances liquid permeation by facilitating the directional flow of liquids through the pore spaces. High interconnectivity of the pores promotes liquid and gaseous permeation throughout.[203] In tissue engineering applications, permeation of 3D scaffolds also allows efficient nutrient exchange between the external and internal of the scaffold. An efficient exchange is crucial in transportation of waste metabolites away from the respiring cells within while permitting the delivery of factors such as glucose, salts, and oxygen that are crucial for cellular metabolism and survival.[204] Furthermore, permeable scaffolds can also promote the regulated diffusion of growth factors to stimulate anastomosis between the host tissue circulation and engineered blood vessels within.[205] In catalytic applications, permeability of scaffolds allow high surface area for reactions with immobilized catalysts.[206] For scaffold applications in water filtration, permeability is needed to increase surface contact area for chelating metals and adsorbing of toxins from the treated water,[147,207] while allowing sufficient flux to prevent clogging and rupture of the scaffold due to buildup of pressure.[208]

2.4.1 Batteries

Electronic devices demand higher performance batteries that can hold enough energy for their efficient operations. Most of the batteries usually have a low power capacity and lose electrical conductivity over time. To solve these problems, porous sponge materials have been incorporated into the batteries characterized by the presence of hybrid electrodes that contain

polymers and are designed to accommodate different architectures.[209,210] Anodes based on 3D microporous nickel foam scaffold have been incorporated in batteries, where the foam is able to withstand stress in volume fluctuations during charging and discharging. This thus prevent delamination and results in a columbic efficiency that is very much improved.[211] Furthermore, 3D porous carbon derived from bamboo has been used as efficient scaffolds for construction of lithium metal anodes for battery applications, and optimized porosity has been shown to be essential in the modulated deposition of lithium within the scaffold.[212] Freeze-dried and electrospun silk fibroin scaffolds have also been proposed recently to be an environmentally-friendly alternative to the materials used in the components of lithium ion batteries (Table 2.2).[213] The trend of utilizing natural polymers such as cellulose and chitin while adopting the natural porosity associated with them are currently gaining traction in battery applications, due to their newly-discovered advantages of suppressing dendritic lithium deposition while maintaining environmental friendliness and economic viability.[214-218]

2.4.2 Wound Healing

The skin is considered the largest organ in the vertebrates' human body, which comprises the epidermis, dermis, and hypodermis. It is mainly exposed to injuries caused by burns, or sometimes that they can be exposed to leg ulcers that lead to the loss of the epidermis. Generally, there are limited skin donors as donor grafts cannot be widely used due to incompatibility with the recipient.[219,220] Due to limited skin autografts, the development of skin grafts as a substitute in the healing processes has been of wide interest in the medical arena. For instance, collagen being a significant component in the connective tissues,[221] has been a choice material for scaffolds used in wound healing because of its biocompatibility and biodegradability aspects.[222] The porosity of

these collagen grafts promotes the infiltration and interconnection between the discontinued skin tissue.[223-225] Porous collagen scaffolds have been utilized in other aspects of tissue engineering such as cartilage and bone grafts. Despite them having weak mechanical strength, the cross-linking of collagen-based scaffolds can be optimized to match the mechanical property, physiological porosity and biodegradation rate of the natural ECM of the site of application. Biopolymers such as silk, bacterial cellulose, keratin, gelatin and chitosan are among the recent candidates the generation of tissue scaffolds for wound healing application for the same reasons (Table 2.2).[225-230]

2.4.3 Catalyst support

Porous scaffolds are used as supports for nanoparticles with catalytic properties for use in industrial applications. Suspended nanoparticles have long withstanding issues regards to recovery, and scaffolds as supports provide much alleviation via a facile method of filtration to recover these nanoparticles and avoiding non-environmentally-friendly purification processes.[231] Immobilization on porous supports also mitigates toxicity issues associated with the handling of free nanoparticles.[232]

Cellulose porous scaffolds have been recently used in the immobilization of platinum nanoparticle catalysts for ethylene decomposition. Immobilization on the scaffold improves the distribution of the nanoparticles, and hence improves its catalytic activity.[232] Agar, composed of polysaccharides agarose and agaropectin had been utilized as hydrogels for the support of copper (II) oxide nanoparticles for reduction of nitrophenols.[233] Chitosan functionalized with aldehydes have also been fabricated into highly porous aerogels for support of copper complex catalysts, leading to high efficiency for the Huisgen [3+2] cycloaddition reactions.[234]

Porous scaffolds are also used as an encapsulation and storage of catalysts and its resultant products. Due to hydrogen's low volumetric energy density, nanopores formed by Fe_3O_4 efficiently binds to $LiBH_4$ and improves the overall hydrogen storage properties of the latter.[235]

2.4.5 Pressure Detection

Porous sponge structures have recently been utilized in pressure sensing, due to its ability to enhance the sensing and response time, and lowering detection limit of pressure-sensing piezoresistive sensors. 3D porous dielectric layer incorporated into the sensor enhances the detecting range of the piezoresistive sensors. Synergetic conductive material coated onto sponges ensure that the sensor exhibits high outstanding sensitivity with changes to compression. Recently, fabricated graphene sponges were demonstrated to enhance sensor sensitivity largely due to its relatively low density, high surface area, and high elasticity which serves to amplify minute changes in pressure accompanying changes in hand motion.[236] More importantly, being low cost and renewable, cellulose has been widely explored as a suitable natural alternative. Cellulose-based composite sponges and silk fibroin have both shown potential as flexible wearable pressure sensors as well as highly-responsive strain sensors.[237-240]

2.4.4 Water Treatment and Oil-Water Separation

The combination of carbon water filtration with reverse osmosis is commonly employed in water treatment.[241] While carbon filtration enhances permeability by adsorbing volatile organics and their by-products,[242] engineered materials employed as reverse osmosis membranes require a high degree of permeability to allow consistently high flux to minimize the chance of failure due to rupture of the scaffold as a consequence buildup of pressure.[208] While typically antifouling

materials that aid in the maintenance of flux are utilized, hydrophilic polymers also ensures the stream of water flows through with minimal resistance.[243-247] Porosity and permeability of the scaffold also increase surface contact area for chelating of metals and adsorbing of toxins from the treated water.[147,207] Although natural polymers are typically hydrophilic in nature, they usually do not have the tensile strength required for such applications. Nevertheless, cellulose acetate and nitrocellulose polymers have been successfully fabricated and employed for such applications.[149,248] 3D porous materials are also utilized for use in oil remediation in due to it having well-defined pores and large surface area, and thus having a high capacity of absorption.[249-251] These scaffolds generally operate via oil–water separation or oil adsorption. Materials utilized in oil-water separation are usually composed of highly hydrophilic polymers that allow free flow of water through while retaining or rejecting oil, whereas materials utilized in oil absorption are highly hydrophobic. Silica, polydimethylsiloxane (PDMS) or polytetrafluoroethylene (PTFE) coated membranes are commonly employed industrially as oil-absorbing materials.[252] In both methods, highly interconnected pore structures would aid in their respective functions, either by free passage of water for the former, or increased absorption capacity of the latter.[253] Furthermore, it is highly advantageous to utilize porous materials composed of natural polymers due to its potential low-cost, eco-friendliness, renewable and sustainable source, recyclability and biodegradability.[254]

Applications of porous scaffolds	Biopolymers used and their performance
Electro chemical	• 3D porous carbon from bamboo used as scaffolds for construction of lithium metal anodes for battery applications reduces volumetric changes during charging cycles, lowers current density and induces lithium deposition.[212] • Cellulose/Si carbon scaffold as anodes for lithium ion batteries gives high reversible capacity and 70% capacity retention after 200 cycles.[255] • Electrospun lignin/polyacrylonitrile membrane show 74% porosity and no thermal shrinkage at 150 ºC.[256] • Alginate/attapulgite mesoporous membrane separator show 82% retention rate after 700 cycles, displayed no thermal shrinkage at 250 ºC and naturally biodegradable.[257] • Silk fibroin membranes in $LiPF_6$ displayed high ionic conductivity of up to 1.00 mS/cm due to presence of β-sheet crystalline regions.[213]
Tissue engineering	• Gelatin-coated porous membrane induces human dermal fibroblasts migration for in vitro wound healing models.[224] • MatriDerm® (lyophilized bovine collagen coated with elastin hydrolysate) promotes adhesion and infiltration of adipocytes for reconstruction of subcutaneous tissues.[258] • Electrospun silk fibroin scaffolds with pore size of 37.2 ± 12.9 μm allows efficient infiltration of mouse fibroblasts.[225] • Chitosan/alginate/hyaluronate scaffolds incorporating RGD motifs promote complete regeneration of rabbit knee cartilage within 6 months.[230]
Catalysis	• Recyclable iron catalyst immobilized onto silk fibroin supports for phenol hydroxylation reactions into dihydroxybenzenes demonstrated conversion rates of up to 80.3 % with no significant leaching of iron catalysts.[259] • Hierarchical porous cellulose scaffolds combined with cerium-doped TiO_2 as support for Pt catalysts successfully decomposes 100% ethylene at 25 ºC.[232] • Agar-CuO nanocomposite hydrogel displayed high catalytic activity in reduction of nitroarenes into aminophenols among other hydrogel supports, with recyclability of up to 5 times, potentially beneficial for other water-based chemical reduction reactions.[233] • 83 % loading of copper(I) complexes anchored on chitosan aerogel polymer network yields a 99% conversion rate into triazole products with EtOH as solvent.[234]

Piezoelectric sensors	• Flexible cellulose thermoelectric sponge able to generate a voltage of 0.3 mV when attached to skin, suitable for wearable pressure sensor applications.[237] • Conductive cellulose nanocrystal/carbon nanotubes/rubber composites with high resistivity (gauge factor of ~43.5) for flexible strain sensors.[239] • Highly-responsive and flexible ZnO nanorod-embedded paper (cellulose) with good sensitivity and linearity at various frequencies for self-powered strain sensing applications.[238] • *In situ* polymerization of polypyrrole on cellulose surface demonstrated capacitance with good linearity and reversibility for use as flexible temperature and humidity sensor.[260] • Carbonized silk nanofiber electrospun flexible membranes display high transparency, highly-sensitive pressure sensing, low detectable pressure limit (0.8 Pa), rapid response time (< 16.7 ms) and high stability for skin-like pressure sensors.[240]
Water treatment	• Cellulose acetate membranes fabricated via electrospinning and hot-pressing reduced water turbidity to 0.135 NTU with initial flow flux of ~20000 L/m^2 h at 14 psi.[248] • Electrospun cellulose acetate coated with chitin nanocrystal substantially increased the membranes mechanical properties, surface hydrophilicity (0 º), resistance to biofouling and water flux up to ~14000 L/m^2 h at 0.5 bar for water microfiltration applications.[149] • Highly-oriented silk nanofiber porous aerogels with high hydrophobicity (140.9°) show high selectivity to soybean oil in an emulsion, with a quality factor of up to 40.3 ± 0.7, composed of up to 99 % oil content.[261] • Chitin nanofibrous membranes displaying superhydrophilicity and underwater superoleophobicity effectively separates oil/water emulsions with > 95 % efficiency, for applications in water treatment.[262] • Methyltrichlorosilane-coated freeze-dried chitin porous sponge with high elasticity and durability efficiently absorbs up to 58 times its own weight in organics from water. [263]

Table 2.2. Performance of porous scaffold fabricated from natural or nature-derived polymer in various applications

2.5 Conclusion

Development in synthetic polymers have led to many groundbreaking accomplishments, and their usage have been intimately intertwined in our daily lives. However, usage reliance on synthetic polymers has been unsustainable and its impact on the environment has been recently in the spotlight due to toxicity associated with the polymers, the harmful processing methods of generating the polymers, as well as the environmental concerns upon discard of the materials fabricated from these polymers. While natural polymers have obvious limitations especially in terms of mechanical aspect and biodegradation, research is gaining traction on circumventing these issues while exploiting the advantageous aspects such as renewable and sustainable sources, low toxicity, and its inherent biologically friendly characteristics.

Nevertheless, there is a novel need to seek suitable alternatives to synthetic polymers, especially in terms of recapitulating its inertness and strength. In addition, research in engineering novel materials have always been incremental improvements of presently available materials, and there is thus motivation to source out for completely new class of materials, especially from untapped natural and renewable sources (Figure 2.4). These materials should have innate toughness and inertness to allow it to match those of synthetic polymers, while having flexibility of being manipulated to form higher order structures and scaffolds using presently available fabrication methods.

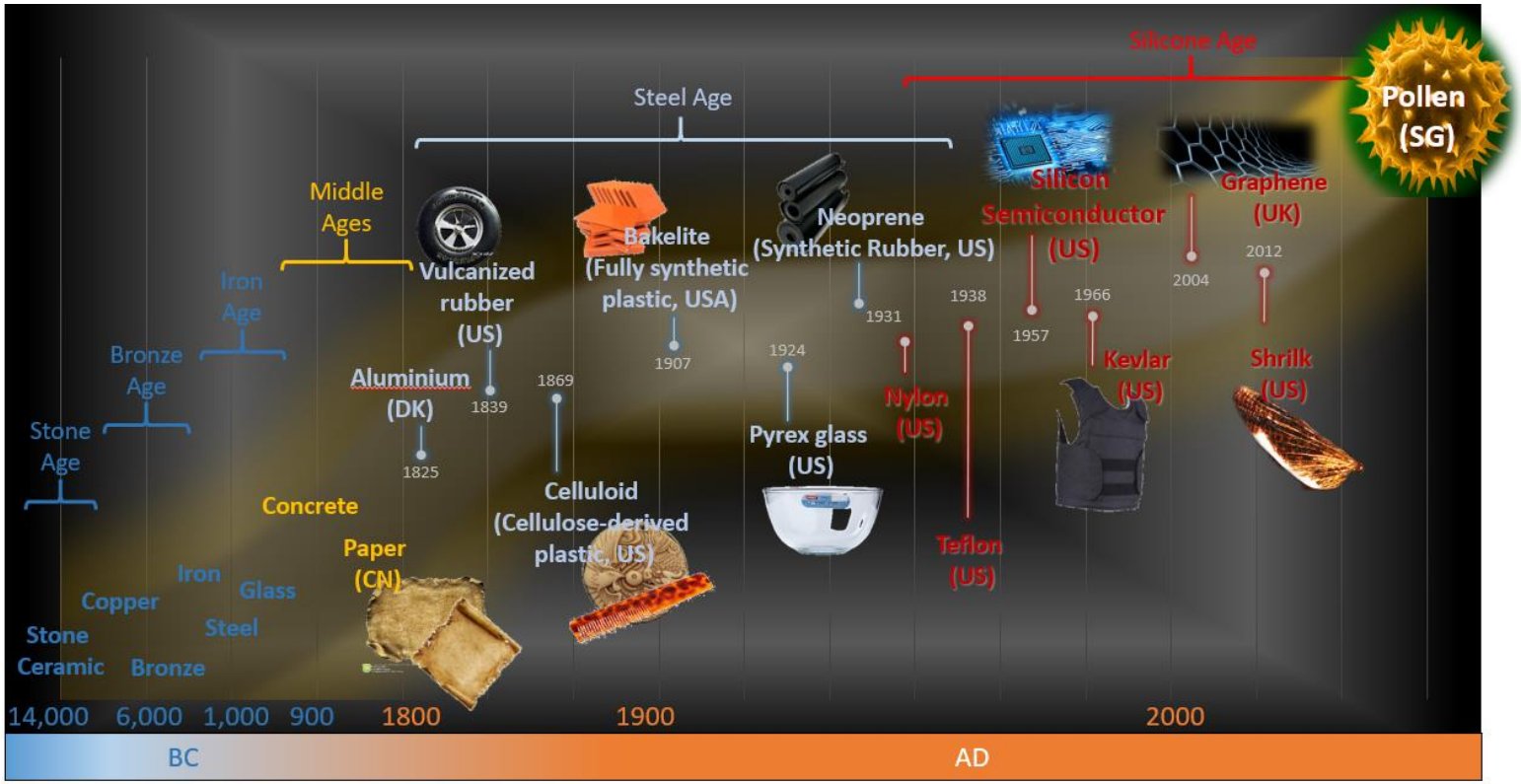

Figure 2.4. Condensed timeline of novel material discoveries. Will pollen be the next breakthrough?

2.6 References

53 Balaji, Pakalapati, Khalid, Walvekar & Siddiqui. Natural and synthetic biocompatible and biodegradable polymers. *Navinchandra Gopal Shimpi. Biodegradable and biocompatible polymer composites. Oxford: Elsevier*, 3-32 (2018).

54 Asghari, Samiei, Adibkia, Akbarzadeh & Davaran. Biodegradable and biocompatible polymers for tissue engineering application: a review. *Artificial cells, nanomedicine, and biotechnology* **45**, 185-192 (2017).

55 Joyce, Fabra, Bozkurt & Pandit. Bioactive potential of natural biomaterials: identification, retention and assessment of biological properties. *Signal transduction and targeted therapy* **6**, 1-28 (2021).

56 Sbrodov. in *IOP Conference Series: Materials Science and Engineering.* 012016 (IOP Publishing).

57 Malujda & Wilczyński. Mechanical properties investigation of natural polymers. *Procedia engineering* **136**, 263-268 (2016).

58 Ghalia & Abdelrasoul. in *Mechanical and physical testing of biocomposites, fibre-reinforced composites and hybrid composites* 123-140 (Elsevier, 2019).

59 Ardalan, Emamzadeh, Rasekh, Joshaghani & Samali. Physical and mechanical properties of polymer modified self-compacting concrete (SCC) using natural and recycled aggregates. *Journal of Sustainable Cement-Based Materials* **9**, 1-16 (2020).

60 Terlikowski, Sobczyńska, Gregoriou-Szczepaniak & Wasilewski. in *IOP Conference Series: Materials Science and Engineering.* 012135 (IOP Publishing).

61 Pintea & Manea. Influence of natural organic polymers upon plaster mortar workability. *Procedia Manufacturing* **46**, 158-164 (2020).

62 Ngwuluka, Ochekpe & Aruoma. Naturapolyceutics: the science of utilizing natural polymers for drug delivery. *polymers* **6**, 1312-1332 (2014).

63 George, Shah & Shrivastav. Guar gum: Versatile natural polymer for drug delivery applications. *European Polymer Journal* **112**, 722-735 (2019).

64 Anwunobi & Emeje. Recent applications of natural polymers in nanodrug delivery. *J Nanomedic Nanotechnol S* **4** (2011).

65 Gavasane & Pawar. Synthetic biodegradable polymers used in controlled drug delivery system: an overview. *Clin Pharmacol Biopharm* **3**, 1-7 (2014).

66 Patel & Goyal. Applications of natural polymer gum arabic: a review. *International Journal of Food Properties* **18**, 986-998 (2015).

67 Celli, Gandini, Gioia, Lacerda, Vannini & Colonna. Polymers from pristine and modified natural monomers. *Chemicals and Fuels from Bio-Based Building Blocks* **1** (2016).

68 Caillol. (Multidisciplinary Digital Publishing Institute, 2021).

69 Mallakpour & Dinari. Progress in synthetic polymers based on natural amino acids. *Journal of Macromolecular Science, Part A* **48**, 644-679 (2011).

70 Namazi. Polymers in our daily life. *BioImpacts: BI* **7**, 73 (2017).

71 Kulkarni Vishakha, Butte Kishor & Rathod Sudha. Natural polymers–A comprehensive review. *International journal of research in pharmaceutical and biomedical sciences* **3**, 1597-1613 (2012).

72 Abedini, Ebrahimi, Roozbehani, Domb & Hosseinkhani. Overview on natural hydrophilic polysaccharide polymers in drug delivery. *Polymers for Advanced Technologies* **29**, 2564-2573 (2018).

73 Schmidt. Hydrophilic Polymers. *Polymers* **11**, 693 (2019).

74 Rajeswari, Prasanthi, Sudha, Swain, Panda & Goka. Natural polymers: a recent review. *World J. Pharm. Pharm. Sci* **6**, 472-494 (2017).

75 Ceglia, Merlin, Viot, Schmitt & Mondain-Monval. Porous materials with tunable mechanical properties. *Journal of Porous Materials* **21**, 903-912 (2014).

76 Li, Huang, Gao, Zhong, Cao, Chen, Zhang & Cai. Reinforced mechanical properties and tunable biodegradability in nanoporous cellulose gels: poly (l-lactide-co-caprolactone) nanocomposites. *Biomacromolecules* **17**, 1506-1515 (2016).

77 Abid, Khan & Iqbal. A study on optical and thermal properties of natural polymer-based hemicellulose compounds. *Journal of Biomaterials Science, Polymer Edition*, 1-14 (2021).

78 Birajdar, Joo, Koh & Park. Natural bio-based monomers for biomedical applications: a review. *Biomaterials Research* **25**, 1-14 (2021).

79 de Moraes Porto. Polymer biocompatibility. *Polymerization. Croatia: InTech* **2012**, 47-63 (2012).

80 Bhatia. in *Natural Polymer Drug Delivery Systems* 95-118 (Springer, 2016).

81 Cao & Uhrich. Biodegradable and biocompatible polymers for electronic applications: A review. *Journal of Bioactive and Compatible Polymers* **34**, 3-15 (2019).

82 Altuntaş, Özkan & Yener. in *Nanobiomaterials Science, Development and Evaluation* 27-59 (Elsevier, 2017).

83 Samadian, Maleki, Allahyari & Jaymand. Natural polymers-based light-induced hydrogels: Promising biomaterials for biomedical applications. *Coordination Chemistry Reviews* **420**, 213432 (2020).

84 Albuquerque, Coelho, Teixeira & Carneiro-da-Cunha. Approaches in biotechnological applications of natural polymers. (2016).

85 Torres, Troncoso, Pisani, Gatto & Bardi. Natural polysaccharide nanomaterials: an overview of their immunological properties. *International journal of molecular sciences* **20**, 5092 (2019).

86 Banwell, Pollard, Liu & Connal. Exploiting Nature's Most Abundant Polymers: Developing New Pathways for the Conversion of Cellulose, Hemicellulose, Lignin and Chitin into Platform Molecules (and Beyond). *Chemistry–An Asian Journal* **16**, 604-620 (2021).

87 Acquavia, Pascale, Martelli, Bondoni & Bianco. Natural polymeric materials: A solution to plastic pollution from the agro-food sector. *Polymers* **13**, 158 (2021).

88 Liu, Holzwarth & Ma. Functionalized synthetic biodegradable polymer scaffolds for tissue engineering. *Macromolecular bioscience* **12**, 911-919 (2012).

89 Oh & Lee. Hydrophilization of synthetic biodegradable polymer scaffolds for improved cell/tissue compatibility. *Biomedical materials* **8**, 014101 (2013).

90 Bou-Gharios, Abraham & de Crombrugghe. in *Principles of bone biology* 295-337 (Elsevier, 2020).

91 Abedinia, Mohammadi Nafchi, Sharifi, Ghalambor, Oladzadabbasabadi, Ariffin & Huda. Poultry gelatin: Characteristics, developments, challenges, and future outlooks as a sustainable alternative for mammalian gelatin. *Trends in Food Science & Technology* **104**, 14-26, doi:https://doi.org/10.1016/j.tifs.2020.08.001 (2020).

92 Cao, Wang, Hao, Zhang & Zhou. Antihypertensive Effects in Vitro and in Vivo of Novel Angiotensin-Converting Enzyme Inhibitory Peptides from Bovine Bone Gelatin Hydrolysate. *Journal of Agricultural and Food Chemistry* **68**, 759-768, doi:10.1021/acs.jafc.9b05618 (2020).

93 Mony, Shenoy, Raj, Geetha, Pratheesh, Nair, Purnima & Anilkumar. Gelatin-Modified Cholecyst-Derived Scaffold Promotes Angiogenesis and Faster Healing of Diabetic Wounds. *ACS Applied Bio Materials* **4**, 3320-3331, doi:10.1021/acsabm.0c01648 (2021).

94 Alipal, Mohd Pu'ad, Lee, Nayan, Sahari, Basri, Idris & Abdullah. A review of gelatin: Properties, sources, process, applications, and commercialisation. *Materials Today: Proceedings* **42**, 240-250, doi:https://doi.org/10.1016/j.matpr.2020.12.922 (2021).

95 Wang, Ao, Tian, Fan, Tong, Hou & Bai. Gelatin-based hydrogels for organ 3D bioprinting. *Polymers* **9**, 401 (2017).

96 Lin, Regenstein, Lv, Lu & Jiang. An overview of gelatin derived from aquatic animals: Properties and modification. *Trends in Food Science & Technology* **68**, 102-112, doi:https://doi.org/10.1016/j.tifs.2017.08.012 (2017).

97 Wilson, Amirkhani & Taylor. Evaluation of Gelatin as a Biostimulant Seed Treatment to Improve Plant Performance. *Frontiers in Plant Science* **9**, doi:10.3389/fpls.2018.01006 (2018).

98 Karim & Bhat. Fish gelatin: properties, challenges, and prospects as an alternative to mammalian gelatins. *Food Hydrocolloids* **23**, 563-576, doi:https://doi.org/10.1016/j.foodhyd.2008.07.002 (2009).

99 Jongjareonrak, Rawdkuen, Chaijan, Benjakul, Osako & Tanaka. Chemical compositions and characterisation of skin gelatin from farmed giant catfish (Pangasianodon gigas). *LWT - Food Science and Technology* **43**, 161-165, doi:https://doi.org/10.1016/j.lwt.2009.06.012 (2010).

100 Roy & Rhim. Preparation of Gelatin/Carrageenan-Based Color-Indicator Film Integrated with Shikonin and Propolis for Smart Food Packaging Applications. *ACS Applied Bio Materials* **4**, 770-779, doi:10.1021/acsabm.0c01353 (2021).

101 Campiglio, Contessi Negrini, Farè & Draghi. Cross-Linking Strategies for Electrospun Gelatin Scaffolds. *Materials* **12**, doi:10.3390/ma12152476 (2019).

102 Tytgat, Van Damme, Van Hoorick, Declercq, Thienpont, Ottevaere, Blondeel, Dubruel & Van Vlierberghe. Additive manufacturing of photo-crosslinked gelatin scaffolds for adipose tissue engineering. *Acta Biomaterialia* **94**, 340-350, doi:https://doi.org/10.1016/j.actbio.2019.05.062 (2019).

103 Soltan, Ning, Mohabatpour, Papagerakis & Chen. Printability and Cell Viability in Bioprinting Alginate Dialdehyde-Gelatin Scaffolds. *ACS Biomaterials Science & Engineering* **5**, 2976-2987, doi:10.1021/acsbiomaterials.9b00167 (2019).

104 Ferracci, Zhu, Ibrahim, Ma, Fan, Lee & Cho. Photocurable Albumin Methacryloyl Hydrogels as a Versatile Platform for Tissue Engineering. *ACS Applied Bio Materials* **3**, 920-934 (2020).

105 Fox, Li, Xu & Edgar. Regioselective Esterification and Etherification of Cellulose: A Review. *Biomacromolecules* **12**, 1956-1972, doi:10.1021/bm200260d (2011).

106 Zhao, Kwak, Wang, Franz, White & Holladay. Effects of Crystallinity on Dilute Acid Hydrolysis of Cellulose by Cellulose Ball-Milling Study. *Energy & Fuels* **20**, 807-811, doi:10.1021/ef050319a (2006).

107 Thakur & Thakur. Processing and characterization of natural cellulose fibers/thermoset polymer composites. *Carbohydrate polymers* **109**, 102-117 (2014).

108 Liu, Du, Zhang, Liu, Liu, Xie, Zhang & Si. Bacterial Cellulose-Based Composite Scaffolds for Biomedical Applications: A Review. *ACS Sustainable Chemistry & Engineering* **8**, 7536-7562, doi:10.1021/acssuschemeng.0c00125 (2020).

109 Dugan, Gough & Eichhorn. Bacterial cellulose scaffolds and cellulose nanowhiskers for tissue engineering. *Nanomedicine* **8**, 287-298, doi:10.2217/nnm.12.211 (2013).

110 Modulevsky, Lefebvre, Haase, Al-Rekabi & Pelling. Apple derived cellulose scaffolds for 3D mammalian cell culture. *PloS one* **9**, e97835 (2014).

111 Courtenay, Johns, Galembeck, Deneke, Lanzoni, Costa, Scott & Sharma. Surface modified cellulose scaffolds for tissue engineering. *Cellulose* **24**, 253-267 (2017).

112 Abitbol, Rivkin, Cao, Nevo, Abraham, Ben-Shalom, Lapidot & Shoseyov. Nanocellulose, a tiny fiber with huge applications. *Current Opinion in Biotechnology* **39**, 76-88, doi:https://doi.org/10.1016/j.copbio.2016.01.002 (2016).

113 Dufresne. Nanocellulose: a new ageless bionanomaterial. *Materials today* **16**, 220-227 (2013).

114 Kyle, Jessop, Al-Sabah, Hawkins, Lewis, Maffeis, Charbonneau, Gazze, Francis, Iakovlev, Nelson, Eichhorn & Whitaker. Characterization of pulp derived nanocellulose hydrogels using AVAP® technology. *Carbohydrate Polymers* **198**, 270-280, doi:https://doi.org/10.1016/j.carbpol.2018.06.091 (2018).

115 Kim, Shim, Kim, Lee, Min, Jang, Abas & Kim. Review of nanocellulose for sustainable future materials. *International Journal of Precision Engineering and Manufacturing-Green Technology* **2**, 197-213 (2015).

116 Auad, Contos, Nutt, Aranguren & Marcovich. Characterization of nanocellulose-reinforced shape memory polyurethanes. *Polymer International* **57**, 651-659, doi:https://doi.org/10.1002/pi.2394 (2008).

117 Thomas, Raj, B, H, Joy, Moores, Drisko & Sanchez. Nanocellulose, a Versatile Green Platform: From Biosources to Materials and Their Applications. *Chemical Reviews* **118**, 11575-11625, doi:10.1021/acs.chemrev.7b00627 (2018).

118 Frey, Widner, Segmehl, Casdorff, Keplinger & Burgert. Delignified and Densified Cellulose Bulk Materials with Excellent Tensile Properties for Sustainable Engineering. *ACS Applied Materials & Interfaces* **10**, 5030-5037, doi:10.1021/acsami.7b18646 (2018).

119 Khan & Khan. Use of collagen as a biomaterial: An update. *Journal of Indian Society of Periodontology* **17**, 539 (2013).

120 Brodsky & Ramshaw. The collagen triple-helix structure. *Matrix biology* **15**, 545-554 (1997).

121 Brodsky & Persikov. Molecular structure of the collagen triple helix. *Advances in protein chemistry* **70**, 301-339 (2005).

122 Egli, Schnitzer, Dietschreit, Ochsenfeld & Wennemers. Why proline? Influence of ring-size on the collagen triple helix. *Organic letters* **22**, 348-351 (2019).

123 Zhang, Gopalakrishnan, Li, Wang, Han & Rotello. Fabrication of Collagen Films with Enhanced Mechanical and Enzymatic Stability through Thermal Treatment in Fluorous Media. *ACS Applied Materials & Interfaces* **12**, 6590-6597, doi:10.1021/acsami.9b18256 (2020).

124 Kim, Yun & Kim. An innovative cell-laden α-TCP/collagen scaffold fabricated using a two-step printing process for potential application in regenerating hard tissues. *Scientific Reports* **7**, 3181, doi:10.1038/s41598-017-03455-9 (2017).

125 Zarei, Samimi, Khorram, Abdi & Golestaneh. Fabrication and characterization of conductive polypyrrole/chitosan/collagen electrospun nanofiber scaffold for tissue engineering application. *International Journal of Biological Macromolecules* **168**, 175-186, doi:https://doi.org/10.1016/j.ijbiomac.2020.12.031 (2021).

126 Seong, Kang, Song, Kim & Jeong. Calcium Phosphate–Collagen Scaffold with Aligned Pore Channels for Enhanced Osteochondral Regeneration. *Advanced Healthcare Materials* **6**, 1700966, doi:https://doi.org/10.1002/adhm.201700966 (2017).

127 Yang, Ding, Tang, Deng, Yang, Wu, Chen, Ni, Huang & Zhang. Novel modification of collagen: Realizing desired water solubility and thermostability in a conflict-free way. *ACS omega* **5**, 5772-5780 (2020).

128 Avila Rodríguez, Rodriguez Barroso & Sánchez. Collagen: A review on its sources and potential cosmetic applications. *Journal of cosmetic dermatology* **17**, 20-26 (2018).

129 Rapson, Christley-Balcomb, Jackson & Sutherland. Enhancement of metallomacrocycle-based oxygen reduction catalysis through immobilization in a tunable silk-protein scaffold. *Journal of inorganic biochemistry* **204**, 110960 (2020).

130 Belda Marín, Fitzpatrick, Kaplan, Landoulsi, Guénin & Egles. Silk Polymers and Nanoparticles: A Powerful Combination for the Design of Versatile Biomaterials. *Frontiers in chemistry* **8**, 604398-604398, doi:10.3389/fchem.2020.604398 (2020).

131 Marín, Fitzpatrick, Kaplan, Landoulsi, Guénin & Egles. Silk polymers and nanoparticles: a powerful combination for the design of versatile biomaterials. *Frontiers in Chemistry* **8** (2020).

132 Zhang, Zhang, Hu, Fei, Liu, Huang, Wang, Ruan, Heng, Chen & Shen. Systematic Review of Silk Scaffolds in Musculoskeletal Tissue Engineering Applications in the Recent Decade. *ACS Biomaterials Science & Engineering* **7**, 817-840, doi:10.1021/acsbiomaterials.0c01716 (2021).

133 Gu, Jiang & Hu. Scalable Spider-Silk-Like Supertough Fibers using a Pseudoprotein Polymer. *Advanced Materials* **31**, 1904311 (2019).

134 Mu, Wang, Guo, Li, Ling, Huang, Cebe, Hsu, De Ferrari & Jiang. 3D Printing of Silk Protein Structures by Aqueous Solvent-Directed Molecular Assembly. *Macromolecular bioscience* **20**, 1900191 (2020).

135 Agostinacchio, Mu, Dirè, Motta & Kaplan. In situ 3D printing: opportunities with silk inks. *Trends in Biotechnology* (2020).

136 Huang, Yuan, Hong, Fan, Yao, Ren, Song, Yang & Zhang. 3D printed hydrogels with oxidized cellulose nanofibers and silk fibroin for the proliferation of lung epithelial stem cells. *Cellulose* **28**, 241-257 (2021).

137 Gore, Naebe, Wang & Kandasubramanian. Progress in silk materials for integrated water treatments: Fabrication, modification and applications. *Chemical Engineering Journal* **374**, 437-470, doi:https://doi.org/10.1016/j.cej.2019.05.163 (2019).

138 Lu, Hu, Wang, Kluge, Lu, Cebe & Kaplan. Water-insoluble silk films with silk I structure. *Acta Biomaterialia* **6**, 1380-1387, doi:https://doi.org/10.1016/j.actbio.2009.10.041 (2010).

139 Zheng, Zhong, Qi, Ling & Kaplan. Isolation of Silk Mesostructures for Electronic and Environmental Applications. *Advanced Functional Materials* **28**, 1806380, doi:https://doi.org/10.1002/adfm.201806380 (2018).

140 Rinaudo. Chitin and chitosan: Properties and applications. *Progress in Polymer Science* **31**, 603-632, doi:https://doi.org/10.1016/j.progpolymsci.2006.06.001 (2006).

141 Ravi Kumar. A review of chitin and chitosan applications. *Reactive and Functional Polymers* **46**, 1-27, doi:https://doi.org/10.1016/S1381-5148(00)00038-9 (2000).

142 Croisier & Jérôme. Chitosan-based biomaterials for tissue engineering. *European polymer journal* **49**, 780-792 (2013).

143 Jayakumar, Menon, Manzoor, Nair & Tamura. Biomedical applications of chitin and chitosan based nanomaterials—A short review. *Carbohydrate Polymers* **82**, 227-232, doi:https://doi.org/10.1016/j.carbpol.2010.04.074 (2010).

144 Jayakumar, Chennazhi, Srinivasan, Nair, Furuike & Tamura. Chitin Scaffolds in Tissue Engineering. *International Journal of Molecular Sciences* **12**, doi:10.3390/ijms12031876 (2011).

145 Shamshina, Berton & Rogers. Advances in Functional Chitin Materials: A Review. *ACS Sustainable Chemistry & Engineering* **7**, 6444-6457, doi:10.1021/acssuschemeng.8b06372 (2019).

146 Madhumathi, Kumar, Abhilash, Sreeja, Tamura, Manzoor, Nair & Jayakumar. Development of novel chitin/nanosilver composite scaffolds for wound dressing applications. *Journal of Materials Science: Materials in Medicine* **21**, 807-813 (2010).

147 Yoon, Kim, Wang, Fang, Hsiao & Chu. High flux ultrafiltration membranes based on electrospun nanofibrous PAN scaffolds and chitosan coating. *Polymer* **47**, 2434-2441 (2006).

148 Zhao, Zheng, Wang, Zhang & Han. High performance ultrafiltration membrane based on modified chitosan coating and electrospun nanofibrous PVDF scaffolds. *Journal of membrane science* **394**, 209-217 (2012).

149 Goetz, Jalvo, Rosal & Mathew. Superhydrophilic anti-fouling electrospun cellulose acetate membranes coated with chitin nanocrystals for water filtration. *Journal of Membrane Science* **510**, 238-248 (2016).

150 Asghar & Henrickson. Chemical, biochemical, functional, and nutritional characteristics of collagen in food systems. *Advances in food research* **28**, 231-372 (1982).

151 Gómez-Guillén, Giménez, López-Caballero & Montero. Functional and bioactive properties of collagen and gelatin from alternative sources: A review. *Food Hydrocolloids* **25**, 1813-1827, doi:https://doi.org/10.1016/j.foodhyd.2011.02.007 (2011).

152 Bello, Kim, Kim, Park & Lee. Engineering and functionalization of gelatin biomaterials: From cell culture to medical applications. *Tissue Engineering Part B: Reviews* **26**, 164-180 (2020).

153 Xing, Yates, Vogt, Qian, Frost & Zhao. Increasing mechanical strength of gelatin hydrogels by divalent metal ion removal. *Scientific reports* **4**, 1-10 (2014).

154 Shoulders & Raines. Collagen structure and stability. *Annual review of biochemistry* **78**, 929-958 (2009).

155 Tanaka, Inoue & Mizuno. Hydrophobic interaction of P25, containing Asn-linked oligosaccharide chains, with the HL complex of silk fibroin produced by Bombyx mori. *Insect biochemistry and molecular biology* **29**, 269-276 (1999).

156 Zhou, Confalonieri, Jacquet, Perasso, Li & Janin. Silk fibroin: structural implications of a remarkable amino acid sequence. *Proteins: Structure, Function, and Bioinformatics* **44**, 119-122 (2001).

157 Asakura, Ito, Okudaira & Kameda. Structure of Alanine and Glycine Residues of Samia c ynthia r icini Silk Fibers Studied with Solid-State 15N and 13C NMR. *Macromolecules* **32**, 4940-4946 (1999).

158 Gage & Manning. Internal structure of the silk fibroin gene of Bombyx mori. I The fibroin gene consists of a homogeneous alternating array of repetitious crystalline and amorphous coding sequences. *Journal of Biological Chemistry* **255**, 9444-9450 (1980).

159 Fedic, Z˘urovec & Sehnal. Correlation between fibroin amino acid sequence and physical silk properties. *Journal of Biological Chemistry* **278**, 35255-35264 (2003).

160 Huang, Ling, Li, Omenetto & Kaplan. Silkworm silk-based materials and devices generated using bio-nanotechnology. *Chemical Society Reviews* **47**, 6486-6504 (2018).

161 Husmann, Pawelec, Burdett, Best & Cameron. Numerical simulations to determine the influence of mould design on ice-templated scaffold structures. *genesis* **6**, 8 (2015).

162 Asuncion, Goh & Toh. Anisotropic silk fibroin/gelatin scaffolds from unidirectional freezing. *Materials Science and Engineering: C* **67**, 646-656 (2016).

163 Pawelec, Husmann, Best & Cameron. A design protocol for tailoring ice-templated scaffold structure. *Journal of the Royal Society Interface* **11**, 20130958 (2014).

164 Shao, Hanaor, Shen & Gurlo. Freeze Casting: From Low-Dimensional Building Blocks to Aligned Porous Structures—A Review of Novel Materials, Methods, and Applications. *Advanced Materials* **32**, 1907176, doi:https://doi.org/10.1002/adma.201907176 (2020).

165 Martoïa, Cochereau, Dumont, Orgéas, Terrien & Belgacem. Cellulose nanofibril foams: Links between ice-templating conditions, microstructures and mechanical properties. *Materials & Design* **104**, 376-391 (2016).

166 Deville, Viazzi & Guizard. Ice-structuring mechanism for zirconium acetate. *Langmuir* **28**, 14892-14898 (2012).

167 Wu, Li, Xue, Liu, Fan, Bai & Wang. Size Controllable, Transparent, and Flexible 2D Silver Meshes Using Recrystallized Ice Crystals as Templates. *ACS Nano* **11**, 9898-9905, doi:10.1021/acsnano.7b03821 (2017).

168 Zhang, Li, Lv, Zhao & Qu. Vertically Aligned Graphene Sheets Membrane for Highly Efficient Solar Thermal Generation of Clean Water. *ACS Nano* **11**, 5087-5093, doi:10.1021/acsnano.7b01965 (2017).

169 Wu, Zhu, He, Xue, Fan, Song, Francisco, Zeng & Wang. Ion-specific ice recrystallization provides a facile approach for the fabrication of porous materials. *Nature communications* **8**, 1-8 (2017).

170 Baheti, Kumar & Bansal. Excipients used in lyophilization of small molecules. *Journal of Excipients and Food Chemicals* **1**, 1135 (2016).

171 Whang, Thomas, Healy & Nuber. A novel method to fabricate bioabsorbable scaffolds. *Polymer* **36**, 837-842 (1995).

172 Owen, Sherborne, Evans, Reilly & Claeyssens. Combined porogen leaching and emulsion templating to produce bone tissue engineering scaffolds. *International Journal of Bioprinting* **6** (2020).

173 Yıldırım, Demirtaş, Dinçer, Yıldız & Karakeçili. Preparation of polycaprolactone/graphene oxide scaffolds: A green route combining supercritial CO2 technology and porogen leaching. *The Journal of Supercritical Fluids* **133**, 156-162 (2018).

174 Yin, Qian, Zhang, Lin, Li, Xu & Li. Engineering porous poly (lactic acid) scaffolds with high mechanical performance via a solid state extrusion/porogen leaching approach. *Polymers* **8**, 213 (2016).

175 Chen & Ma. Nano-fibrous poly(l-lactic acid) scaffolds with interconnected spherical macropores. *Biomaterials* **25**, 2065-2073, doi:https://doi.org/10.1016/j.biomaterials.2003.08.058 (2004).

176 Salerno, Fernández-Gutiérrez, del Barrio & Domingo. Bio-safe fabrication of PLA scaffolds for bone tissue engineering by combining phase separation, porogen leaching and scCO2 drying. *The Journal of Supercritical Fluids* **97**, 238-246 (2015).

177 Janik & Marzec. A review: Fabrication of porous polyurethane scaffolds. *Materials Science and Engineering: C* **48**, 586-591, doi:https://doi.org/10.1016/j.msec.2014.12.037 (2015).

178 Yu, Hua, Yang, Fu, Teng, Niu, Zhao & Yi. Fabrication and characterization of electrospinning/3D printing bone tissue engineering scaffold. *RSC advances* **6**, 110557-110565 (2016).

179 Do, Khorsand, Geary & Salem. 3D printing of scaffolds for tissue regeneration applications. *Advanced healthcare materials* **4**, 1742-1762 (2015).

180 Maroulakos, Kamperos, Tayebi, Halazonetis & Ren. Applications of 3D printing on craniofacial bone repair: A systematic review. *Journal of Dentistry* **80**, 1-14 (2019).

181 Ventola. Medical applications for 3D printing: current and projected uses. *Pharmacy and Therapeutics* **39**, 704 (2014).

182 Ko, Pan, Grigoropoulos, Luscombe, Fréchet & Poulikakos. All-inkjet-printed flexible electronics fabrication on a polymer substrate by low-temperature high-resolution selective laser sintering of metal nanoparticles. *Nanotechnology* **18**, 345202 (2007).

183 Costantini & Barbetta. in *Functional 3D Tissue Engineering Scaffolds* 127-149 (Elsevier, 2018).

184 Chen, Zhou, Tang, Weir, Bao & Xu. Gas-foaming calcium phosphate cement scaffold encapsulating human umbilical cord stem cells. *Tissue Engineering Part A* **18**, 816-827 (2012).

185 Song, Zhou, Fan, Zhang, Pei, Fan, Jiang, Bao, Yang & Dong. Novel 3D porous biocomposite scaffolds fabricated by fused deposition modeling and gas foaming combined technology. *Composites Part B: Engineering* **152**, 151-159 (2018).

186 Gorna & Gogolewski. Preparation, degradation, and calcification of biodegradable polyurethane foams for bone graft substitutes. *Journal of Biomedical Materials Research Part A: An Official Journal of The Society for Biomaterials, The Japanese Society for Biomaterials, and The Australian Society for Biomaterials and the Korean Society for Biomaterials* **67**, 813-827 (2003).

187 Kim & Hollinger. Recombinant human bone morphogenetic protein-2 released from polyurethane-based scaffolds promotes early osteogenic differentiation of human mesenchymal stem cells. *Biomedical materials* **7**, 045008 (2012).

188 Kim, Park, Kim, Cho & Kim. Gas foaming fabrication of porous biphasic calcium phosphate for bone regeneration. *Tissue Engineering and Regenerative Medicine* **9**, 63-68 (2012).

189 Quirk, France, Shakesheff & Howdle. Supercritical fluid technologies and tissue engineering scaffolds. *Current Opinion in Solid State and Materials Science* **8**, 313-321 (2004).

190 Ramakrishna, Fujihara, Teo, Yong, Ma & Ramaseshan. Electrospun nanofibers: solving global issues. *Materials today* **9**, 40-50 (2006).

191 Dror, Salalha, Khalfin, Cohen, Yarin & Zussman. Carbon nanotubes embedded in oriented polymer nanofibers by electrospinning. *Langmuir* **19**, 7012-7020 (2003).

192 Kanani & Bahrami. Review on electrospun nanofibers scaffold and biomedical applications. *Trends Biomater Artif Organs* **24**, 93-115 (2010).

193 Yang, Chen, Wang, Zhu, Xu, Chen, Ma & Li. A facile electrospinning method to fabricate polylactide/graphene/MWCNTs nanofiber membrane for tissues scaffold. *Applied Surface Science* **362**, 163-168 (2016).

194 Liang, Zhang, Huang, Xu & Fong. Superhydrophobic and elastic 3D conductive sponge made from electrospun nanofibers and reduced graphene oxide for sweatproof wearable tactile pressure sensor. *Polymer*, 124025, doi:https://doi.org/10.1016/j.polymer.2021.124025 (2021).

195 Karki, Kafle, Ojha, Song & Kim. Three-dimensional nanoporous polyacrylonitrile-based carbon scaffold for effective separation of oil from oil/water emulsion. *Polymer* **153**, 597-606, doi:https://doi.org/10.1016/j.polymer.2018.08.069 (2018).

196 Desai, Kit, Li & Zivanovic. Morphological and surface properties of electrospun chitosan nanofibers. *Biomacromolecules* **9**, 1000-1006 (2008).

197 Makaremi, De Silva & Pasbakhsh. Electrospun nanofibrous membranes of polyacrylonitrile/halloysite with superior water filtration ability. *The Journal of Physical Chemistry C* **119**, 7949-7958 (2015).

198 Xu, Zheng, Chen, Ding, Liang, Liu, Zhu & Fong. Halloysite nanotubes sponges with skeletons made of electrospun nanofibers as innovative dye adsorbent and catalyst support. *Chemical Engineering Journal* **360**, 280-288 (2019).

199 Xu, Miszuk, Zhao, Sun & Fong. Electrospun polycaprolactone 3D nanofibrous scaffold with interconnected and hierarchically structured pores for bone tissue engineering. *Advanced healthcare materials* **4**, 2238-2246 (2015).

200 Nam, Huang, Agarwal & Lannutti. Materials selection and residual solvent retention in biodegradable electrospun fibers. *Journal of Applied Polymer Science* **107**, 1547-1554, doi:https://doi.org/10.1002/app.27063 (2008).

201 Lannutti, Reneker, Ma, Tomasko & Farson. Electrospinning for tissue engineering scaffolds. *Materials Science and Engineering: C* **27**, 504-509, doi:https://doi.org/10.1016/j.msec.2006.05.019 (2007).

202 Zhang, Feng & Zhang. Emulsion electrospinning: Fundamentals, food applications and prospects. *Trends in Food Science & Technology* **80**, 175-186, doi:https://doi.org/10.1016/j.tifs.2018.08.005 (2018).

203 Al-Handarish, Omisore, Duan, Chen, Zebang, Akinyemi, Du, Li & Wang. Facile Fabrication of 3D Porous Sponges Coated with Synergistic Carbon Black/Multiwalled Carbon Nanotubes for Tactile Sensing Applications. *Nanomaterials* **10**, 1941 (2020).

204 Gu, Jeong, Na, Seon, Lee & Kang. Application of semi-permeable membrane for a scaffold in a nature-mimicking vascular system. *Journal of Membrane Science* **611**, 118384, doi:https://doi.org/10.1016/j.memsci.2020.118384 (2020).

205 Mazio, Casale, Imparato, Urciuolo, Attanasio, De Gregorio, Rescigno & Netti. Pre-vascularized dermis model for fast and functional anastomosis with host vasculature. *Biomaterials* **192**, 159-170, doi:https://doi.org/10.1016/j.biomaterials.2018.11.018 (2019).

206 Quintanilla, Casas, Miranzo, Osendi & Belmonte. 3D-Printed Fe-doped silicon carbide monolithic catalysts for wet peroxide oxidation processes. *Applied Catalysis B: Environmental* **235**, 246-255, doi:https://doi.org/10.1016/j.apcatb.2018.04.066 (2018).

207 Sinha, Cha & Kim. Three-dimensional macroporous alginate scaffolds embedded with akaganeite nanorods for the filter-based high-speed preparation of arsenic-free drinking water. *ACS Applied Nano Materials* **1**, 1940-1948 (2018).

208 Fan, Liu, Quan & Chen. Highly permeable thin-film composite forward osmosis membrane based on carbon nanotube hollow fiber scaffold with electrically enhanced fouling resistance. *Environmental science & technology* **52**, 1444-1452 (2018).

209 Cheng. Porous graphene sponge additives for lithium ion batteries with excellent rate capability. *Scientific reports* **7**, 1-11 (2017).

210 Ma, Wang, Zeng & Fang. Amorphous Ge/C Composite Sponges: Synthesis and Application in a High-Rate Anode for Lithium Ion Batteries. *Langmuir* **33**, 2141-2147, doi:10.1021/acs.langmuir.6b04444 (2017).

211 Sengupta, Patra, Mitra, Jena, Das, Majumder & Das. Melt impregnation as a post processing treatment for performance enhancement in high capacity 3D microporous tin-copper-nickel intermetallic anode for Li-ion battery supported by electrodeposited nickel scaffold: A structural study. *Applied Surface Science* **441**, 965-977, doi:https://doi.org/10.1016/j.apsusc.2018.01.311 (2018).

212 Jin, Sheng, Luo, Yuan, Fang, Zhang, Huang, Gan, Xia, Liang, Zhang & Tao. 3D lithium metal embedded within lithiophilic porous matrix for stable lithium metal batteries. *Nano Energy* **37**, 177-186, doi:https://doi.org/10.1016/j.nanoen.2017.05.015 (2017).

213 Pereira, Brito-Pereira, Gonçalves, Silva, Costa, Silva, de Zea Bermudez & Lanceros-Méndez. Silk Fibroin Separators: A Step Toward Lithium-Ion Batteries with Enhanced Sustainability. *ACS Applied Materials & Interfaces* **10**, 5385-5394, doi:10.1021/acsami.7b13802 (2018).

214 Liu, Yuan, Cheng, Chen, Titirici, Huang, Yuan & Zhang. A review of naturally derived nanostructured materials for safe lithium metal batteries. *Materials Today Nano* **8**, 100049, doi:https://doi.org/10.1016/j.mtnano.2019.100049 (2019).

215 You, Zhang, Deng, Li, Zheng, Li, Zhou, Huang & Sun. Suppressing Li dendrite by a protective biopolymeric film from tamarind seed polysaccharide for high-performance Li metal anode. *Electrochimica Acta* **299**, 636-644 (2019).

216 Zhang, Gao, Wang, Lu, Deng, You, Li, Zhou, Huang & Zhou. A natural biopolymer film as a robust protective layer to effectively stabilize lithium-metal anodes. *Small* **14**, 1801054 (2018).

217 Chang, Chung & Manthiram. Dendrite-Free Lithium Anode via a Homogenous Li-Ion Distribution Enabled by a Kimwipe Paper. *Advanced Sustainable Systems* **1**, 1600034 (2017).

218 Kim, Kim, Joo, Choi, Cha, Kim, Kwon, Kwak, Kang & Jin. Hierarchical chitin fibers with aligned nanofibrillar architectures: a nonwoven-mat separator for lithium metal batteries. *ACS nano* **11**, 6114-6121 (2017).

219 Ye, Zhong, Xu, Chang, Yang, Wang, Ye & Zhang. Construction of cellulose/nanosilver sponge materials and their antibacterial activities for infected wounds healing. *Cellulose* **23**, 749-763, doi:10.1007/s10570-015-0851-4 (2016).

220 Nguyen, Nguyen & Hsieh. Curcumin-Loaded Chitosan/Gelatin Composite Sponge for Wound Healing Application. *International Journal of Polymer Science* **2013**, 106570, doi:10.1155/2013/106570 (2013).

221 Ramanathan, Seleenmary Sobhanadhas, Sekar Jeyakumar, Devi, Sivagnanam & Fardim. Fabrication of Biohybrid Cellulose Acetate-Collagen Bilayer Matrices as Nanofibrous Spongy Dressing Material for Wound-Healing Application. *Biomacromolecules* **21**, 2512-2524, doi:10.1021/acs.biomac.0c00516 (2020).

222 Hu, Bi, Yan, Zhou, Sun, Cheng & Chen. Preparation of composite hydroxybutyl chitosan sponge and its role in promoting wound healing. *Carbohydrate Polymers* **184**, 154-163, doi:https://doi.org/10.1016/j.carbpol.2017.12.033 (2018).

223 Tolba, Wang, Ackermann, Neufurth, Muñoz-Espí, Schröder & Müller. In Situ Polyphosphate Nanoparticle Formation in Hybrid Poly(vinyl alcohol)/Karaya Gum Hydrogels: A Porous Scaffold Inducing Infiltration of Mesenchymal Stem Cells. *Advanced Science* **6**, 1801452, doi:https://doi.org/10.1002/advs.201801452 (2019).

224 Ballesteros-Cillero, Davison-Kotler, Kohli, Marshall & García-Gareta. Biomimetic In Vitro Model of Cell Infiltration into Skin Scaffolds for Pre-Screening and Testing of Biomaterial-Based Therapies. *Cells* **8**, doi:10.3390/cells8080917 (2019).

225 Huang, Huang, Shao, Hu, Cao, Fan, Song & Zhang. Silk scaffolds with gradient pore structure and improved cell infiltration performance. *Materials Science and Engineering: C* **94**, 179-189, doi:https://doi.org/10.1016/j.msec.2018.09.034 (2019).

226 Pandey, Singh, Momin & Bhavsar. Chitosan: Application in tissue engineering and skin grafting. *Journal of Polymer Research* **24**, 125, doi:10.1007/s10965-017-1286-4 (2017).

227 Kim, Kim, Ki, Kim & Park. Fabrication of bi-layer scaffold of keratin nanofiber and gelatin-methacrylate hydrogel: Implications for skin graft. *International Journal of Biological Macromolecules* **105**, 541-548, doi:https://doi.org/10.1016/j.ijbiomac.2017.07.067 (2017).

228 Shan, Li, Wu, Li & Liao. Hybrid cellulose nanocrystal/alginate/gelatin scaffold with improved mechanical properties and guided wound healing. *RSC advances* **9**, 22966-22979 (2019).

229 Bouhlouli, Pourhadi, Karami, Talebi, Ranjbari & Khojasteh. Applications of Bacterial Cellulose as a Natural Polymer in Tissue Engineering. *ASAIO Journal* **67** (2021).

230 Hsu, Whu, Hsieh, Tsai, Chen & Tan. Evaluation of chitosan-alginate-hyaluronate complexes modified by an RGD-containing protein as tissue-engineering scaffolds for cartilage regeneration. *Artificial organs* **28**, 693-703 (2004).

231 Poupart, Grande, Carbonnier & Le Droumaguet. Porous polymers and metallic nanoparticles: A hybrid wedding as a robust method toward efficient supported catalytic

systems. *Progress in Polymer Science* **96**, 21-42, doi:https://doi.org/10.1016/j.progpolymsci.2019.05.003 (2019).

232 Guo, Warnicke, Griffa, Müller, Chen, Schaeublin, Zhang & Luković. Hierarchical Porous Wood Cellulose Scaffold with Atomically Dispersed Pt Catalysts for Low-Temperature Ethylene Decomposition. *ACS Nano* **13**, 14337-14347, doi:10.1021/acsnano.9b07801 (2019).

233 Kamal. Aminophenols formation from nitrophenols using agar biopolymer hydrogel supported CuO nanoparticles catalyst. *Polymer Testing* **77**, 105896, doi:https://doi.org/10.1016/j.polymertesting.2019.105896 (2019).

234 Chtchigrovsky, Primo, Gonzalez, Molvinger, Robitzer, Quignard & Taran. Functionalized Chitosan as a Green, Recyclable, Biopolymer-Supported Catalyst for the [3+2] Huisgen Cycloaddition. *Angewandte Chemie International Edition* **48**, 5916-5920, doi:https://doi.org/10.1002/anie.200901309 (2009).

235 Wang, Gao, Yao, Liu, Wu, Li, Liu, Sun & Pan. A nanoconfined-LiBH4 system using a unique multifunctional porous scaffold of carbon wrapped ultrafine Fe3O4 skeleton for reversible hydrogen storage with high capacity. *Chemical Engineering Journal* **428**, 131056, doi:https://doi.org/10.1016/j.cej.2021.131056 (2022).

236 Zhu, Wang, Mei & Wu. Highly sensitive and flexible tactile sensor based on porous graphene sponges for distributed tactile sensing in monitoring human motions. *Journal of Microelectromechanical Systems* **28**, 154-163 (2018).

237 Cheng, Du, Wang, Mao, Xu, Zhang, Zhong, Jiang, Wang & Sui. Flexible cellulose-based thermoelectric sponge towards wearable pressure sensor and energy harvesting. *Chemical Engineering Journal* **338**, 1-7 (2018).

238 Gullapalli, Vemuru, Kumar, Botello-Mendez, Vajtai, Terrones, Nagarajaiah & Ajayan. Flexible piezoelectric ZnO–paper nanocomposite strain sensor. *small* **6**, 1641-1646 (2010).

239 Wang, Zhang, Wu & Lu. Tailoring percolating conductive networks of natural rubber composites for flexible strain sensors via a cellulose nanocrystal templated assembly. *Soft Matter* **12**, 845-852 (2016).

240 Wang, Jian, Wang & Zhang. Carbonized silk nanofiber membrane for transparent and sensitive electronic skin. *Advanced Functional Materials* **27**, 1605657 (2017).

241 Wang, Peng, Yu, Chen, Ge & Uyama. Hierarchically porous sponge for oily water treatment: Facile fabrication by combination of particulate templates and thermally induced phase separation method. *Journal of Industrial and Engineering Chemistry* **62**, 192-196, doi:https://doi.org/10.1016/j.jiec.2017.12.057 (2018).

242 Filina, Yousefi, Okshevsky & Tufenkji. Antimicrobial Hierarchically Porous Graphene Oxide Sponges for Water Treatment. *ACS Applied Bio Materials* **2**, 1578-1590, doi:10.1021/acsabm.9b00008 (2019).

243 Wang, Chen, Yoon, Fang, Hsiao & Chu. High Flux Filtration Medium Based on Nanofibrous Substrate with Hydrophilic Nanocomposite Coating. *Environmental Science & Technology* **39**, 7684-7691, doi:10.1021/es050512j (2005).

244 Ismail, Salleh, Ismail, Hasbullah, Yusof, Aziz & Jaafar. Hydrophilic polymer-based membrane for oily wastewater treatment: A review. *Separation and Purification Technology* **233**, 116007, doi:https://doi.org/10.1016/j.seppur.2019.116007 (2020).

245 Li, Li, Zhou, Xian, Shui, Wu & Yao. Super-hydrophilic electrospun PVDF/PVA-blended nanofiber membrane for microfiltration with ultrahigh water flux. *Journal of Applied Polymer Science* **137**, 48416, doi:https://doi.org/10.1002/app.48416 (2020).

246 Hu, Chen, Lu, Fan, Li, Li, Zeng & Liu. A self-supported gel filter membrane for dye removal with high anti-fouling and water flux performance. *Polymer* **201**, 122531, doi:https://doi.org/10.1016/j.polymer.2020.122531 (2020).

247 Chen, Su, Peng, Zhao, Jiang, Dong, Zhang, Liang & Liu. Efficient Wastewater Treatment by Membranes through Constructing Tunable Antifouling Membrane Surfaces. *Environmental Science & Technology* **45**, 6545-6552, doi:10.1021/es200994n (2011).

248 Zhou, Lin & Wu. Electrospinning ultrathin continuous cellulose acetate fibers for high-flux water filtration. *Colloids and Surfaces A: Physicochemical and Engineering Aspects* **494**, 21-29, doi:https://doi.org/10.1016/j.colsurfa.2015.11.074 (2016).

249 Chu & Seeger. Multifunctional Hybrid Porous Micro-/Nanocomposite Materials. *Advanced Materials* **27**, 7775-7781, doi:https://doi.org/10.1002/adma.201503502 (2015).

250 Yu, Yu, Cui, Song, Zhao, Ma & Jiang. Facile Preparation of the Porous PDMS Oil-Absorbent for Oil/Water Separation. *Advanced Materials Interfaces* **4**, 1600862 (2017).

251 Guan, Cheng & Pan. Superwetting Polymeric Three Dimensional (3D) Porous Materials for Oil/Water Separation: A Review. *Polymers* **11**, doi:10.3390/polym11050806 (2019).

252 El-Samak, Ponnamma, Hassan, Ammar, Adham, Al-Maadeed & Karim. Designing flexible and porous fibrous membranes for oil water separation—A review of recent developments. *Polymer Reviews* **60**, 671-716 (2020).

253 Yang, Yin, Zhang, Zhu & Zhang. Fabrication of emulsion-templated macroporous poly(ε-caprolactone) towards highly effective and sustainable oil/water separation. *Polymer* **204**, 122852, doi:https://doi.org/10.1016/j.polymer.2020.122852 (2020).

254 Cheng, Guan, Meng & Wang. Dual-Functional Porous Wood Filter for Simultaneous Oil/Water Separation and Organic Pollutant Removal. *ACS Omega* **5**, 14096-14103, doi:10.1021/acsomega.0c01606 (2020).

255 Shen, Huang, Gan, Liu, Gong & Long. Rational design of Si@ SiO2/C composites using sustainable cellulose as a carbon resource for anodes in lithium-ion batteries. *ACS applied materials & interfaces* **10**, 7946-7954 (2018).

256 Zhao, Wang, Chong, Yu, Wang & Shi. An electrospun lignin/polyacrylonitrile nonwoven composite separator with high porosity and thermal stability for lithium-ion batteries. *Rsc Advances* **5**, 101115-101120 (2015).

257 Song, Li, Shi, Qian, Feric, Fu, Zhang, Li, Wang & Li. Thermally stable, nano-porous and eco-friendly sodium alginate/attapulgite separator for lithium-ion batteries. *Energy Storage Materials* **22**, 48-56 (2019).

258 Keck, Haluza, Selig, Jahl, Lumenta, Kamolz & Frey. Adipose tissue engineering: three different approaches to seed preadipocytes on a collagen-elastin matrix. *Annals of plastic surgery* **67**, 484-488 (2011).

259 Pekşen, Üzelakçil, Güneş, Malay & Bayraktar. A novel silk fibroin-supported iron catalyst for hydroxylation of phenol. *Journal of Chemical Technology & Biotechnology: International Research in Process, Environmental & Clean Technology* **81**, 1218-1224 (2006).

260 Mahadeva, Yun & Kim. Flexible humidity and temperature sensor based on cellulose–polypyrrole nanocomposite. *Sensors and Actuators A: Physical* **165**, 194-199 (2011).

261 Xie, Zheng, Wang & Lee Kaplan. Low-Density Silk Nanofibrous Aerogels: Fabrication and Applications in Air Filtration and Oil/Water Purification. *ACS Nano* **15**, 1048-1058, doi:10.1021/acsnano.0c07896 (2021).

262 Yan, Li, Zhou, Wang, Fan, Chen, Fang & Liu. Shrimp Shell-Inspired Antifouling Chitin Nanofibrous Membrane for Efficient Oil/Water Emulsion Separation with In Situ Removal of Heavy Metal Ions. *ACS Sustainable Chemistry & Engineering* **7**, 2064-2072, doi:10.1021/acssuschemeng.8b04511 (2019).

263 Duan, Gao, He & Zhang. Hydrophobic Modification on Surface of Chitin Sponges for Highly Effective Separation of Oil. *ACS Applied Materials & Interfaces* **6**, 19933-19942, doi:10.1021/am505414y (2014).

Chapter 3 Hard Pollen to Stimuli-Responsive Soft Microgels

Chapter Abstract

Pollen is generated in large amounts in flowering plants, but a majority of these end up as biological waste. Harvesting and modulating the properties of pollen could potentially turn pollen into a sustainable source of materials with specialized purposes. However, the understanding of how the mechanical and chemical properties of pollen are biologically controlled are limited, and strategies to manipulate pollen's robust shell beyond its natural performance limits would have tremendous advantages. In this chapter, a facile method to transform pollen grains into soft microgel by remodeling pollen shells was optimized. Utilizing a range of characterization techniques, marked increase in the level of carboxyl groups present in the intine and reduced Young's modulus of the exine gave rise to pollen with tunable mechanical characteristics resembling microgels, while exhibiting physical properties that rapidly respond to stimuli, reminiscent of smart polymers. Collectively, these findings provide a deep insight into the factors that govern the shift in pollen property in nature, while the resultant pollen microgel particles open new fields and pave the way for future applications of sustainable materials.

Keywords : Pollen, microgel, smart polymers, pectin, pH-responsive, ion-responsive, swell, renewable, sustainable materials.

3.1 Introduction

Pollen, the male microgametophyte of seed plants, plays a critical role in plant reproduction and transfers viable cellular material (i.e., male gametes or sperm cells) between different reproductive parts of plants[2,264]. Widely regarded as virtually indestructible,[7,265] pollen's tough characteristic are in fact highly dynamic and possess unique material characteristics.[4,10,266] Common physical features of pollen across various plant species include a microcapsule structure, function-driven shape, and ornamental architecture that greatly influences its method of dispersion.[3] Pollen wall plays a primary role in determining the toughness of pollen and serves to protect the reproductive cells housed within from environmental hazards such as desiccation, microorganisms, ultraviolet irradiation, environmental oxidants, mechanical stress and chemical exposure.[7,43,267-269] Sporopollenin, a highly robust, crosslinked biopolymer inherently found only on pollen,[4] makes up the primary composition of the tough outer exine layer of the pollen wall and is detrimental in the pollen's resilience to these external factors. Cellulose/hemicellulose microfibrils and pectin make up the major composition of the elastic inner intine layer of the pollen shell (Figure 3.1).[5,6] The presence of defined gaps in the exine layer, known as apertures, serve to facilitate the process of germination by providing a breach in the tough outer wall for emergence of the pollen tube. However, it is still essential that this process requires a marked decrease in the stiffness of the pollen wall to allow flexibility and elasticity for the opening of the aperture. De-esterification of pectin into pectate of the intine by pectin methylesterase (PME) enzyme has been shown to be essential in controlling wall elasticity to allow germination to occur.[17] This de-esterification process leads to the increased presence of carboxyl functional moieties that provide greater surface charge density, hence altering the intine structural arrangement.[17] Biologically, this enzymatic activity is spatially-controlled within the pollen wall structure.[15,16]

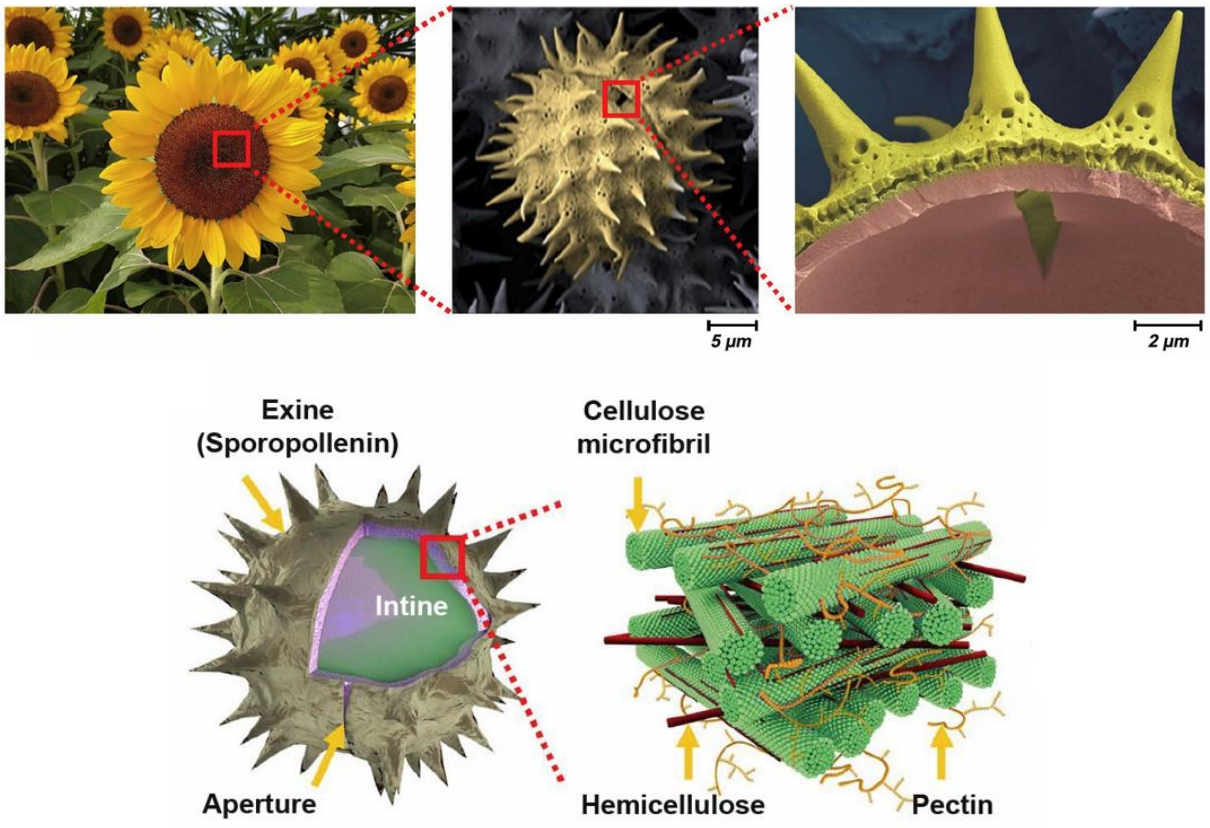

Figure 3.1. Pollen structural components. Cellulose microfibrils organized by hemicellulose and pectin in the intine layer.[270]

Upon their release from anthers, pollen become dehydrated and fold onto themselves in a process termed "harmomegathy",[11,12] to protect its content. Under the right stimulus for germination to occur, pollen grains undergo architectural remodeling during pollen tube growth, a process guided by an evolution-optimized sequence of enzymatically controlled reactions.[14,271] Understanding and replication of the biochemical mechanisms that plants utilize to modulate the shift in physicochemical properties of pollen grains has the potential to turn pollen from biological waste to precious resources.

Motivated by this, a strategy to induce elasticity of the pollen wall was developed. In this aspect, pollen from sunflower plants (*Helianthus annuus*), which have spiky appendages and a tripartite structure (Figure 3.2) were selected as our model of study. Defatted sunflower pollen was first treated with potassium hydroxide (KOH) for 2 h under reflux at 80 °C and continuous stirring to efficiently remove cytoplasmic components. The pollen was then incubated without stirring in fresh KOH at 80 °C for an extended period of up to 90 h before neutralization was performed to terminate the reaction, yielding a series of soft pollen microgel with varied mechanical properties. The level of de-esterification of pectin to pectate was then analyzed to ascertain if the KOH-induced microgel formation process had indeed artificially paralleled the biological mechanism of softening the hard pollen wall for the process of germination to proceed. Furthermore, the influence of parameters involved in the synthesis on the physical and chemical properties of the resultant pollen microgel were explored. Dynamic image particle analysis (DIPA), Fourier-transform infrared (FTIR) spectroscopy analysis and atomic force microscopy (AFM) were employed to analyze and characterize the chemo-mechanical changes of the pollen as a result of various processing conditions. The findings show that alterations in the pectin and sporopollenin are the main source of influence in the substantial and reversible swelling of the obtained pollen

microgel. The obtained pollen-derived microgel have the potential to give rise to a whole new class of natural renewable materials with unique performance and properties for sustainable engineering applications.

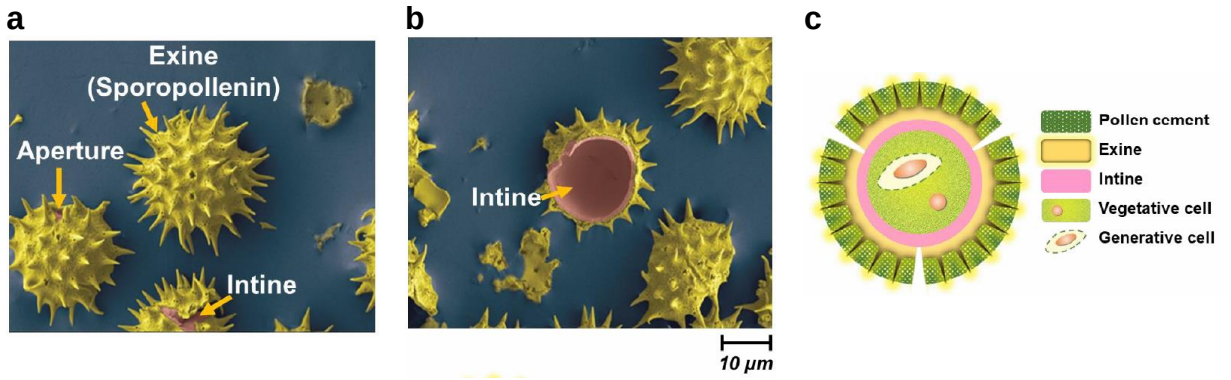

Figure 3.2. Scanning electron microscope (SEM) images and schematic illustration of sunflower pollen grains. a,b) Pseudo-colored SEM images show distinctive features of pollen grains, including the exine, apertures, and intine. c) Schematic illustration of pollen cement, exine, intine, and genetic material.[270]

3.2 Methods

3.2.1 Pollen microgel synthesis

Readily defatted pollen grains from the sunflower (*Helianthus annuus* L.) were purchased from Greer Laboratories, Inc. (Lenoir, NC, USA). Sunflower bee pollen granules were purchased from GTL Biotech (Xi'an, Shaanxi, China) and requires defatting prior to synthesis of pollen microgels to remove the lipid-rich pollenkitt that surrounds individual pollen grains. For this purpose, bee pollen granules (500 g) were refluxed in acetone (1000 mL) for 3 h in a round-bottom flask under magnetic stirring (50 °C, 220 rpm). Then, acetone was decanted, and deionized (dI) water (1000 mL, 50 °C) was added to the sample, mixed, and stirred for 1 h. The pollen suspension was passed through a nylon mesh (with 300 μm diameter pores) to filter away any contaminating particulate matter. The resulting filtrate was subsequently passed through filter paper (with 6 μm diameter pores) in a common Büchner funnel and flask setup and vacuumed to retain the pollen while removing the solvent and solubilized lipids. The resulting pollen was again resuspended and refluxed in acetone (500 mL, 50 °C) with magnetic stirring (400 rpm) for 3 h before being vacuum filtered as before, with copious washing with acetone until the filtrate runs colorless. The acetone-treated pollen was then transferred and spread evenly on a glass petri dish and covered loosely with paper wipe to be air-dried in a clean chemical fume hood overnight. The dried pollen was then dispersed in diethyl ether (1000 mL) with stirring (25 °C, 400 rpm, 2 h) in order to further remove any traces of lipids that were not effectively soluble in acetone previously. The suspension was then vacuum filtered as before, and the diethyl ether treatment and filtration process was repeated. The pollen was then resuspended in fresh diethyl ether and left to stir overnight (25 °C, 400 rpm) before being vacuum filtered with washing by copious amounts of diethyl ether until the filtrate runs colorless. This acetone-treated and diethyl ether-treated pollen was transferred to a

petri dish and air-dried in a fume hood overnight as before. The fully defatted pollen was then kept in a polytetrafluoroethylene (PTFE) bottle and stored in a dehumidifying cabinet until use.

The pollen microgel synthesis follows a well-regulated two-step hydrolysis process below

1. Cytoplasmic removal (1st KOH treatment step): Defatted pollen (2 g) was mixed with 20 mL aqueous 10, 20 or 30% w/v KOH (Sigma-Aldrich) in a 100 mL PTFE round-bottom flask and the suspension was refluxed for 2 h at 80 °C with stirring at 400 rpm. PTFE flask were used to prevent alkali-silica reactions (ASR) occurring at elevated temperatures for prolonged periods.[272] The suspension was transferred to a 50 mL conical centrifuge tube, and then centrifuged at 5000 × *g* for 5 min. The supernatant was decanted and the sample resuspended with fresh respective KOH to a final volume of 20 mL. The mixture was vortexed at high speed for 2 min to ensure thorough resuspension and centrifuged as before. This was repeated for 2 more times. Finally, the supernatant was decanted and the pollen suspension was left in the tube for the next treatment step.
2. Microgel formation (2nd KOH treatment step): Fresh respective KOH was added to the pollen sample up to a total volume of 20 mL, followed by vortexing at high speed for 2 min. The sample was left to incubate in an oven (Memmert, Schwabach, Germany) set to 80 °C for a specific period (3,6, 12, 24, 48, and 90 h). At the end of the specified duration of incubation, the samples were taken out and the suspension was neutralized via a series of centrifugation and resuspension with dI water. The pollen was collected by centrifugation (5000 × *g*, 5 min) and the supernatant was decanted. The pollen sample was resuspended with deionized water up to a total volume of 40 mL, vortexed at high speed (2500 rpm) for 2 min and centrifuged as before. This process was repeated until the suspension effectively

achieved the power of hydrogen (pH) level of 7.5, measured via pH-indicator strips (MilliporeSigma, Burlington, MA, USA). The resulting pollen suspension was collected by a final centrifugation followed by the supernatant removal, and then stored at 4 °C until further use.

3.2.2 Dynamic image particle analysis (DIPA)

DIPA was performed using a benchtop Fluid Imaging FlowCAM system (Fluid Imaging Technologies, Scarborough, ME, USA) with a 200 μm flow cell and a 10X optical lens. To optimize the focus and other measurement settings, the system was calibrated with 50 μm diameter polystyrene beads (Thermo Fisher Scientific, Waltham, MA, USA). The pollen suspension to be analyzed was drawn into the flow chamber via a syringe pump at a speed of 0.25 m/ min. When a pollen particle passes through the flow cell and into the path of the laser light causing significant light scatter that exceeds a certain threshold, the camera captures time-lapse images in the corresponding field of view at 15 images per second. The optical settings were set as follows: brightness 100, contrast 40, sharpness 6, and gain 400. Based on image data and analysis conducted using the Visual Spreadsheet software (Fluid Imaging Technologies), particle characteristics such as number concentration, edge gradient, and circularity were computed.

For pH-dependent studies, the various pH conditions were prepared by the addition of 2 M HCl or 2 M KOH to deionized water. For each pH condition, 3 μL of pollen microgel sample was resuspended in 700 μL of each respective pH solution. After an incubation period of 5 min, the pollen particles were homogenously dispersed by pipetting and 200 μL of the pollen suspension was dispensed through the flow cell for each analysis.

For ion-dependent studies, aqueous solutions of 10 mM potassium chloride (KCl), magnesium chloride ($MgCl_2$), calcium chloride ($CaCl_2$), strontium chloride ($SrCl_2$), or ferric nitrate ($Fe(NO_3)_3$) in dI water were used. For each condition, 200 µL of pollen microgel was mixed thoroughly with 3 mL of the ion solution in a 10 mL conical centrifuge tube and incubated for 5 min. For control, dI water was used as the dispersion medium in the absence of added ions. After an incubation period of 5 min, 200 µL of the pollen microgel suspension was passed through the flow cell. The rest of the mixture was centrifuged at 5000 × *g* for 5 min. The resulting supernatant was discarded and 600 µL of an aqueous solution containing an equivalent molar concentration of ethylenediaminetetraacetic (EDTA) was added. After vortexing and an incubation period of 5 min, 200 µL of the EDTA solution was dispensed through the flow cell for each analysis. All the experiments were conducted in triplicate and 500 particles were evaluated for analysis.

3.2.3 Fourier-transform infrared (FTIR) spectroscopy

Before experiment, the pollen microgel suspension were resuspended in dI water to form a dilute solution, frozen at –20 °C for 24 h and then lyophilized in a freeze dryer (Labconco, Kansas City, MO, USA) under 0.008 mbar vacuum pressure for 2 days. FTIR spectroscopy measurements were performed on the freeze-dried samples by using a PerkinElmer spectrometer (PerkinElmer, Waltham, MA, USA) with a diamond cell attenuated total reflection (ATR) accessory module. Reflectance infrared spectra were collected at 4000 – 650 cm^{-1}, with 16 scans per measurement and 3 replicate measurements per sample. Background spectra were collected prior to sample readings and automatically subtracted from each measurement. A baseline correction procedure was carried out using the Spectrum 10 software (PerkinElmer). Following baseline correction, each spectrum was standardized as previously reported.[273]

3.2.4 *Field-Emission Scanning electron microscopy (FE-SEM)*

For the defatted samples, the pollen particles were dried in a freeze dryer (Labconco) under 0.008 mbar vacuum pressure for two days. For the microgel samples, 3 μL of the sample was resuspended in 200 μL of the respective medium condition in a 1.5 mL microcentrifuge tube and then frozen with liquid nitrogen for 15 min. The frozen samples were freeze-dried for two days. The dried samples were spread and immobilized on a sample holder with copper tape and sputter-coated with a 10-nm thick gold film using a JFC-1600 Auto Fine Coater (JEOL, Tokyo, Japan; operating settings, 20 mA for 40 s). For cross-sectional observation, the dried samples were adhered onto a piece of double-sided copper tape (2 cm × 1.3 cm) and dipped into liquid nitrogen for 5 min. Then, multiple cuts were conducted across the frozen sample with a surgical blade (B. Braun Melsungen AG, Melsungen, Germany). Finally, the pollen-adhered copper tape was dried in a freeze dryer for two days. Field-emission SEM imaging was performed using a JSM-7600F Schottky field-emission scanning electron microscope (JEOL) at an accelerating voltage of 5.00 kV under various magnification levels.

3.2.5 *NHS/EDC activation of pollen particles*

The carboxyl acid functional groups on the surface of pollen particles were activated by treatment with N-hydroxysuccinimide (NHS, Sigma-Aldrich) and 1-ethyl-3-(3-dimethylaminopropyl) carbodiimide hydrochloride (EDC, Sigma-Aldrich). Pollen samples (20 mg) were first dispersed in 0.5 mL of 100 mM 2-(N-morpholino) ethanesulfonic acid (MES, Sigma-Aldrich) buffer (0.5 M NaCl, pH 6.0). Then, EDC (5 mg) and NHS (15 mg) were added to the pollen suspension and quickly dispersed by vortexing. After an incubation period of 30 min on a rocking platform shaker, the suspension was centrifuged (555 × g, 5 min) to remove the

supernatant containing unreacted EDC and NHS. Then, 0.5 mL of PBS (pH 7.4) was added to re-suspend the pollen. Immediately after resuspension, the pollen samples were either used immediately or frozen by liquid nitrogen and placed in a freeze-dryer under 0.008 mbar vacuum pressure for 4–6 h. Freeze-dried pollen samples were stored in a dehumidifying cabinet until further use.

3.2.6 Immobilization of pollen particles on glass

Glass coverslips (25 mm × 75 mm, ibidi GmbH, Planegg, Germany) were sequentially rinsed with water and ethanol, dried with a stream of nitrogen gas, and treated with oxygen plasma for 1 min using an Expanded Plasma Cleaner (PDC-002, Harrick Plasma, Ithaca, NY, USA). After cleaning, the glass coverslips were immediately soaked in a 2 % v/v solution of (3-Aminopropyl) triethoxysilane (APTES, Sigma-Aldrich) in 95% ethanol to functionalize the surface. After 30 min, the coverslips were sequentially rinsed with dI water and 95% ethanol for a total of 3 times before drying with a stream of nitrogen gas. As-prepared APTES-treated coverslips were kept in a dry cabinet and used within 2 weeks. Then, activated pollen particles were dispersed in PBS buffer and injected onto an APTES-treated glass coverslip that was enclosed within a microfluidic flow-through chamber (sticky-Slide VI 0.4, ibidi GmbH) at a flow rate of 300 μL/min, as controlled by an Ismatec Reglo Digital peristaltic pump (Cole-Parmer GmbH, Wertheim, Germany). After checking that the density of attached pollen particles was within a sufficient range, the chamber was thoroughly washed by flowing PBS buffer at a flow rate of 3 mL/min.

3.2.7 *Confocal laser scanning microscopy (CLSM)*

Pollen gel samples in suspension (~20 µL) were pipetted onto a thin glass slide (24 mm × 75 mm, CellPath Ltd, Newton, UK). CLSM imaging was performed using a Zeiss LSM710 microscope (Carl Zeiss, Oberkochen, Germany) equipped with three spectral reflection/fluorescence detection channels, six laser lines (405/458/488/514/561/633 nm) and connected to a Z1 inverted microscope (Carl Zeiss). A ×20 optical lens was used for imaging and at least two images were obtained per sample. Imaging was performed under the laser excitation channel at 488 nm (12.0%). Fluorescence signals from the samples were collected in photomultiplier tubes equipped with emission filters at 495–550 nm. Plane mode scanning was performed with a pixel dwell of 12.6 µs. Optimized imaging conditions were used for other types of pollen samples as follows: For immunolabeled-pollen particles, the samples were suspended by shaking gently and then pipetted (~20 µL) onto a thin glass slide. Laser excitation channels were set at 488 nm (3.5%) and the emission filter was set at 493–634 nm. Plane mode scanning was performed with a pixel dwell of 1.0 µs. For the immunolabeling studies, all imaging conditions were identical to allow a semi-quantitative comparison of the fluorescence intensity of each sample. For tethered pollen samples, imaging was performed with two excitation channels, 405 nm and 488 nm, and with two respective emission filters: 416–477 nm and 430–740 nm. Plane mode scanning was performed with a pixel dwell of 1.0 µs. Image processing was performed with Fiji software (available at http://fiji.sc/).

3.2.8 *Time-Lapse microscopy imaging*

Microscopy experiments were conducted using an Eclipse Ti-E inverted microscope (Nikon, Tokyo, Japan) with a CFI Super Plan Fluor ELWD ×20 or ×40 (NA = 0.45 or 0.60)

objective lens (Nikon), and images were collected with an iXon3 512 × 512 pixel Electron Multiplying Charge-Coupled Device (EMCCD) camera (Andor Technology, Belfast, UK). A halogen lamp, light power supply (TI-PS100W, Nikon) connected to TI-DH diascopic pillar illuminator (Nikon), was used to illuminate the pollen samples. As described above, the pollen particles were immobilized on an APTES-treated glass coverslip and the coated coverslip was then enclosed within a microfluidic flow-through chamber (25.5 mm × 75.5 mm) with a ~200 µL volume channel. In a separate time-lapse microscopy experimental setup, pollen microgels suspension were also dropped onto a 100 µm pore size nylon mesh placed on a glass coverslip, and then the sample was enclosed with a microfluidic flowthrough chamber (sticky slide VI 0.4, ibidi GmbH). In both experimental setups, prepared solutions of HCl_{aq} (pH 2), KOH_{aq} (pH 10), 10 mM $CaCl_2$, and 10 mM EDTA were dispensed by a Ismatec Reglo Digital peristaltic pump (Cole-Parmer GmbH, Wertheim, Germany) sequentially at a flow rate of 300 µL/min. During the swelling/deswelling experiments, the bulk solution in the measurement chamber was exchanged and time-lapse images were captured in 0.4 s time intervals. Data processing was performed in MATLAB (MathWorks, Natick, MA, USA), ImageJ (National Institutes of Health, Bethesda, MD, USA) and OriginPro 8.5 (OriginLab, Northampton, MA, USA) software programs (Figure 3.3).

3.2.9 Immunolabeling studies

In order to detect the presence and esterification state of pectin molecules within the intine layer, JIM5 and JIM7 antibodies were used according to previously defined protocols.[16,274] Defatted pollen grain (10 mg) or as-prepared pollen microgel (10 µL) samples were washed with PBS (1 mL) and then blocked in 2 % w/v bovine serum albumin (BSA) in PBS (1 mL) for 30 min. The pollen particles were then incubated overnight in an orbital shaker (Gaia Science

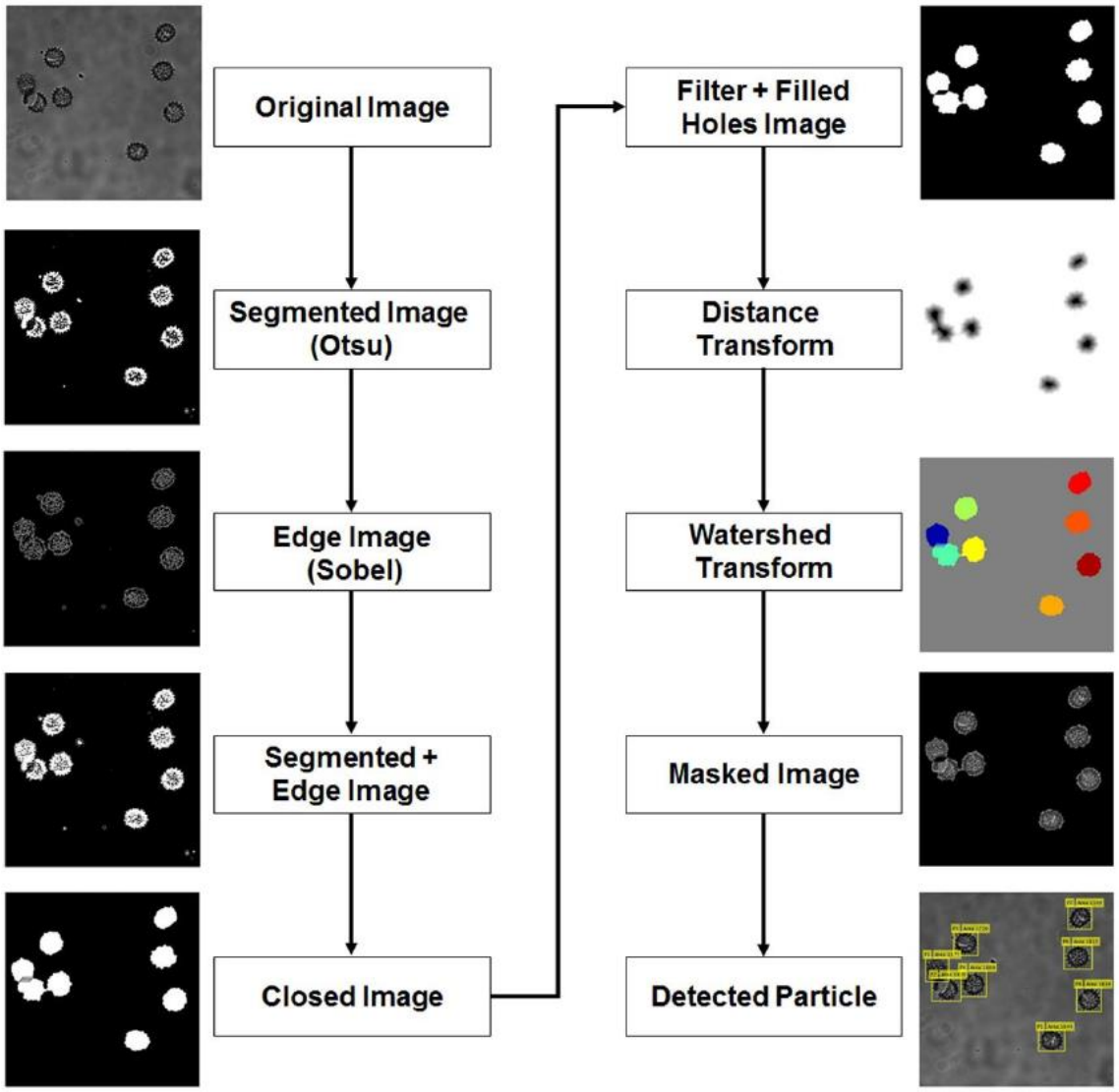

Figure 3.3. Image analysis procedure to measure the area of pollen grains. A series of processing steps were undertaken on original microscopy images using an in-house built MATLAB code utilizing a computer vision system toolbox.[270]

Pte Ltd, Singapore) with a rotation speed of 200 rpm at 4 °C in the presence of a primary antibody (JIM5 or JIM7) (PlantProbes, Leeds, UK, Cat. No. JIM5 and Cat. No. JIM7) at 1:20 dilutions in PBS containing 0.2 % w/v BSA. After washing twice with fresh PBS, the samples were incubated with Alexa Fluor 488 AffiniPure Goat Anti-Rat IgG (H + L) secondary antibody (Jackson ImmunoResearch Laboratories, West Grove, PA, USA, Cat. No. 112-545-003), diluted 1:100 in PBS containing 0.2% BSA, for 1 h in a dark environment. Antibody-labeled pollen particles were examined immediately with a confocal laser scanning microscope (Zeiss LSM 710) and without any antifade reagents. Pollen grains without primary and/or secondary antibodies were used as controls to determine baseline background fluorescence.

3.2.10 Discrete particle mechanical characterization via Atomic Force Microscopy (AFM)

The mechanical properties of defatted pollen and microgel particles were characterized by conducting AFM force-distance (or load versus displacement) measurements. This depth-sensing AFM indentation approach enables the quantitative determination of the Young's modulus of the shell material.[275,276] For wet samples, pollen microgel samples (5 μL) were suspended in dI water, and 50 μL of this suspension was spread onto a polystyrene petri dish. Excess liquid was aspirated by micropipette, leaving the partially hydrated samples on the dish for immediate analysis. For dry specimens, the pollen sample was directly spread onto the surface of a petri dish before measurement. Intact pollen particles were carefully selected for measurements of the Young's modulus of the exine layer, whereas randomly broken pollen particles, which exposed the inner layer, were chosen to determine the Young's modulus of the intine layer. To avoid the influence of the modulus of the underlying substrate (substrate effect), the 10% depth rule was employed where the indentation depth should be less than 1/10th of the thickness of the material measured.[277]

The average thickness of the exine layer was approximately 0.6 μm for defatted pollen particles and 0 h KOH-treated pollen specimens, and became thinner with increasing KOH treatment time (~0.5 μm). Thus, the depths of indentation for exine measurements were set in the range of 20–60 nm under indentation loads of 3–6 μN. On the other hand, the intine layer was swollen in wet conditions, with a thickness range from 0.5 to 1.5 μm. Thus, the indentation depths for wet samples were in the range of 50 to 100 nm. For all measurements, the NX-10 AFM instrument (Park Systems, Suwon, South Korea) was used with two AFM probes: (i) an aluminum reflex-coated silicon cantilever PPP-NCHR (Nanosensors, Neuchâtel, Switzerland) with a typical spring constant of ~42 N m^{-1} and a tip end radius of 5 nm; and (ii) a diamond cantilever TD26135 (Micro Star Technology, Huntsville, TX) with a spring constant of 150 N m^{-1} and a tip end radius of 5 nm. The tips were shaped as polygon-based pyramid with a half-cone angle of 20°. Both AFM probes provided almost identical values of Young's moduli for exine and intine layers regardless of the various indenting parameters such as maximum contact forces, contact time or approach speed (Appendix 3x1). Before experiments, the AFM cantilever was rinsed with water and ethanol, and treated with a UV light cleaner for 30 min in order to remove any organic contaminants. The spring constant and sensitivity of the deflection signal were also calibrated by recourse to the thermal vibration of the AFM cantilever[278] by employing the commercial software (XEP, Park Systems). A minimum of 16 measurements were conducted at various positions within a 5 μm × 5 μm area at an approach speed of 0.8 μm/s with a maximum loading force of 4.8 μN and zero contact time. The force-displacement curves were normalized by subtracting the deflection distance of the AFM probe from the total displacement.

For data analysis, it was assumed that both the exine and intine layers were isotropic. As the AFM probe used had a tip end radius of 5 nm, the indentation depths employed in this

methodology were significantly larger than the tip end radius. Thus, the classical Hertz model was used for data analysis.[276,279].The Hertz model[275] was fitted to the force-displacement curves using a commercial software analysis program (XEI, Park Systems) and the Python script language (Appendix 3x1). The geometry of the AFM tip was taken as a parabolic model whereby it has a tip radius of R_c, and therefore the force (F) can be expressed as:

$$F = \frac{4\sqrt{R_c}}{3} \cdot \frac{E}{1-\nu^2} \cdot \delta^{3/2}$$

where E is Young's modulus, ν is the Poisson's ratio, and δ is the indentation depth. The Poisson's ratio ν was set at 0.5, which is typical for natural materials.

3.2.11 Statistical analysis

Statistical analysis was performed using the Origin 2018 software package (OriginLab). Unpaired Student's t-test and one-way analysis of variance (ANOVA) with Tukey's multiple comparison tests were used to calculate the statistical significance of data sets. A p-value of less than 0.05 was considered statistically significant. Data were presented as the mean ± standard deviation, wherever appropriate.

3.3 Results and Discussion

3.3.1 Alkaline incubation transforms hard pollen into microgel

The preparation of the pollen microgel begins with the removal of the protein- and lipid-rich pollenkitt that encapsulates the pollen particle during the defatting process. This exposes the porous exine layer and aperture of the pollen grain (Figures 3.4a, d). Proteins present in the pollenkitt that makes up the pollen cement is responsible for most allergenic reactions associated to pollen, and efficient removal of the pollenkitt effectively reduces this.

The first cytoplasmic removal step was performed via treatment of the pollen with 10% w/v KOH solution refluxed at 80 °C for 2 h. This method successfully induced cytoplasmic extrusion within a short period, thus allowing the cavity of the pollen grain to be filled with KOH solution (Figures 3.4b,e). The efficiency of the extrusion was qualitatively assessed via comparison of the confocal laser scanning microscopy images of the defatted and KOH-treated pollen grains (Figure 3.5). Fluorescence signals from the pollen wall and inner cytoplasmic content were visually present and easily observable in the non-treated defatted samples. In the KOH-treated pollen however, the fluorescence signals obtained were present only from the pollen wall, which is direct evidence of the absence of cytoplasmic contents due to efficient extrusion. SEM images also showed a porous surface of the pollen grain due to the cavity in the pollen (Figure 3.4 e). Further incubation of the pollen particles in a second incubation step in 10 % w/v of KOH solution at 80 °C induces the transformation of the pollen suspension from a wet sand slurry to an agar-like consistency (Figure 3.6). The presence of the spike structure on the surface of the pollen microgel (Figure 3.4f) demonstrates that although the KOH treatment removes the inner content of the pollen grain, the inherent morphology of the pollen shell remained intact. Coinciding with

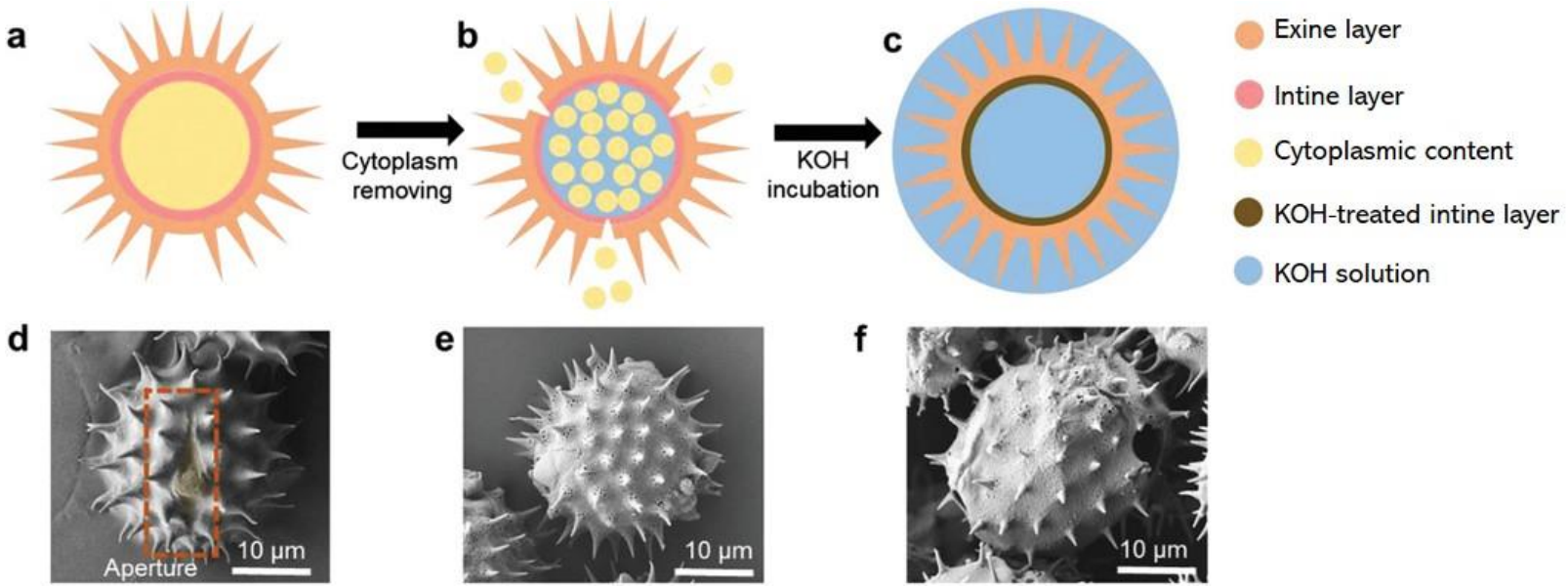

Figure 3.4. The process of transforming defatted sunflower pollen into pollen microgel. a) Intact defatted sunflower pollen grain. b) Extrusion of cytoplasm. c) Pollen microgel formed after KOH incubation. d) SEM image of defatted sunflower pollen grain with an open aperture. e) SEM image of a pollen grain after cytoplasm removal. f) SEM image of freeze-dried pollen microgel.[280]

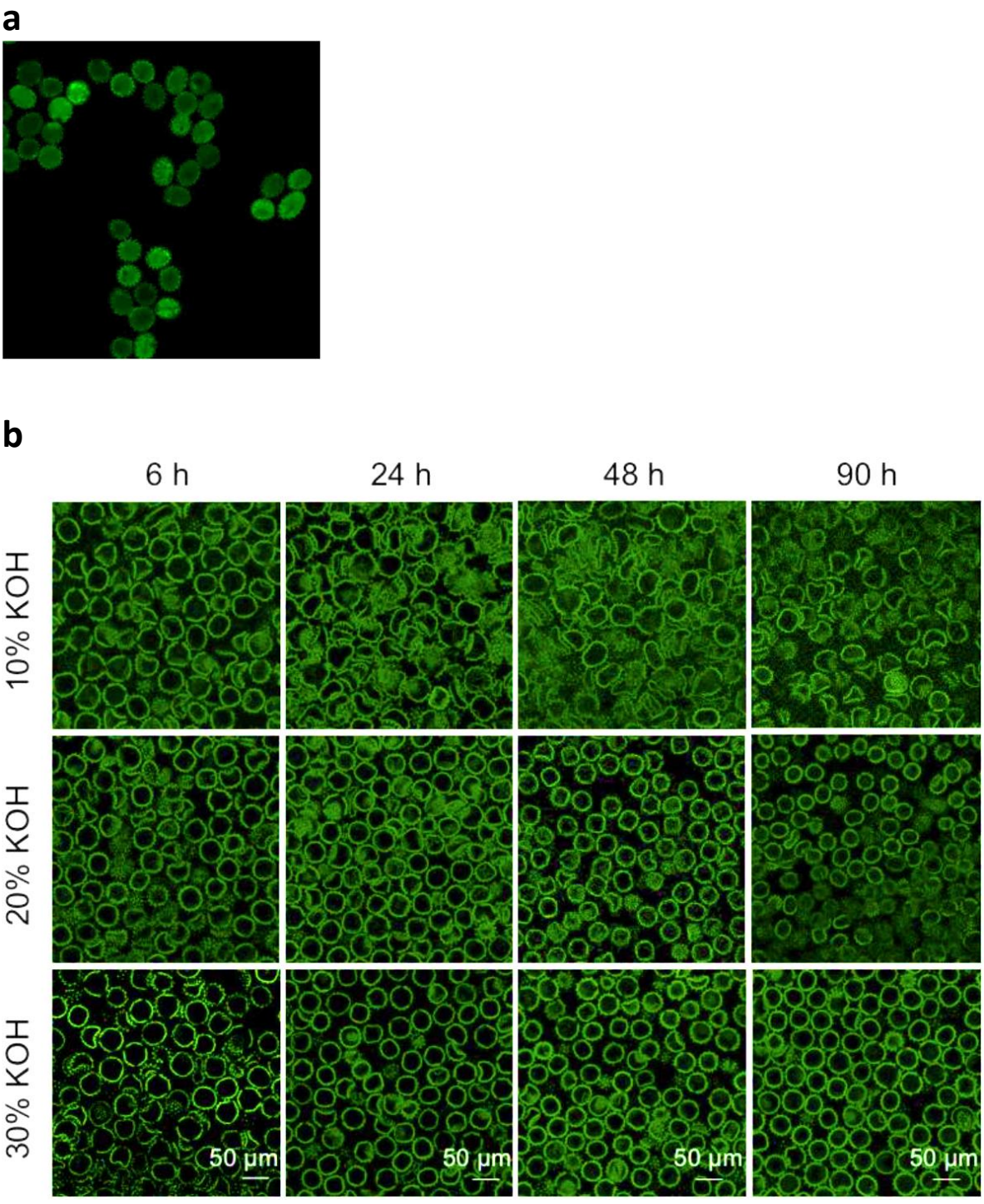

Figure 3.5. Confocal laser scanning microscopy of a) defatted pollen, b) pollen microgel of various incubation time and KOH concentration.[280]

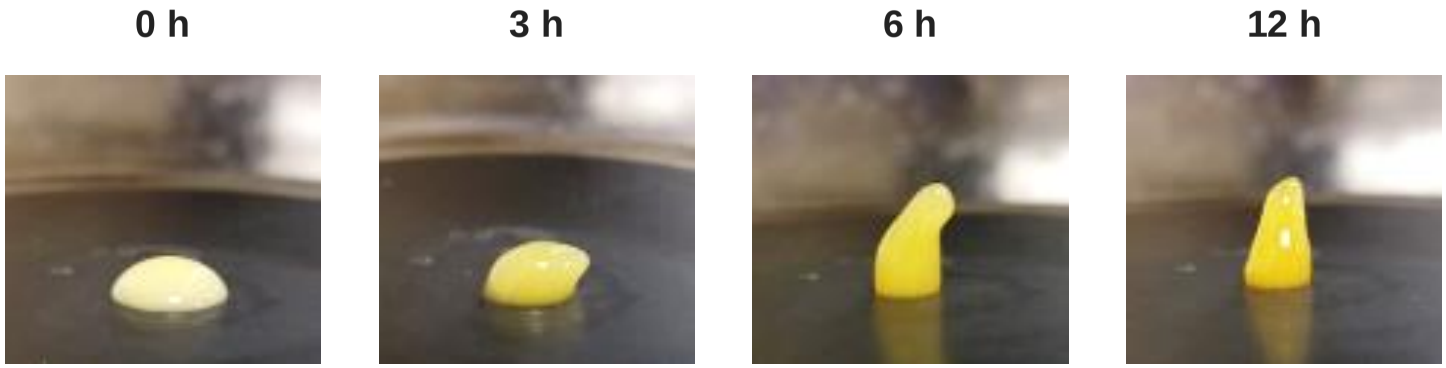

Figure 3.6. Photograph images of 75 µl of resultant pollen pipetted onto a platform show that the suspension consistency transforms from a wet sand slurry to an agar-like consistency with increasing KOH incubation from 0 h to 12 h.

an increase in gel-like properties, CLSM images revealed that chemical processing caused the pollen particles to swell and be in close contact with each other remaining structurally discrete and intact, essentially qualifying these particles as microgels (Figure 3.7).[281]

3.3.2 Pollen gelation is due to de-esterification of pectin in intine

To verify de-esterification, a series of experiments were performed to evaluate the state of the pectin present in the intine layer. Immunolabelling of KOH-treated pollen using the monoclonal JIM5 antibody that recognizes and binds to epitopes of pectin that has a low content of ester bonds[282] and observation via immunofluorescence microscopy experiments were performed. The results confirmed successful processing as indicated by increased de-esterification after 3 h incubation while longer incubation periods resulted in more extensive de-esterification of pectin molecules (Figure 3.8a).[283] These results were complemented by immunolabeling experiments with JIM7 antibody, which recognizes highly esterified epitopes of pectin (Figure 3.8b).[282]

To attempt to characterize and analyze the changes of chemical moieties induced by the KOH treatment, FTIR spectroscopy was performed on freeze-dried pollen microgel samples. By measuring the absorbance of infra-red light absorbed at each discrete wavelength associated to known chemical groups, the changes in amount of these moieties in the respective samples can be quantified after normalization to a reference sample. The spectra of KOH-treated pollen grains up to 12 h appear nearly identical regardless of the treatment time, whereas the defatted sample exhibited more complex and convoluted spectral features along with peaks corresponding to

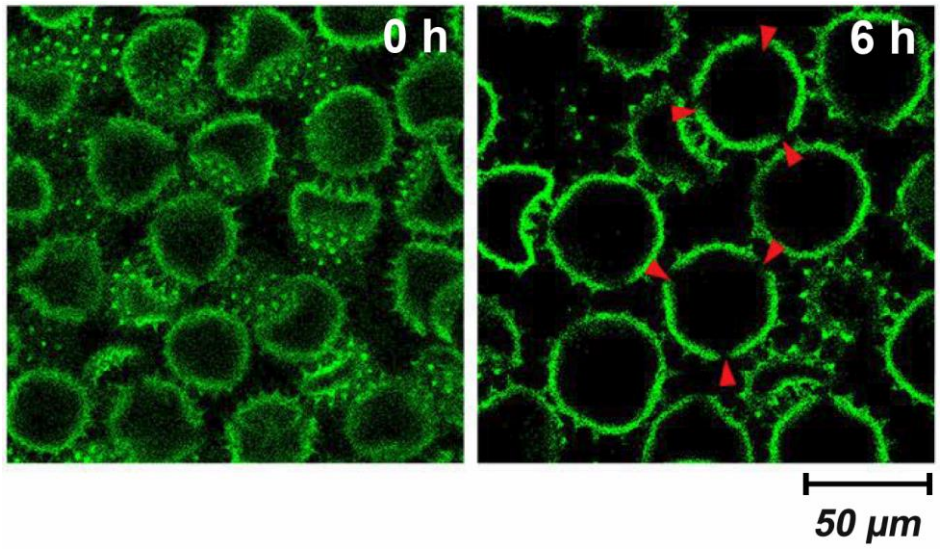

Figure 3.7. Cross-sectional CLSM images of pollen-derived microgel particles. Red arrows indicate aperture openings.[270]

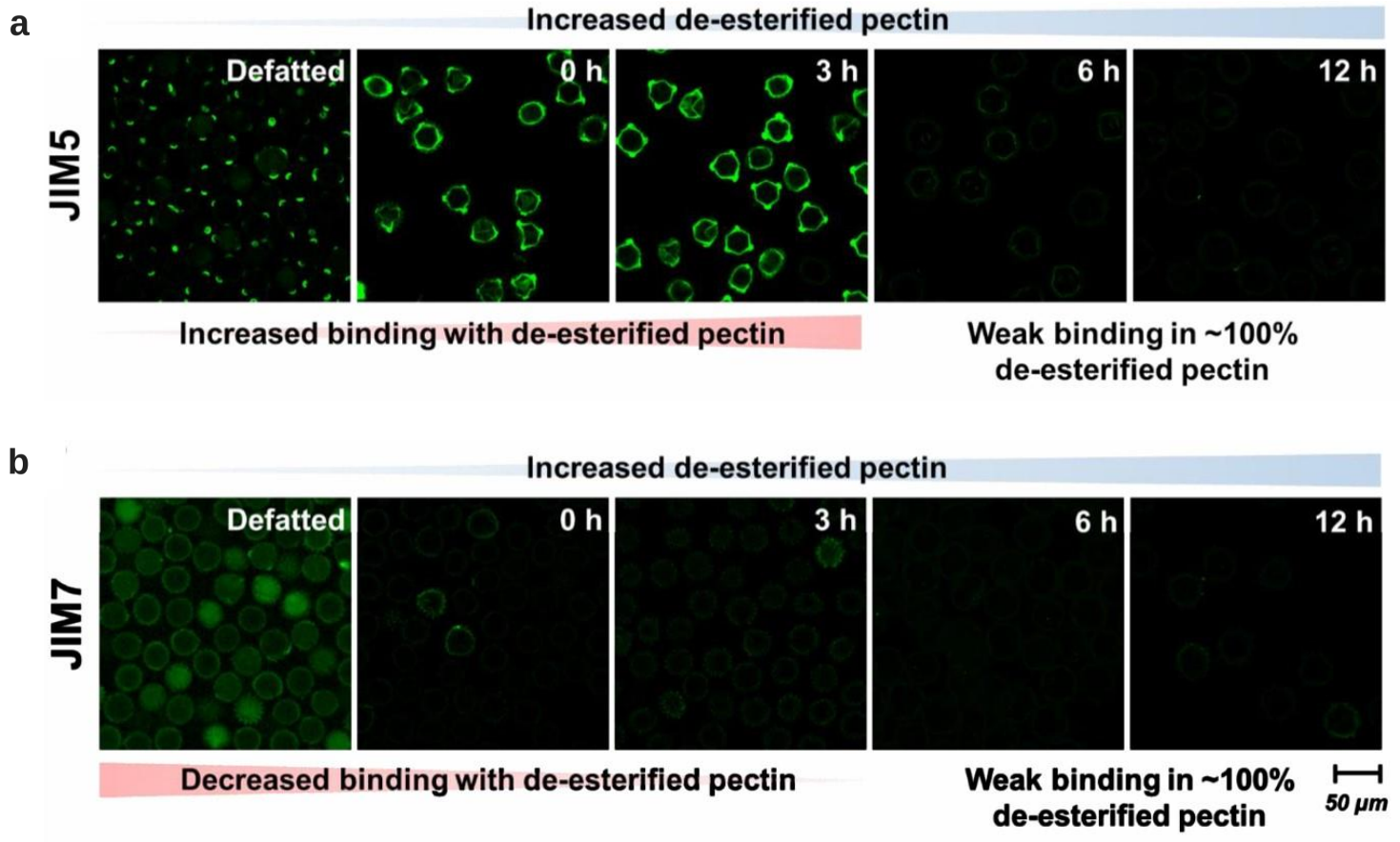

Figure 3.8. Immunofluorescence microscopy used for the detection of de-esterified pectin within pollen shells.[270] Prior to experiments, the pollen microgel samples were incubated with a) JIM5 and b) JIM7 which recognize weakly esterified pectin molecules. antibodies cannot detect fully de-esterified pectin samples.[271]

pectin molecules due to residual cytoplasmic contents (Figure 3.9).

Since the process of de-esterification would result in an increase of the carboxyl group on the intine layer,[17,283] which enables the gelation of the pollen grains, a systematic approach of evaluating the chemical changes of the pollen microgel was performed. Pollen was treated with KOH of various concentrations and incubation duration. KOH concentration of 10, 20, and 30 % w/v was used to perform the first cytoplasm removal and second microgel incubation step for up to 90 h.

Figure 3.10 shows the absorbance spectra of 24, 48, and 90 h-treated samples in 10, 20, and 30 % w/v KOH solution, normalized to that of 6 h-treated samples from 4000 to 3000 cm^{-1}, respectively. Although the peaks between 3500 and 3600 cm^{-1} (corresponding to O-H bonds in carboxyl groups) show negligible changes in 10 %-24 h and 10 %-48 h-treated pollen microgel, pollen microgel in other conditions showed a positive shift in 3550 cm^{-1}. This result imply that the longer incubation time and high KOH concentration induced generation of more O-H groups in pectin.[284,285] Beyond 6 h and up to 90 h incubation, another peak was identified to be consistently shifted, from 1071 cm^{-1} to 1053 cm^{-1} in 10 % w/v KOH, from 1068 cm^{-1} to 1049 cm^{-1} in 20 % w/v KOH, and from 1068 cm^{-1} to 1041 cm^{-1} in 30 % w/v KOH, inferring that there was degradation of pectin in the pollen wall, especially from the intine layer.[286] Additionally, longer incubation time (from 6 to 90 h) and a higher concentration of KOH from 10to 30 % w/v led to a gradual change in color intensity from pale yellow to dark brown. The increase of peak at 1581 and 1584 cm^{-1} suggests that this was due to formation of C-C bonds in aromatic rings within sporopollenin's chemical backbone (Figure 3.11).[287]

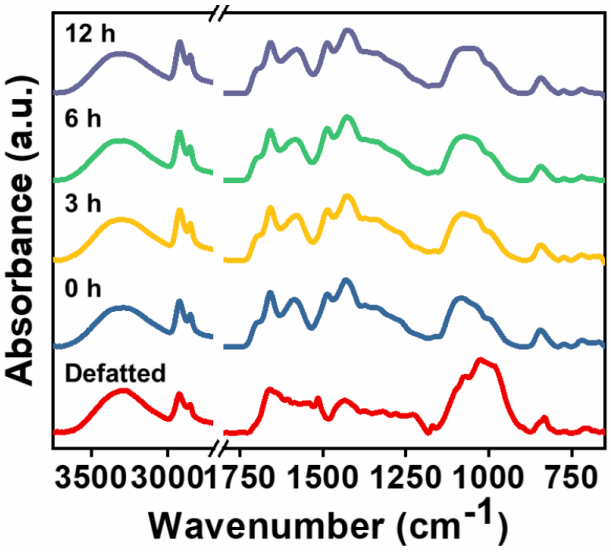

Figure 3.9. FTIR characterization of 10 % w/v KOH-treated defatted sunflower pollen grains. The FTIR spectra of pollen microgel dispersions as a function of incubation time in 10 % w/v KOH are presented. Pectin peaks (~1620 cm^{-1}) were more clearly observed for KOH-treated pollen grains than defatted pollen. The characteristic absorbance peaks of all KOH-treated pollen grains appear almost identical, regardless of the alkali treatment time.[270]

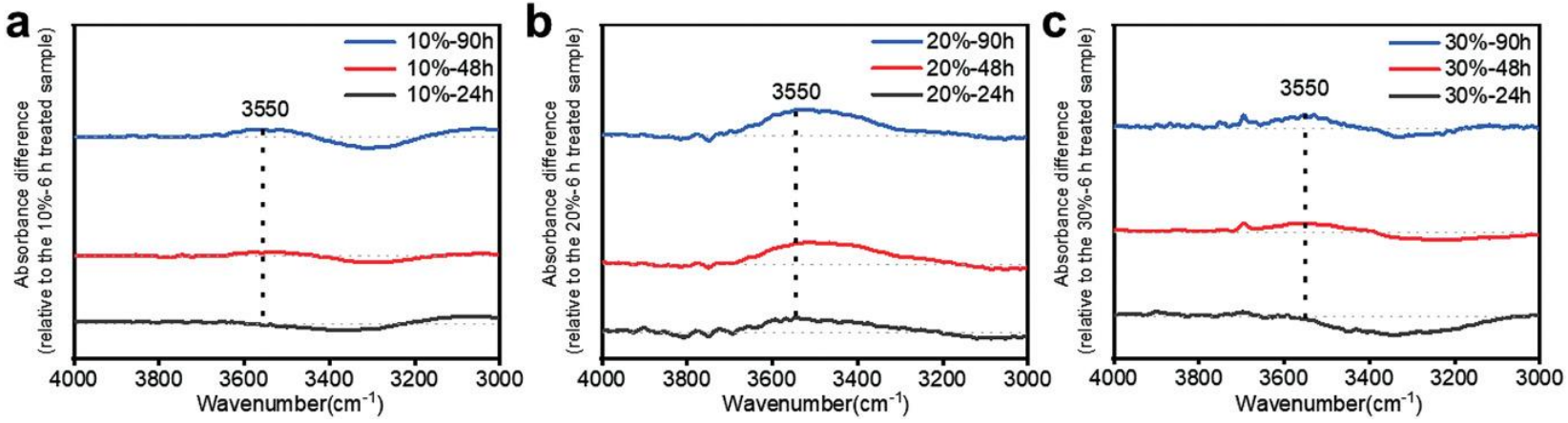

Figure 3.10. FTIR absorbance difference spectra of the sunflower pollen microgel after different KOH treatment showing the mean spectrum minus the mean spectrum of samples treated for 6 h. a) Absorbance difference spectra of the sunflower pollen microgel treated with 10 % w/v aqueous KOH for 24, 48, and 90 h. b) Absorbance difference spectra of the sunflower pollen microgel treated with 20 % w/v KOH aqueous for 24, 48, and 90 h. c) Absorbance difference spectra of the sunflower pollen microgel treated with 30 % w/v KOH aqueous for 24, 48, and 90 h. Grey dashed line indicates no shift (i.e., no difference between experimental samples and 6 h treated sample).[280]

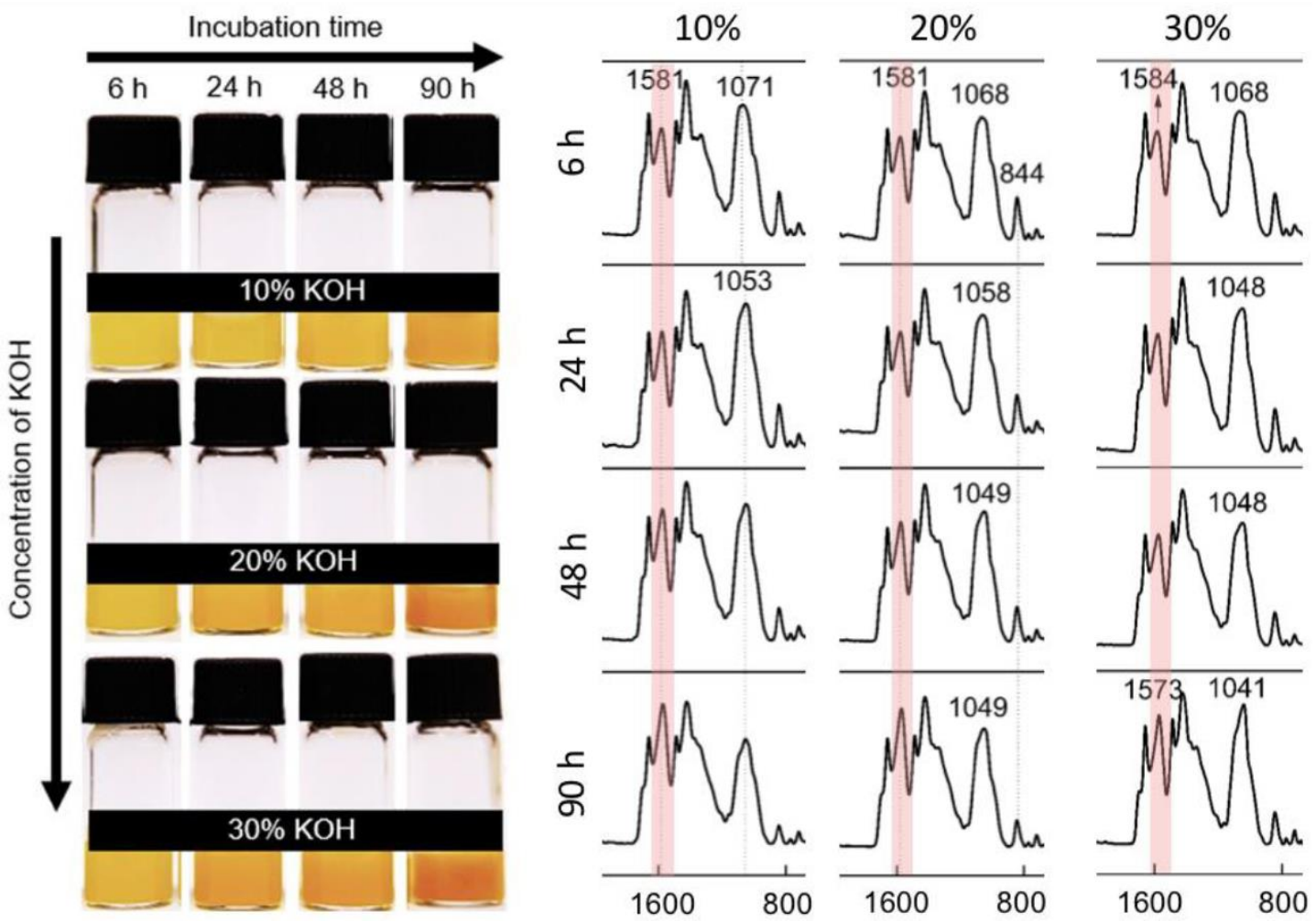

Figure 3.11. The color change of pollen microgel along with their chemical changes during the KOH treatment. Left: Optical images of condensed sunflower pollen gel under different KOH treatment, such as different incubation time and different concentration of KOH. Right: FTIR spectrum of sunflower pollen microgel after different KOH treatment.[280]

Taken together, the findings reveal that incubating pollen in well-controlled alkaline conditions for extended periods of time can result in the transformation of hard pollen grains into pliable, soft microgel particles via de-esterification of pectin within the intine.

3.3.3 Reversible chemo-mechanical response of pollen microgel

Noting the significant but gradual changes in texture of the microgel suspensions during the neutralization process for termination of the incubation at specified timepoints, it was theorized that there was a pH-induced change in the physical property of the microgel that was not observed in suspensions of unprocessed pollen. While the carboxylic acid functional groups on the de-esterified pectin molecules are expected to be protonated under acidic pH conditions, the same functional groups would exhibit a higher degree of deprotonation, and hence greater anionic surface charge, under increasingly basic pH conditions (Figure 3.12). To evaluate how KOH-treatment and pectin de-esterification affect the chemomechanical responsiveness of individual pollen particles, the fully neutralized synthesized pollen microgels were visually analyzed for the resultant particle size change as a function of the different pH by employing the DIPA method. Using this method, the morphology of pollen microgels at different conditions can be visually observed and the diameter effectively quantified in a high-throughput manner (Figure 3.13).

Pollen microgel with 10 % w/v KOH treatment showed the largest change of diameter from 22.17 ± 1.52 to 52.48 ± 5.52 µm. As the concentration of KOH increases to 30 % w/v the maximum diameter at pH 10 was lower at 42.51 ± 2.68 µm and 40.56 ± 2.21 µm for 20 and 30 % w/v KOH respectively (Figure 3.14). This trend is highly believed to be due to the degradation of the pectin in the intine layer resulting in a decrease of the maximum diameter. As shown in

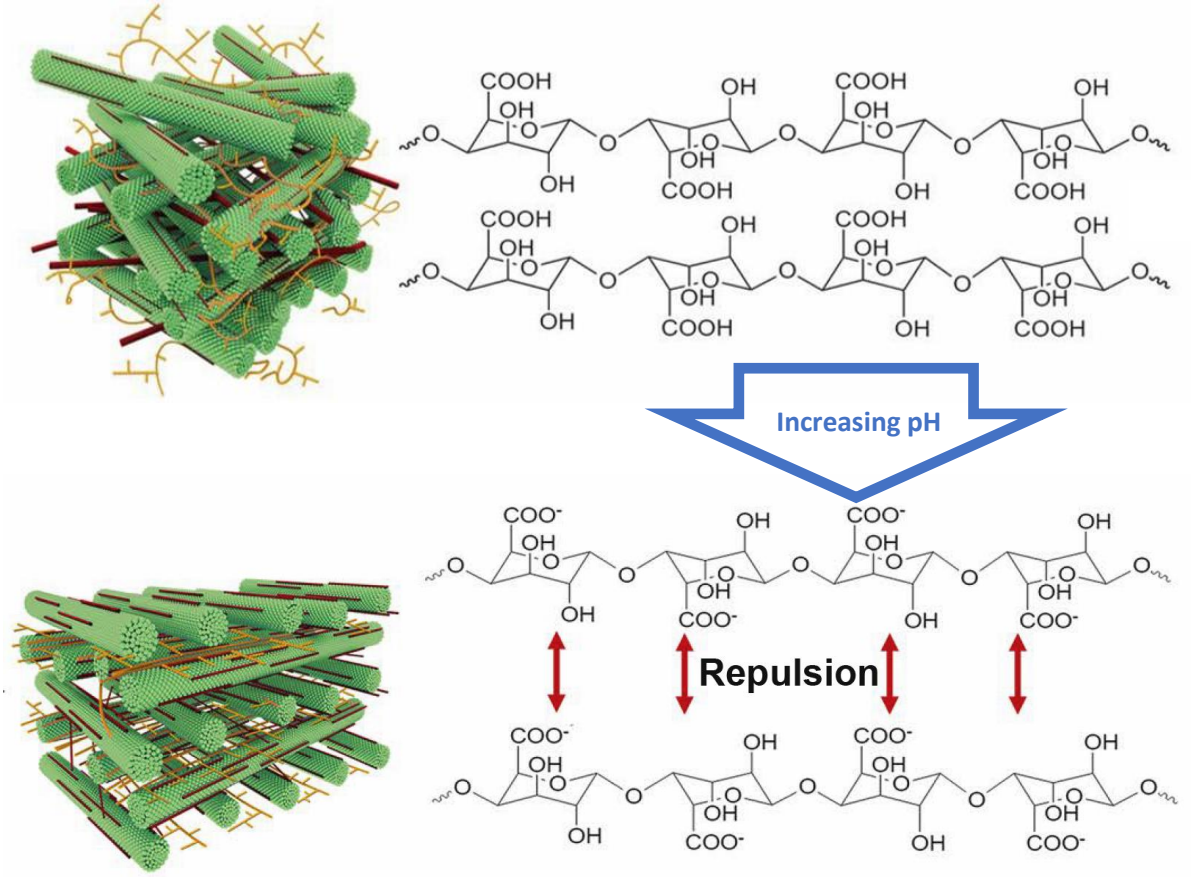

Figure 3.12. Schematic illustration of pH-dependent effects on pectin structure and corresponding intermolecular repulsion events.[270]

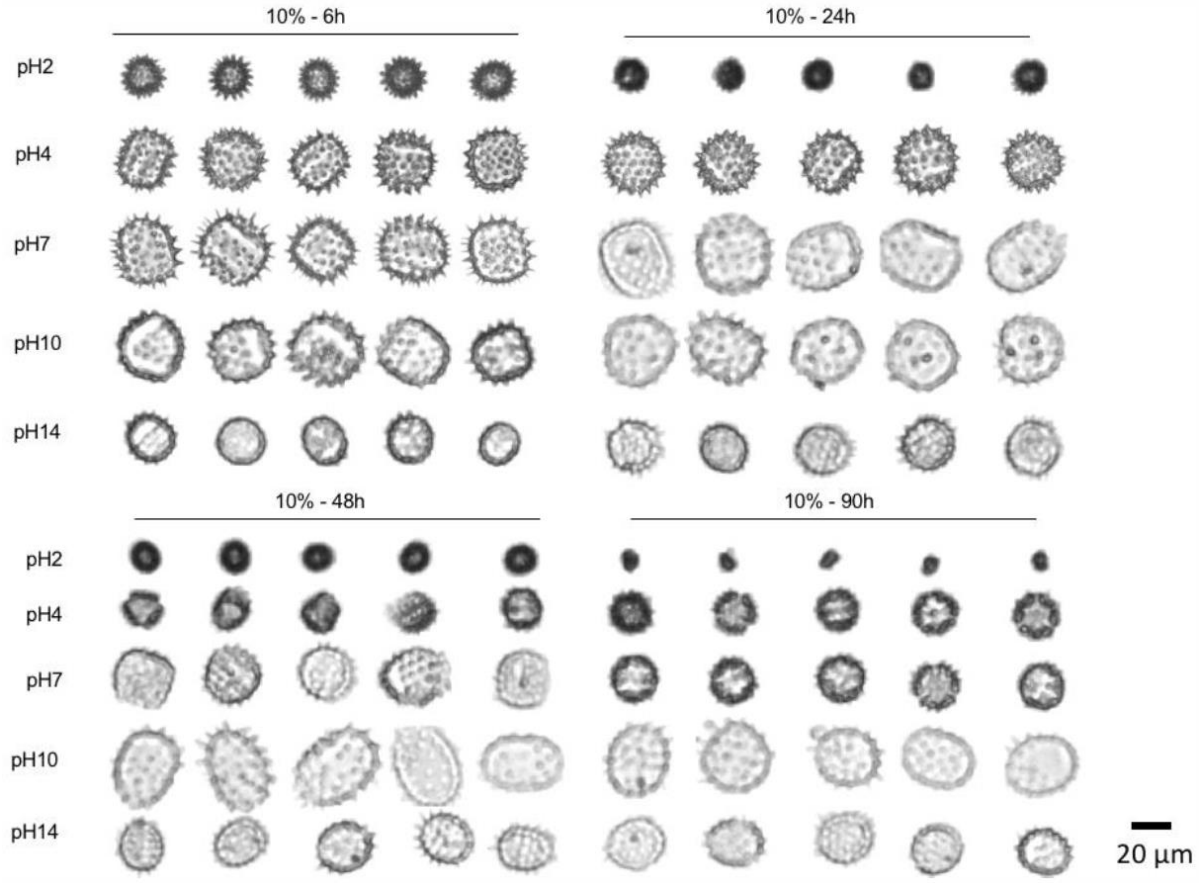

Figure 3.13. Optical micrographs of representative sunflower pollen microgel (10 % w/v KOH - 6, 24, 48, and 90 h) in different pH conditions obtained via DIPA. Images were taken at 10× magnification.[280]

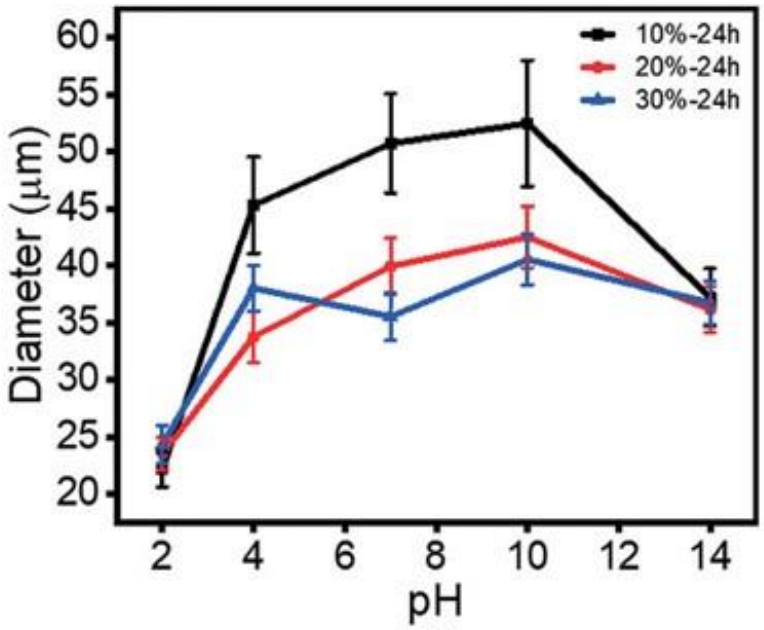

Figure 3.14. Influence of pH on the size of sunflower pollen microgel prepared with different concentrations of KOH solution (10, 20, and 30 % w/v).[280]

earlier studies, pectin can be degraded through saponification and β-elimination in alkaline and high temperature conditions.[288,289] Interestingly, all samples show the maximum diameter at pH 10 before progressively decreasing as the pH continued to 14. It is likely that the carboxyl groups of pectin was fully deprotonated at pH 10, and further increases of pH to 14 led to neutralization of the negative charge of the carboxyl groups due to excess of K^+ ion present in the KOH_{aq} solution.[290] The effect of the incubation time in 10 % w/v KOH solution for the swelling/deswelling behavior of pollen microgel was also thoroughly investigated (Figure 3.15). The minimum diameters of pollen microgel after 6, 24, 48, and 90 h incubation were 22.84 ± 1.63, 22.17 ± 1.52, 22.38 ± 3.30, and 13.28 ± 2.15 μm in pH 2. It is noteworthy that all the samples have similar minimum diameter at pH 2, and this is likely due to the size being limited to the maximum constriction and packing of the sporopollenin shell during the de-swelling/shrinking. In the case of 90 h incubation, a significantly smaller diameter was recorded compared to other pollen microgels, due to the irreversible low pH-induced rupture of pollen microgel and the recording of fragments (not shown). This rupture was highly likely to be attributed to the exine being weak from the prolonged incubation. Pollen microgel after 24 h incubation in 10 % w/v KOH exhibited the largest diameter at pH 10 compared to those of pollen microgel after 6, 48, and 90 h incubation. 6, 48 and 90 h-treated pollen microgel show a slightly lower maximum diameter at pH 10. For 6 h pollen microgel sample, this is likely due to the sporopollenin shell still being stiff, leading to resistance and restrictions on the swelling of the pollen microgel. In contrast for 48 and 90 h pollen microgel sample, the lower maximum size would be more likely due to a more extensive degradation of pectin, leading the decrease of the internal force to swell the pollen microgel.[291] Analysis of the volume of the pollen microgel particles at maximum/minimum diameters (Figure 3.16) gave 54,605 μm^3 / 6,239 μm^3 for 6 h-treated sample, 75,680 μm^3 / 5,706 μm^3 for 24 h-treated

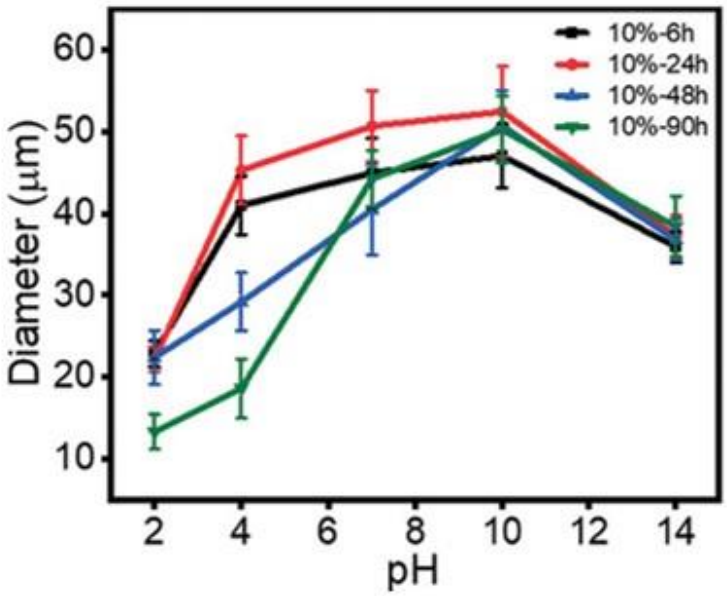

Figure 3.15. Influence of pH on the diameter of pollen microgel prepared with different incubation time (6, 24, 48, and 90 h) in 10 % w/v KOH solution.[280]

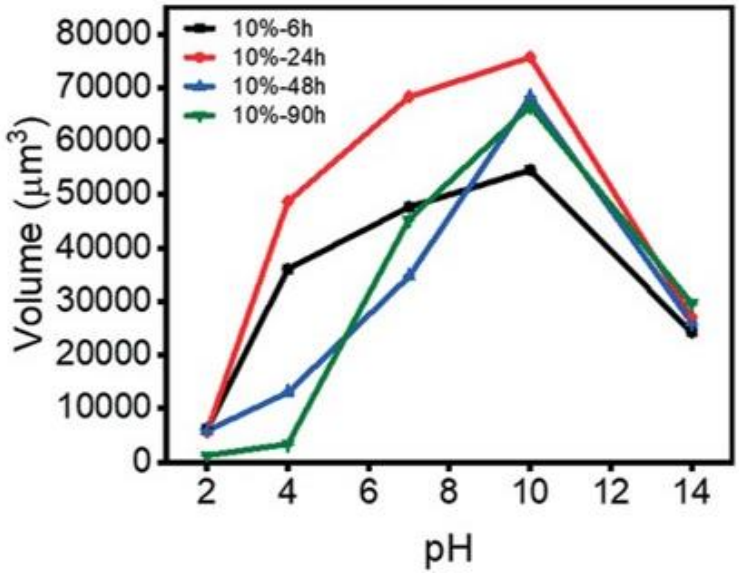

Figure 3.16. Influence of pH on the volume of pollen microgel prepared with different incubation time (6, 24, 48, and 90 h) in 10 % w/v KOH solution.[280]

sample, 68,237 μm^3 / 5,869 μm^3 for 48 h-treated sample. For pollen microgels synthesized in 10 % w/v KOH and incubated for 24 h, the volume of the pollen particle in a fully swollen state at pH 10 was 13 times that of its fully deswollen/shrunken state at pH 2, demonstrating the dynamic pH-responsive behavior of the synthesized pollen microgels.

To demonstrate the cyclical reversibility of pH-induced swelling, time-lapsed optical microscopy was performed on pollen microgel particles captured in nylon mesh show the dynamic swelling/de-swelling behavior of individual pollen microgel according to the pH change (pH 10 to pH 2 and pH 2 to pH 10) (Figure 3.17). Fully swollen 24 h-treated pollen microgel in a 10 % w/v KOH solution in pH 10 solution rapidly de-swelled/shrank within 3 s after subjecting the pollen with pH 2 HCl solution. De-swelled/shrunken pollen microgel fully recovered its swollen size upon flow of excess pH 10 KOH solution. As it was challenging to closely criticize the other changing features of the pollen shell using the nylon mesh entrapment method due to flow-induced displacement of the pollen particles, an alternate method to immobilize the pollen microgel particles was employed. Utilizing well-established NHS/EDC conjugation to tether the carboxyl group present on the KOH-treated pollen microgel onto an APTES-functionalized glass surface, 6 h-treated pollen microgel in a 10 % w/v KOH solution pollen microgel particles were discretely and securely immobilized. Similarly, the particles were subjected to rapid changes in solution pH and morphological changes were recorded via time-lapse optical microscopy (Figure 3.18). When the solution pH was changed from 2 to 12, the microgel particles underwent extensive swelling. Similarly, as the solution pH was changed from 12 to 2 and back, the microgel particles underwent relatively faster de-swelling/shrinking. In marked contrast, pollen grains that were not KOH-treated (“Defatted”) exhibited negligible pH-responsive behavior. It was noted that the swelling

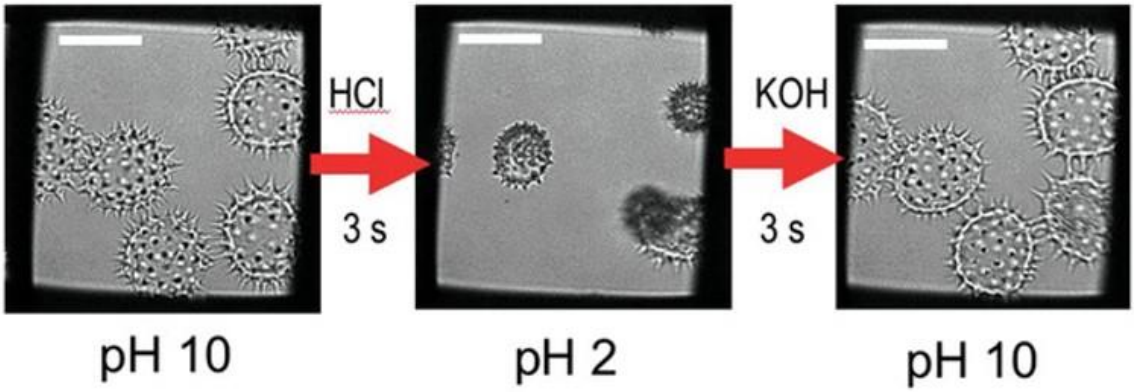

Figure 3.17. Time-lapsed optical micrographs of sunflower pollen microgel under pH 2 and pH 10.[280] Scale bar: 50 µm

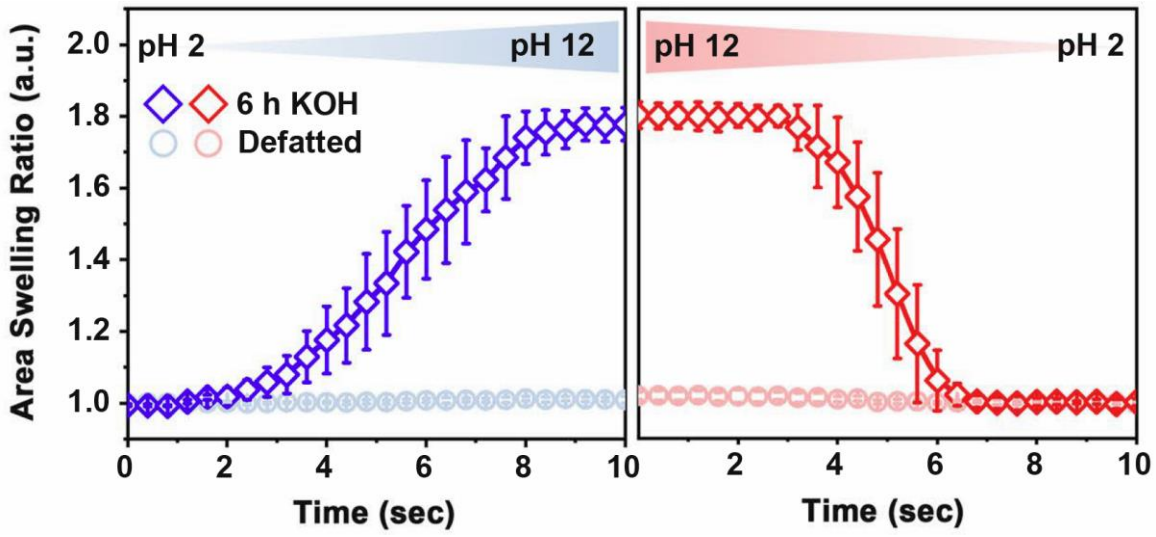

Figure 3.18. Quantitative comparison of pH-induced pollen swelling and de-swelling behavior as the solution pH was changed from pH 2 to 12 and from pH 12 to 2.[270]

and de-swelling kinetics were markedly different between 6 h and 24 h incubated pollen microgel, with the 24 h microgel displaying a faster response time (not shown). Observation of the aperture stretching during the pH- induced swelling allowed measurement of the opening angle during the swelling and deswelling process (Figure 3.19). The observed pH-dependent swelling response is analogous to that of ionizable polymer networks whose time scales for de-swelling occur similarly within seconds.[292,293] It is worthy to mention that this pH-induced swelling observed behavior is distinct from harmomegathy as it is triggered by a different stimulus and involves more uniform morphological responses.

As de-esterification generates presence of negative charges of the carboxyl group in the intine, providing repulsion forces leading to swelling of the pollen microgel, positive charges were expected to reduce the repulsion force between the pectin polymers. The effect of different ions in altering the swelling/de-swelling properties of pollen microgel particles under neutral pH conditions were thus evaluated. At this state, the carboxylic acid functional groups in the pectin molecules are predominately deprotonated[294] and thus would be sensitive to presence of cations.[295] Time-lapse optical microscopy experiments on immobilized pollen particles provided direct evidence of the microgel response in the presence of Ca^{2+} ions. However, the Ca^{2+}-induced swelling and shrinking of the pollen microgel was noted to proceed at a slower rate (approximately 12 s to swell and 12 s to de-swell/shrink) than pH-induced swelling/deswelling response (Figure 3.20a). DIPA data shows the $CaCL_2$ and EDTA response of pollen microgel (Figure 3.20b, c). Subjecting pollen microgels to 10 mM of $CaCl_2$ solution induced the de-swelling of pollen microgel as expected. In addition, the pollen microgels fully recovered and reswelled upon flow of 10 mM of EDTA solution, a known cation chelator. The minimum diameters of pollen microgel

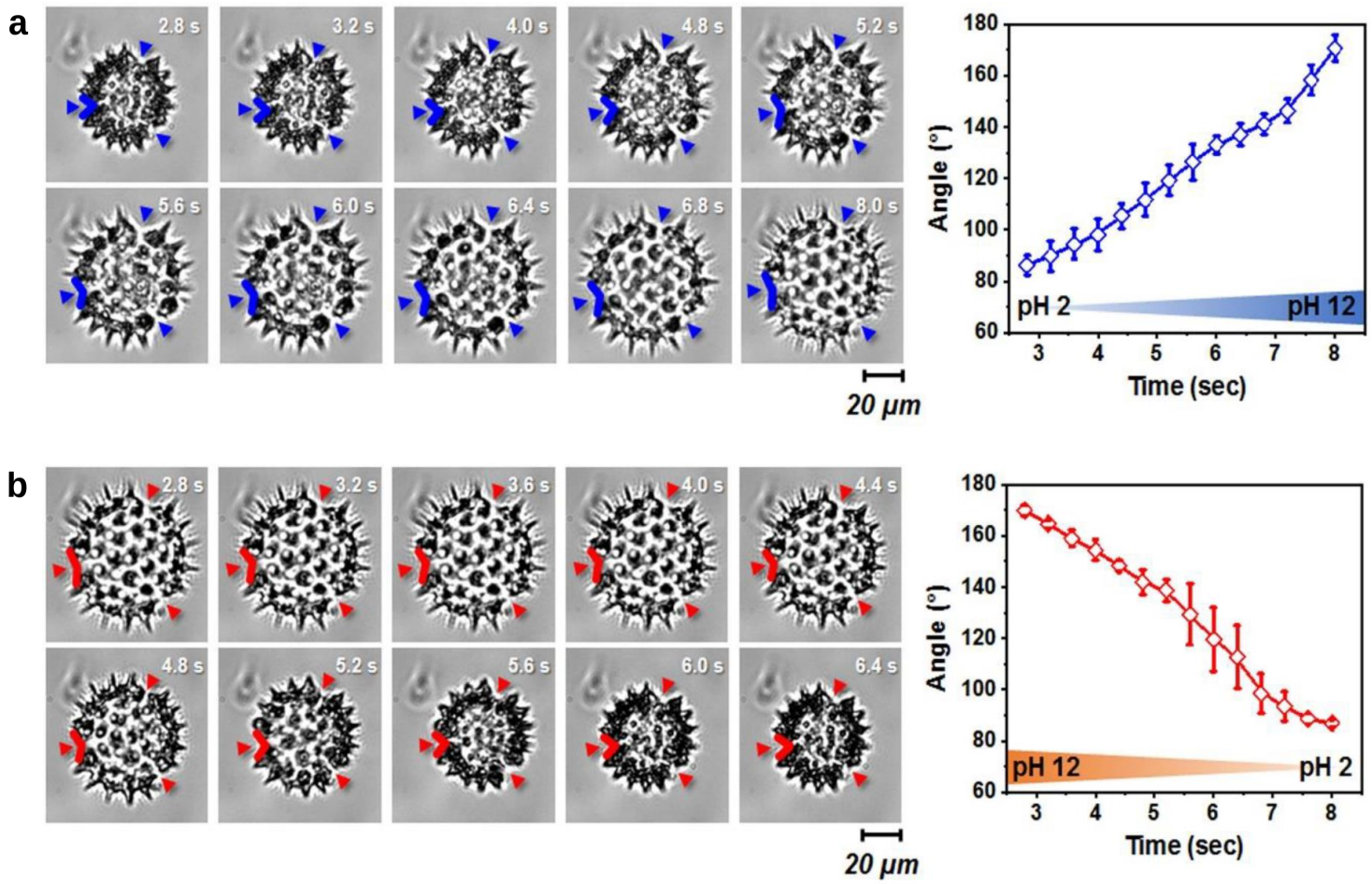

Figure 3.19. Time-lapse micrographs of 6 h KOH-treated pollen grains.[270] a) When the solution pH was increased from 2 to 12, the apertures become larger due to swelling and exhibited a larger angle of opening. b) When the solution pH was decreased from 12 to 2, the apertures become smaller due to de-swelling and exhibited a smaller angle of opening. The average and standard deviations were obtained for 6 samples and the imaging interval was 0.4 s. Data are presented as mean ± s.d.

treated with 10, 20, and 30 % w/v KOH solution respectively were 32.1 ± 2.61 µm, 31.58 ± 1.15 µm, and 31.06 ± 1.09 µm.; The maximum diameters of the pollen microgel were 55.2 ± 0.96 (10 % w/v), 50.44 ± 3.54 (20 % w/v), and 49.46 ± 2.88 µm (30 % w/v) (Figure 3.20b). For pollen microgels incubated for 6, 24, 48, and 90 h in 10 % w/v KOH solution, the minimum diameters of the pollen microgel are 32.44 ± 1.75 (6 h), 32.10 ± 2.61 (24 h), 32.25 ± 3.16 (48 h), and 31.47 ± 2.49 µm (90 h). The maximum diameters of the pollen microgel are 51.80 ± 3.25 (6 h), 55.20 ± 0.96 (24 h), 47.61 ± 2.94 (48 h), and 45.58 ± 3.86 µm (90 h) (Figure 3.20c). Similar effects were observed with other cations as well (Figure 3.21). In all cases, the addition of 10 mM EDTA caused re-swelling of the microgel particles.

3.3.4 Resultant swell size is dependent on exine stiffness and intine swelling

The effect of KOH-treatment on the structural and mechanical properties of the pollen substructure layers were also analyzed. SEM imaging show the gradual increment in porosity of the pollen shell with increasing KOH incubation time (Figure 3.22), suggestive of a progressive decline in structural integrity of the exine. Moreover, AFM measurements revealed that prolonged alkaline treatment caused a significant decrease in the Young's modulus of the exine layer (Figure 3.23), indicating a lowered stiffness of the exine. In turn, the ratio of the Young's modulus values of the exine and intine layers ($M_{E/I}$) decreased from 2.7 in defatted pollen to 1.2 in 24 h KOH-treated pollen.

Collectively, these findings strongly point to two interplaying factors that govern the swelling capability and size for the pollen microgel; 1) The pectin de-esterification process, which leads to deprotonation of the carboxyl group to provide the internal force for swelling and de-swelling, and 2) The resultant stiffness of the sporopollenin exine that determines the upper

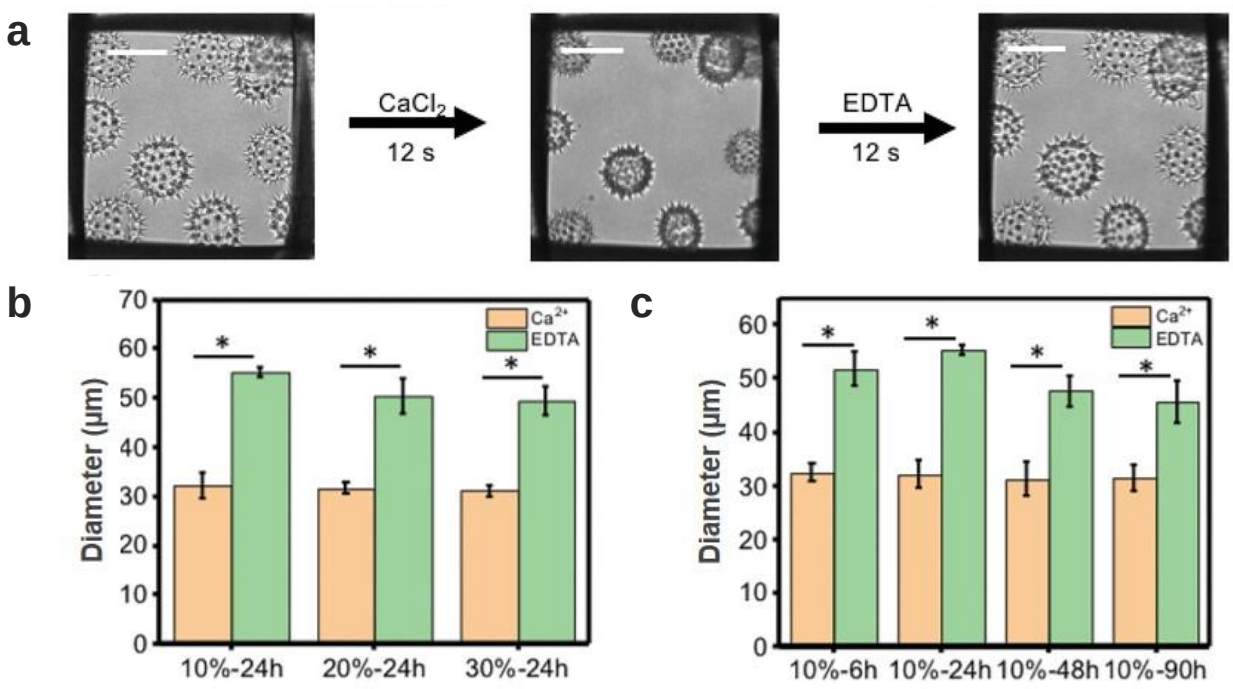

Figure 3.20. Ca^{2+}-EDTA induced swelling behavior of sunflower pollen microgel.[280] a) Time-lapsed optical micrographs of sunflower pollen microgel stimulated by Ca^{2+} (10 mM) and EDTA (10 mM). Scale bar: 50 μm. b) Diameter of pollen microgel prepared with 10, 20, and 30 % w/v KOH solution. c) Diameter of pollen microgel prepared with 6, 24, 48 and 90 h incubation duration.

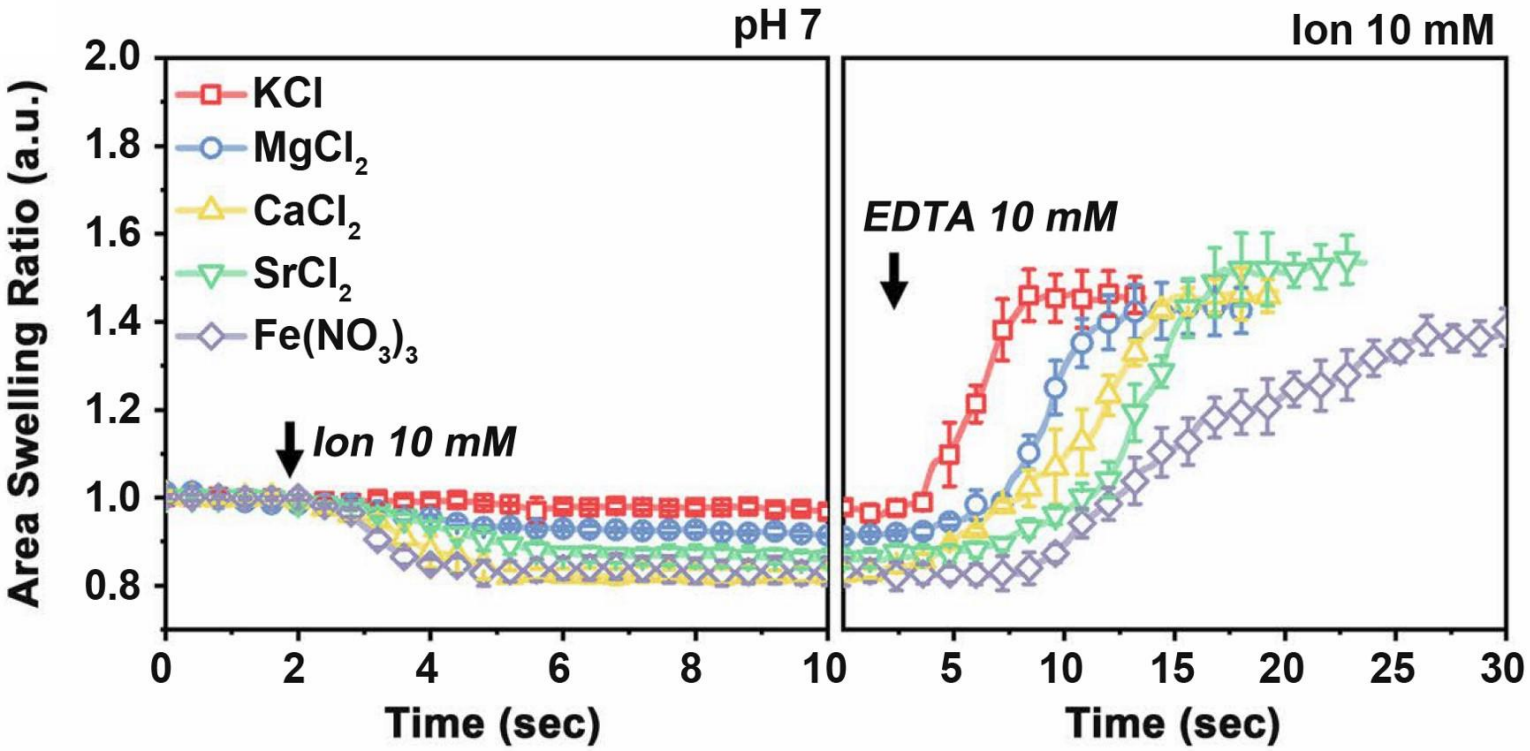

Figure 3.21. Quantitative comparison of cation-induced pollen de-swelling and swelling behaviors (n = 5). The area swelling ratio were normalized to pollen particles at pH 7.[270]

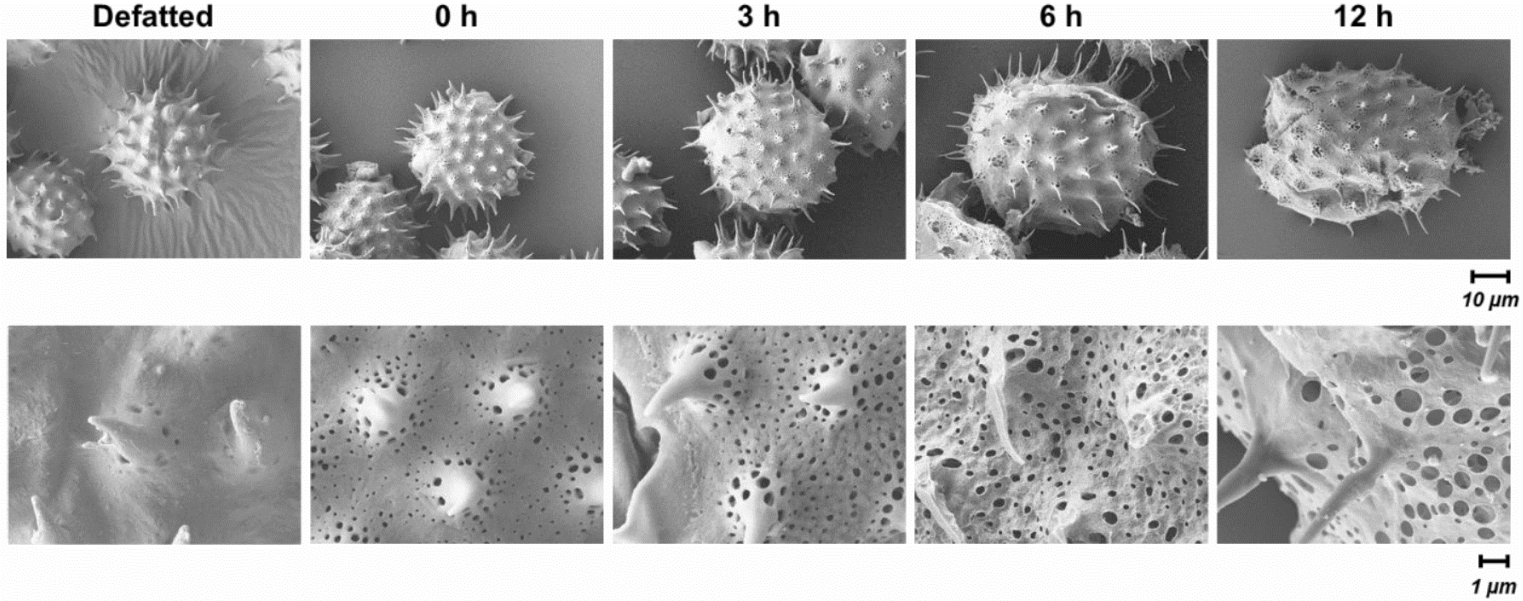

Figure 3.22. SEM images of pollen grains before and after 10 % w/v KOH treatment.[270] Top row: SEM images of pollen microgels at various incubation duration in 10 % w/v KOH. Longer KOH incubation duration resulted in greater opening of the apertures. Bottom row: Surface morphology of exine of corresponding microgels. Defatted pollen grain exhibited a dense and smooth surface morphology with few microscale pores around the spikes, whereas KOH-treated pollen were porous. The increased porosity of the exine surface was attributed to the release of remaining pollen cement as a result of KOH hydrolysis.[3,14]

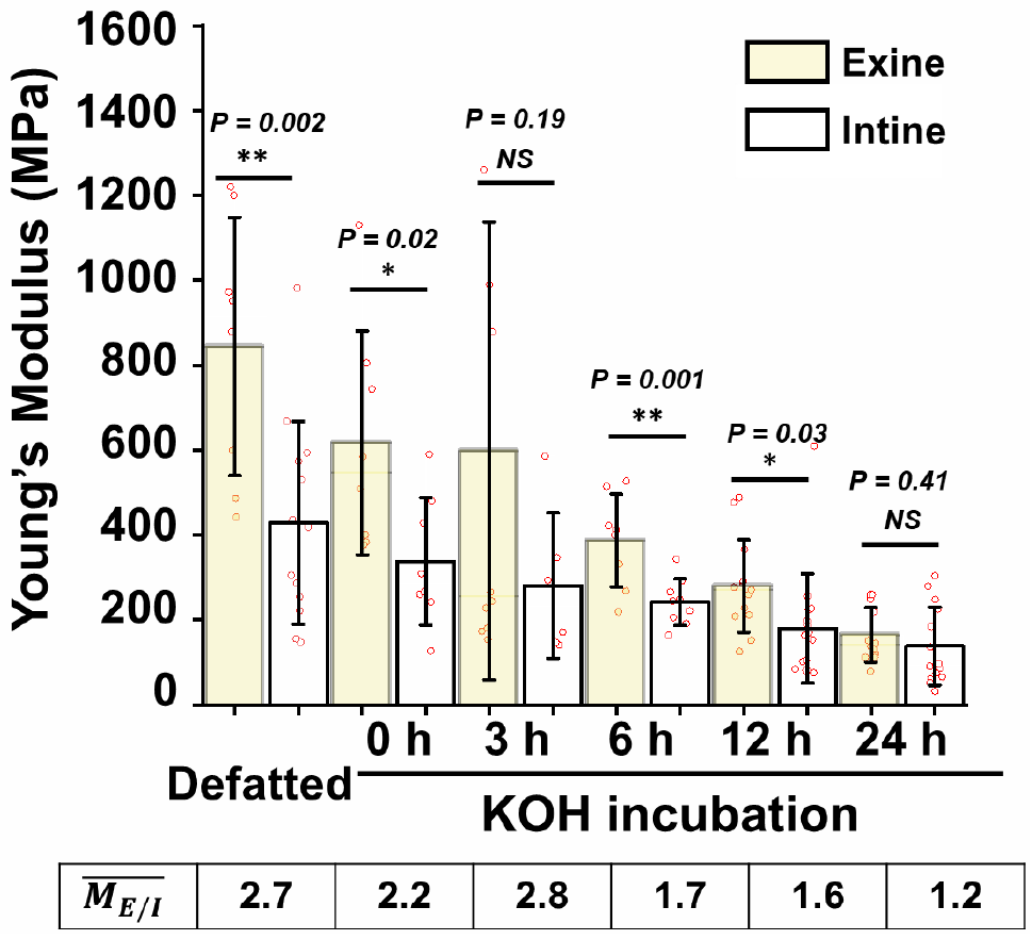

$\overline{M_{E/I}}$	2.7	2.2	2.8	1.7	1.6	1.2

Figure 3.23. Young's modulus values of exine and intine layers of pollen microgels incubated over various duration in 10 % w/v KOH. The pollen microgels were fully hydrated in aqueous solution at pH 7 prior to measurement. Mean ± s.d. are reported with statistical analysis (n > 16, one-way ANOVA with Tukey's multiple comparisons test, *P < 0.05 and **P < 0.01).[270]

swell limit of the pollen microgel, whereas the lower limit is limited spatially by maximum constriction of the pollen shell, which was similar for all the synthesized microgels.

3.4 Conclusion

Manipulation of the properties of natural materials holds promise for sustainable materials design and application. While these results may be significant and relevant in deciphering the evolutionary adaptations that pollen have adopted in ensuring continued reproductive success in nature, the modulation of pollen property and formation of microgels are explicit demonstrations of how the limits of natural processes can be surpassed. The present findings broadly extend this potential by illustrating how a robust pollen grain, regarded as the diamond of the plant world, can be transformed into a soft microgel exhibiting properties of a smart polymer by a simple alkaline hydrolysis process. Inherent properties of these microgels are conveniently controlled and tuned by tweaking KOH concentration and incubation duration. These synthesized microgels have advantageous properties over synthetically produced microgels in terms of naturally derived biocompatibility, high uniformity, and stimuli-responsiveness while remaining sustainable. The findings presented here would thus have great significance in the design and application of pollen-derived sustainable materials for a wide range of engineering and medical applications, such as in high-performance sensors and actuators, scaffolds, and drug delivery.

This chapter is a slightly modified version of "Transformation of hard pollen into soft matter." (Nature Communications 11, no. 1 (2020): 1-10) and "Influence of Chemical and Physical Change of Pollen Microgels on Swelling/De-Swelling Behavior." (Macromolecular Rapid Communications 41, no. 21 (2020): 2000155) and has been reproduced here with the permission of the copyright holder.

3.5 References

2 Tylianakis. The global plight of pollinators. *Science* **339**, 1532-1533 (2013).

3 Erdtman. *Pollen morphology and plant taxonomy: angiosperms*. Vol. 1 (Brill Archive, 1986).

4 Mackenzie, Boa, Diego-Taboada, Atkin & Sathyapalan. Sporopollenin, the least known yet toughest natural biopolymer. *Frontiers in Materials* **2**, 66 (2015).

5 Rojas, Hotton & Dumais. Chemically mediated mechanical expansion of the pollen tube cell wall. *Biophysical journal* **101**, 1844-1853 (2011).

6 Heslop-Harrison & Heslop-Harrison. The microfibrillar component of the pollen intine some structural features. *Annals of Botany* **50**, 831-842 (1982).

7 Birks, Birks & Ammann. The fourth dimension of vegetation. *Science* **354**, 412-413 (2016).

10 Blackmore, Wortley, Skvarla & Rowley. Pollen wall development in flowering plants. *New Phytologist* **174**, 483-498 (2007).

11 Katifori, Alben, Cerda, Nelson & Dumais. Foldable structures and the natural design of pollen grains. *Proceedings of the National Academy of Sciences* **107**, 7635-7639 (2010).

12 Couturier, Dumais, Cerda & Katifori. Folding of an opened spherical shell. *Soft Matter* **9**, 8359-8367 (2013).

14 Bosch & Hepler. Pectin methylesterases and pectin dynamics in pollen tubes. *The Plant Cell* **17**, 3219-3226 (2005).

15 Wolf, Hématy & Höfte. Growth control and cell wall signaling in plants. *Annual review of plant biology* **63**, 381-407 (2012).

16 Vieira & Feijó. Hydrogel control of water uptake by pectins during in vitro pollen hydration of Eucalyptus globulus. *American Journal of Botany* **103**, 437-451 (2016).

17 Bosch, Cheung & Hepler. Pectin methylesterase, a regulator of pollen tube growth. *Plant physiology* **138**, 1334-1346 (2005).

43 Quilichini, Grienenberger & Douglas. The biosynthesis, composition and assembly of the outer pollen wall: A tough case to crack. *Phytochemistry* **113**, 170-182 (2015).

264 Faegri & Van der Pijl. Principles of pollination ecology. (2013).

265 Ferreira, Reinhard & Araújo. *Foundations of paleoparasitology*. (Editora Fiocruz, 2014).

266 Radja, Horsley, Lavrentovich & Sweeney. Pollen cell wall patterns form from modulated phases. *Cell* **176**, 856-868. e810 (2019).

267 Prabhakar. *Pine pollen for molecular encapsulation and oral delivery applications*, (2018).

268 Brooks & Shaw. Chemical structure of the exine of pollen walls and a new function for carotenoids in nature. *Nature* **219**, 532-533 (1968).

269 Ariizumi & Toriyama. Genetic Regulation of Sporopollenin Synthesis and Pollen Exine Development. *Annual Review of Plant Biology* **62**, 437-460, doi:10.1146/annurev-arplant-042809-112312 (2011).

270 Fan, Park, Shi, Zhang, Liu, Song, Chin, Ibrahim, Mokrzecka & Yang. Transformation of hard pollen into soft matter. *Nature communications* **11**, 1-10 (2020).

271 Heslop-Harrison. Pollen germination and pollen-tube growth. *International review of cytology* **107**, 1-78 (1987).

272 Thomas. The effect of supplementary cementing materials on alkali-silica reaction: A review. *Cement and Concrete Research* **41**, 1224-1231, doi:https://doi.org/10.1016/j.cemconres.2010.11.003 (2011).

273 Jardine, Abernethy, Lomax, Gosling & Fraser. Shedding light on sporopollenin chemistry, with reference to UV reconstructions. *Review of Palaeobotany and Palynology* **238**, 1-6 (2017).

274 Clausen, Willats & Knox. Synthetic methyl hexagalacturonate hapten inhibitors of anti-homogalacturonan monoclonal antibodies LM7, JIM5 and JIM7. *Carbohydrate Research* **338**, 1797-1800 (2003).

275 Parre & Geitmann. More than a leak sealant. The mechanical properties of callose in pollen tubes. *Plant Physiology* **137**, 274-286 (2005).

276 Qu & Meredith. The atypically high modulus of pollen exine. *Journal of The Royal Society Interface* **15**, 20180533 (2018).

277 Zeng & Tan. AFM nanoindentation to quantify mechanical properties of nano-and micron-sized crystals of a metal–organic framework material. *ACS applied materials & interfaces* **9**, 39839-39854 (2017).

278 Hutter & Bechhoefer. Calibration of atomic-force microscope tips. *Review of scientific instruments* **64**, 1868-1873 (1993).

279 Neumann. Determining the elastic modulus of biological samples using atomic force microscopy. *JPK Instruments Application Report*, 1-9 (2008).

280 Fan, Hwang, Ibrahim, Ferracci & Cho. Influence of Chemical and Physical Change of Pollen Microgels on Swelling/De-Swelling Behavior. *Macromolecular Rapid Communications* **41**, 2000155, doi:https://doi.org/10.1002/marc.202000155 (2020).

281 Saunders, Laajam, Daly, Teow, Hu & Stepto. Microgels: From responsive polymer colloids to biomaterials. *Advances in colloid and interface science* **147**, 251-262 (2009).

282 Knox, Linstead, King, Cooper & Roberts. Pectin esterification is spatially regulated both within cell walls and between developing tissues of root apices. *Planta* **181**, 512-521 (1990).

283 Parre & Geitmann. Pectin and the role of the physical properties of the cell wall in pollen tube growth of Solanum chacoense. *Planta* **220**, 582-592 (2005).

284 Gnanasambandam & Proctor. Determination of pectin degree of esterification by diffuse reflectance Fourier transform infrared spectroscopy. *Food chemistry* **68**, 327-332 (2000).

285 Balaria & Schiewer. Assessment of biosorption mechanism for Pb binding by citrus pectin. *Separation and Purification Technology* **63**, 577-581 (2008).

286 Diaz, Anthon & Barrett. Nonenzymatic degradation of citrus pectin and pectate during prolonged heating: effects of pH, temperature, and degree of methyl esterification. *Journal of agricultural and food chemistry* **55**, 5131-5136 (2007).

287 Yule, Roberts & Marshall. The thermal evolution of sporopollenin. *Organic Geochemistry* **31**, 859-870, doi:https://doi.org/10.1016/S0146-6380(00)00058-9 (2000).

288 Sułkowski, Pentak, Nowak & Sułkowska. The influence of temperature, cholesterol content and pH on liposome stability. *Journal of molecular structure* **744**, 737-747 (2005).

289 Renard & Thibault. Degradation of pectins in alkaline conditions: kinetics of demethylation. *Carbohydrate Research* **286**, 139-150 (1996).

290 Wehr, Menzies & Blamey. Alkali hydroxide-induced gelation of pectin. *Food Hydrocolloids* **18**, 375-378 (2004).

291 Maciel, Yoshida & Franco. Chitosan/pectin polyelectrolyte complex as a pH indicator. *Carbohydrate polymers* **132**, 537-545 (2015).

292 Kiser, Wilson & Needham. A synthetic mimic of the secretory granule for drug delivery. *Nature* **394**, 459-462 (1998).

293 Zhao & Moore. Fast pH-and ionic strength-responsive hydrogels in microchannels. *Langmuir* **17**, 4758-4763 (2001).

294 BeMiller. An introduction to pectins: structure and properties. (1986).

295 Michard, Simon, Tavares, Wudick & Feijó. Signaling with ions: the keystone for apical cell growth and morphogenesis in pollen tubes. *Plant Physiology* **173**, 91-111 (2017).

Chapter 4 Influence of Variables and Mechanism of Formation of 3-Dimensional Pollen Microgel-derived Sponge Scaffold

Chapter Abstract

3D porous materials possess immense potential for applications in various fields such as energy generation and storage, wearable electronics, separation, catalysis and tissue engineering. In this study, the ability of pollen microgels to form 3D porous sponges via freeze-drying and the various factors that influence the sponge characteristics were investigated. Regulation of stiffness of pollen microgels, the swell state of the microgels and the freezing rate of the microgel slurry greatly influences the morphology, porosity, hydrophilicity and compression modulus of the fabricated 3D sponges. The interparticle bonding mechanism during the sponge formation process was also investigated. Two hypotheses were put forward. Firstly, the pressure from the ice crystals was sufficient to provide proximity to allow formation of bonds between microgel particles, allowing the pore walls to form. Secondly, the removal of "bound water" during the secondary drying stage was necessary to provide sufficient proximity to allow bonds to form. Observations in this study suggests that both factors were essential to form strong chemical bonds that conjugates adjacent pollen particles. A 'zipping' mechanism of the interface of pollen microgel was proposed.

Keywords: pollen, microgel, 3D, scaffold, sponge, freeze-drying, porous, bound water.

4.1 Introduction

Being a male microgametophyte of seed plants, pollen is usually produced in largely excessive amounts beyond what is efficiently necessary for fertilization of the female flower. A large proportion of the pollen released are thus regarded as biological waste, largely due to the pollen's robust nature, which limits its propensity to be processed into useful products other than health supplements in the form of bee pollen and in encapsulation applications, which exploit the pollen's natural microcapsule form and its renowned robust yet porous outer shell.

Previously, a detailed yet simple method to significantly soften hard pollen particles was established, with the resultant pollen particles exhibiting physical properties resembling discrete colloidal microgel. These ion-responsive highly dynamic pollen microgels were explicitly shown to have swelling capabilities that were reminiscent of the pollen tube germination process, and its properties can be conveniently modulated by the regulation of potassium hydroxide (KOH) concentration and duration of incubation in KOH at elevated temperatures[270,280]. These newfound malleability opens multiple avenues of using pollen for applications that were not possible prior, largely due to the natural pollen's resistance to manipulations via mechanical deformations and its inherent inertness to external factors.

The possibility of utilizing these pliable pollen microgels for the fabrication of three dimensional (3D) scaffolds was explored. Employing the simple and well-understood ice-templating and lyophilization process, or freeze-drying, which is suitable for thermolabile compounds such as microgels,[170] a porous sponge-like scaffold was fabricated from aqueous suspension of the pollen microgel. The mechanical properties of the scaffold were reliant on the softness of the microgel, which was in turn dependent on the duration of KOH incubation during the microgel synthesis, the swell state of the pollen microgel and the freezing temperature during

ice-templating. Analysis of the mechanism of interparticle interaction indicates that a critical interparticle distance threshold needs to be overcome before a permanent bond can form that is resistant to disintegration and reversion of the scaffold wall to discrete microgels by capillary effect of evaporating water.

4.2 Methods

4.2.1 Fabrication of 3D scaffolds from pollen microgel suspension

Sunflower bee pollen granules were purchased from GTL Biotech (Xi'an, Shaanxi, China) and defatted as previously described. Briefly, 250 g of the bee pollen was dispersed in deionized water (1000 mL) and stirred. The suspension was filtered through nylon mesh with 200 µm pore size (ELKO Filtering Co., USA). The dispersed pollen in the filtrate was collected via vacuum filtration using a Büchner funnel lined with filter paper. The collected pollen was refluxed in 500 mL acetone (Aik Moh, Singapore) at 50 °C for 3 h under continuous stirring. The acetone in the suspension was removed by vacuum filtration as before and the collected pollen was rinsed with fresh acetone followed by vacuum filtration. The acetone reflux and filtration was repeated. The washing step was repeated until the filtrate runs clear. The resulting pollen powder was transferred into an open glass petri dish, covered with wipes and air-dried overnight in a fume hood.

The dried pollen powder (~120 g) was suspended in 200 mL diethyl ether (Sigma Aldrich, Singapore) and continuously stirred at room temperature for 2 h. The diethyl ether in the suspension was removed by vacuum filtration, and the collected pollen was rinsed with fresh diethyl ether followed by vacuum filtration. The collected pollen was suspended in diethyl ether (200 mL) again and continuously stirred at room temperature overnight, and the rinsing and

filtration process was repeated until the filtrate runs clear. The resulting pollen powder was transferred to an open glass petri dish, covered with wipes and air-dried overnight in a fume hood.

The defatted pollen was then transformed into microgel particles following previous protocols.[270] Briefly, the defatted pollen was suspended in 10% (w/v) KOH at a concentration 1 g pollen per 10 mL KOH solution in a polytetrafluoroethylene (PTFE) round-bottom flask. The suspension was continuously stirred and refluxed for 2 h at 80 °C. The pollen was collected via filtration using a nylon mesh with 20 µm pore size, and the collected pollen was rinsed with 20 mL of 10% (w/v) KOH followed by filtration. The rinsing and filtration process were repeated a total of three times. The rinsed pollen was transferred to a 50 mL conical centrifuge tube and topped up to a total volume of 20 mL with fresh KOH solution. The solution was resuspended using a vortex mixer at high speed for 2 min and was incubated at 80 °C in an oven (Memmert, Schwabach, Germany) for defined periods. The incubation was terminated at the defined time by isolating the pollen particles via filtration using a nylon mesh of 20 µm pore size. The collected pollen was rinsed with copious amounts of deionized (dI) water followed by filtration. The rinsing and filtration processes were repeated until the pH of the suspension reached 7, as measured using pH-indicator strips (Millipore Sigma, Burlington, MA). The resulting pollen microgel suspension was transferred to a 50 mL conical centrifuge and centrifuged at 3000 rpm (Beckman Coulter, Allegra X-15 R, rotor SX4750) for 5 min. Any residual water supernatant was then decanted.

For the respective microgel slurry, a volume that was equivalent to 0.2 g of defatted pollen material were pipetted into individual wells of NUNC 24-well tissue culture dishes (Thermo Scientific, Rochester, NY). This ensures that the absolute number of pollen particles that make up each sponge was consistent among the various fabricated scaffolds. The plates were centrifuged at 3000 rpm (Beckman Coulter, Allegra X-15 R, rotor SX4750µ) for 15 min to remove any residual

water and to level the microgel surface. The plates were then frozen in respective freezer, before lyophilization of the frozen microgel suspension was performed (Labconco, Kansas City, MO) for 48 h under 0.008 mbar vacuum. The obtained dry pollen sponges were kept in a dehumidifying cabinet until further characterizations.

4.2.2 Morphological Analysis of Pollen Sponges

High-magnification images of pollen sponge cross sections were obtained via field emission-scanning electron microscopy (FESEM). For sponges that were rehydrated, liquid nitrogen was used to rapidly freeze the wet sponges and lyophilization was performed as before. Rapid freezing would generate small ice crystals that would not alter the inherent porosity of the prepared sponges. Fully dried pollen sponges were gently sliced with a sharp blade along the transverse plane and immobilized on the sample holder with carbon tape and sputter-coated with platinum to a thickness of 5 nm (20 mA, 40 s) using a JFC-1600 Auto Fine Coater (JEOL, Tokyo, Japan) to improve the sample conductivity. Thick samples were further held in place using copper tape. Images were taken with a JSM-7600F Schottky microscope (JEOL) at an acceleration voltage of 5 kV. Pollen sponge cross-sectional pore area was determined via measurement of the obtained images via ImageJ (NIH, USA). A minimum of 30 pores showing intact borders was used to calculate the results for each sample.

4.2.3 Mechanical analysis

The rheological properties of microgel samples were characterized by performing oscillatory measurements at 25 °C with a stress-controlled rheometer (MCR 501, Anton Paar,

Graz, Austria) using a cone/plate geometry (CP 25-1, angle of 0.982°, diameter of 24.990 mm, gap of 47 μm). For each experiment, 75 μL of microgel sample was loaded onto the measurement stage. The linear viscoelastic (LVE) region for the samples were initially determined by performing a strain sweep, by increasing the strain logarithmically from 0.1% to 100% at a frequency of 6.28 rad/s (1 Hz). The storage (G′) and loss (G″) moduli and the loss tangent (tanδ) were calculated as functions of the strain (data not shown). Frequency sweeps were then performed in triplicates on fresh microgel samples by increasing the frequency logarithmically from 0.1 to 10 Hz, keeping within the LVE region at a strain amplitude of 0.5%. Storage moduli of respective microgel samples were calculated as functions of the angular frequency

The compressive Young's modulus values of the pollen sponges were analyzed using a DMA Q800 dynamic mechanical analyzer (TA Instruments, USA) in a controlled force mode. The pollen sponge samples were held between parallel-plate compression clamps and were then compressed from 0.1 to 18.0 N at a ramp rate of 1 N/min. The compressive Young's modulus was calculated from the slope of the elastic region of the stress–strain curve, between 40% and 50% compressive strain.

4.2.4 Discrete particle mechanical characterization via Atomic Force Microscopy (AFM)

The mechanical properties of defatted pollen and microgel particles were characterized by conducting AFM force-distance (or load versus displacement) measurements. This depth-sensing AFM indentation approach enables the quantitative determination of the Young’s modulus of the shell material[275,276]. For wet samples, pollen microgel samples (5 μL) were suspended in dI water, and 50 μL of this suspension was spread onto a polystyrene petri dish. Excess liquid was aspirated by micropipette, leaving the partially-hydrated samples on the dish for immediate analysis. For

dry specimens, the pollen sample was directly spread onto the surface of a petri dish before measurement. Intact pollen particles were carefully selected for measurements of the Young's modulus of the exine layer, whereas randomly broken pollen particles, which exposed the inner layer, were chosen to determine the Young's modulus of the intine layer. To avoid the influence of the modulus of the underlying substrate (substrate effect), the 10% depth rule was employed where the indentation depth should be less than 1/10th of the thickness of the material measured[277]. The average thickness of the exine layer was approximately 0.6 μm for defatted pollen particles and 0 h KOH-treated pollen specimens and became thinner with increasing KOH treatment time (~0.5 μm). Thus, the depths of indentation for exine measurements were set in the range of 20–60 nm under indentation loads of 3–6 μN. On the other hand, the intine layer was swollen in wet conditions, with a thickness range from 0.5 to 1.5 μm. Thus, the indentation depths for wet samples were in the range of 50 to 100 nm. For all measurements, the NX-10 AFM instrument (Park Systems, Suwon, South Korea) was used with two AFM probes: (i) an aluminum reflex-coated silicon cantilever PPP-NCHR (Nanosensors, Neuchâtel, Switzerland) with a typical spring constant of ~42 N m^{-1} and a tip end radius of 5 nm; and (ii) a diamond cantilever TD26135 (Micro Star Technology, Huntsville, TX) with a spring constant of 150 N m^{-1} and a tip end radius of 5 nm. The tips were shaped as polygon-based pyramid with a half-cone angle of 20°. Both AFM probes provided almost identical values of Young's moduli for exine and intine layers regardless of the various indenting parameters such as maximum contact forces, contact time or approach speed (Appendix 3.1). Before experiments, the AFM cantilever was rinsed with water and ethanol, and treated with a UV light cleaner for 30 min in order to remove any organic contaminants. The spring constant and sensitivity of the deflection signal were also calibrated by recourse to the thermal vibration of the AFM cantilever[278] by employing the commercial software (XEP, Park Systems).

A minimum 16 measurements were conducted at various positions within a 5 μm × 5 μm area at an approach speed of 0.8 μm/s with a maximum loading force of 4.8 μN and zero contact time. The force-displacement curves were normalized by subtracting the deflection distance of the AFM probe from the total displacement.

For data analysis, it was assumed that both the exine and intine layers were isotropic. As the AFM probe used had a tip end radius of 5 nm, the indentation depths employed in this methodology were significantly larger than the tip end radius. Thus, the classical Hertz model was used for data analysis[276,279]. The Hertz model[275] was fitted to the force-displacement curves using a commercial software analysis program (XEI, Park Systems) and the Python script language (Appendix 3.1). The geometry of the AFM tip was taken as a parabolic model whereby it has a tip radius of R_c, and therefore the force (F) can be expressed as:

$$F = \frac{4\sqrt{R_c}}{3} \cdot \frac{E}{1-v^2} \cdot \delta^{3/2}$$

where E is Young's modulus, v is the Poisson's ratio, and δ is the indentation depth. The Poisson's ratio v was set at 0.5, which is typical for natural materials.

4.2.5 Fourier-Transform Infrared Spectroscopy

FTIR spectroscopic analysis of the pollen sponge was conducted using the PerkinElmer Spectrometer (PerkinElmer, UK) equipped with a diamond cell attenuated total reflection (ATR) accessory. Reflectance infrared spectra were obtained between 4000 and 600 cm^{-1} by 16-times scanning per measurement. For each sample, three different areas were measured. Background spectra were collected prior to sample readings and subtracted from each sample spectrum

automatically by Spectrum 10 Software (PerkinElmer, UK). To correct spectra with sloped baselines and reduce the amount of noise in the spectrum, a baseline correction and smoothing process were conducted after sample measurements using the software.

4.2.6 Freezing profile measurement

The pollen microgel was pipetted into individual wells of 24-well tissue culture dishes (each well containing an amount of microgel approximately equal to 0.2 g worth of pollen, ie. each sample is separately pipetted into 10 wells), and the plates were centrifuged at 3000 rpm for 15 min to remove any residual water. The plates were then placed into a freezer set at −20°C. The temperature profile of the freezing microgel was monitored in real-time using a Type-K thermocouple (Omega, USA), with the electrode suspended within the core of the pipetted volume of microgel suspension.

4.2.7 Hydrophobic coating & Freeze-drying

Hydrophobic coating of microgels was performed via conjugation of norbonene on pollen microgel surface. 1 g of pollen was suspended in 50 mL of prepared 2-(N-morpholino) ethanesulfonic acid (MES, MW: 195.2. CAS No. 4432-31-9, Sigma-Aldrich, USA) buffer (0.1 M, pH 6). 0.8 g of 1-Ethyl-3-(3-dimethylaminopropyl)-carbodiimide·HCl (EDC, MW: 191.7, CAS No. 25952-53-8, Sigma-Aldrich, USA) and 2 g of N-hydroxysuccinimide (NHS, MW: 115.09, CAS No. 6066-82-6, Sigma-Aldrich, USA) were then added to the suspension and stirred for 2 h at room temperature. 0.64 g of 5-Norbornene-2-methylamine (MW: 123.20, CAS: 95-10-3. TCI Chemicals, USA) was slowly added to the mixture and stirred for 18 h at room temperature. pH

correction, if needed, was done using 0.1 M HCl solution. The reaction was terminated by quenching the suspension in excess PBS, centrifuging the suspension (1500 rpm, 5 min), and decanting the supernatant. The pollen-norbornene pellet was resuspended in dI water. The centrifuge, decant and resuspension step was performed for 5 cycles. The washed pollen-norbornene particles were finally resuspended in 40 mL dI water, frozen in liquid nitrogen for 15 min, and lyophilized over a period of 48 h to obtain the dried pollen-norbornene particles.

4.3 Results and Discussion

4.3.1 Formation of 3D porous scaffolds

The ability of pollen microgel to form higher order structures was observed during the process of dehydration of pollen microgels suspensions in the preparation for certain assay characterizations. While the suspensions of defatted pollen remain as loose powders upon drying, suspensions of pollen microgels, especially those that had a longer period of incubation, tend to aggregate, and form films on the walls of the vessels in which they were stored in. These observations suggests that these novel pollen microgels were able to form interparticle interactions and would thus be able to function as discrete building blocks for modular assembly into larger more complex physical structures.

Expounding on this phenomenon, a freeze-drying method was applied onto prepared suspensions of pollen microgel in an attempt to control the interparticle fusion and fabricate 3D-scaffolds (Figure 1). Freeze-drying is a method for forming porous materials and microstructures in which ice acts as the pore-shaping agent, or porogen. This process consists of three steps: (1) freezing, (2) primary drying and (3) secondary drying.[296-300] In the freezing stage, ice crystals nucleate and grow, excluding molecules or particles from the ice fronts. This crystallization process thus forces the particles into close proximity with each other. The freezing conditions such as freezing rate or direction of freezing, greatly influences the resultant size and morphology of the ice crystals, which then acts as a negative template to the scaffold's final macrostructure.[296] even at complete freezing, a small percentage of water remains 'bound' to the solute phase, unable to be included in the ice crystal formation, and thus remain unfrozen.[297,301] In the primary stage of the freeze-drying process, a high vacuum is applied to lower the pressure below the triple point of water (Figure 2).[170] This results in sublimation of the ice crystals to vapor, and thus avoiding the

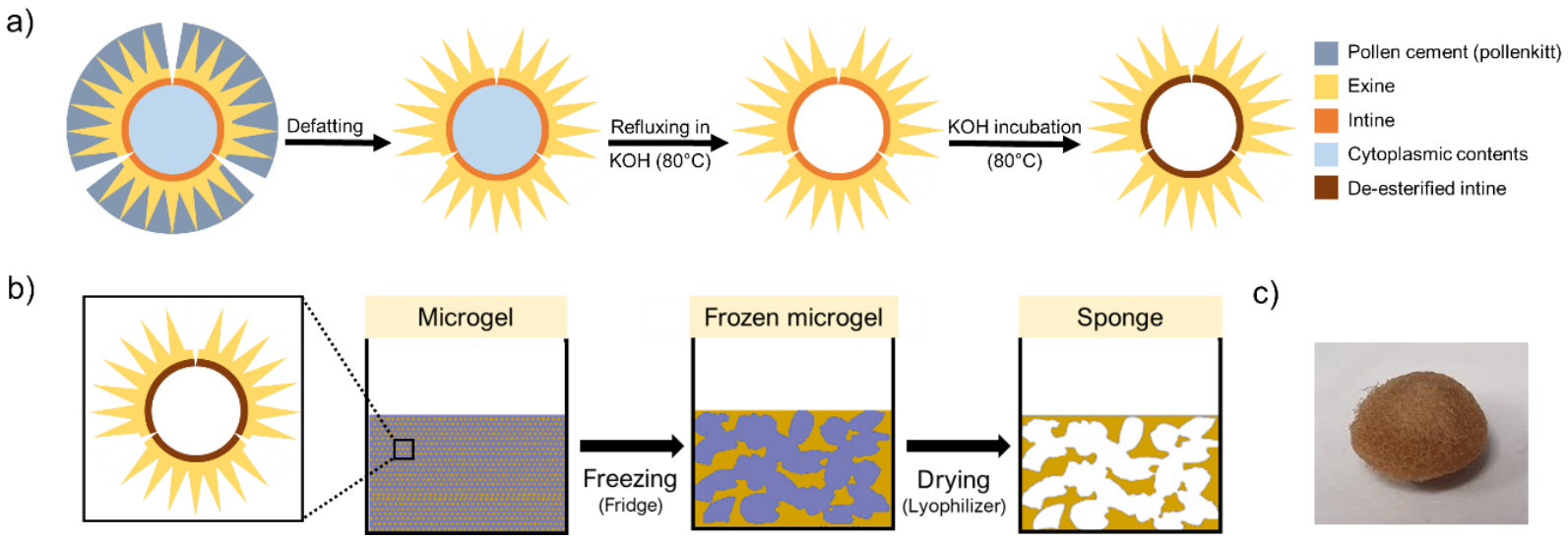

Figure 4.1. Schematic illustrating (a) the process of converting pollen grains to microgel particles and (b) the process of fabricating sponges from the microgel. (c) Image of a pollen sponge.

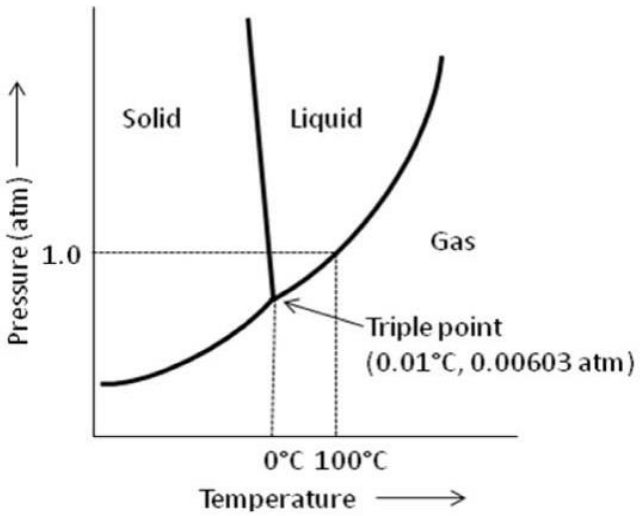

Figure 4.2 Phase diagram showing the triple point of water at 0.01°C, 0.00603 atm. Lyophilization is carried out below the triple point to enable conversion of ice into vapor, without entering the liquid phase (known as sublimation).[170]

capillary effects brought about by evaporation of the liquid phase of water. This sublimation process thus removes the ice crystals formed during freezing. In the event that the particles excluded from the ice crystal front are of sufficient density to be packed into a structure, this sublimation process would preserve the morphology of the formed particulate wall. Absolute removal of the ice crystals during this first drying stage is succeeded by the secondary drying stage, where desorption of bound water surrounding the particles occur. The water vapor diffuses and bound water is continually transported outside of the porous matrix to be subsequently removed.[296]

Naïve defatted pollen were unable to form structures likely due to limited interparticle interactions, exacerbated by their micron-sized topography and high stiffness that prevents adequate, efficient and robust interactions to occur. Therefore, conditions that promote high surface contact area were hypothesized to promote interparticle interactions and thus scaffold formation. A reduced particle stiffness was therefore able to promote surface contact area for interparticle interaction due to the particle's ability to conform to the topography of adjacent particles. The influence of various factors that may positively influence the surface contact area of adjacent pollen particles were carefully selected from the different stages of the freeze-drying method process of scaffold fabrication. These include the duration of incubation at the microgel synthesis stage, which affects the resultant softness of the pollen microgel,[270] the pH environment of the microgel suspension, which affects the swell state of the pollen microgel,[270,280] and the influence of freezing rate at the freeze-casting stage, which affects the force generated by growing ice crystals within the pores of the scaffold.[302,303]

4.3.2 Influence of incubation duration

Pollen microgels prepared in 10 % w/v KOH were chosen as our base condition as it had been previously shown to result in pollen microgels with the most dynamic swelling across the pH range.[280] Previously, it had been adequately illustrated that the duration of incubation during pollen microgel synthesis negatively influences the stiffness of the resultant pollen particles (Figure 3.23).[270]

Pollen was transformed into microgels using the previously employed KOH hydrolysis method[270] with increasing duration of incubation. AFM measurement of the stiffness of the

resultant microgel at wet and dry conditions shows a decreasing trend in Young's modulus values (Figure 4.3). Furthermore, the modulus ratio of wet/dry pollen particles show a decreasing trend

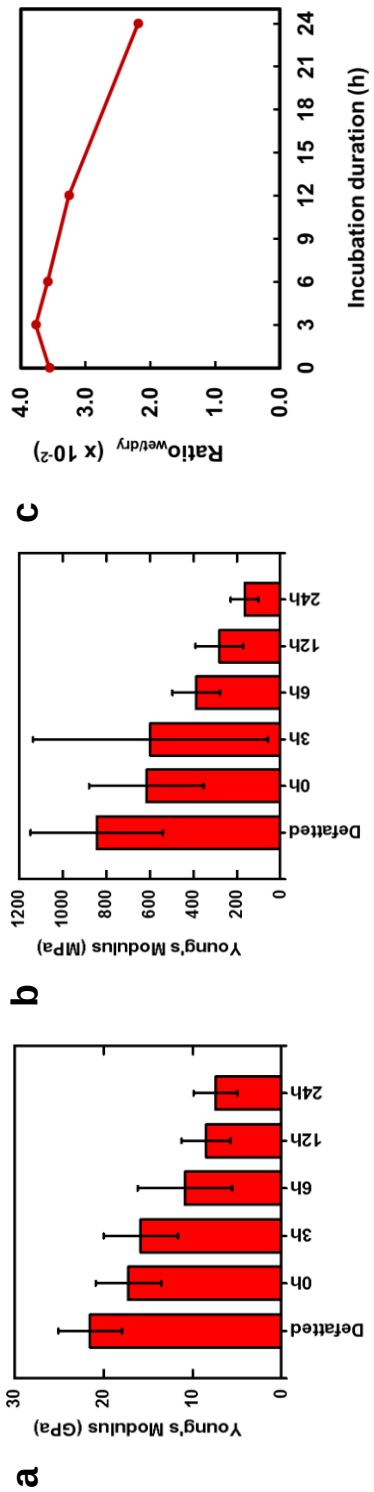

Figure 4.3. Young's modulus of discrete pollen particles subjected to increasing duration of incubation in a) dry and b) wet conditions, and the corresponding ratio of modulus for wet/dry.

as the incubation duration increased from 3 h to 24 h, showing that the difference in modulus between wet and dry state was increasing and that the presence of water plays a crucial role in the flexibility of the pollen particle (Figure 4.3c). Pollen sponge scaffolds were fabricated by casting respectively prepared pollen microgel of amounts approximately equal to 0.2 g worth of initial defatted pollen into individual wells of 24-well tissue culture plate. This volume differs across the different pollen microgels due to their various degrees of swelling upon subjected to different incubation period (Figure 4.4, Figure 3.15).

These processes resulted in the formation of pollen sponges with 3D porous architectures. Scanning electron microscopy (SEM) imaging further verified that longer incubation times up to 72 h improved sponge fabrication quality, as indicated by a progressively lower number of defects in the sponge walls (Figure 4.5). It is easily noticeable that the pore sizes of the sponge were relatively similar, indicating a similar freezing rate throughout the samples. However, differences of the topographical features of the wall were immediately noticeable. Boundary of individual pollen grains were visible in the wall that makes up the pore of the 0 h sponge. Furthermore, the texture of the walls exhibited the spiky appendages that is characteristic of the sunflower pollen utilized in this study, although they resembled deflated and flattened particles. As the incubation duration progresses to 72 h, there is a marked decrease in observable interparticle boundaries and a corresponding marked decrease in visibility of spiky appendages on the pore wall. This observation correlates well with the decreasing Young's modulus of the microgel. As the microgel gets softer, the pressure from the growing ice crystal was able to overcome the force of that retains the particle's physical. The particles at the front of the growing ice crystal are thus compressed together, leading to formation of the pore wall upon lyophilization. This mechanism of pore wall formation would be akin to compressing multiple particles of putty,

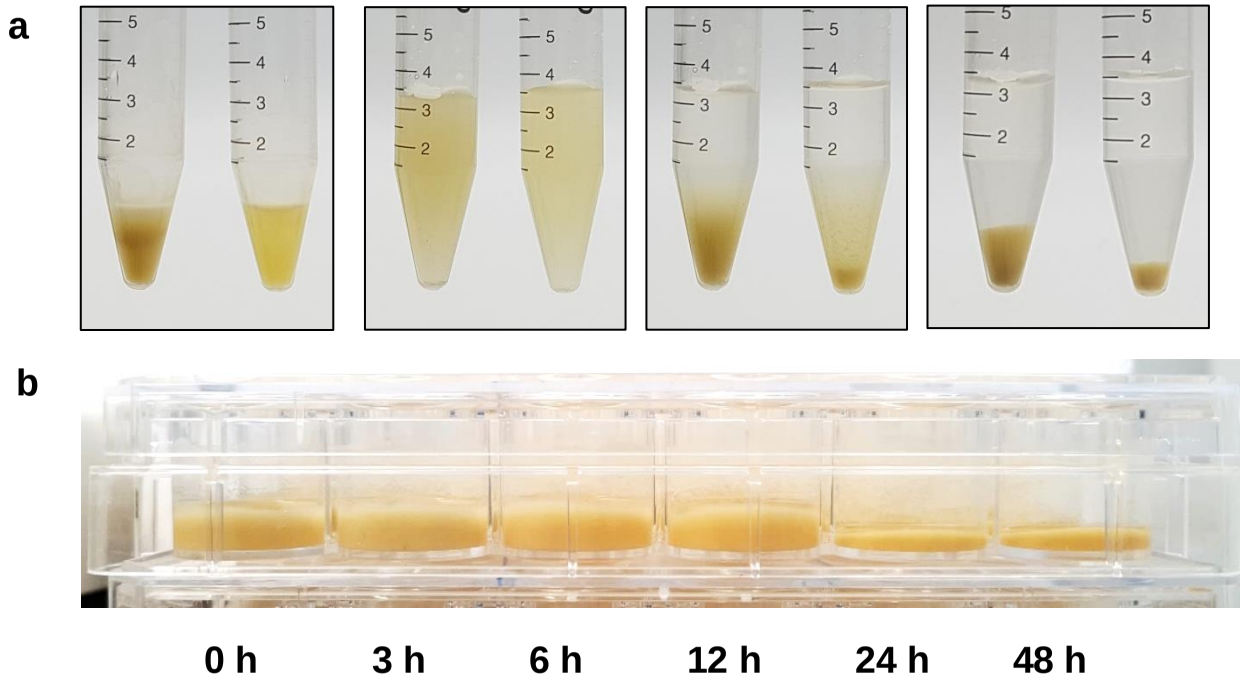

Figure 4.4. a) 0 h and 24 h microgel of i) equal initial pollen volume, ii) reconstituted in pH 4 solution, iii) 30 min later and iv) centrifuged to visualize the resultant pollen microgel pellet is of a smaller volume, especially for the 24h microgel. b) Equivalent initial pollen microgel of various incubation duration at pH 4 and post-centrifuge show that 24 h microgel is the timepoint where drastic dynamic swelling occurs

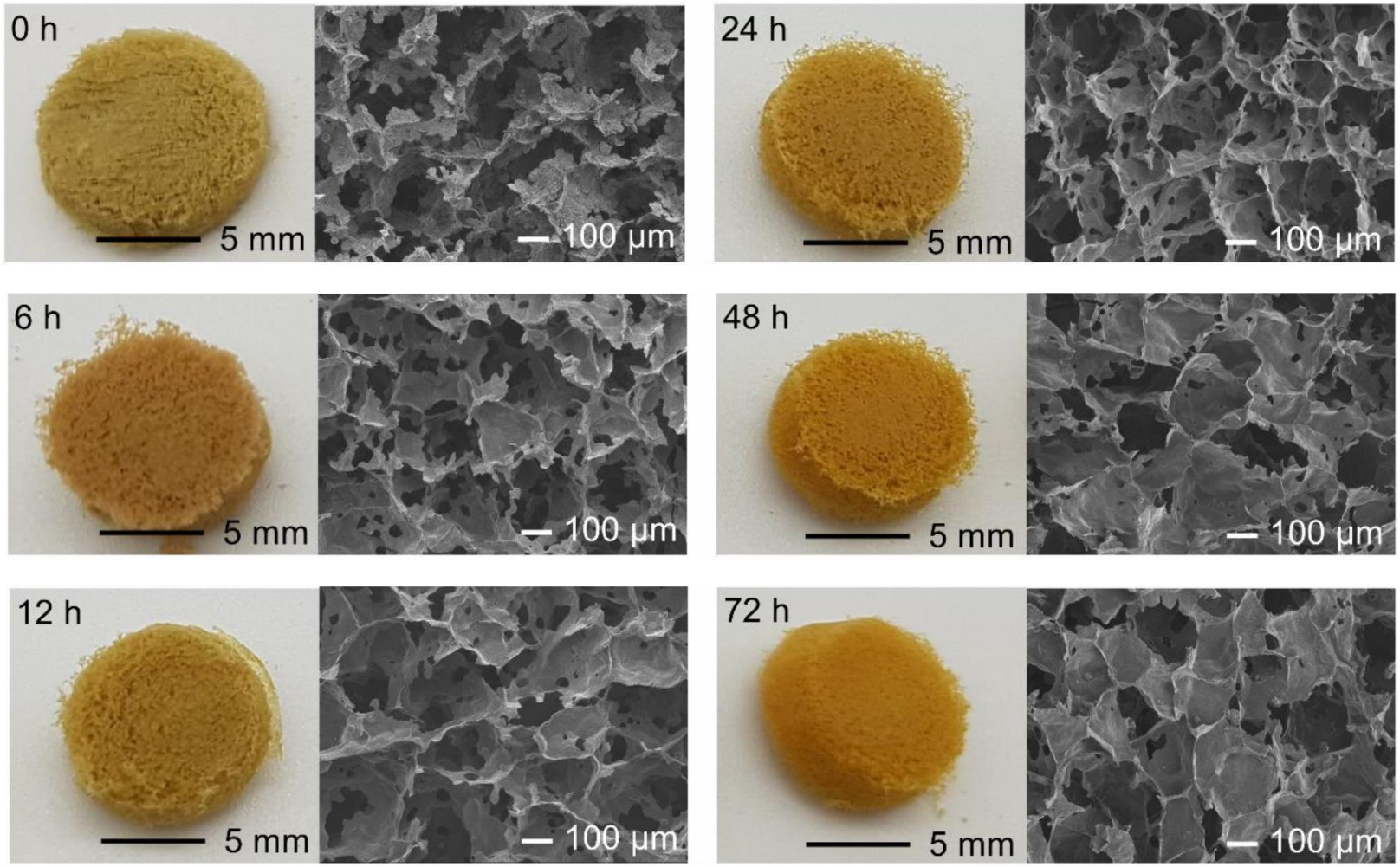

Figure 4.5. Photographs and SEM images of bare pollen sponges.[304] The pollen sponges had been prepared using the standard fabrication protocol with 0, 6, 12, 24, 48, and 72 h KOH incubation time durations during the second incubation step.

with softer particles leading to an increasingly seamless and smooth wall. Since 0 h microgel had a significantly higher modulus, the force generated by the ice crystal was not able to fully overcome the stiffness of the pollen particle, and thus the interparticle boundary and spikes were still visible. This also explains why exceedingly high modulus naïve pollen particles suspended in water were unable to form 3D sponges, but simply reverts to its powder form upon freeze-drying. The high Young's modulus of naïve pollen was not easily overcome by the force of the growing ice crystal during freezing, and would be akin to pushing compressing multiple marbles to form a wall. The retention of the spherical shape also means that there is limited surface contact area for any robust interaction to occur.

To characterize the freezing behavior of the microgels, the temperature of the microgels during the freezing stage was measured to obtain the cooling curves (Figure 4.6a). For 0 h incubation time, the microgel particles sunk to the bottom of the well during freezing. As a result, the frozen microgel was not homogeneous and the thermocouple electrode tip was in a water-rich region. Hence, the temperature profile of the 0 h microgel can be assumed to be similar to that of water. 24 h microgel had the lowest rate of freezing, of which longer incubation duration progressively leads to freezing profiles that approaches that of water, indicated by shorter freezing plateaus (Figure 4.6b). This is likely due to increasing water content, consistent with previous studies that demonstrated how longer incubation times resulted in more extensive de-esterification of pectin molecules,[270] thus enhancing the exposure of functional groups available for water adsorption.[305] However, in all the microgel samples, the degree of supercooling prior to ice nucleation was smaller (Figure 4.6c) , indicating that ice nucleation proceeded more readily, probably due to presence of pollen-derived precipitates within the slurry.

This mechanism of pore wall forming was further supported by the decreasing trend in

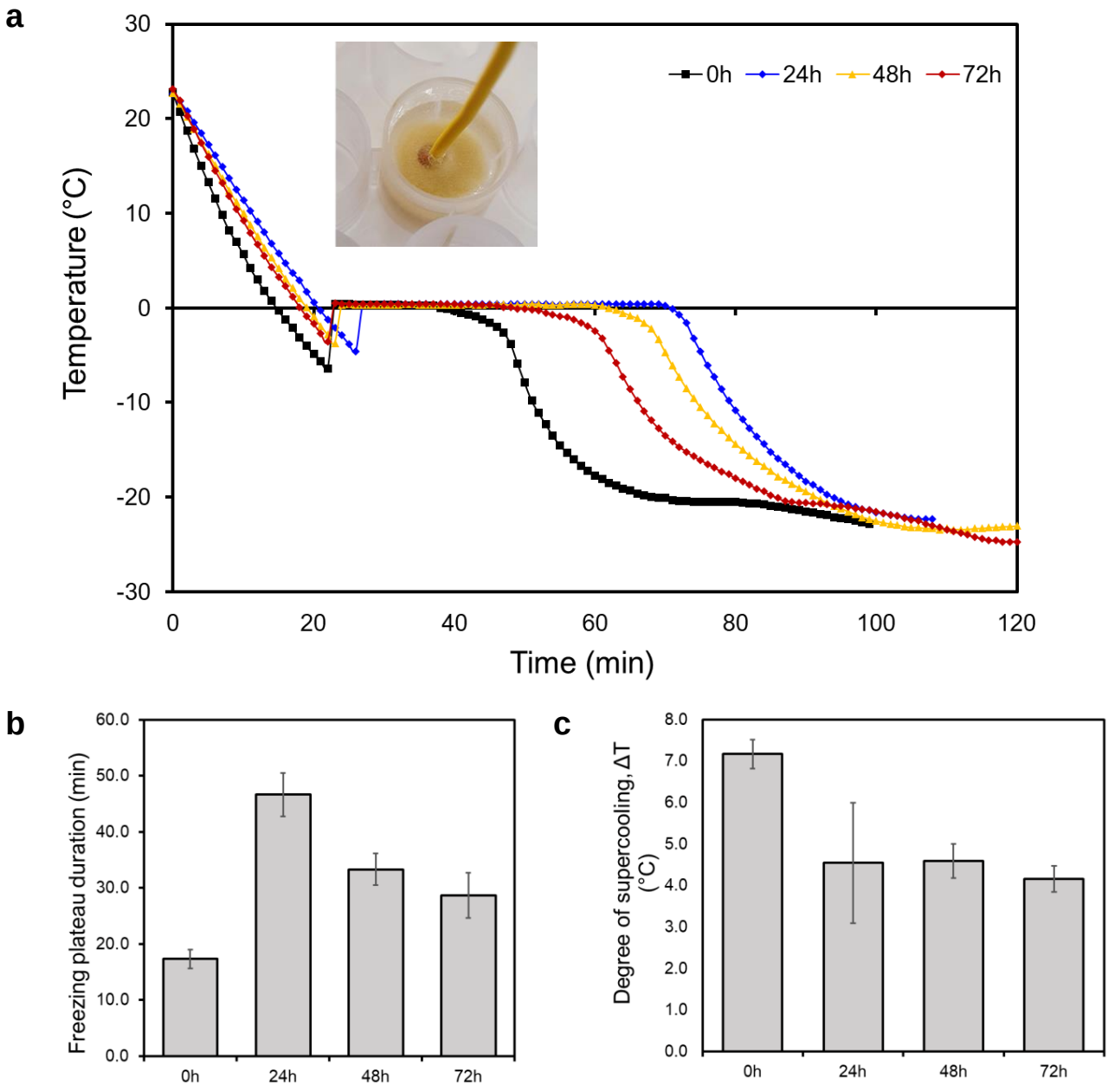

Figure 4.6. a) Temperature profile of 10 % w/v KOH microgels during freezing in -20°C freezer. Inset: Thermocouple electrode submerged in pollen microgel. b) Duration of freezing plateau. c) Degree of supercooling.

both material density and compressive Youngs' modulus of the respective resulting sponges (Figure 4.7a, b). The decrease in density was expected due to degradation of the exine and intine as KOH hydrolysis progresses. While the compressive mechanical strength was reduced, presumably due to softer pollen particles, there was a recorded increase in Young's modulus for 48 h sponge. This spike could possibly be due to an optimized interplay between softness of the pollen microgel particle and the level of interparticle interaction. Prolonged incubation of 72 h saw a reduction in compressive mechanical strength again, possibly due to the increasing influence of the reduced modulus of the pollen microgel particle. The ability of the sponges to absorb water was also characterized by submerging dry sponges into water for 5 min before weighing the wet weight. There was progressive increase in amount of water absorbed when microgel slurries of progressively longer duration of incubation was used, before plateauing at 48 h onwards (Figure 4.7c). Given that the pore sizes of the sponges appeared similar under SEM (Figure 4.5), the difference in amount of water absorption would be due to the increase in hydrophilicity of the sponges, probably resulting from the increase in free hydroxyl group as a result of the increasing de-esterification. Characterization of the hydrophilicity via a goniometer was unsuccessful due to absorption of water into the pollen material (not shown).

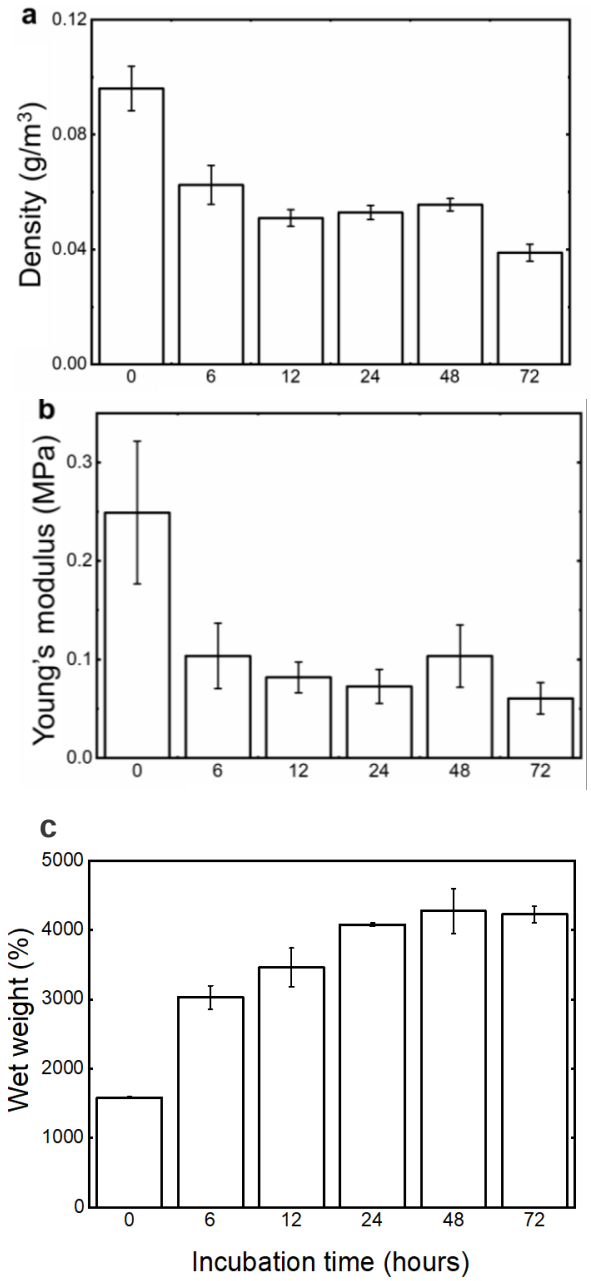

Figure 4.7. Physical characterization of bare pollen sponges after various KOH incubation times.[304] a) Density, b) Young's modulus and c) wet weight values of pollen sponges that had been prepared using the standard fabrication protocol with 0, 6, 12, 24, 48, and 72 h KOH incubation time durations during the second incubation step.

4.3.3 Influence of freezing rate

To evaluate the influence of freezing rate on the morphology of the fabricated sponge scaffolds during the freeze-casting stage, 48 h microgels in multi-well plates were frozen overnight in respective freezers at −20 °C or −80 °C, or at −196 °C by floating the plate on a vessel of liquid nitrogen for 30 min to induce patterning of the pollen scaffold wall resulting from ice crystal growth.[306,307] This method utilizes the magnitude of differences in temperature between ambient and the freezer to vary the freezing rate.[308,309] Therefore the slowest freezing rate would be when the microgel was placed in the -20 °C freezer, and the fastest freezing rate was experienced when the microgel was subjected to the liquid nitrogen bath. The rate of freezing determines the size of the ice crystal, with faster freezing rates leading to formation of smaller ice crystals due to an increased rate of nucleation of ice crystals.[308]

Robust homogenous sponges were obtained when freeze-casted at −20 °C, as indicated by relatively smooth, partially delaminated walls that are advantageous for high levels of surface attachment (Figure 4.8). These morphological features stand out in comparison to the typically observed, highly porous walls of 3D sponge scaffolds formed from fibril-like natural materials,[310,311] and the use of highly uniform pollen grains in this fabrication strategy provides a similar templating function to colloidal microparticles used in designing inverted colloidal crystal scaffolds.[312] Sponges obtained at -80 °C freezing were noticeably softer and did not have pores that were as homogenous. Furthermore, the pore sizes were also noticeably reduced in size, and this was expected due to the more rapid freezing and smaller ice crystals. Sponges obtained from freeze-casting at -196 °C had almost no defined pores, following the trend. More interestingly, no integrated pore wall was observed, and the discrete spherical pollen was explicitly observed via SEM. These sponges were fragile and crumbled upon handling. The retention of the spherical

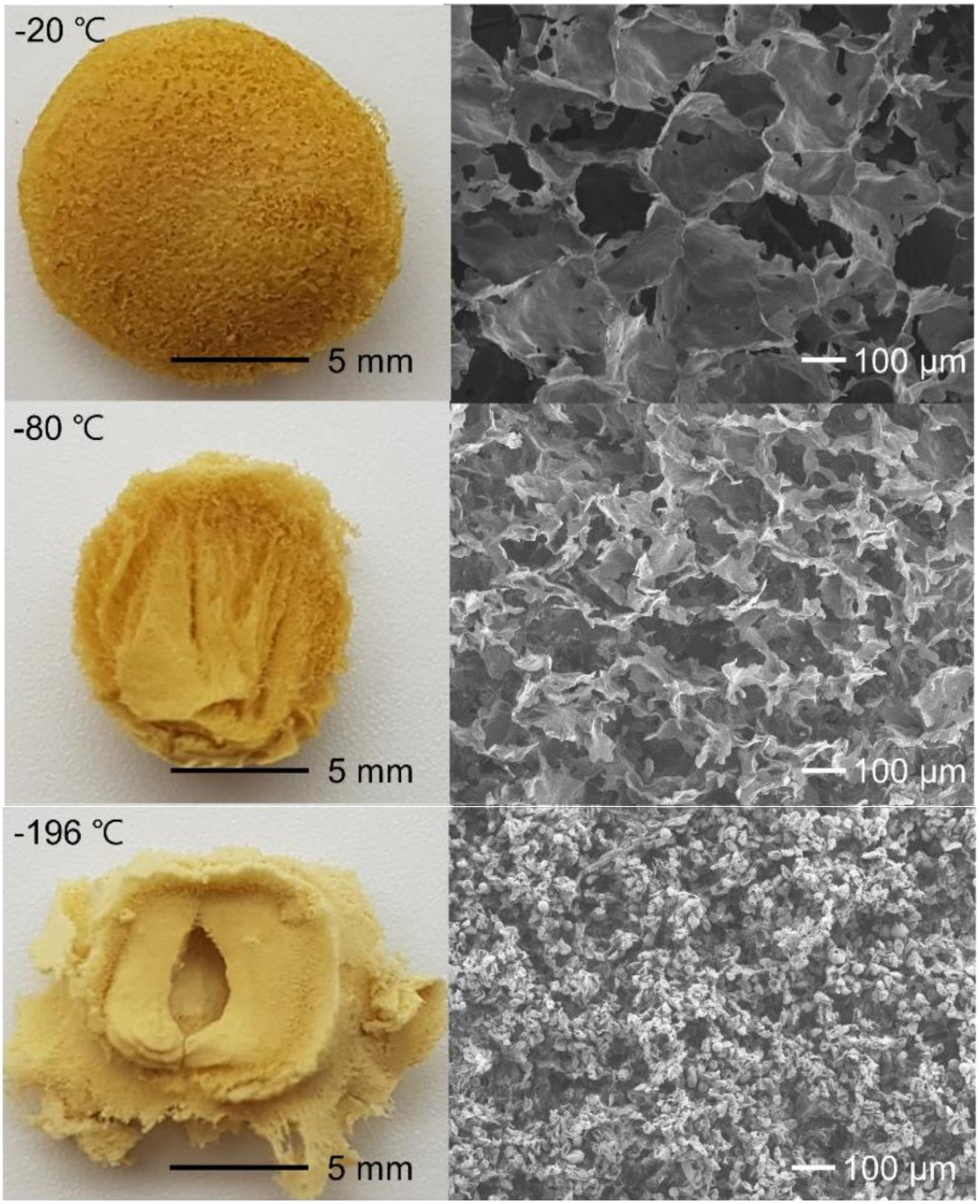

Figure 4.8. Photographs and SEM images of pollen sponges prepared using different temperatures during the freeze-casting process (-20, -80, and -196 ℃) to vary freezing rates.[304]

morphology of the pollen grain at a rapid freezing rate is indicative of inadequate force by the growing ice crystals to compress the pollen particles at the freezing front. The reduced interparticle interaction, seen by greater distances between pollen particles would be the result of the extensive nucleation sites from rapid cooling, thus increasing the grain boundary network and leading to a thin distribution of pollen particles per unit area. Both these factors resulted in sponges that were excessively brittle and powdery. This would thus parallel the earlier observation of naïve defatted pollen's inability to form sponges even at slow freezing rates, which is a result of inadequate compressive force by the growing ice crystal to overcome the stiffness of pollen particles and compress them together at the freezing front.

4.3.4 Influence of swelling state of microgel

To study the influence of the state of microgel swelling on the morphology of fabricated scaffold, microgels were first resuspended in a medium of varying pH, namely pH 4, 7 and 10. pH 4 was chosen as the lower range to exclude any possibility of pollen rupture at extremely low pH (as earlier observed for 90 h-incubated pollen microgels at pH 2), while pH 10 was chosen as the upper range as this was the pH where most of the microgels characterized exhibited their maximum swollen state (Figures 3.14, 3.15 and 3.16). Furthermore, within the pH range of 4 to 10, there is a positive correlation between the increase in pH and the swollen size of the discrete microgels. Given the difference in bulk volume at the different pH, the amount of microgel suspension used for the casting of each sponge was maintained at the equivalent of 0.2 g weight of defatted pollen, of which pH 4 would have the least volume (Figure 4.4b). Sponges fabricated from microgel suspensions under pH 4 conditions exhibited a flat and packed morphology, as compared to the plump and cushiony appearance of those derived from pH 7 and 10 (Figure 4.9). Furthermore, pH

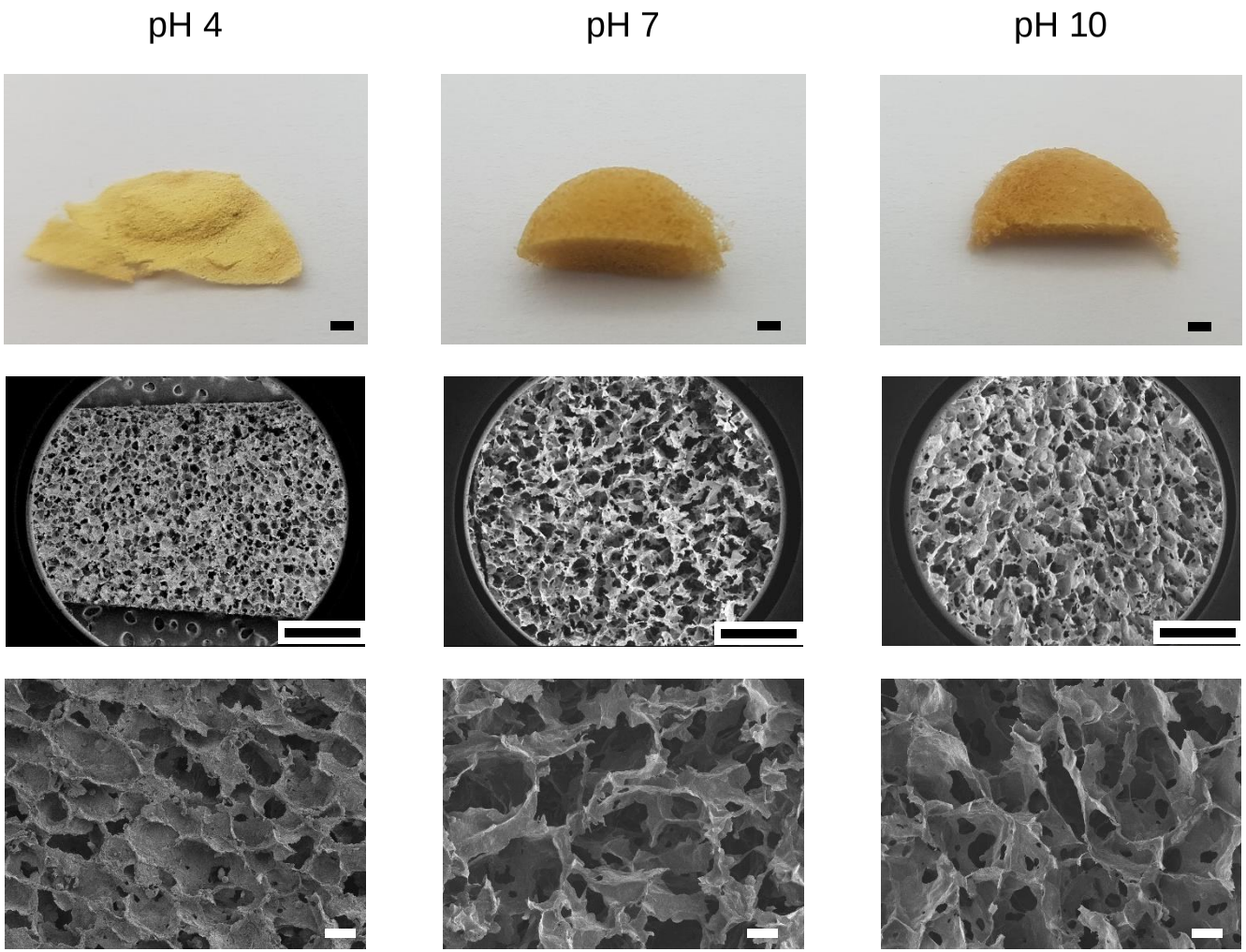

Figure 4.9. Photographs and SEM images of pollen sponges prepared using microgels suspensions at pH 4, 7 and 10 prior to freezing. Black scale bars: 1 mm. White scale bars: 100 µm.

4 sponges were fragile upon handling, with cracks observed after slight flexion of the sponge. SEM cross-section of the sponges show stark differences between the respective sponge morphology. pH 4 sponges exhibited the smallest pore size, despite the same freeze-drying conditions. This could be attributed to the lower volume of pH 4 microgel suspension, leading to a higher freezing rate. Furthermore, the walls of the pore had a significantly rougher topography, with the periphery of the discrete pollen grain and the spikes being visible. This observation was similar to when pollen microgel had a higher modulus, due to lower duration of incubation. It thus can be inferred that when the pH of the microgel slurry was lowered to pH 4, the associated shrinkage of the pollen microgel led to an increase in the modulus of the pollen microgel, thus exhibiting the wall topography and the resulting physical brittleness. In comparison, the pore walls of sponges fabricated from pH 10 microgel suspensions exhibited a smooth appearance and was more seamless than when microgel suspensions of pH 7 was used. This was likely due to a low modulus of the pollen microgels as a result of the maximum swollen state of the microgel, thus allowing greater compression and integration by the force of the growing ice crystals.

These results show that the physical properties of the fabricated sponges can be conveniently modulated and tailored to suit various applications by using microgels of specific incubation durations, casting slurries of specific pH to influence the microgel swell state or choosing appropriate freezing conditions. The physical properties of the resultant pollen sponge positively correlate to the modulus of the pollen microgel particles.

4.3.5 Mechanism of microgel interaction for scaffold wall formation

It had been previously reported that the interparticle bonding between pollen microgels were thought to be due to hydrogen bonding.[305] However, no conclusive study has been performed to explore the actual mechanism of how the pollen microgels interact with each other. Given that pollen sponges that were immersed were able to retain their morphology indicates that hydrogen bonds are not the primary interparticle interactions, but a more robust chemical bond, likely to be covalent bonding, holds the particles. Understanding of the pollen interaction would thus be necessary to allow the possibility of scaling up, currently limited by the lyophilization step.

The mechanism of interaction between pollen microgels that make up the sponge pore walls were investigated. Given that the pollen sponges were able to form via the freeze-drying method, and that soft pollen microgels formed sponges readily with smooth seamless pore walls, it was hypothesized that the force generated on the freezing front of the growing ice crystals during freeze-casting was able to sufficiently compress adjacent pollen microgel particles to close proximity that allowed efficient interparticle conjugation occurs to permanently form the pore wall, and that removal of ice within the pore would not affect the integrity of the pore wall as long as it remains submerged. This would mean that a freeze-thawing process would be sufficient to form pollen sponges without the need for lyophilization. Removing reliance of lyophilization step would be advantageous as it is a very energy intensive process, leading to high operational costs and consequently low scaleup potential.[296] Previous studies using cellulose have shown that freeze-thawing was able to achieve robust scaffolds, although this method would not allow post-fabrication drying to obtain dry scaffolds due to collapse of pores as a result of surface tension from the water evaporation.[313] However, this was not observed for the pollen microgels as pollen microgel slurry frozen at -20 ºC reverted to discrete microgel particles to become a slurry again

after it was left to thaw at room temperature (Figure 4.10). While it was possible that surface tension of the water solvent during the process of melting was able to overcome any formed interparticle bond, this would suggest that the freeze-dried formed sponges would crumble upon being wetted and dried, which was not observed. Nevertheless, these results show that a robust bond was not formed solely by the compression of pollen particles.

To investigate the influence of hydrophilicity of microgels on interparticle interactions, reduction of the hydrophilicity of the microgel to disrupt bound water surrounding the microgel was performed. Pollen microgels were coated with a hydrophobic layer of norbonene (Appendix 4.1) to disrupt the interactions between pollen grain and water molecules (Figure 4.11a). The resultant pollen microgels were observed to be of smaller diameter, likely due to the reduction of water absorption (Figure 4.11b,c). Freeze-drying of the prepared pollen-norbonene microgels did not yield a sponge, characterized by its brittleness upon handling. Although it was possible that the decrease in swell size and the corresponding increase in stiffness may contribute to the reduction of bond formation, the magnitude of brittleness indicates that hydrophilicity of microgels plays a more significant role in the pore wall and sponge formation. This result further supports that compression by the freezing front of growing ice crystals on its own was inadequate to stimulate interparticle bond formation, and that the lyophilization process was essential.

Beyond the sublimation of ice in the primary drying stage, lyophilization also removed bound water in the secondary drying stage. Bound water is water tightly bound to the particle, and is thus unable to participate in the ice crystal formation during the freezing process.[314-316] Given that removal of ice crystal via thawing was seen to be inadequate in forming a sponge, the removal of bound water was thought to be the essential process for formation of interparticle bond between pollen microgel, although it is believed that freeze-drying process does not influence the final

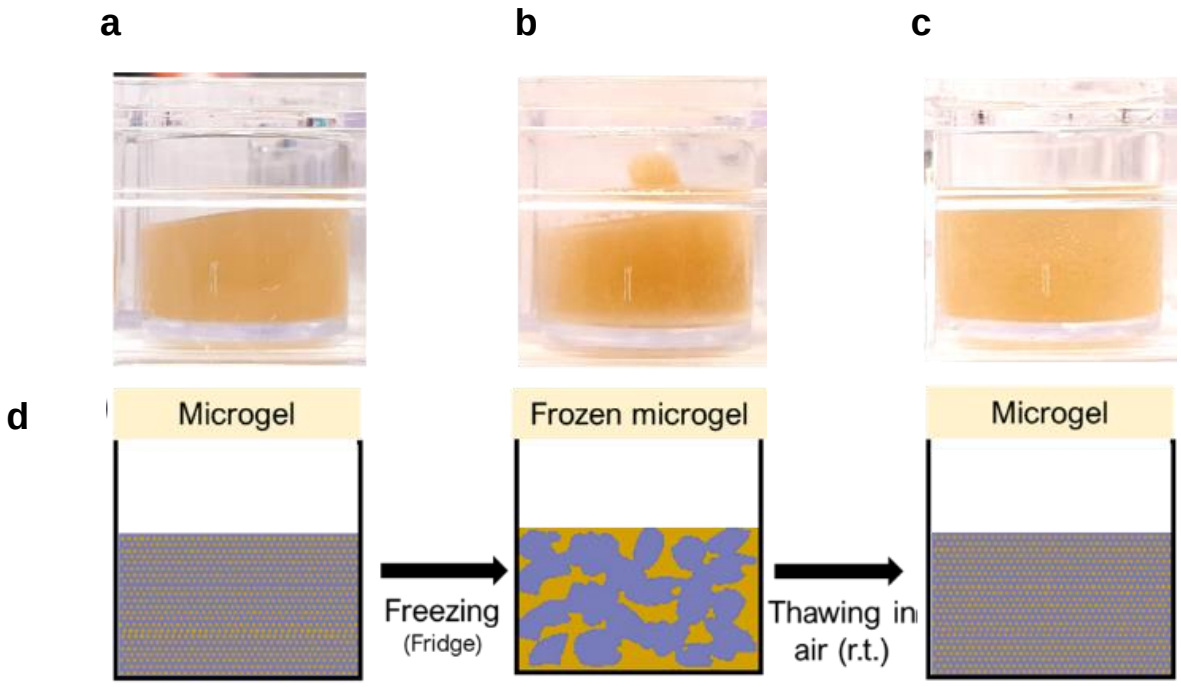

Figure 4.10. Images of 24 h incubated pollen microgel slurry a) before freezing, b) after freezing, c) after thawing at room temperature. d) Schematic of pollen microgel slurry during freeze-thaw process.

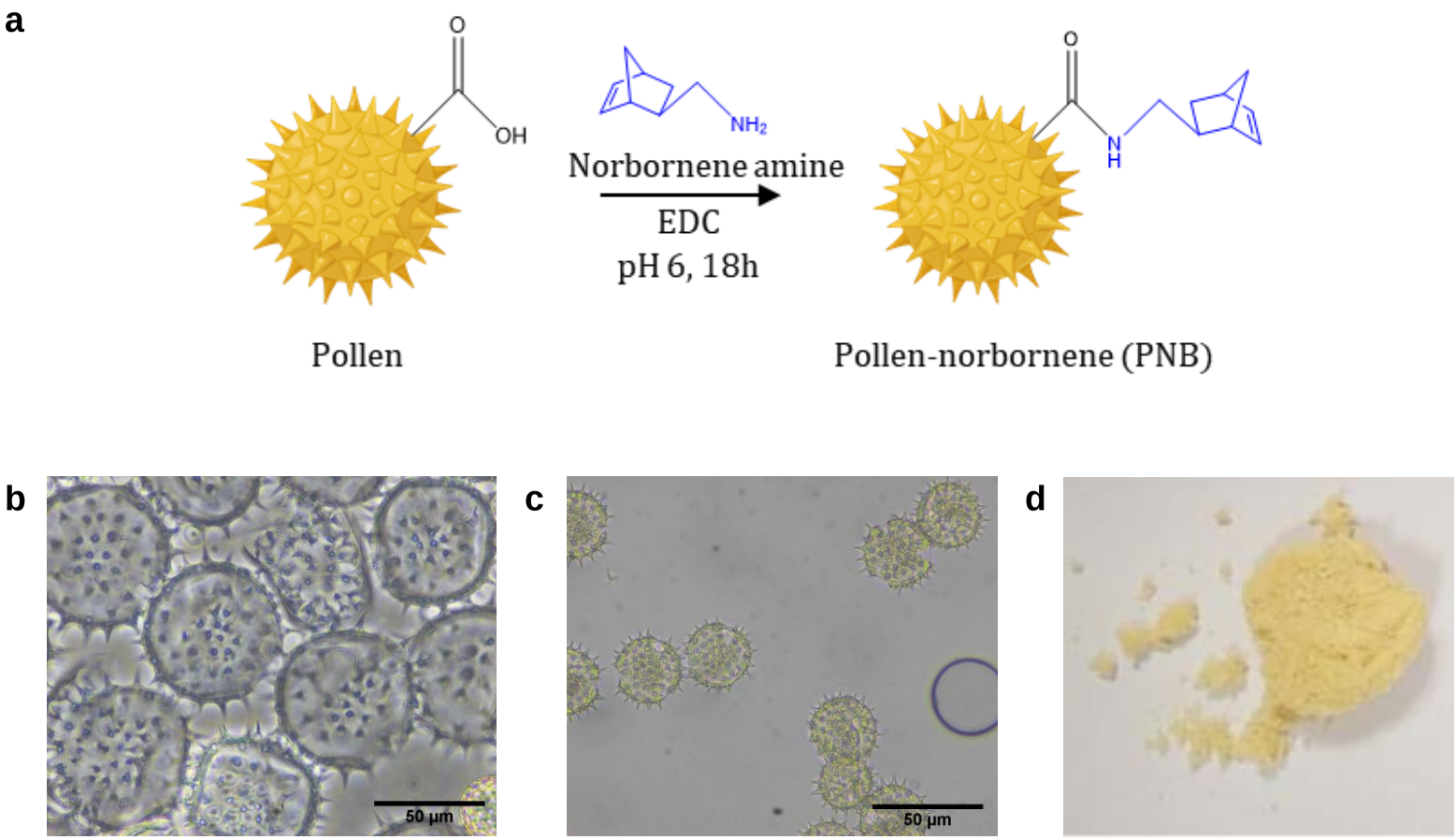

Figure 4.11. a) Synthesis schematic of pollen-norbonene. Pollen microgel b) before and c) after norbonene conjugation. d) Freeze-dried pollen-norbonene was brittle and was unable to form a robust sponge.

microstructure of the scaffolds.[164] Thus, it is hypothesized that gradual removal of the bound water would lessen the absolute distance between adjacent microgel surfaces. Coupled with water's high surface tension, the process of capillary action as the water evaporates and bringing adjacent surface together would be akin to 'zipping' of the walls of adjacent microgels as the bound water gets removed during the secondary drying stage of the lyophilization process. In addition, the possibility of pollen microgels to be able to bond to neighboring pollen microgels during the gradual drying process of 2D pollen sheet fabrication at ambient conditions[305] indicates that removal of bound water to a level that matches the ambient humidity was sufficient to bring two microgel surfaces within the threshold proximity that allow robust interactions to occur.

To test this hypothesis, thawing of frozen pollen microgel in excess of ethanol, a water miscible solvent of significantly lower surface tension, was performed. As soon as the ice crystals surrounding the pollen microgel recedes to expose the microgel surface, solvent exchange between bound water and the miscible solvent would occur via diffusion. Given that the solvent is in excess and assuming that every microgel particle is physically connected as a network, there will be a continuous solvent exchange until all the bound water is replaced with ethanol, and this exchange may proceed faster than the thawing process given that the bound solvent would be more mobile. The relatively low surface tension of ethanol would lead to a thinner solvent shell around each microgel, thus translating to a greater proximity between adjacent microgels surface. If this proximity falls below the threshold distance for interactions to occur, a chemical bond would be formed, and the pore wall would remain intact upon complete thawing of the ice crystal within (Figure 4.12).

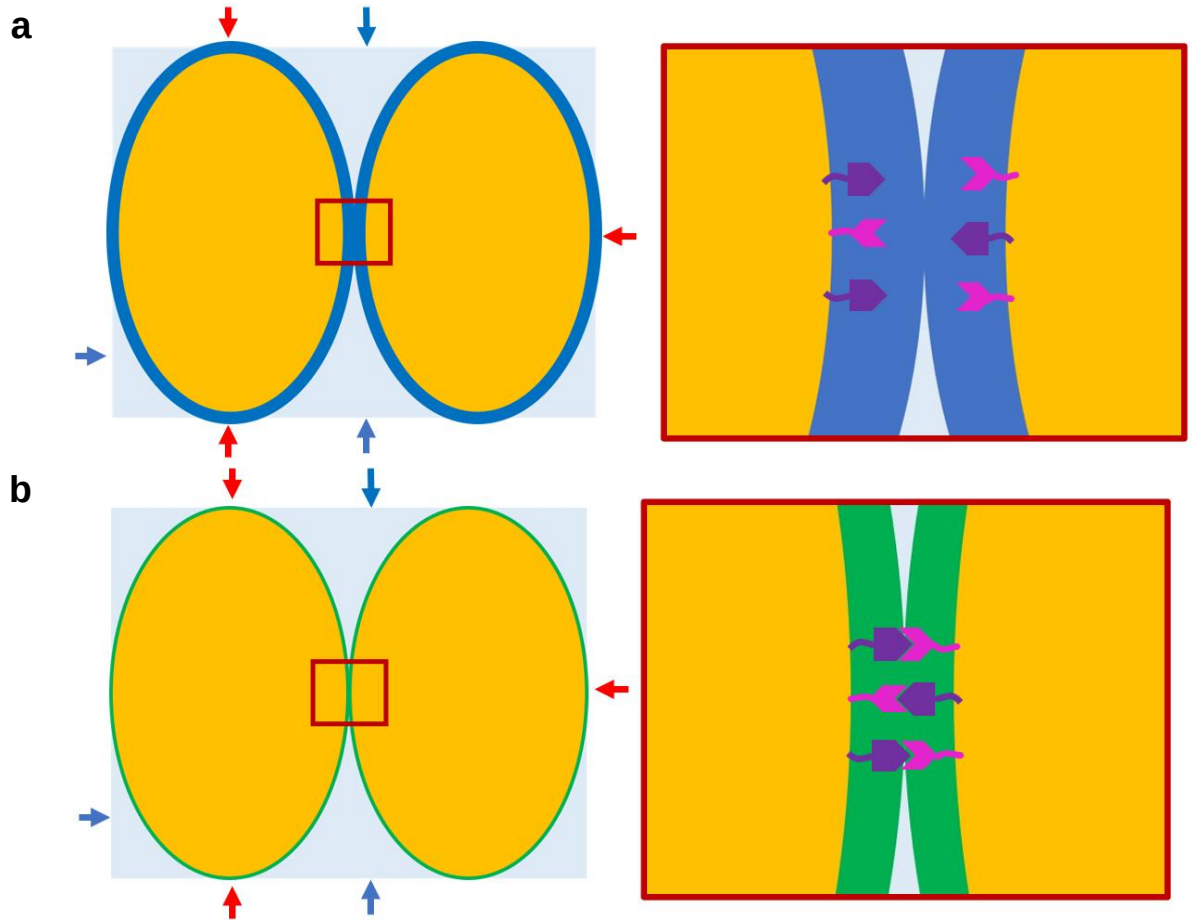

Figure 4.12. Schematic of bound solvent shell around adjacent pollen microgels. Red boxes represent magnified view of interface between adjacent pollen microgels. Blue arrows represent receding ice surface during process of thawing. Red arrows represent regions of microgel exposed as ice recedes. A) blue boundary represents water shell during thawing in water solvent and b) green boundary represents ethanol shell upon thawing in ethanol solvent and solvent exchange. Purple and pink symbols represent complementary chemical moieties present on pollen microgel surface.

Frozen pellets of pollen microgel slurry were removed from the freezer and immediately submerged in excess ethanol in increasing concentrations (25, 50, 75, 100 % v/v) for 2 h at room temperature until the pellet was completely thawed. Upon complete thawing, intact pollen scaffolds were obtained (Figure 4.13a-d). With the exception of 100 % ethanol thawed scaffold, all the other scaffolds swelled upon complete thawing, although they retained their scaffold morphology. Upon gentle agitation of the still submerged scaffolds, the mechanical stability of the scaffolds was apparent with varying ethanol concentration (Figure 4.13e-g), with scaffold formed via thawing in 25 % ethanol to be the weakest and completely disintegrating while scaffold formed in 100 % ethanol to be most robust, remaining intact despite shaking. The trend of increasing mechanical stability with increasing ethanol concentration would be due to a progressively lowered concentration of water and thus a lowered surface tension of the resultant liquid that makes up the bound solvent. This would hence allow the adjacent microgel particles to be closer together and increase the amount of interparticle interactions, and hence improved the stability of the scaffold.

This 100 % ethanol thawed scaffold was slightly smaller than scaffolds obtained via the lyophilization method, showing that complete exchange of water with ethanol solvent leads to overall contraction of the scaffold. In addition, the scaffold was springy and stable enough to be lifted by forceps to be transferred to a bath of excess dI water. Almost immediately, swelling of the scaffold was observed (Figure 4.13h). Overnight submersion of this scaffold in dI water resulted in a brittle swollen scaffold, which broke into pieces upon handling. To mediate this, 100 % ethanol thawed scaffolds were dried in an oven at 60 °C to evaporate off residual ethanol (Figure 4.14). Upon drying, the scaffolds appeared flat and darker brown (Figure 4.14b). Immersion of these scaffold in water readily reverted the swelling of the scaffold (Figure 4.14c). SEM of the

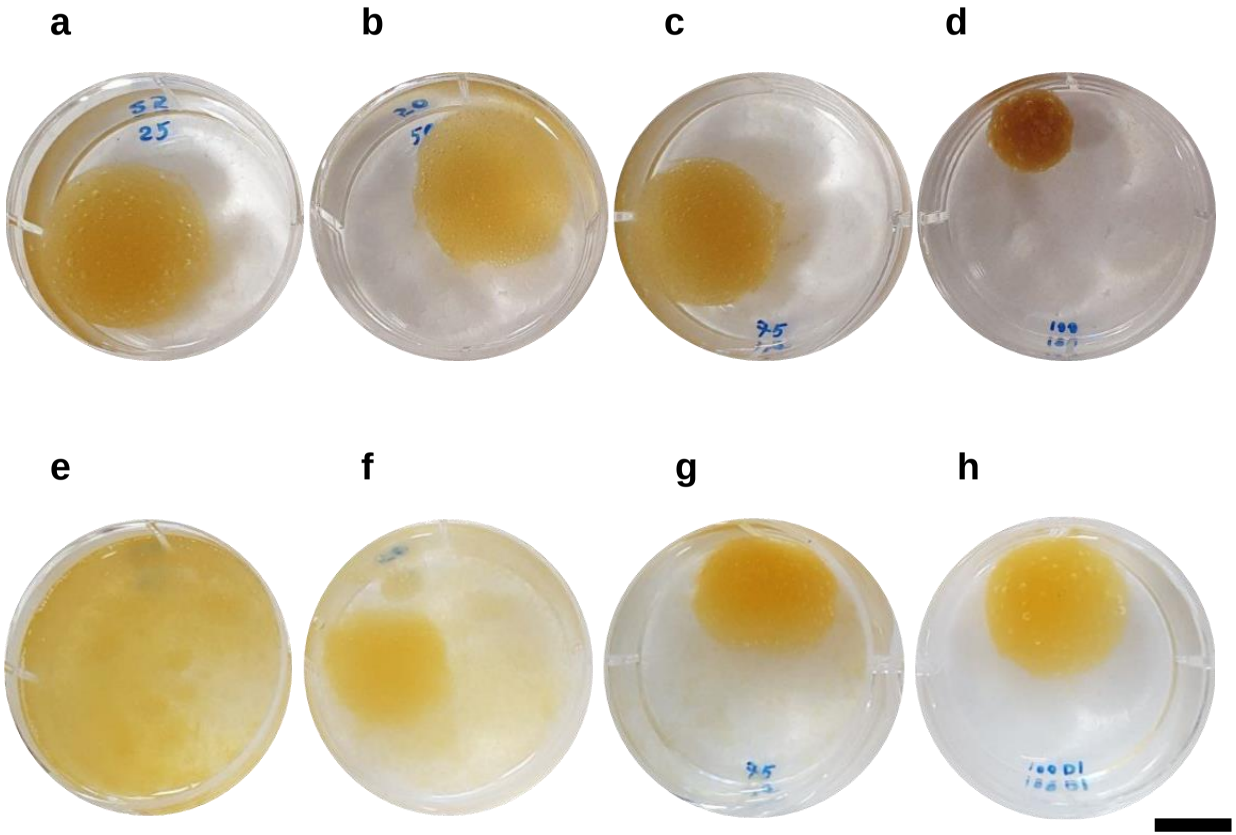

Figure 4.13. Formed pollen scaffolds after 2 h thawing of frozen pollen microgel pellets in a) 25 % b) 50 %, c) 75 %, d) 1 00 % ethanol. Gentle agitation of the still submerged scaffolds show an increasing trend in robustness of the scaffolds, showing e) complete disintegration of scaffolds in 25 % ethanol, f) diffused erosion of scaffold in 50 % Ethanol, g) slight disintegration of scaffold in 75 % ethanol. Scaffold thawed in 100 % ethanol were robust and remained unchanged. h) Transfer of scaffold from 100 % ethanol to 100 % dI water led to an almost immediate and drastic swelling. Scale bar: 1 cm

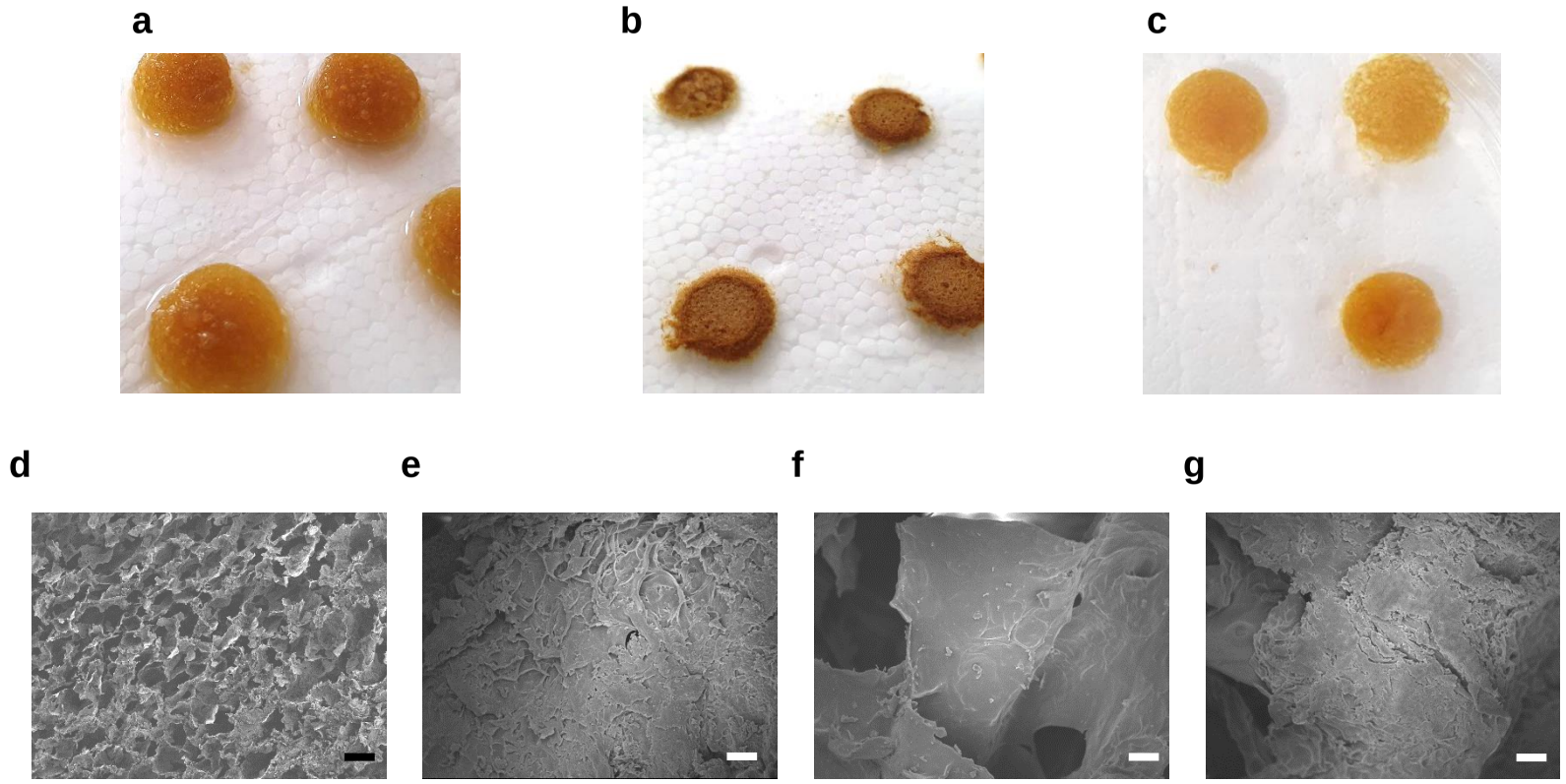

Figure 4.14. a) 100 % ethanol thawed scaffold are robust even when taken out of solvent bath. b) Scaffolds after drying in oven at 60 °C. c) Scaffold reverts to swollen state upon immersion in water. d) scaffold pores are open upon resubmersion and rehydration of dried scaffolds in water. High magnification topography of rehydrated scaffold pore wall after e) 1 h, f) 2 h, g) 4 h drying in oven. Black scale bar: 200 µm. White scale bars: 10 µm.

cross-section of these rehydrated scaffolds show that the pores were efficiently reopened to recover the porosity of the scaffold (Figure 4.14d). Varying oven drying times of the 100 % ethanol thawed scaffold from 1 h to 4 h led to pore wall of varying topography. 1 h drying gave rise to scaffolds with pore walls still displaying some spikes characteristic of the pollen, while 4 h drying lead to walls that appear to be cracked, probably due to excessive dehydration. 2 h drying time was optimal as it led to very smooth scaffold pore wall (Figure 4.14e-g). Furthermore, 100 % ethanol thawed scaffold dried for 2 hours and rehydrated with water could be dried again at ambient conditions to its flattened state and rehydrated to its swollen state repeatedly for over 10 cycles without any noticeable disintegration or increase in fragility. Furthermore, these scaffolds did not swell to the same extent as 100 % ethanol thawed scaffold that were immediately submerged in water (without oven drying stage).

100% ethanol thawed scaffolds that were immediately placed in water immediately swelled likely due to the bound solvent of ethanol reverting to water, and thus leading to an overall increase in absolute distance between adjacent microgels due to water's higher surface tension. This would therefore lead to loss of any present interparticle interaction between the microgel surfaces, and thus the whole scaffold becomes increasingly fragile the longer the scaffold was submerged in water. Removal of the bound ethanol via oven drying similarly leads to zipping of the microgel surfaces, leading to direct and permanent bond of two microgel surfaces. Given that the scaffolds remained robust even upon repeated and extensive durations of rehydration, it would thus be logical to theorize that the interparticle bonds involved would not be easily overcome by the surrounding water, and that these bonds were stronger than the bonds formed with water. This is further proof that the bonds involved in the interactions of microgel surfaces that allow the scaffold pore wall formation was not simply physical hydrogen bonds, but likely to be a chemical bond,

and would likely be interparticle ester bonds that were brought about by the generation of free carboxyl and hydroxyl groups during the process of pectin de-esterification during the microgel synthesis process. Nevertheless, hydrogen bonds would still contribute to the general stability of the scaffold in its dry state, as observed by swelling of pollen sheet in high humidity.[305] To investigate if solvent exchange of water with ethanol was sufficient to promote bond formation, pollen microgel was pipetted directly into excess ethanol (Figure 4.15). However, no interparticle interactions were observed, and the pollen microgel become dispersed. This shows that the interparticle interaction of microgel surface requires that the adjacent microgels to remain sufficiently immobilized to each other and allow the complete solvent exchange to occur before the forces that immobilize the particles can be removed. In these examples, this immobilizing force is provided by the ice crystals.

Thawing of freeze-casted biopolymers in ethanol in place of lyophilization has been shown previously on cellulose scaffolds. However, the motivation for that was due to the collapse of the scaffold leading to a permanent sealing of the pores as a result of the withdrawing water during the thawing and subsequent evaporation process.[313] This shows that in their system, the materials that form the scaffold were able to for strong interparticle interaction during the freeze-casting stage itself. However, for the pollen, freeze-casting alone was insufficient as the slurry of discrete microgels were obtained upon thawing (Figure 4.10).

This series of studies show that sufficient pressure brought about by the freezing front of growing ice crystals during freezing to physically compress adjacent microgels, coupled with the further enhanced proximity of the microgel surface brought about by the removal of bound water was essential to form robust bonds between microgel surfaces. Absence of either of these would not allow the microgel surfaces to be in sufficient proximity for interactions to occur. While the

growing ice crystals physically brings pollen microgel particles within close contact, the distance was still limited by the presence of bound water that remains unfrozen. Thinning this bound water by means of solvent exchange with ethanol stimulates bond formation. However, there appears to exist a threshold of absolute distance that needs to be overcome before the microgels were able to interact permanently, and this involves total removal of bound solvent. Coupled with the capillary action of drawn solvents, would be reminiscent of 'zipping' of interface of adjacent microgels. Furthermore, the drawing away of the bound solvent needs to occur while the interface is immobilized (in this study, the interface was maintained by the ice crystals holding the microgels in place), and this can be achieved either by lyophilizing a frozen pollen microgel pellet, or via thawing the pellet in excess ethanol before oven drying.

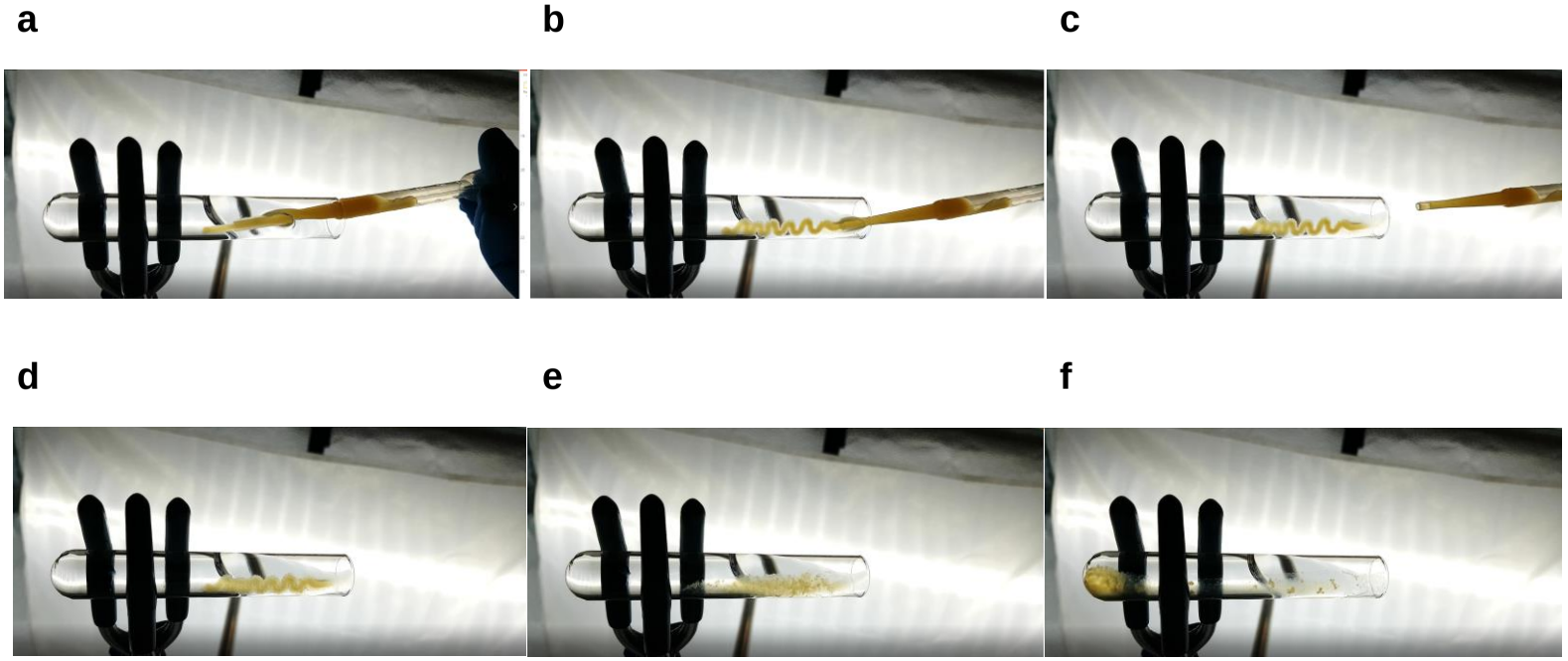

Figure 4.15. Time-lapsed images of bottom-up view of pollen microgel slurry dispensed into excess 100 % ethanol in a glass tube. Glass tube was held stationary via a retort clamp at 30° elevation. a,b) Dispensing of pollen microgel on wall of tube, c) region of first dispensing has its boundary appearing dispersed, d-f) continued dispersion of the microgel slurry.

4.4 Conclusion

The physical properties of fabricated pollen sponges had been shown to be dependent upon several variables during the microgel preparation process, the pH-induced swell state of the resultant microgel as well as the freezing rate of the pollen microgel slurry. Soft, and fully swollen microgels coupled with slow freezing rate was shown to form favorable scaffold pore wall, determined by the absence of visible particle boundary or spikes, and well-defined pore shapes. Pollen microgel synthesized with an incubation duration of 24 h was required to reduce the modulus of the pollen enough to be overcome by growing ice crystals, with pollen microgels incubated for 48 h giving robust pollen sponges. Pollen microgels at pH 7 was sufficient in giving homogenous pores in the formed scaffolds and freezing at -20 °C was optimal to achieve ice crystals with enough pressure to overcome the microgel stiffness. Faster freezing rates gave rise to brittle scaffolds with weak walls and poorly defined pores.

Analysis of the mechanism of microgel interactions shows that physical compression of microgels and removal of bound water solvent while still under compression was necessary for the bond formation between adjacent microgels. The removal of bound solvent, coupled with the capillary action brought about by surface tension leads to a ‘zipping’ of the interface of pollen microgel surfaces. The results here provide further insights on the mechanism of bond formation between two pollen particles. Complete understanding of the mechanism would allow efficient application of pollen microgels as modular building blocks for the formation of higher order structures for diverse fields ranging from sensors, tissue engineering, drug delivery and possibly energy storage applications.

This chapter is a slightly modified version of "Influence of Chemical and Physical Change of Pollen Microgels on Swelling/De-Swelling Behavior." (Macromolecular Rapid Communications 41, no. 21 (2020): 2000155) and "Colloid-Mediated Fabrication of a 3D Pollen Sponge for Oil Remediation Applications." (Advanced Functional Materials (2021): 2101091) and has been reproduced here with the permission of the copyright holder.

4.5 References

164 Shao, Hanaor, Shen & Gurlo. Freeze Casting: From Low-Dimensional Building Blocks to Aligned Porous Structures—A Review of Novel Materials, Methods, and Applications. *Advanced Materials* **32**, 1907176, doi:https://doi.org/10.1002/adma.201907176 (2020).

170 Baheti, Kumar & Bansal. Excipients used in lyophilization of small molecules. *Journal of Excipients and Food Chemicals* **1**, 1135 (2016).

270 Fan, Park, Shi, Zhang, Liu, Song, Chin, Ibrahim, Mokrzecka & Yang. Transformation of hard pollen into soft matter. *Nature communications* **11**, 1-10 (2020).

275 Parre & Geitmann. More than a leak sealant. The mechanical properties of callose in pollen tubes. *Plant Physiology* **137**, 274-286 (2005).

276 Qu & Meredith. The atypically high modulus of pollen exine. *Journal of The Royal Society Interface* **15**, 20180533 (2018).

277 Zeng & Tan. AFM nanoindentation to quantify mechanical properties of nano-and micron-sized crystals of a metal–organic framework material. *ACS applied materials & interfaces* **9**, 39839-39854 (2017).

278 Hutter & Bechhoefer. Calibration of atomic-force microscope tips. *Review of scientific instruments* **64**, 1868-1873 (1993).

279 Neumann. Determining the elastic modulus of biological samples using atomic force microscopy. *JPK Instruments Application Report*, 1-9 (2008).

280 Fan, Hwang, Ibrahim, Ferracci & Cho. Influence of Chemical and Physical Change of Pollen Microgels on Swelling/De-Swelling Behavior. *Macromolecular Rapid Communications* **41**, 2000155, doi:https://doi.org/10.1002/marc.202000155 (2020).

296 Zhang. *Ice templating and freeze-drying for porous materials and their applications*. (John Wiley & Sons, 2018).

297 MacKenzie. Factors affecting the mechanism of transformation of ice into water vapor in the freeze-drying process. *NYASA* **125**, 522-547 (1965).

298 Oetjen & Haseley. *Freeze-drying*. (John Wiley & Sons, 2004).

299 Franks & Auffret. *Freeze-drying of Pharmaceuticals and Biopharmaceuticals*. (royal Society of Chemistry, 2008).

300 Ohtake, Izutsu & Lechuga-Ballesteros. *Drying Technologies for Biotechnology and Pharmaceutical Applications*. (Wiley Online Library, 2020).

301 Rey. *Freeze-drying/lyophilization of pharmaceutical and biological products*. (CRC Press, 2016).

302 Zheng, Winnubst, Velianti, Fang & Salamon. Manipulation of Sintering Behavior by Initial Freeze Pressing an Aqueous Alumina Suspension. *Advanced Engineering Materials* **13**, 77-81, doi:https://doi.org/10.1002/adem.201000199 (2011).

303 Vidovskii. Experimental determination of pressure during ice expansion. *Hydrotechnical Construction* **6**, 791-792, doi:10.1007/BF02377294 (1972).

304 Hwang, Ibrahim, Deng, Jackman & Cho. Colloid-Mediated Fabrication of a 3D Pollen Sponge for Oil Remediation Applications. *Advanced Functional Materials*, 2101091 (2021).

305 Zhao, Hwang, Yang, Fan, Song, Suresh & Cho. Actuation and locomotion driven by moisture in paper made with natural pollen. *Proceedings of the National Academy of Sciences* **117**, 8711-8718 (2020).

306 Xie, Zhou, Bi, Yin, Wan & Sun. Large-range control of the microstructures and properties of three-dimensional porous graphene. *Scientific reports* **3**, 1-6 (2013).

307 Chen, Huang, Li, Yu & Yan. Preparation of a macroporous flexible three dimensional graphene sponge using an ice-template as the anode material for microbial fuel cells. *Rsc Advances* **4**, 21619-21624 (2014).

308 Hobbs. *Ice physics*. (Oxford university press, 2010).

309 O'Brien, Harley, Yannas & Gibson. The effect of pore size on cell adhesion in collagen-GAG scaffolds. *Biomaterials* **26**, 433-441, doi:https://doi.org/10.1016/j.biomaterials.2004.02.052 (2005).

310 Wu, Li, Zhang, Zhong, Xu, Mao, Wang & Sui. Thiol–ene click reaction on cellulose sponge and its application for oil/water separation. *Rsc Advances* **7**, 20147-20151 (2017).

311 Guo, Chen, Lyu, Fu & Wang. Highly flexible cross-linked cellulose nanofibril sponge-like aerogels with improved mechanical property and enhanced flame retardancy. *Carbohydrate polymers* **179**, 333-340 (2018).

312 Zhang, Wang, Eghtedari, Motamedi & Kotov. Inverted-colloidal-crystal hydrogel matrices as three-dimensional cell scaffolds. *Advanced Functional Materials* **15**, 725-731 (2005).

313 Antonini, Wu, Zimmermann, Kherbeche, Thoraval, Nyström & Geiger. Ultra-porous nanocellulose foams: A facile and scalable fabrication approach. *Nanomaterials* **9**, 1142 (2019).

314 Meryman. Review of biological freezing. *Cryobiology* **1**, 114 (1966).

315 Kuprianoff. in *Conference on Fundamental aspects of the Dehydration of Foodstuffs.* 14-23.

316 Caurie. Bound water: its definition, estimation and characteristics. *International Journal of Food Science & Technology* **46**, 930-934, doi:https://doi.org/10.1111/j.1365-2621.2011.02581.x (2011).

Chapter 5 Optimization and Functionalization of Pollen Sponge for Oil Remediation Applications

Chapter Abstract

There is tremendous interest in developing 3D scaffolds from natural materials for a wide range of healthcare, energy, photonic, and environmental science applications. To date, most natural materials that are used to make 3D scaffolds consist of fibril structures; however, it would be advantageous to explore the development of scaffolds from natural materials with distinct supramolecular structures. Herein, the fabrication of a mechanically responsive pollen sponge that exhibits tunable 3D scaffold properties and is useful for oil remediation applications is reported. By using pollen-based microgel particles as colloidal building blocks, the sponge fabrication process is optimized by tuning the processing conditions during freeze-drying and thermal annealing steps. Stearic acid functionalization transforms the pollen sponge into a hydrophobic scaffold that can readily and repeatedly absorb oil and other organic solvents from contaminated water sources, with similar performance levels to commercial, synthetic polymer-based absorbents and an improved environmental footprint.

Keywords: pollen, sponge, scaffold, water treatment, oil absorbent, sustainable.

5.1 Introduction

3D microporous scaffolds are highly versatile materials that can be used in a wide range of healthcare, energy, photonic, and environmental science applications.[317-321] Most design progress in the field has focused on using synthetic polymers such as polyurethane (PU), polydimethylsiloxane (PDMS), and poly(3,4-ethylenedioxythiophene) (PEDOT).[322-325] Rationally tuning the chemical composition and other molecular features of synthetic polymers enables scaffolds to have advantageous properties, including low density, high surface area, high absorption capacity, and excellent mechanical properties.[326-330] The functionality of polymer-based scaffolds can be further enhanced by incorporating inorganic components such as 1D and 2D nanomaterials, e.g., carbon nanotubes and graphene, that can modulate various scaffold properties, including conductivity, porosity, and compressibility.[331-333]

Simultaneously, there are growing concerns about the environmental impact of synthetic polymer-based scaffolds and a desire to instead use natural materials such as cellulose, collagen, and silk that are affordable, plentiful, renewable, and biodegradable.[23-26] Attention to this topic falls in line with current trends to view renewable biomass as a promising source for developing advanced materials.[27-29] To date, most natural materials that are used to make 3D scaffolds consist of fibril structures, while it would be advantageous to explore the development of scaffolds from natural materials that self-assemble into other types of supramolecular structures. One excellent candidate is natural pollen grains, which are renewably produced in abundant supply by plants and possess many attractive material properties, including hollow microcapsule structure, chemical stability, mechanical strength, species-specific architectural details, and high monodispersity among each species of pollen grains.[11,43-47]

For a long time, the basic structural properties of pollen grains were regarded as unchangeable, in large part owing to the presence of sporopollenin—considered the "diamond of biopolymers"—in the outer layer of the pollen shell called the exine.[334] As such, most investigations focused on exploring discrete pollen grains as markers for environmental dating (palynology) as well as drug delivery carriers.[335-337] More recently, it was reported that hard pollen grains are in fact pliable and can be converted into soft, stimuli-responsive microgel particles based on a simple chemical process akin to soapmaking, which adjusts the mechanical properties of the pollen shell layers.[270] This discovery has opened the door to developing self-actuating paper sheets derived from self-assembling microgel particles and further motivates the exploration of advanced material fabrication strategies to create 3D scaffolds composed exclusively of pollen grains.[305] It is also advantageous that pollen grains—both in the natural form and as isolated exine capsules—possess a myriad of useful functional groups, including extensive surface hydroxylation, that can facilitate covalent and noncovalent attachment depending on the application.[334,338]

In this thesis chapter, the fabrication of a mechanically-responsive pollen sponge that exhibits tunable 3D scaffold properties for oil remediation applications was explored. Oil remediation is an increasingly important goal due to increasing oil pollution from various industries worldwide.[339] By using pollen-based microgel particles as colloidal building blocks, the sponge fabrication process was optimized by tuning the processing conditions during the hydrolysis duration, freezing, lyophilization and thermal annealing steps. Subsequently, the simple attachment of stearic acid—one of the most common fatty acid molecules in nature—transformed the pollen sponge into a hydrophobic scaffold that could readily and repeatedly absorb oil and other organic solvents from contaminated water sources, with similar performance levels to commercial, synthetic polymer-based absorbents and an improved environmental footprint.

5.2 Methods

5.2.1 Defatting of Sunflower Bee Pollen Granules

Sunflower bee pollen granules were purchased from GTL Biotech (Xi'an, Shaanxi, China) and defatted by first dispersing 250 g of the sample in deionized water (1000 mL) and stirring. The suspension was filtered through nylon mesh with 200 µm pore size (ELKO Filtering Co., USA). The dispersed pollen in the filtrate was collected via vacuum filtration using a Büchner funnel lined with filter paper. The collected pollen was refluxed in 500 mL acetone (Aik Moh, Singapore) at 50 °C for 3 h under continuous stirring. The acetone in the suspension was removed by vacuum filtration as before and the collected pollen was washed with fresh acetone followed by vacuum filtration. This washing step was repeated five times. The acetone reflux and washing processes were repeated. The resulting pollen powder was transferred into a glass petri dish and air-dried overnight in a fume hood.

The dried pollen powder (~120 g) was suspended in 200 mL diethyl ether (Sigma Aldrich, Singapore) and continuously stirred at room temperature for 2 h. The diethyl ether in the suspension was removed by vacuum filtration, and the collected pollen was washed with fresh diethyl ether followed by vacuum filtration. This washing process was repeated three times. The collected pollen was suspended in diethyl ether (200 mL) again and continuously stirred at room temperature overnight, and the washing process was repeated. The resulting pollen powder was transferred to a glass petri dish and air-dried overnight in a fume hood. The dry defatted pollen was collected in a plastic bottle and stored in a desiccator cabinet under low humidity conditions until use.

5.2.2 Sponge Fabrication

Defatted pollen was initially transformed into microgel particles following previous protocols[270] with slight modifications. 2 g of defatted sunflower pollen was suspended in 20 mL of 10 % w/v KOH solution in a polytetrafluoroethylene (PTFE) round-bottom flask. The suspension was continuously stirred and refluxed for 2 h at 80 °C. The pollen was isolated via filtration using a nylon mesh with 20 µm pore size, and the collected pollen was rinsed with 20 mL of 10 % w/v KOH followed by filtration. The rinsing and filtration process were repeated a total of three times. The rinsed pollen was transferred to a 50 mL conical centrifuge tube and topped up to a total volume of 20 mL with fresh KOH solution. The solution was resuspended using a vortex mixer at high speed for 2 min and was incubated at 80 °C in an oven (Memmert, Schwabach, Germany) for defined periods of time (6, 12, 24, 48, and 72 h).

After incubation, the pollen particles were isolated via filtration using a nylon mesh with 20 µm pore size. The collected pollen was rinsed with copious amounts of deionized water followed by filtration. The rinsing and filtration processes were repeated until the pH of the suspension reached 7, as measured by using pH-indicator strips (Millipore Sigma, Burlington, MA). The resulting neutral-pH pollen microgel suspension was transferred to a 50 mL conical centrifuge and centrifuged at 3000 rpm (Beckman Coulter, Allegra X-15 R, rotor SX4750) for 5 min. The residual water supernatant was then decanted.

The as-prepared pollen microgel was then pipetted into individual wells of Nunc 24-well tissue culture dishes (Thermo Scientific, Rochester, NY), and the plates were centrifuged at 3000 rpm (Beckman Coulter, Allegra X-15 R, rotor SX4750µ) for 15 min to remove any residual water. The plates were then frozen in the freezers overnight or in liquid nitrogen for 15 min. The plates containing the frozen microgel were lyophilized (Labconco, Kansas City, MO) under 0.008 mbar

vacuum for 48 h to obtain the bare pollen sponges. Heat-treated pollen sponges were prepared by incubating the bare pollen sponges in a furnace (XST-3-0-12-1V2, Thermcraft, USA) at the specified temperature for 30 min. Coated pollen sponges were prepared by immersing heat-treated sponges in ethanolic solutions of stearic acid for 60 min and left to dry at room temperature overnight. Individual pollen sponge samples were weighed, and geometrical dimensions were measured via Vernier calipers to determine their density. Contact angle measurements were performed using an Attension Theta Optical Tensiometer (Biolin Scientific AB, Sweden) via the sessile drop method. 20 µL of deionized water was dispensed onto the pollen sponge surface, and the shape of the drop was recorded by high-resolution imaging. For analysis, the drop shape was fitted to the Young–Laplace equation, with a duration of 10 s for each measurement.

5.2.3 Mechanical Testing

The compressive Young's modulus values of the pollen sponges were analyzed using a DMA Q800 dynamic mechanical analyzer (TA Instruments, USA) in a controlled force mode. The pollen sponge samples were held between parallel-plate compression clamps and were then compressed from 0.1 to 18.0 N at a ramp rate of 1 N/min. The compressive Young's modulus was calculated from the slope of the elastic region of the stress–strain curve, between 40% and 50% compressive strain. Cyclical compression recovery analyses of the pollen sponges were performed on the MTS Criterion Model 42 instrument (MTS Systems Corporation, USA). Pollen sponges were subjected to 100 cycles of 1 mm/min compression up to the determined compressive strain and 0.01 mm/min decompression back to the original sample height.

5.2.4 *Morphological Analysis of Pollen Sponges*

High-magnification images of pollen sponge cross sections were obtained via field emission-scanning electron microscopy (FE-SEM). Pollen sponges were gently sliced with a sharp blade along the transverse plane and immobilized on the sample holder with carbon tape and sputter-coated with platinum to a thickness of 5 nm (20 mA, 40 s) using a JFC-1600 Auto Fine Coater (JEOL, Tokyo, Japan) to improve the sample conductivity. Thick samples were further held in place using copper tape. Images were taken with a JSM-7600F Schottky microscope (JEOL) at an acceleration voltage of 5 kV. Pollen sponge cross-sectional pore area was determined via measurement of the obtained images via ImageJ (NIH, USA). A minimum of 30 pores showing intact borders was used to calculate the results for each sample.

5.2.5 *Fourier-Transform Infrared Spectroscopy*

FTIR spectroscopic analysis of the pollen sponge was conducted using the PerkinElmer Spectrometer (PerkinElmer, UK) equipped with a diamond cell attenuated total reflection (ATR) accessory. Reflectance infrared spectra were obtained between 4000 and 600 cm^{-1} by 16-times scanning per measurement. For each sample, three different areas were measured. Background spectra were collected prior to sample readings and subtracted from each sample spectrum automatically by Spectrum 10 Software (PerkinElmer, UK). To correct spectra with sloped baselines and reduce the amount of noise in the spectrum, a baseline correction and smoothing process were conducted after sample measurements using the software.

5.2.6 Oil Absorption Capacity Measurement

Silicone oil ($\rho = 0.971$ g/cm^3, Sigma-Aldrich) and dichloromethane ($\rho = 1.33$ g/cm^3, VWR Chemicals) were mixed with lipophilic Oil Red O dye (molecular weight = 408.49 g/mol, Sigma-Aldrich) for high optical contrast and then mixed with water samples. A coated pollen sponge after drying in an oven at 60 °C for 2 h was used for the testing. To test oil absorption to various oils and organic solvents, the oil absorption capacity (g/g) was calculated by the following equation:

$$\text{Absorption capacity (g/g)} = \frac{w - w0}{w0} \quad (1)$$

where w_0 is the weight of the coated pollen sponge after drying, and w is the weight of the coated pollen sponge after oil absorption. The pollen sponge was immersed into the various oils and organic solvents [toluene ($\rho = 0.865$ g/cm^3, Sigma-Aldrich), chloroform ($\rho = 1.49$ g/cm^3, Sigma-Aldrich), dichloromethane ($\rho = 1.33$ g/cm^3, VWR Chemicals), n-hexane ($\rho = 0.659$ g/cm^3, Sigma-Aldrich), gasoline (Synergy Extra 5000, Esso), silicone oil ($\rho = 0.971$ g/cm^3, Sigma-Aldrich), pump oil ($\rho = 0.859$ g/cm^3, Edwards), motor oil ($\rho = 0.861$ g/cm^3, 7100 10w40, Motul), and coconut oil (Marico) for 5 min.

5.3 Results and Discussion

5.3.1 Fabrication and optimization of robust pollen sponge scaffolds

Figure 1 presents an overview of the pollen sponge fabrication process, starting with the sourcing of natural pollen grains from sunflower plants (*Helianthus annuus*) that had been collected by bees. The natural pollen grains of ~20 μm diameter are microcapsules with a two-layer wall structure that is perforated by apertures, and the entire grain surface is covered with lipidic components commonly referred to as pollen cement (Figure 5.1a and Figure 5.2). To first remove this lipidic cement ("defatting"), the pollen was sequentially rinsed with water, acetone, and diethyl ether (Figure 5.1b). The pollen grains were then refluxed in an aqueous potassium hydroxide solution (KOH, 10 % w/v) at 80 °C for 2 h to remove inner contents, resulting in the pollen shell consisting of just the exine and intine only (Figure 5.1c). As determined previously, pollen sponges obtained via freeze-casting of pollen microgels incubated for 48 h in 10 % w/v KOH, slurry conditions of pH 7 and frozen at -20 °C gave homogenous porosity, seamless pore walls, robustness and the best mechanical strength.

The as-obtained pollen sponges were then briefly heated at 150, 200, 250, or 300 °C for 10 min and sponge structures heated at 200 °C or higher temperatures remained morphologically stable after aqueous hydration and subsequent dehydration (Figure 5.3) without any noticeable collapse in structure associated with capillary forces of the evaporating liquid[296,313]. Sponges heated at 250 °C and beyond not only showed a more intense browning, but also a considerable reduction in size. Thermogravimetric analysis of the sponges showed decomposition above temperatures of 220.08 °C (Figure 5.4). Therefore, a thermal treatment temperature of 200 °C was chosen as the upper limit. Furthermore, the Young's modulus value of the sponge structure upon heating was observed to increase by over twofold of that of the non-heated sponge (Figure 5.5),

indicating increased rigidity of the scaffold wall likely due to heat-induced interparticle sintering or pyrolysis-induced ceramization.[164]

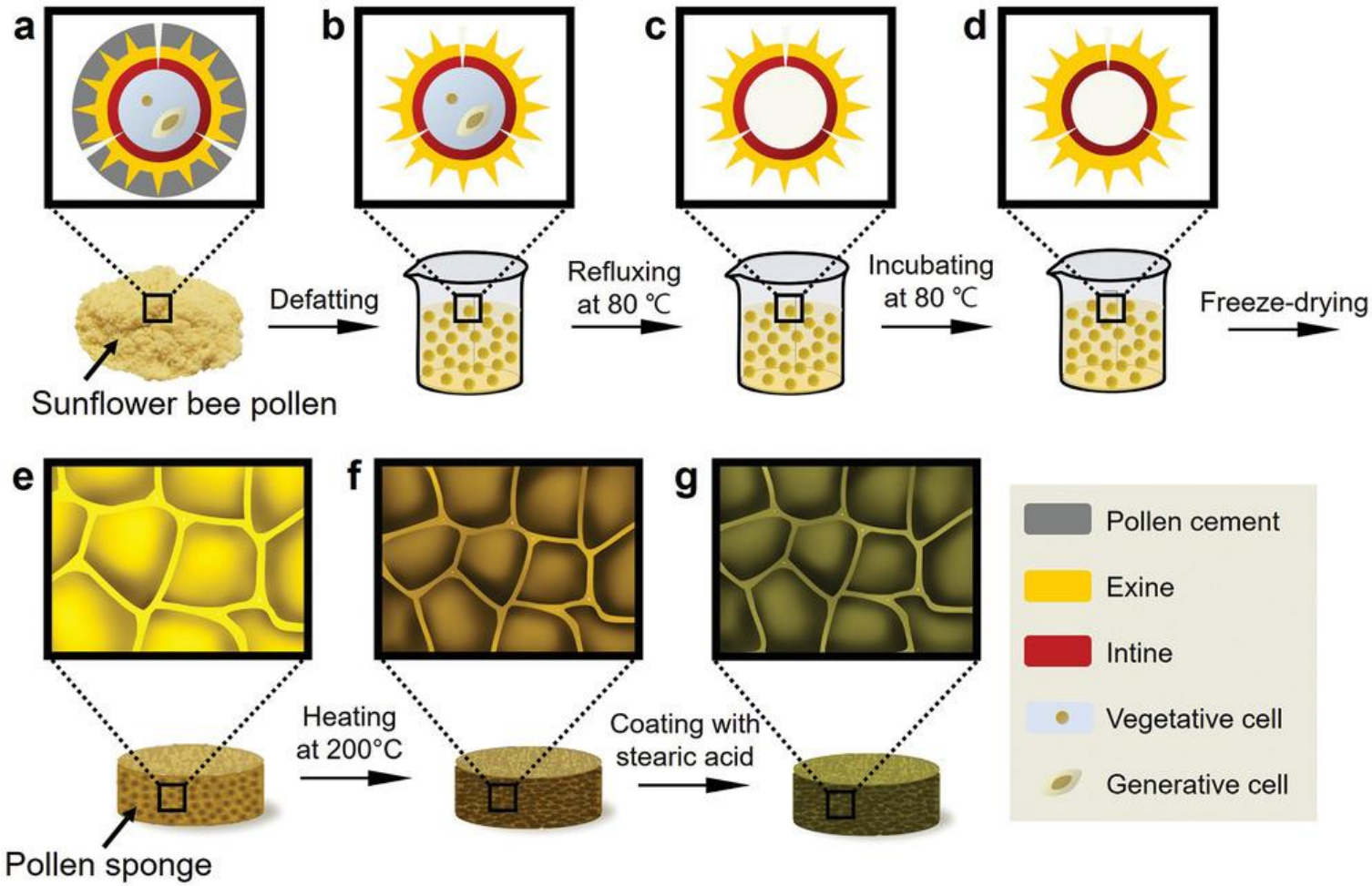

Figure 5.1. Schematic illustration of the step-by-step fabrication process to prepare oil-absorbing pollen sponges.[304]

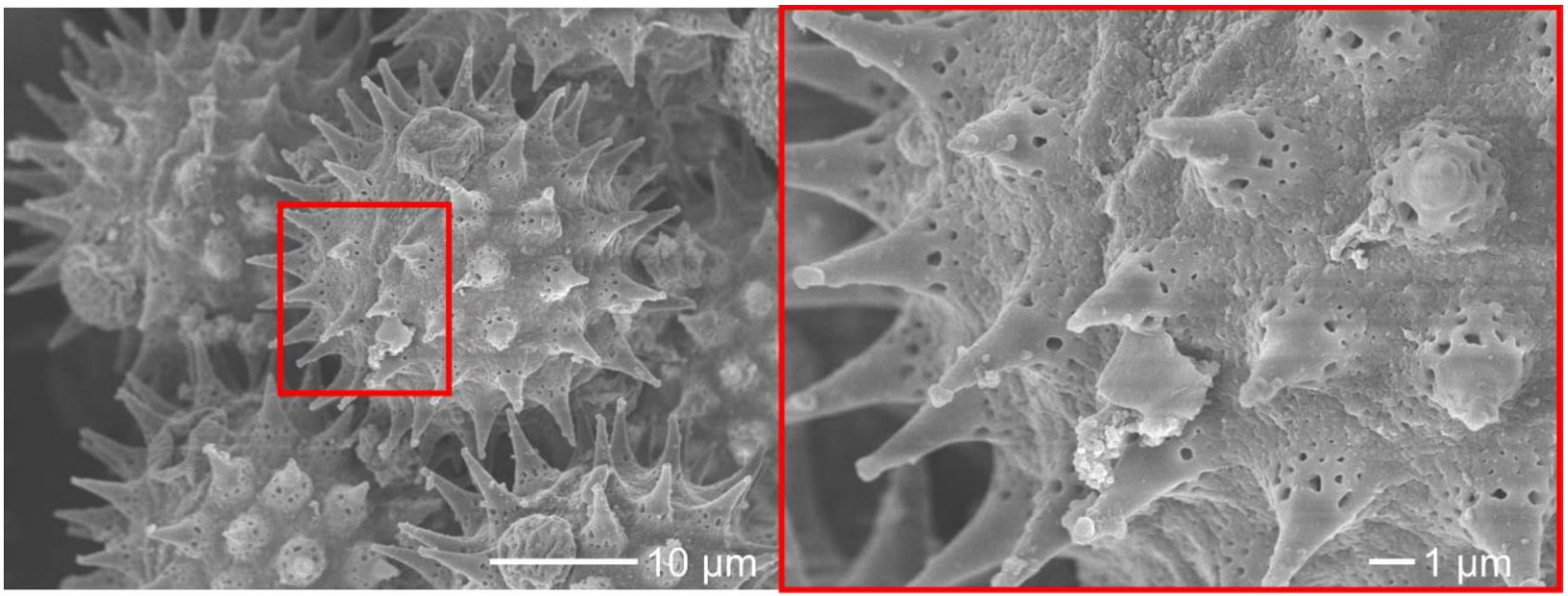

Figure 5.2. SEM image of defatted sunflower pollen particles.[304] The red box corresponds to a magnified image of the selected area.

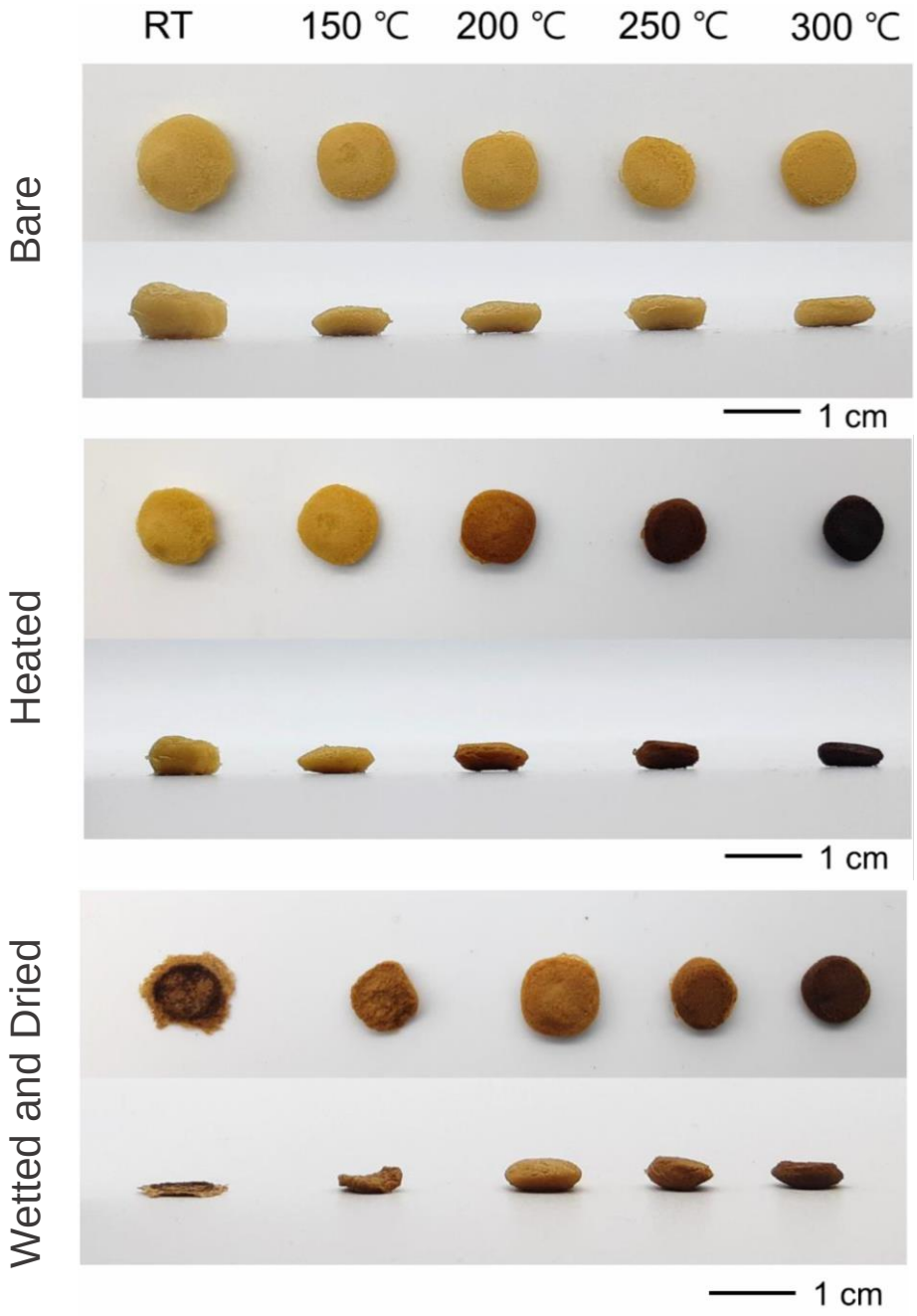

Figure 5.3. Effects of heating on pollen sponge stability upon hydration.[304] Photographs of bare pollen sponges are shown before (top row) and after (middle row) 10 mins heating at the specific temperature, and after subsequent hydration with deionized water and drying (bottom).

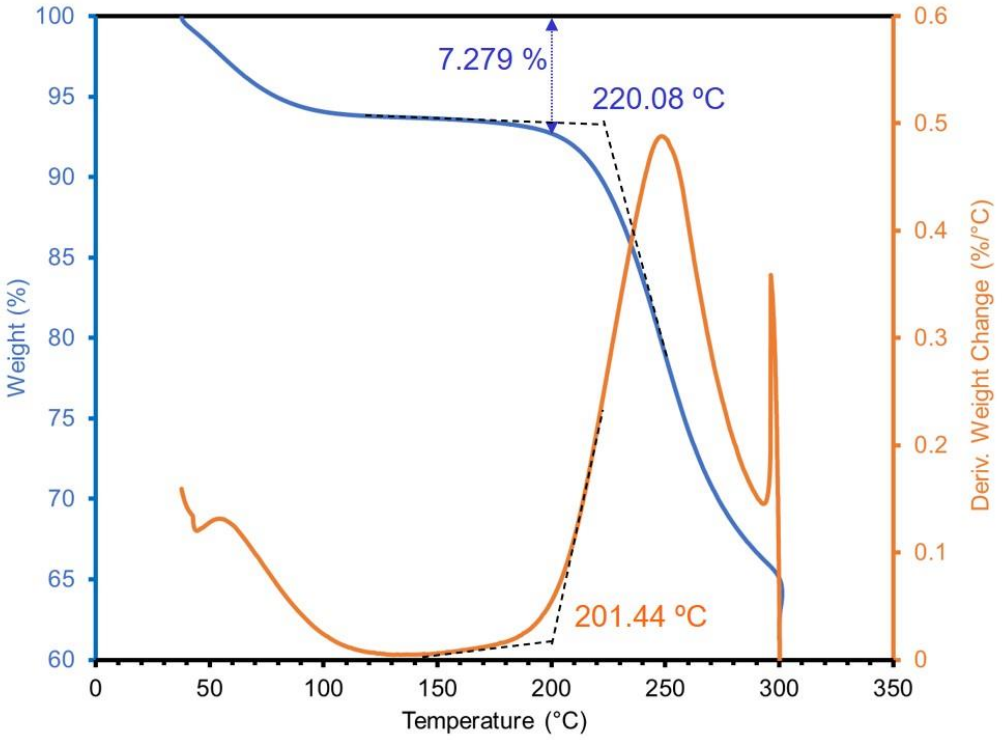

Figure 5.4. Thermogravimetric analysis profile of pollen sponge heated to 300 °C.

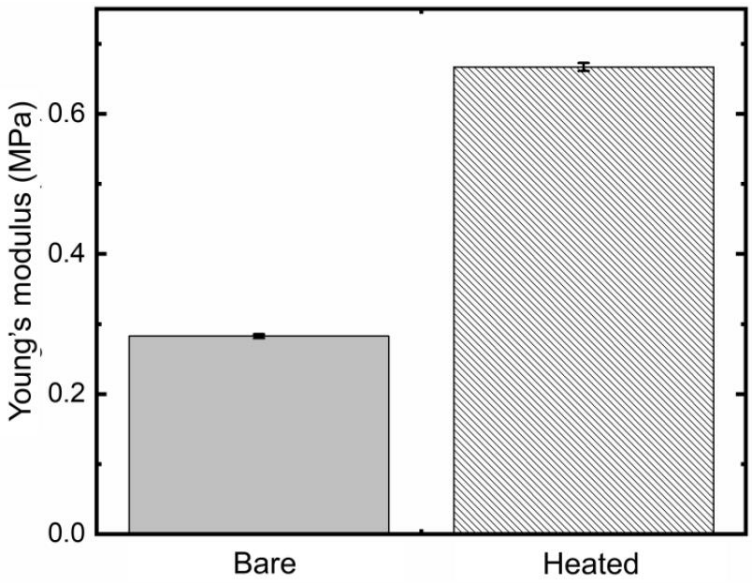

Figure 5.5. Young's modulus value of bare pollen sponge before and after heating.[304] The sample was heated at 200 °C for 10 min.

5.3.2 Sustainable fatty acid coating for optimal pollen sponge hydrophobicity

The fabricated pollen sponges had a water contact angle (WCA) measurement of 100° (Figure 5.6). To imbue increased hydrophobic properties to the sponge to allow it to be used as an oil absorbent, a green and sustainable method of utilizing hydrophobic fatty acid was employed. The 18-carbon saturated fatty acid stearic acid was chosen due to it being one of the most common fatty acids found in nature, following palmitic acid.[340] As stearic acid has a low solubility in water (0.00029 g/100 g at 20 °C), ethanol was utilized as a solvent instead (2.25 g/100 g at 20 °C).[341]

Since the process of stearic acid coating needs to be performed by submerging the pollen sponge into a prepared steric acid solution, the significant increase in rigidity and strength of the sponge, which allows its wetting and subsequent drying without disruption to the sponge morphology, becomes critical. The sponge structure was incubated in an ethanolic solution containing stearic acid for 1 h before being air-dried overnight to allow the stearic acid molecules to attached noncovalently to the sponge walls and render the walls highly hydrophobic.

The fabricated pollen sponges were characterized by SEM imaging before and after heating and after stearic acid functionalization. The bare sponge had a light brown color and highly porous structure owing to lamination of the pollen particles to form the scaffold walls (Figure 5.7 a). Upon heating, the sponge structure assumed a dark brown color while retaining microstructural features of the bare sponge (Figure 5.7 b). After stearic acid coating, the sponge structure had a brown color and maintained the 3D porous architecture along with apparently decreased pore area owing to ethanol-induced shrinkage (Figure 5.7 c). This ethanol-induced shrinkage phenomenon had also been observed on pollen sheets fabricated in the lab.

The effect of stearic acid concentration used to coat heat-treated sponges and the resultant sponge hydrophobicity was investigated. Concentration-dependent increments in sponge

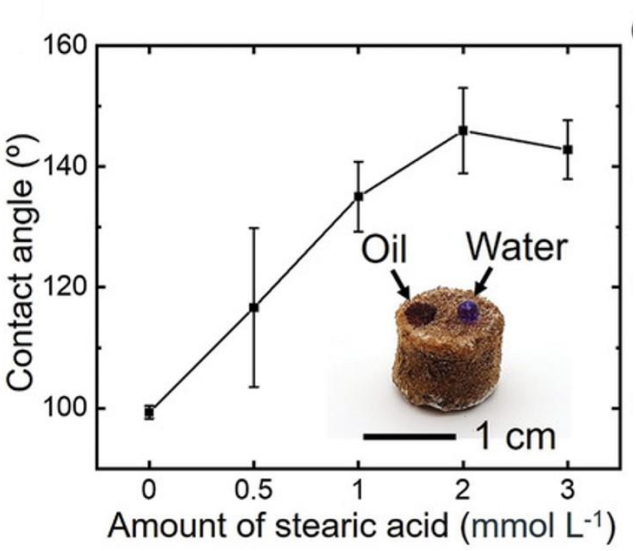

Figure 5.6. Water contact angle of the pollen sponge after coating with different concentrations of stearic acid.[304] Inset illustrates the selectivity of coated sponge to oil. Water droplet has been dyed for visualization purposes.

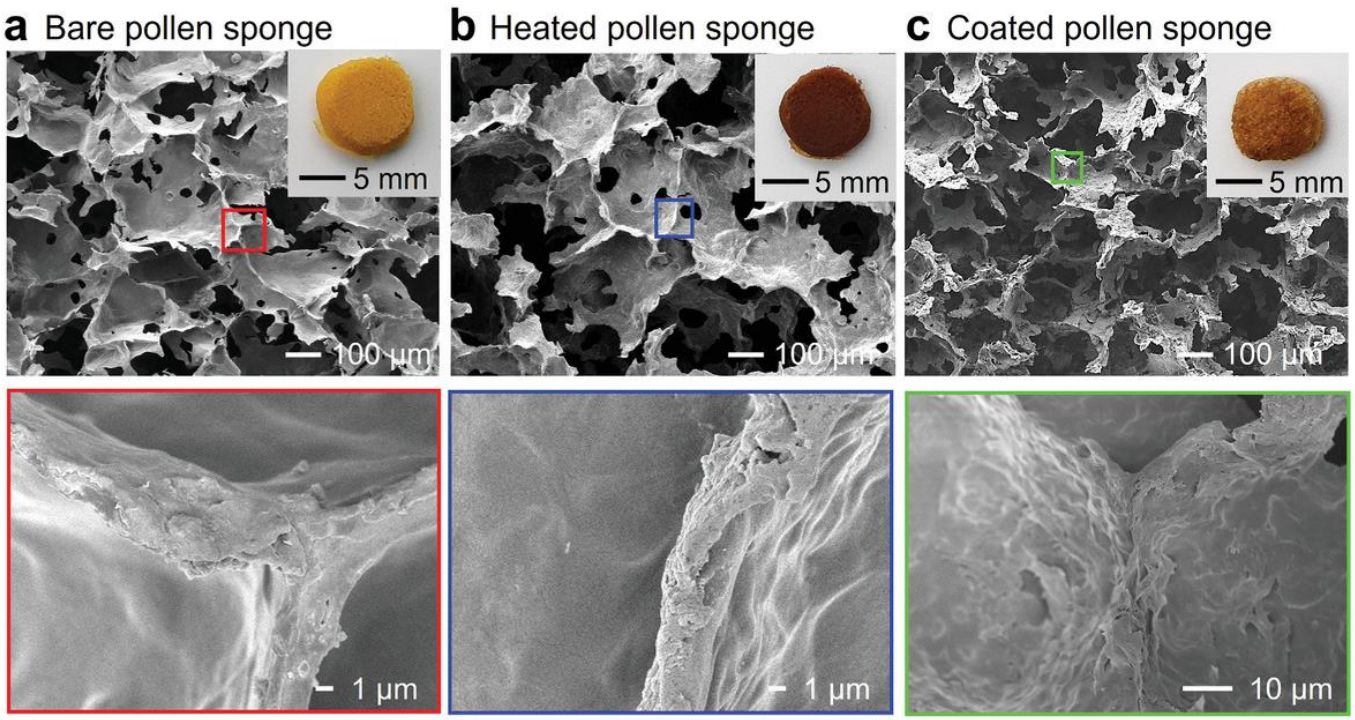

Figure 5.7. Cross-sectional SEM images of a) bare, b) heated, and c) coated pollen sponges.[304] The red, blue, and green boxes correspond to magnified images of the selected areas in each image.

hydrophobicity was observed for up to 2×10^{-3} M stearic acid concentrations and resulted in a maximum WCA of 145° (Figure 5.6), which signifies that the maximum binding capacity of the sponge was reached. At higher concentrations, the hydrophobicity was lower, which may have resulted from stearic acid forming a double layer on the sponge wall surface that would expose hydrophilic carboxylic acid groups.[342,343] Hence, 2×10^{-3} M stearic acid was selected as the optimal coating condition. FTIR spectroscopy experiments were performed to characterize structural changes related to heat treatment and stearic acid coating (Figure 5.8). It was observed that the peaks at 2917, 2849, and 719 cm^{-1}, which are related to C-H bonds, decreased after heating owing to degradation of residual protein and lipid, while the peaks increased again upon stearic acid coating.[287,344,345] In line with these results, cross-sectional SEM images supported that the coated sponges had smaller pore areas than the other sponges (Table 5.1). The coated sponges had a final density around 0.065 g cm^{-3}, which is comparable to the densities of sponges fabricated from bacterial cellulose, graphene, and carbon nanotubes (Figure 5.9).[346]

5.3.3 Absorption and recovery of oil, and reusability of pollen sponges

Another important property of oil-absorbing materials is compressibility, whereby oil-laden sponges can be compressed to release the oil waste and then reused. Mechanical tests were conducted on the coated sponges with varying degrees of compressive strain (20%, 40%, 60%, and 80%, respectively). Figure 5.10 shows sequential photographs of a pollen sponge before compression, 40% compressive strain, and in the recovered state upon release, in which the pollen sponge recovered approximately 90% of its original height. Measurements of the stress–strain curve at compressive strains of 20%, 40%, 60%, and 80% were also performed. The hysteresis

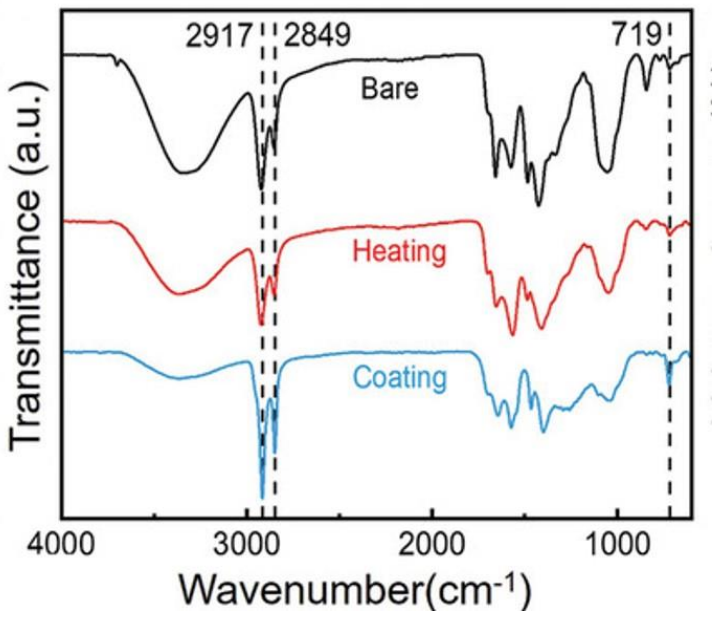

Figure 5.8. FTIR spectroscopic analysis of bare, heated, and coated pollen sponges.[304]

Sample	Density [g/cm^3]	Pore area [µm^2]
Bare	$2.9 \times 10^{-5} \pm 3.0 \times 10^{-6}$	$7.3 \times 10^{4} \pm 1.2 \times 10^{4}$
Heated	$5.1 \times 10^{-5} \pm 8.4 \times 10^{-6}$	$5.7 \times 10^{4} \pm 1.3 \times 10^{4}$
Coated	$6.5 \times 10^{-5} \pm 9.1 \times 10^{-6}$	$3.4 \times 10^{4} \pm 8.2 \times 10^{3}$

Table 5.1. Density and pore area of pollen sponges.[304]

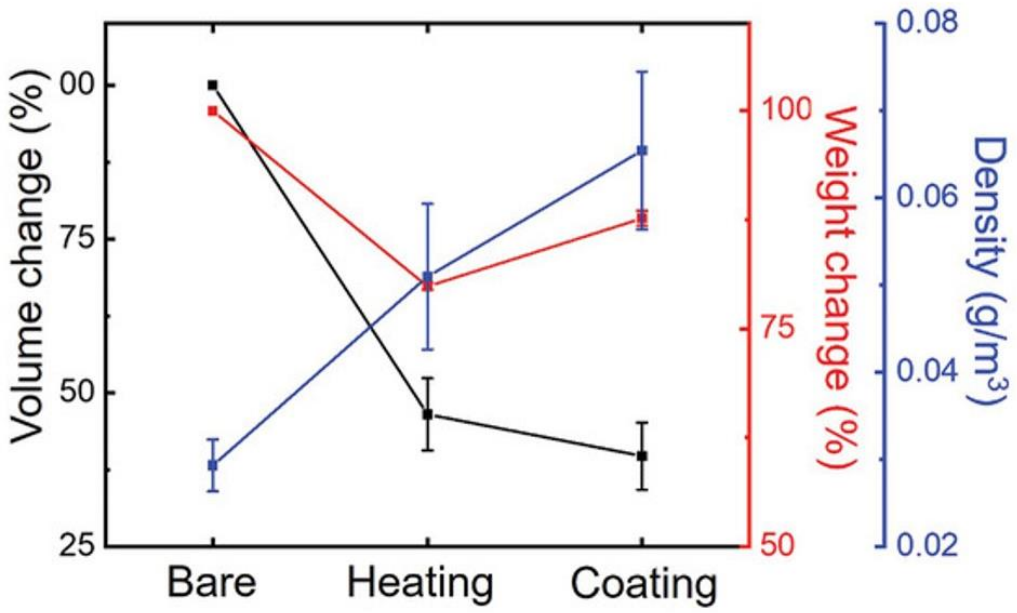

Figure 5.9. Volume, weight, and density of pollen sponges at different fabrication stages.[304]

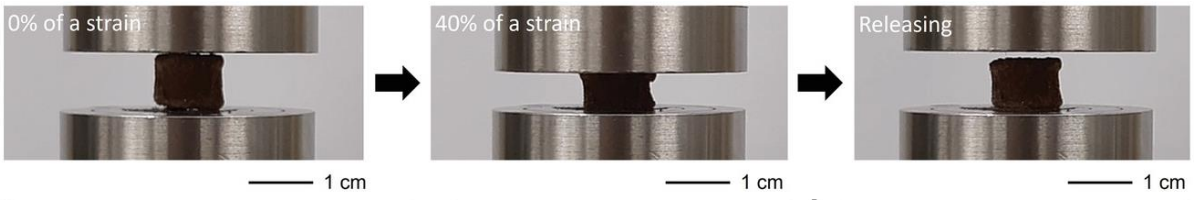

Figure 5.10. Mechanical characterization of pollen sponges. Photographs of reversible compression of pollen sponge under 40% compressive strain.[304]

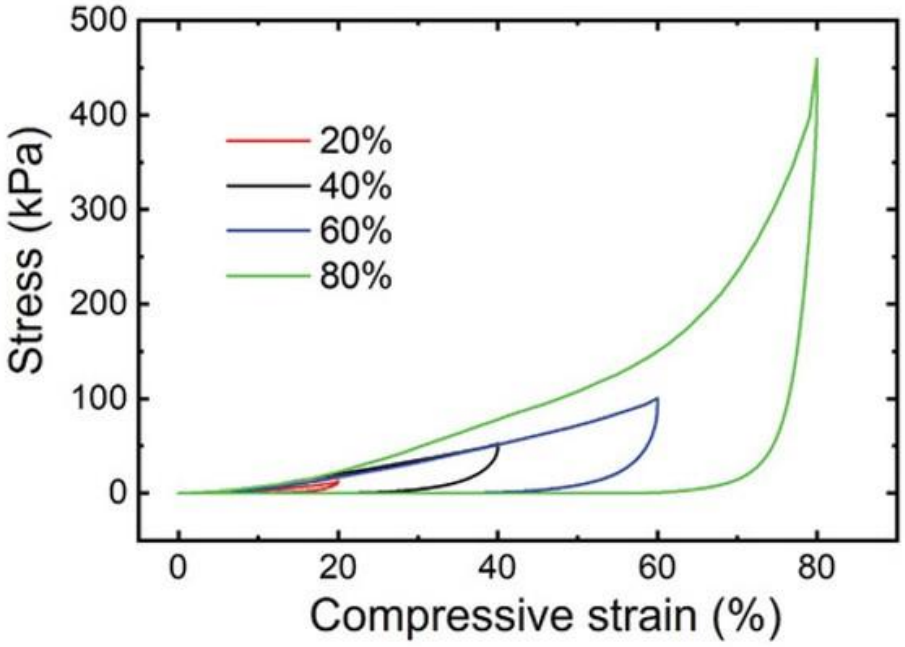

Figure 5.11. Strain–stress curves of pollen sponge under 20%, 40%, 60%, and 80% compressive strains.[304]

loops of the samples under compressive strains of 20%, 40%, and 60% had a cyclical shape indicative of elastic deformation (Figure 5.11). However, with 80% compressive strain, there was structural collapse resulting in a sharp increase in stress recorded due to densification of the sponge structure (Figure 5.12).

Cyclical compression tests at 20%, 40%, and 60% compressive strains were also conducted, and minor changes in the stress–strain curves were observed after the tenth cycle (Figure 5.13). Similar curve profiles were observed at the 50th and 100th cycles. The change in height of the pollen sponge samples were also measured during the cyclical compression testing (Figure 5.14). After the first compression cycle, the pollen sponges recovered about 98% of their original height for up to 80% compressive strain (Figure 5.15). With subsequent compression cycles, the pollen sponges became conditioned and maintained structural integrity with tempered but consistent height recovery trends. After 100 cycles, the pollen sponges retained approximately 92%, 72%, and 59% of their original height upon 20%, 40%, and 60% compressive strains, respectively. Together, these data support that elastic deformation and partial structural collapse ("conditioning") of the pollen sponge occurred during the first few compression cycles and structural stabilization was achieved after five to ten cycles.

5.3.4 Versatility of pollen sponges in absorption of various oils and solvents

To characterize the functional performance of the coated pollen sponge, oil absorption tests with various oils and organic solvents were carried out. Figure 5.16 shows the performance of pollen sponges to remove silicone oil (density of 0.971 g mL–1) and dichloromethane (density of 1.33 g mL–1) from the surface and bottom of water samples, respectively. The oils were labeled with a red, lipophilic dye for visualization and complete absorption of the oils was achieved in

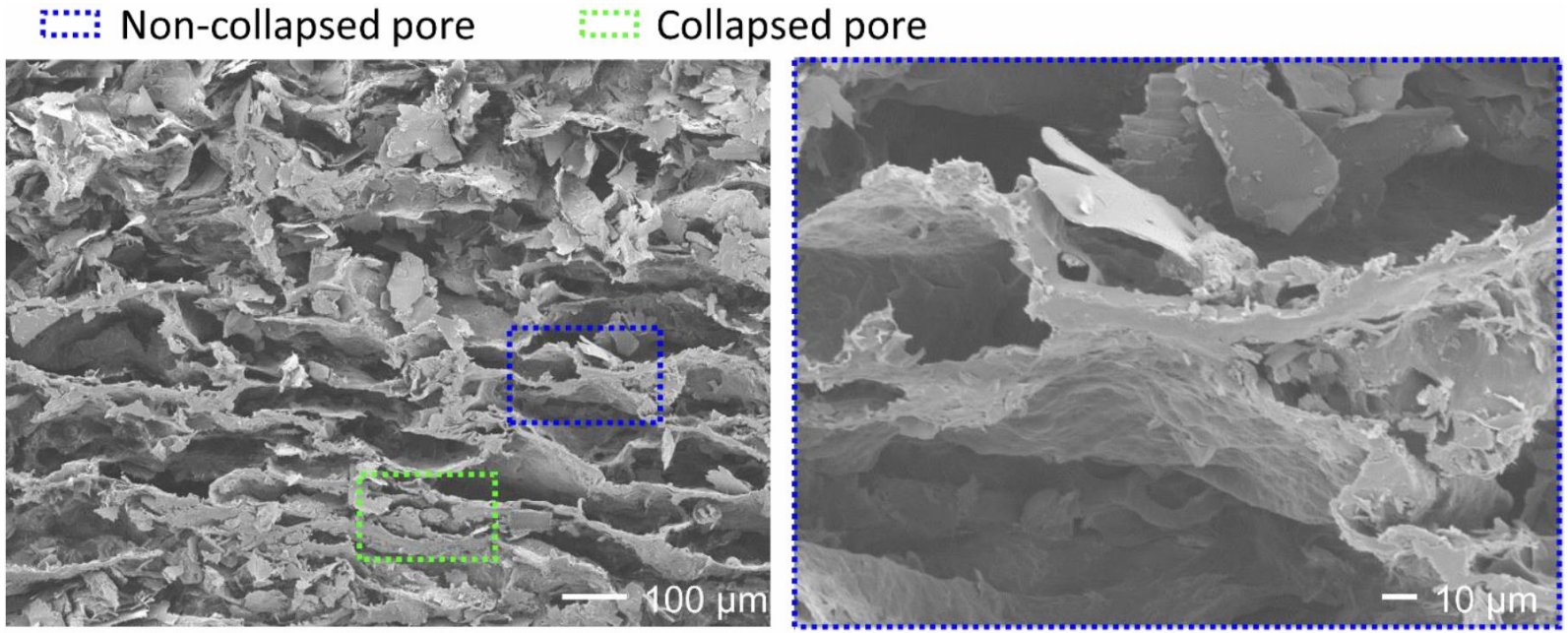

Figure 5.12. Cross-sectional SEM images of a coated pollen sponge after 15 cycles of compression testing at 80% strain.[304] The blue box corresponds to a magnified SEM image of the selected area.

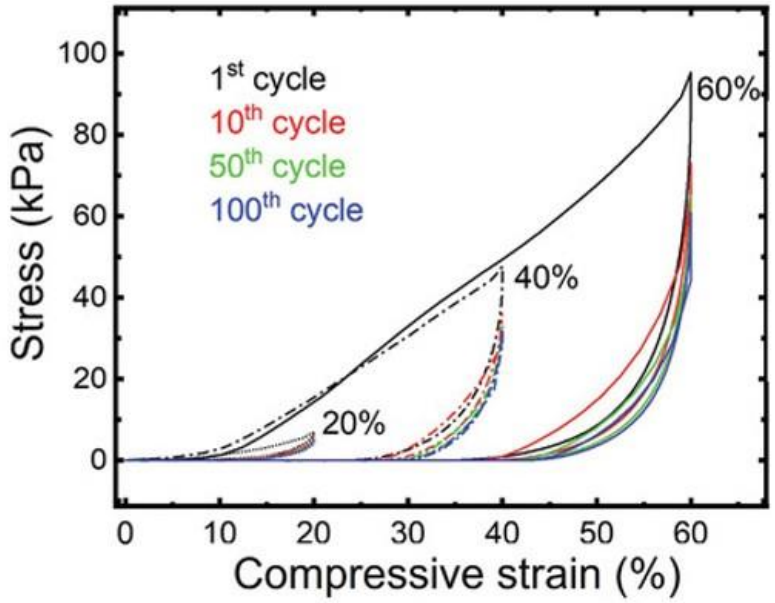

Figure 5.13. Strain–stress curves of pollen sponges with cyclic compression under 20%, 40%, and 60% compressive strains.[304]

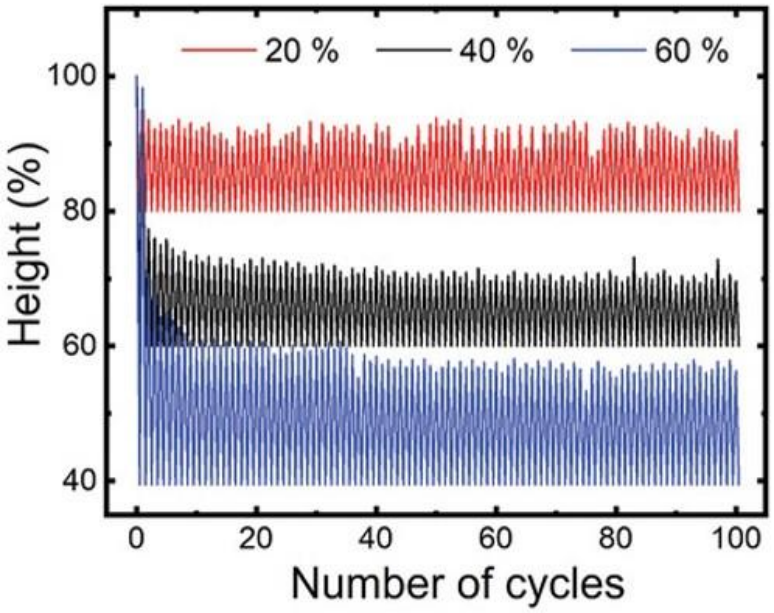

Figure 5.14. Change in height profile of pollen sponges during 100 cycles of compression under 20 %, 40 %, and 60 % compressive strains.[304]

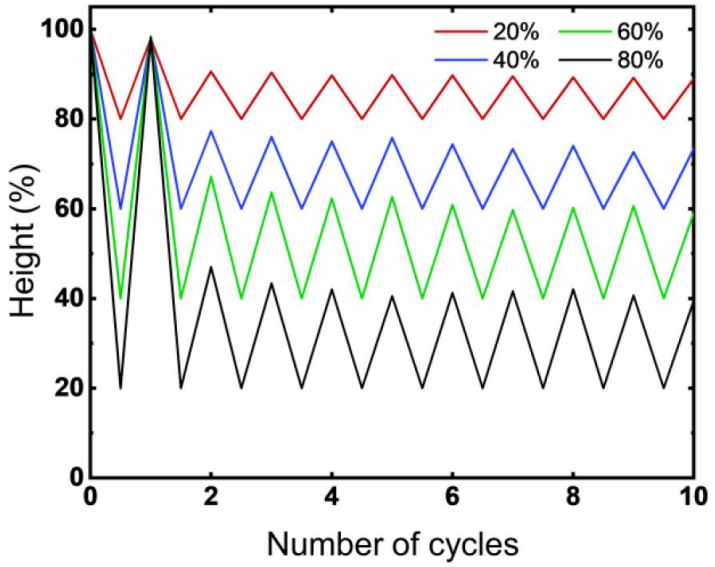

Figure 5.15. Cyclical testing of a coated pollen sponge under 20, 40, 60, and 80% compressive strains.[304]

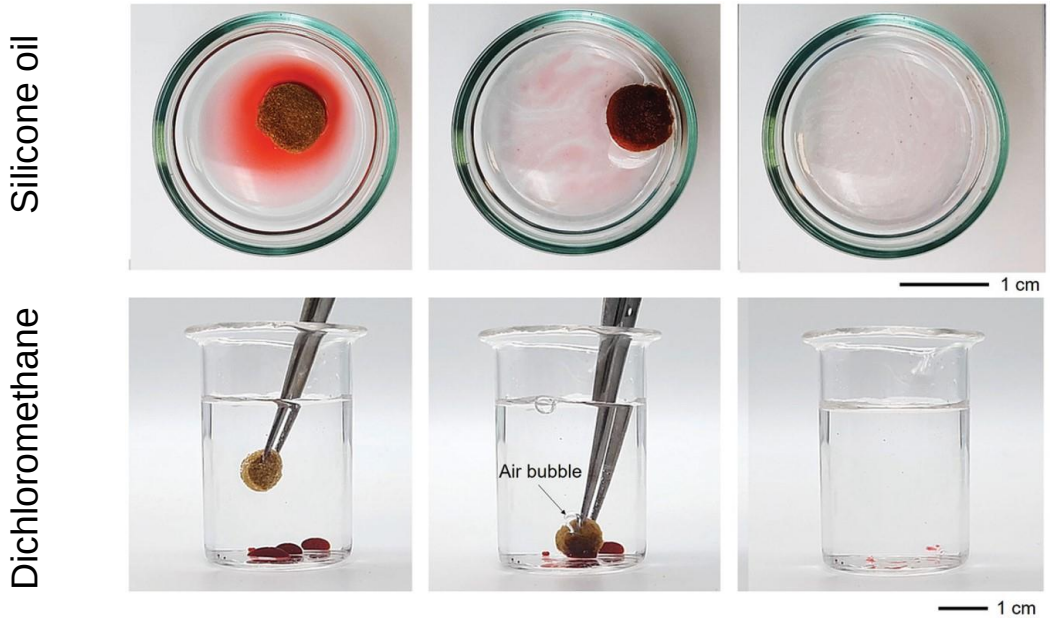

Figure 5.16. Oil absorption capacity of pollen sponge.[304] Photographs of sponge-mediated removal of silicone oil and dichloromethane from contaminated water samples, respectively. Silicone oil and dichloromethane were premixed with lipophilic red dye for optical contrast.

both cases without water absorption. In the latter case of dichloromethane absorption, an air bubble was observed during the extraction process, which indicated mass exchanged between air and dichloromethane within the sponge structure.

The oil absorption capability of the pollen sponge to sequester various types of oils and organic solvents with different densities was also evaluated (Figure 5.17). In general, the pollen sponge exhibited greater than 10 g/g absorption capacity for all tested solvents, with the maximum absorption capacity at 29.3 g/g for chloroform, and the minimum at 9.7 g/g for coconut oil. This performance range is comparable to commercial polypropylene absorbents (8.1–24.6 g/g).[347] To characterize the reusability of the pollen sponge for oil absorption applications in cyclical performance tests, cyclical absorption, and release of silicone oil by the pollen sponge was performed. In each cycle, the sponge was soaked for 5 min, followed by squeezing of the sponge to 45% compression. This process was repeated for a total of 10 cycles. During the first cycle, the pollen sponge absorbed 17.1 g/g of oil, and 9.0 g/g of oil was released by squeezing. In subsequent cycles, the pollen sponge consistently achieved 13.6 g/g absorption and 6.2 g/g release for up to 10 cycles (Figure 5.18), supporting that the fabricated pollen sponges were durable and reusable.

Real application setting was simulated to evaluate the ability of a pollen sponge to remove and recover motor oil from a contaminated water sample (Figure 5.19). The sponge effectively absorbed the motor oil in less than 2 minutes. As tested before, the absorbed motor oil was successfully released into a separate container through the squeezing method. Collectively, these results demonstrate that the pollen sponge can selectively absorb and release oil contaminants and has similar performance levels to commercial oil absorbents while demonstrating compelling properties such as low cost, biocompatibility, and sustainable production. The hydrophobic surface character of the pollen sponge in this case was facilitated by noncovalent attachment of stearic

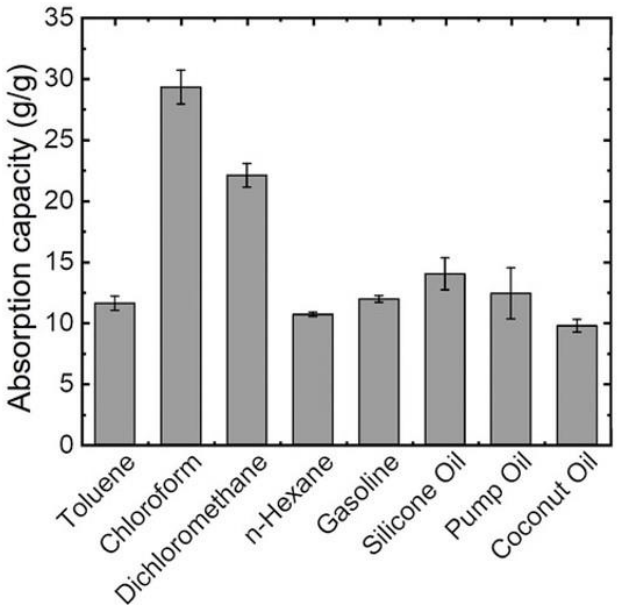

Figure 5.17. Performance testing and reusability of oil-absorbing pollen sponge.[304] a) Mass-based absorption capacity of pollen sponge for various oils and organic solvents.

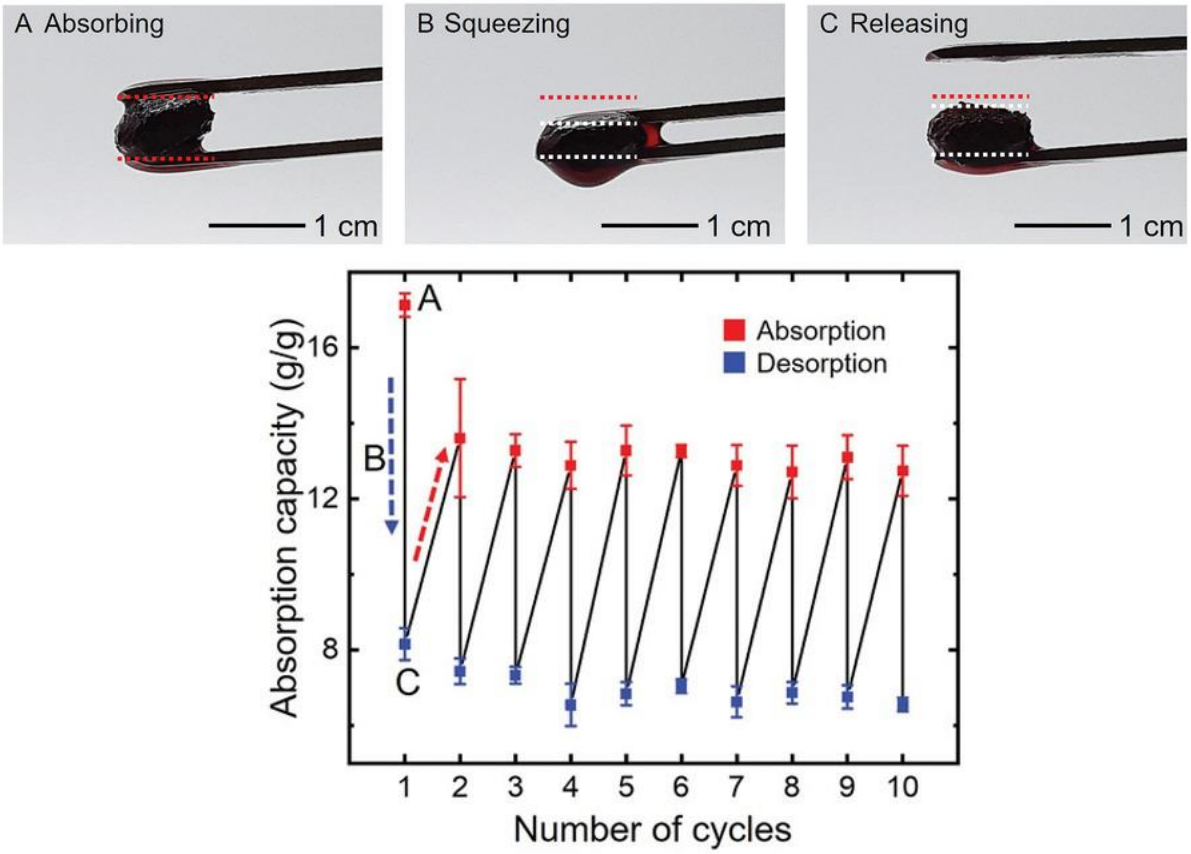

Figure 5.18. Cyclical testing of pollen sponge absorption capacity for silicone oil.[304] The absorption and release amounts are reported for each cycle. Photographs in top row correspond to the absorbing (A), squeezing (B), and releasing (C) steps.

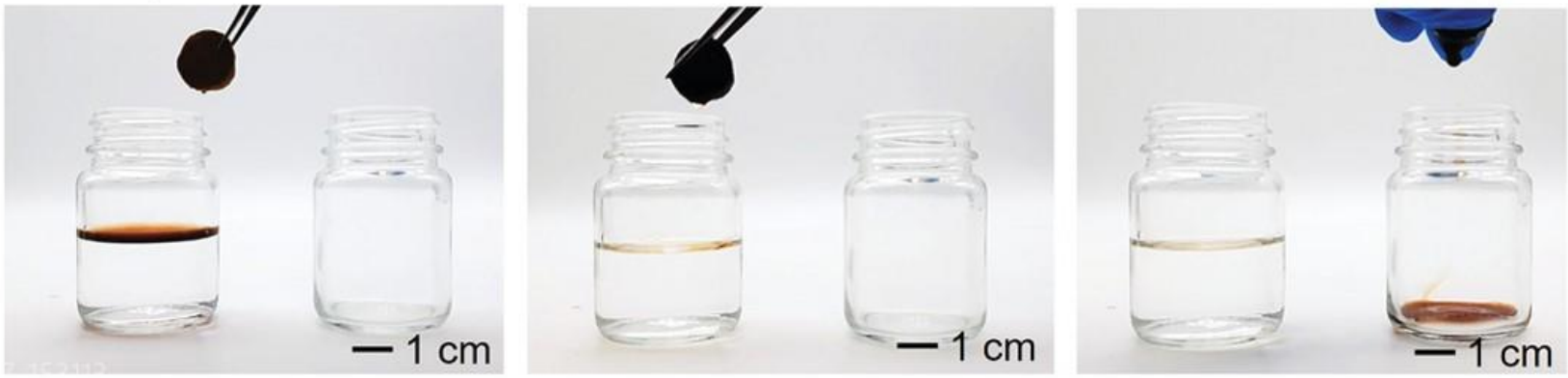

Figure 5.19. Absorption, removal, and squeeze-mediated release of motor oil from contaminated water sample by using a pollen sponge.[304]

acid molecules while there is broad potential to also develop hydrophilic versions of the pollen sponge scaffold by incorporating processing strategies such as ultraviolet–ozone treatment.[348]

5.4 Conclusion

In this study, an efficient oil-absorbing pollen sponge derived from low-cost bee pollen microcapsules was developed. While pollen grains not used for plant pollination are often considered biological waste, this work demonstrate that harvested pollen can be manipulated and readily fabricated into 3D sponge architectures using a colloid-based strategy. Post-treatment of the fabricated sponge with a naturally abundant fatty acid can effectively increase the sponge's capability and selectivity in absorbing oil. Importantly, all the fabrication steps were simple, sustainable and environmentally friendly. While other types of natural materials, typically composed of fibril structures, have been used to fabricate 3D scaffolds in past works, the findings here clearly illustrate the potential of using pliable pollen particles—engineered from natural pollen grains to exhibit microgel-like behavior—as building blocks to fabricate mechanically-responsive sponges. Such findings expand the range of natural materials that can be used to fabricate 3D scaffolds and open the door to new classes of porous, advanced materials derived from pollen particles.

This chapter is a slightly modified version of "Colloid-Mediated Fabrication of a 3D Pollen Sponge for Oil Remediation Applications." (Advanced Functional Materials (2021): 2101091) and has been reproduced here with the permission of the copyright holder.

5.5 References

11 Katifori, Alben, Cerda, Nelson & Dumais. Foldable structures and the natural design of pollen grains. *Proceedings of the National Academy of Sciences* **107**, 7635-7639 (2010).

23 Li, Xu, Xu, Mao, Xu, Zhong, Zhang, Wang & Sui. Cellulose sponge supported palladium nanoparticles as recyclable cross-coupling catalysts. *ACS applied materials & interfaces* **9**, 17155-17162 (2017).

24 Wang, He, Wang, Zhang, Yu, Peng, Wu, Ren, Zeng & Xue. A cellulose sponge with robust superhydrophilicity and under-water superoleophobicity for highly effective oil/water separation. *Green Chemistry* **17**, 3093-3099 (2015).

25 Wang, Gunasekara, Reed, DiSalvo, Bultman, Sims, Magness & Allbritton. A microengineered collagen scaffold for generating a polarized crypt-villus architecture of human small intestinal epithelium. *Biomaterials* **128**, 44-55 (2017).

26 Tozzi, Laurent, Di Buduo, Mu, Massaro, Bretherton, Stoppel, Kaplan & Balduini. Multi-channel silk sponge mimicking bone marrow vascular niche for platelet production. *Biomaterials* **178**, 122-133 (2018).

27 Somsesta, Sricharoenchaikul & Aht-Ong. Adsorption removal of methylene blue onto activated carbon/cellulose biocomposite films: equilibrium and kinetic studies. *Materials Chemistry and Physics* **240**, 122221 (2020).

28 Lu, Xu, Zhang, Pan, Wang, Alshehri, Ahamad, Kim, Na & Hossain. High-Performance Capacitive Deionization by Lignocellulose-Derived Eco-Friendly Porous Carbon Materials. *Bulletin of the Chemical Society of Japan* **93**, 1014-1019 (2020).

29 Guo, Lu, Zhao, Zhou, Shi & Yu. Biomass-Derived Hybrid Hydrogel Evaporators for Cost-Effective Solar Water Purification. *Advanced Materials* **32**, 1907061 (2020).

43 Quilichini, Grienenberger & Douglas. The biosynthesis, composition and assembly of the outer pollen wall: A tough case to crack. *Phytochemistry* **113**, 170-182 (2015).

44 Gonzalez-Cruz, Uddin, Atwe, Abidi & Gill. Chemical treatment method for obtaining clean and intact pollen shells of different species. *ACS biomaterials science & engineering* **4**, 2319-2329 (2018).

45 Bernard, Benzerara, Beyssac, Balan & Brown Jr. Evolution of the macromolecular structure of sporopollenin during thermal degradation. *Heliyon* **1**, e00034 (2015).

46 Bağcıoğlu, Zimmermann & Kohler. A multiscale vibrational spectroscopic approach for identification and biochemical characterization of pollen. *PLoS One* **10**, e0137899 (2015).

47 Liu & Zhang. Mechanical properties of desiccated ragweed pollen grains determined by micromanipulation and theoretical modelling. *Biotechnology and bioengineering* **85**, 770-775 (2004).

164 Shao, Hanaor, Shen & Gurlo. Freeze Casting: From Low-Dimensional Building Blocks to Aligned Porous Structures—A Review of Novel Materials, Methods, and Applications. *Advanced Materials* **32**, 1907176, doi:https://doi.org/10.1002/adma.201907176 (2020).

270 Fan, Park, Shi, Zhang, Liu, Song, Chin, Ibrahim, Mokrzecka & Yang. Transformation of hard pollen into soft matter. *Nature communications* **11**, 1-10 (2020).

287 Yule, Roberts & Marshall. The thermal evolution of sporopollenin. *Organic Geochemistry* **31**, 859-870, doi:https://doi.org/10.1016/S0146-6380(00)00058-9 (2000).

296 Zhang. *Ice templating and freeze-drying for porous materials and their applications*. (John Wiley & Sons, 2018).

304 Hwang, Ibrahim, Deng, Jackman & Cho. Colloid-Mediated Fabrication of a 3D Pollen Sponge for Oil Remediation Applications. *Advanced Functional Materials*, 2101091 (2021).

305 Zhao, Hwang, Yang, Fan, Song, Suresh & Cho. Actuation and locomotion driven by moisture in paper made with natural pollen. *Proceedings of the National Academy of Sciences* **117**, 8711-8718 (2020).

313 Antonini, Wu, Zimmermann, Kherbeche, Thoraval, Nyström & Geiger. Ultra-porous nanocellulose foams: A facile and scalable fabrication approach. *Nanomaterials* **9**, 1142 (2019).

317 Chhetry, Sharma, Yoon, Ko & Park. Enhanced sensitivity of capacitive pressure and strain sensor based on CaCu3Ti4O12 wrapped hybrid sponge for wearable applications. *Advanced Functional Materials* **30**, 1910020 (2020).

318 Fan, Li, Zhang, Zhao, Cao, Yin, Xing, Wang, Guo & Li. A dual-salt gel polymer electrolyte with 3D cross-linked polymer network for dendrite-free lithium metal batteries. *Advanced Science* **5**, 1800559 (2018).

319 Wang, Zhang, Tang, Zhang, Ning, Tian, Li, Zhang, Mao & Liang. Single-electrode triboelectric nanogenerators based on sponge-like porous PTFE thin films for mechanical energy harvesting and self-powered electronics. *Journal of Materials Chemistry A* **5**, 12252-12257 (2017).

320 Giorgianni, Vicario, Shalaby, Tenuzzo, Marcelli, Zhang, Zhao, Chen, Hauri & Lupi. High-Efficiency and Low Distortion Photoacoustic Effect in 3D Graphene Sponge. *Advanced Functional Materials* **28**, 1702652 (2018).

321 Cherukupally, Sun, Wong, Williams, Ozin, Bilton & Park. Surface-engineered sponges for recovery of crude oil microdroplets from wastewater. *Nature Sustainability* **3**, 136-143 (2020).

322 Zhang, Liu, Yang, Shi, Zhang, Shan, Mi, Liu, Shen & Guo. Ultrasensitive and highly compressible piezoresistive sensor based on polyurethane sponge coated with a cracked cellulose nanofibril/silver nanowire layer. *ACS applied materials & interfaces* **11**, 10922-10932 (2019).

323 Zhao & Zhu. High sensitivity and broad range flexible pressure sensor using multilayered porous PDMS/AgNP sponge. *Advanced Materials Technologies* **4**, 1900414 (2019).

324 Zhou, Yang, Zhu, Zheng, Handschuh-Wang, Zhou, Zhang, Liu, Liu & He. Hydrophilic Sponges for Leaf-Inspired Continuous Pumping of Liquids. *Advanced Science* **4**, 1700028 (2017).

325 Qi, Miao, Chi, Zhang, Zhang, Du, An, Ma & Zhang. Ultralight PEDOT: PSS/graphene oxide composite aerogel sponges for electric power harvesting from thermal fluctuations and moist environment. *Nano Energy* **77**, 105096 (2020).

326 Li, Hu, Yang, Zou, Yang, Yu, Wang, Qu, Tan & Wang. Elastic Cu@ PPy sponge for hybrid device with energy conversion and storage. *Nano Energy* **58**, 852-861 (2019).

327 Ruan, Ai, Li & Lu. A superhydrophobic sponge with excellent absorbency and flame retardancy. *Angewandte Chemie* **126**, 5662-5666 (2014).

328 Zhu, Ji, Liu, Mine, Matsuoka, Zhang & Xing. Designing 3D-MoS2 sponge as excellent cocatalysts in advanced oxidation processes for pollutant control. *Angewandte Chemie International Edition* **59**, 13968-13976 (2020).

329 Jiang, Cheong, Nam, Kim, Agarwal & Greiner. High-density fibrous polyimide sponges with superior mechanical and thermal properties. *ACS applied materials & interfaces* **12**, 19006-19014 (2020).

330 Wu, Li, Li, Zhang & Wang. Magnetic, durable, and superhydrophobic polyurethane@ Fe3O4@ SiO2@ fluoropolymer sponges for selective oil absorption and oil/water separation. *ACS applied materials & interfaces* **7**, 4936-4946 (2015).

331 Song, Chen, Su, Chen, Miao, Zhang, Cheng & Zhang. Highly compressible integrated supercapacitor–piezoresistance-sensor system with CNT–PDMS sponge for health monitoring. *Small* **13**, 1702091 (2017).

332 Zhang, Feng, Qin, Gao, Li, Zhao, Zhang, Lv & Feng. Stress controllability in thermal and electrical conductivity of 3D elastic graphene-crosslinked carbon nanotube sponge/polyimide nanocomposite. *Advanced Functional Materials* **29**, 1901383 (2019).

333 Li, Yang, Li, Wang & Liu. From commercial sponge toward 3D graphene–silicon networks for superior lithium storage. *Advanced Energy Materials* **5**, 1500289 (2015).

334 Li, Phyo, Jacobowitz, Hong & Weng. (2019).

335 Wang, Potroz, Jackman, Khezri, Marić, Cho & Pumera. Bioinspired spiky micromotors based on sporopollenin exine capsules. *Advanced Functional Materials* **27**, 1702338 (2017).

336 Mundargi, Potroz, Park, Shirahama, Lee, Seo & Cho. Natural sunflower pollen as a drug delivery vehicle. *Small* **12**, 1167-1173 (2016).

337 Fang, Wang, Yu, Zhang, Baluška, Šamaj & Lin. Isolation of de-exined pollen and cytological studies of the pollen intines of Pinus bungeana Zucc. Ex Endl. and Picea

wilsonii Mast. *Flora-Morphology, Distribution, Functional Ecology of Plants* **203**, 332-340 (2008).

338 Pomelli, D'Andrea, Mezzetta & Guazzelli. Exploiting pollen and sporopollenin for the sustainable production of microstructures. *New Journal of Chemistry* **44**, 647-652 (2020).

339 Chu, Feng & Seeger. Oil/water separation with selective superantiwetting/superwetting surface materials. *Angewandte Chemie International Edition* **54**, 2328-2338 (2015).

340 Gunstone & Harwood. *The lipid handbook with CD-ROM*. (CRC press, 2007).

341 Ralston & Hoerr. The Solubilities of the Normal Saturated Fatty Acids. *The Journal of Organic Chemistry* **07**, 546-555, doi:10.1021/jo01200a013 (1942).

342 Hu, Zen, Gong & Deng. Water resistance improvement of paper by superhydrophobic modification with microsized CaCO3 and fatty acid coating. *Colloids and Surfaces A: Physicochemical and Engineering Aspects* **351**, 65-70 (2009).

343 Dolez, Arfaoui, Dubé & David. Hydrophobic treatments for natural fibers based on metal oxide nanoparticles and fatty acids. *Procedia Engineering* **200**, 81-88, doi:https://doi.org/10.1016/j.proeng.2017.07.013 (2017).

344 Chen, Zhang, Wang, Lv, Zhu & Gao. Fabrication and characterization of novel shape-stabilized stearic acid composite phase change materials with tannic-acid-templated mesoporous silica nanoparticles for thermal energy storage. *RSC advances* **7**, 15625-15631 (2017).

345 Charde, Sonawane, Sonawane & Navin. Influence of functionalized calcium carbonate nanofillers on the properties of melt-extruded polycarbonate composites. *Chemical Engineering Communications* **205**, 492-505 (2018).

346 Fu, Zheng, Liu, Dresselhaus, Dresselhaus, Satcher Jr & Baumann. The Fabrication and Characterization of Carbon Aerogels by Gelation and Supercritical Drying in Isopropanol. *Advanced Functional Materials* **13**, 558-562, doi:https://doi.org/10.1002/adfm.200304289 (2003).

347 Laitinen, Suopajärvi, Österberg & Liimatainen. Hydrophobic, superabsorbing aerogels from choline chloride-based deep eutectic solvent pretreated and silylated cellulose nanofibrils for selective oil removal. *ACS applied materials & interfaces* **9**, 25029-25037 (2017).

348 Tan, Potroz, Ferracci, Jackman, Jung, Wang & Cho. Light-induced surface modification of natural plant microparticles: toward colloidal science and cellular adhesion applications. *Advanced Functional Materials* **28**, 1707568 (2018).

Chapter 6 Conclusion & Future Work

Chapter Abstract

This chapter connects and summarizes the findings obtained in the thesis and further emphasizes how they fulfilled the thesis objectives set at the beginning. Implications, impact, and outlook of pollen-derived microgels and their ability to be used as modular building blocks for the fabrication of higher order structures are discussed in deep. The opportunities and the possible working strategies for this research in the future are recounted.

6.1 Discussion and Concluding Remarks

The objective of this thesis was to realize the potential of utilizing pollen as an untapped natural source of biopolymer for the purpose of fabrication of higher order structures. Being composed of a tough outer sporopollenin shell, which has been regarded as the toughest naturally derived polymer,[4,7] the possibility of natural polymer scaffolds for rigorous industrial applications can finally be realized. Much focus was placed on the physical properties of the pollen microgel and the resultant fabricated 3D scaffolds, and there was emphasis on the chemical mechanism that contributed to the manifestations of these attributes. An ample analytical framework was established to evaluate parameters such as the incubation duration for optimal microgel synthesis, the extent of microgel swelling, cohesiveness of the various microgels interparticle interaction and the robustness of the whole scaffold. The modulation of properties of the scaffold via careful calibrated regulation of the variables during the fabrication process by selecting suitable microgels, regulating the swell state of the microgels, selection of freezing conditions, post-fabrication thermal sintering and wet immersion coating all serve to highlight the flexibility of the scaffold itself, and can be conveniently optimized to serve specific industrial applications, such as oil remediation. The key findings based on the analytical framework are outlined below:

6.1.1 Base hydrolysis of pollen leads to formation of swellable microgel due to de-esterification of pectin in the intine layer and softening of the exine layer.

The results were thoroughly discussed in Chapter 3 of the thesis, where treatment of pollen with KOH for defined periods at elevated temperatures resulted in the synthesis of discrete pollen particles that exhibited properties reminiscent of microgels. The Young's modulus of these base hydrolyzed pollen particles were significantly lower than pollen that were not treated to alkaline

hydrolysis. Interestingly, these microgels displayed a hyperbolic swelling in response to the change in pH of their immediate vicinity, generally shrinking as the pH becomes acidic and swelling as the pH becomes basic up to a pH of 10, before it shrinks again. Furthermore, there appears to be an upper limit to the hydrolysis treatment as KOH concentrations of 20 % and 30 % w/v did not proportionately yield a more dramatic swelling characteristic. Systematic study of the microgel via immunofluorescence staining and FTIR spectroscopy analysis show the increase in amount of O-H moieties present and this was closely correlated with the increase in presence of de-esterified pectins as labelled by JIM5 and JIM7 antibodies. Furthermore, AFM force-distance measurements of the exine shells show a progressive decline in modulus of the pollen shell.

6.1.2 Success of forming scaffolds with seamless walls is dependent on the lowered modulus of the pollen

Chapter 4 explores the various variables that may influence the formation of scaffolds via freeze-drying of pollen. The findings show that pollen with high stiffness, especially those that have not undergone the microgel synthesis process, have a compressive Young's modulus value that cannot be easily overcome by the growing ice crystals during the freeze-casting stage, and thus are unable to be pressed and molded closely to adjacent pollen microgels to attain sufficient surface area for robust interactions to form. Variables that promote or scaffold fabrication processes that are able to overcome of the physical stiffness of the pollen would thus increase the probability of scaffold fabrication. In the freeze-drying method explored in Chapter 4, these variables were 1) using microgels of incubation duration beyond 24 h, 2) subjecting the microgels to a state of maximum swelling (minimum stiffness) via casting of pollen microgel slurry at pH

10, and 3) maximizing the force of freezing front of ice crystals by using a low freezing rate to minimize ice nucleation and maximizing grain size of ice.

6.1.3 Pollen microgel interaction is limited by the spatial distance between adjacent surfaces by surface tension of bound solvents

The second part of Chapter 4 explores the hypothesis that removal of bound water that surrounds the microgel is crucial for robust and permanent bond formation between surfaces of adjacent pollen microgels. This process would be akin to ‘zipping’ of two adjacent surface, drawn by the surface tension of water as the secondary drying process occurs during lyophilization. However, it was also adequately discussed that total removal of the bound water may not be necessary, but only to a level that matches ambient humidity, as how the pollen sheet was formed. Solvent exchange experiments with ethanol, an easily available water miscible solvent with much lower surface tension, proves this hypothesis true. Nevertheless, a permanent interaction between surfaces occurs only when water can no longer penetrate this interface, and this involves drying out of the ethanol to prevent a reverse exchange.

6.1.4 Pollen scaffold properties can be modulated by optimization of fabrication parameters and post-fabrication processes

The flexibility of pollen scaffold to be able to be used in industrial applications was explored. Parameters that allow fabrication of tough scaffolds were identified, and pollen microgels with incubation duration of 48 h, freeze-casted at -20 °C and a swell state at pH 7 for industrial practicality were thermally sintered at 200 °C. These selected parameters allowed the

pollen scaffolds to obtain good recyclability, which would be advantageous for oil remediation and recovery applications. Stearic acid coating of the scaffolds was able to imbue hydrophobic properties to the scaffold that allowed it to selectively and efficiently sequester organic solvent present in water and at amounts that were comparable to currently available oil absorbent pads. The advantage of utilizing pollen for this purpose includes their environmental friendliness and sustainable solutions by utilizing nature-derived products that had been widely discarded before.

Together, all they key findings together had achieved the objectives set out in the commencement of the whole project, with the pollen microgel synthesis process being accelerated to a 24 h process instead of 28-days, successfully proving that with successful manipulation of pollen properties, diverse applications can be realized of which one is fabrication of 3D scaffolds, and that utilization of a tough natural polymer as modular building blocks can translate to fabrication of robust scaffolds that are suitable for industrial applications such as in oil remediations. However, there remains other areas of application that pollen microgel can be applied to, of which some will be discussed further here.

6.2 Implications and Future Impact

The key discoveries that form this thesis provides significant insights to the understanding of how pollen properties can be altered and how their cohesion can be modulated, and thus opens the doors to fabrication of higher order structures or stimuli-responsive materials for smart polymer applications.

While alkaline processing conditions can be used to convert hard pollen grains into soft microgel particles, not all alkaline processing protocols work and different results such as particle fragmentation[349] can occur depending on processing parameters such as incubation time, static or stirred incubation conditions, washing solvents, and drying procedures. In previous experiments, pollen grains and spores from other clades had been evaluated and discovered that those from flowering monocots (cattail) and gymnosperms (pine), as well as spore-bearing lycophytes (lycopodium) did not soften to a similar extent as the sunflower pollen here. Pollen grains from baccharis and camellia plants, which belong to the same eudicot clade as sunflower plants however successfully transformed into microgel particles.[270] The observed variation in susceptibility to being softened among pollen from different plant species may relate to variations in the chemical and physical composition in this other species that may give rise to distinct chemo-mechanical responses and was hence reflective of the branching during the evolution of plants. De-esterification of pectin molecules within the intine layer mimics the activity of key enzymes involved in pollen tube growth that leads to the swelling of pollen in a series of event that occur during the orchestrated sequence of pollen hydration, germination, and tube growth.[350] The results presented here reflect on the variations in the mechanical properties of both the exine and intine layers as a result of evolutionary differences in their chemical makeup.

It can be theorized that there exists an optimum hydrolysis condition whereby the exine is at its softest while the intine can swell to its maximum. From mechanistic studies earlier, this would be achievable via 1) the maximum degradation of the exine, 2) the maximum de-estrification of pectin, 3) the minimum degradation of intine mass. Processing in high KOH concentration of 20% and 30% w/v has been shown to result in microgels that do not swell as dynamically as that in 10% w/v. In synthesis conditions where concentration of KOH utilized was very high, or where excessive duration of incubation stage was excessively long, the exine becomes soft and the de-esterification process is efficient, but there is extensive degradation of the intine layer, leading to a reduced intine mass for swelling to occur.

Utilizing the in depth understanding of fabrication of microgel has allowed the synthesis of microgels that have a much higher degree of swelling while using a much milder reaction condition. It has recently been explored that utilizing lower KOH concentration of 1 % or 2.5 % w/v, even softer microgels with a significantly greater degree of swelling can be achieved (Figure 6.1). Within a 24 h incubation at 2.5 % w/v KOH, a maximum swelling size of 75.9 ± 7.7 μm was achieved, as compared to 52.48 ± 5.52 μm (Figure 3.14). The lower concentrations are advantageous as it further emphasizes the aspect of using pollen as an inexpensive and sustainable substitute to synthetic polymers while being environmentally friendly from the milder processing conditions. Furthermore, these recent experimental conditions may be translatable to the other non-eudicot species that have so far proven resilient to softening.

Studies of scaffold fabrication have also yielded promising results with respect to composite pollen scaffolds. Identification of the modulus of pollen being a limiting factor of pollen microgel surface interaction has allowed the fabrication of scaffolds comprising of multiple pollen species, and in varied permutations, simply by matching their mechanical modulus. Sunflower and

camellia pollen can be casted and fabricated to yield dual layer scaffolds or homogenous composites (Figure 6.2). Careful design would thus generate pollen scaffolds with a variety of unique properties that may benefit specialized applications. In addition, understanding of the factors that govern cohesion of pollen has also allowed the generation of ultra-hard resin-like pollen pieces by the process of continuous pressure exerted during the dehydration process (Figure

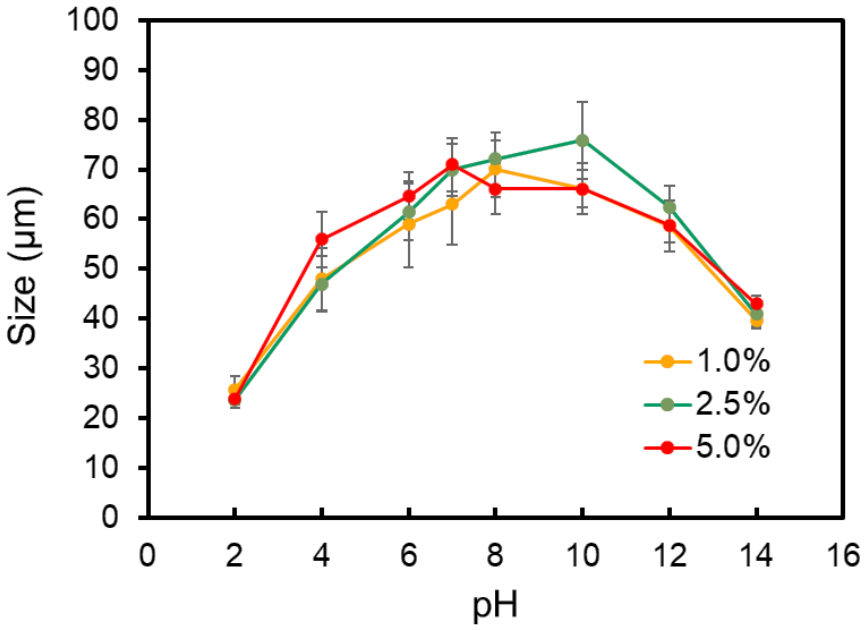

Figure 6.1. pH-dependent swelling of pollen microgel incubated for 24 h in KOH concentrations of 1.0, 2.5 and 5.0 % w/v.

6.3a). On the other end of the spectrum, soft and tacky cotton-like sponges have also been demonstrated to be achievable by extensive duration of incubation of 7 months (Figure 6.3b). The extensive incubation process may have led to extensive degradation of the pollen shell layer, such that there was absence of any intact pollen particle (Figure 6.3c), and this was translatable to the particulate surface of the cotton-like sponges under SEM (Figure 6.3d).

As with every conclusion of a certain aspect of research, more inquisitive questions would be generated. Among them include the exact nature of interparticle bonds that were formed during the interface 'zipping' mechanism. Although it can be hypothesized to be covalent linkages or reformation of ester bonds, van der Waals forces could also be a possibility that is worthy of further investigation. Limitations towards the conclusion also include the propensity of a wider variety of pollen species that can be utilized to form porous scaffolds. Nevertheless, these are some examples of possibilities of the exciting and novel pollen-derived products with yet unknown applications and worthy of further investigations. Pollen applications in engineering would be able to transcend the traditional hollow capsule delivery applications.[267,336,351] Given the versatility of the naturally-derived pollen microgel as highly tunable building blocks to give rise to a diverse range of robust and resilient higher order structures, the possibility of pollen to be utilized in applications that are at the interface of natural and synthetic polymers may become a reality.

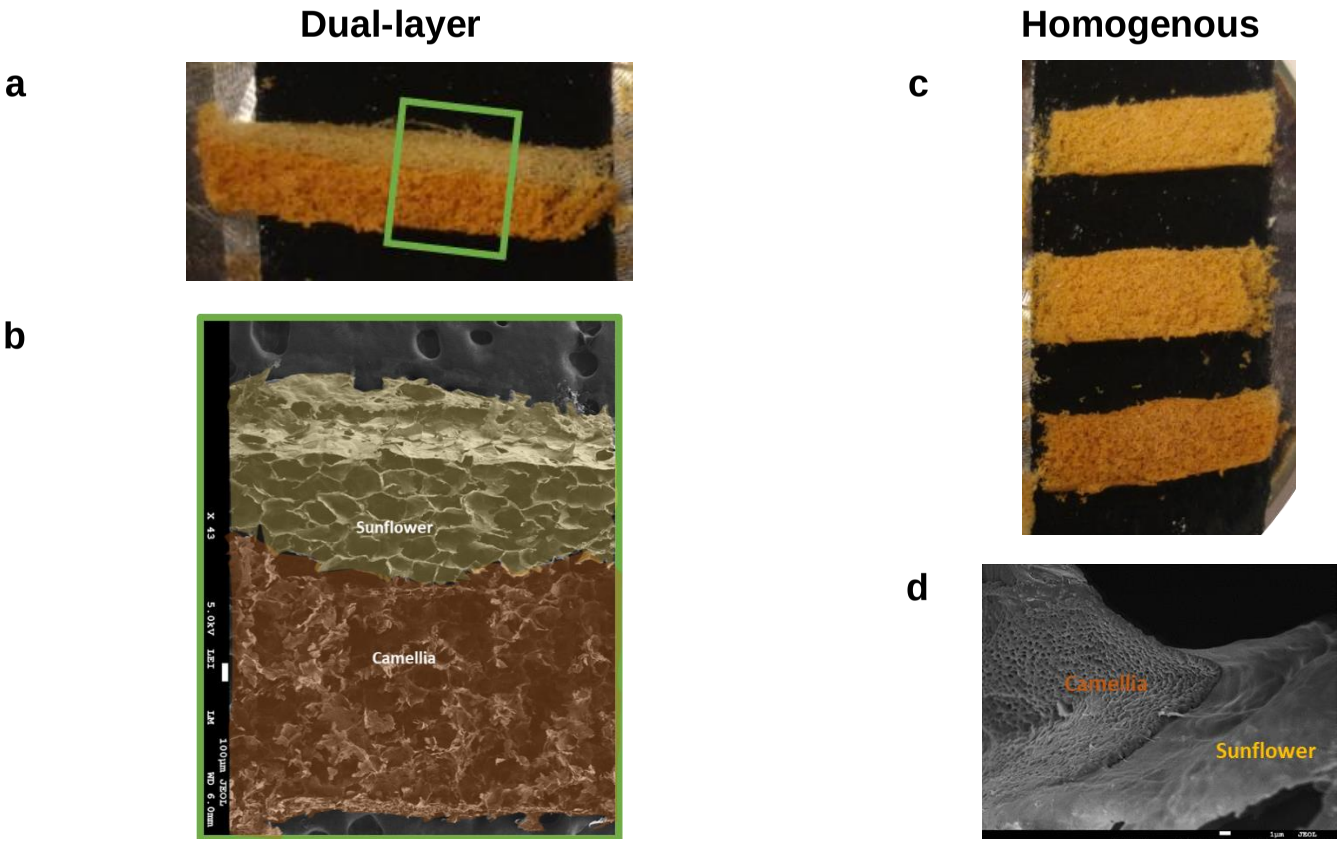

Figure 6.2. Sunflower and camellia pollen composite scaffolds. a) macroscopic cross-section view of distinct boundary of pollen species with b) pseudo-coloured FE-SEM image of highlighted green box showing the distinct pollen species. c) homogenous composite scaffold of increasing ratio of sunflower to camellia pollen (top to bottom, 2:1, :1, 1:2) showing gradient of increasignly intense yellow . d) FE-SEM image showing the interaction of 2 distinct pollen species.

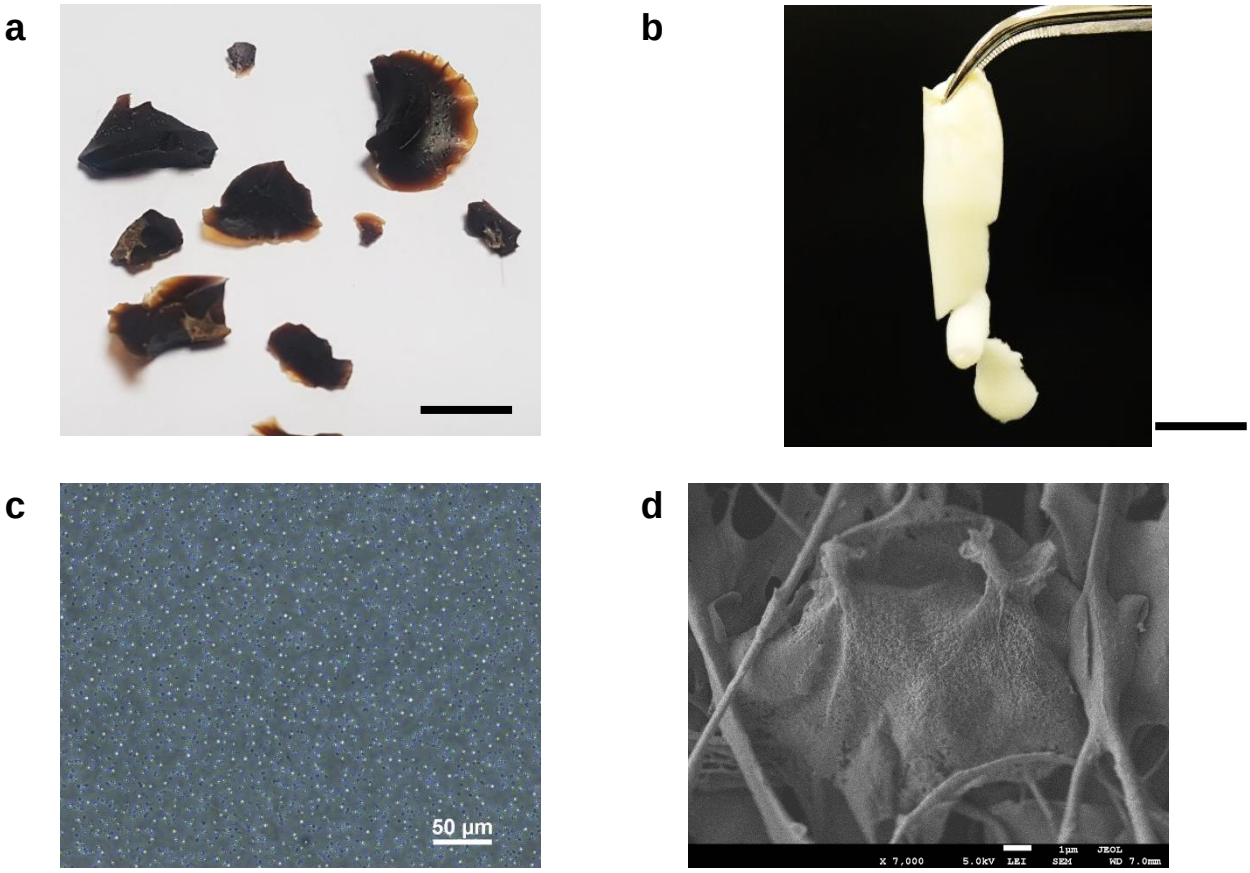

Figure 6.3. Hard and soft products derived from pollen microgels. a) Ultra-hard resin-like pollen pieces. Scale bar: 5 mm. b) Cotton-like sponge derived from 7-month incubation pollen. Scale bar: 1 cm. c) Optical microscope image showing absence of intact pollen after 7 months of incubation in 10 % w/v KOH. d) FE-SEM image of particulate surface of cotton like sponge.

6.3 References

4 Mackenzie, Boa, Diego-Taboada, Atkin & Sathyapalan. Sporopollenin, the least known yet toughest natural biopolymer. *Frontiers in Materials* **2**, 66 (2015).

7 Birks, Birks & Ammann. The fourth dimension of vegetation. *Science* **354**, 412-413 (2016).

267 Prabhakar. *Pine pollen for molecular encapsulation and oral delivery applications*, (2018).

270 Fan, Park, Shi, Zhang, Liu, Song, Chin, Ibrahim, Mokrzecka & Yang. Transformation of hard pollen into soft matter. *Nature communications* **11**, 1-10 (2020).

336 Mundargi, Potroz, Park, Shirahama, Lee, Seo & Cho. Natural sunflower pollen as a drug delivery vehicle. *Small* **12**, 1167-1173 (2016).

349 Mundargi, Potroz, Park, Seo, Lee & Cho. Extraction of sporopollenin exine capsules from sunflower pollen grains. *RSC advances* **6**, 16533-16539 (2016).

350 Matamoro-Vidal, Raquin, Brisset, Colas, Izac, Albert & Gouyon. Links between morphology and function of the pollen wall: an experimental approach. *Botanical journal of the Linnean Society* **180**, 478-490 (2016).

351 Potroz, Mundargi, Gillissen, Tan, Meker, Park, Jung, Park, Cho & Bang. Plant-based hollow microcapsules for oral delivery applications: toward optimized loading and controlled release. *Advanced Functional Materials* **27**, 1700270 (2017).

Appendices

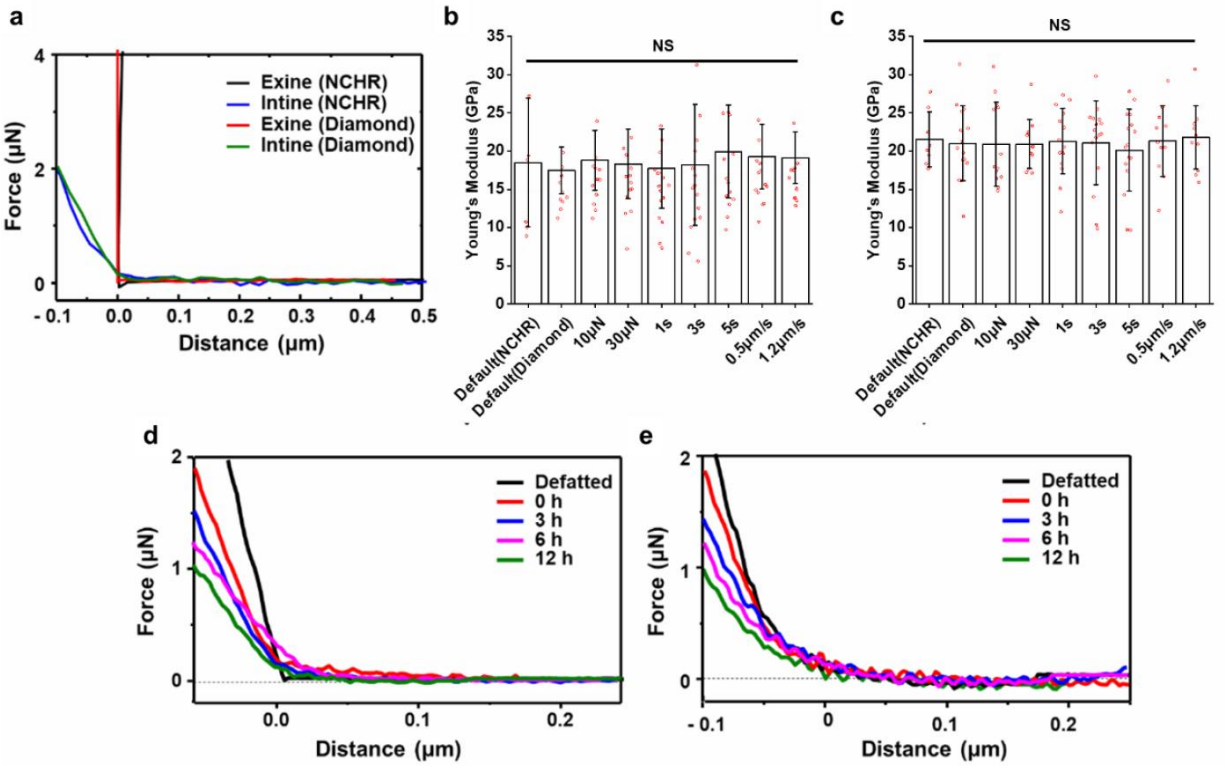

Appendix 3.1. Effects of various AFM parameters on Young's modulus measurement of exine and intine layers of dry, defatted pollen grains. (a) Representative force-displacement curves from AFM measurements using two types of AFM probes, an aluminum reflex-coated silicon cantilever PPP-NCHR (Nanosensors, Neuchâtel, Switzerland) with a typical spring constant of 42 N/m and a tip end radius of 5 nm and a diamond cantilever TD26135 (Micro Star Technology, Texas, USA) with a spring constant of 150 N/m and a tip end radius of 5 nm. Young's moduli of exine (b) and intine (c) retrieved from force-displacement curves after AFM measurements using two AFM probes, NCHR and diamond probes at a maximum contact force of 20 μN with setpoint of 6 μN with zero contact time and an approach speed of 0.8 μN s-1. AFM measurements were performed using the NCHR probe, varying the maximum contact force (10

to 30 μN), contact time (0 to 1, 3, and 5 s), and approach speed (0.5 to 1.2 μN/s). Data are reported as mean ± s.d. from n > 6 particles per condition (one-way analysis of variance (ANOVA) with Tukey's multiple comparisons test). (d) Representative force-displacement curves of exine layer measurements in the wet condition. (e) Representative force-displacement curves of intine layer measurements in the wet condition.

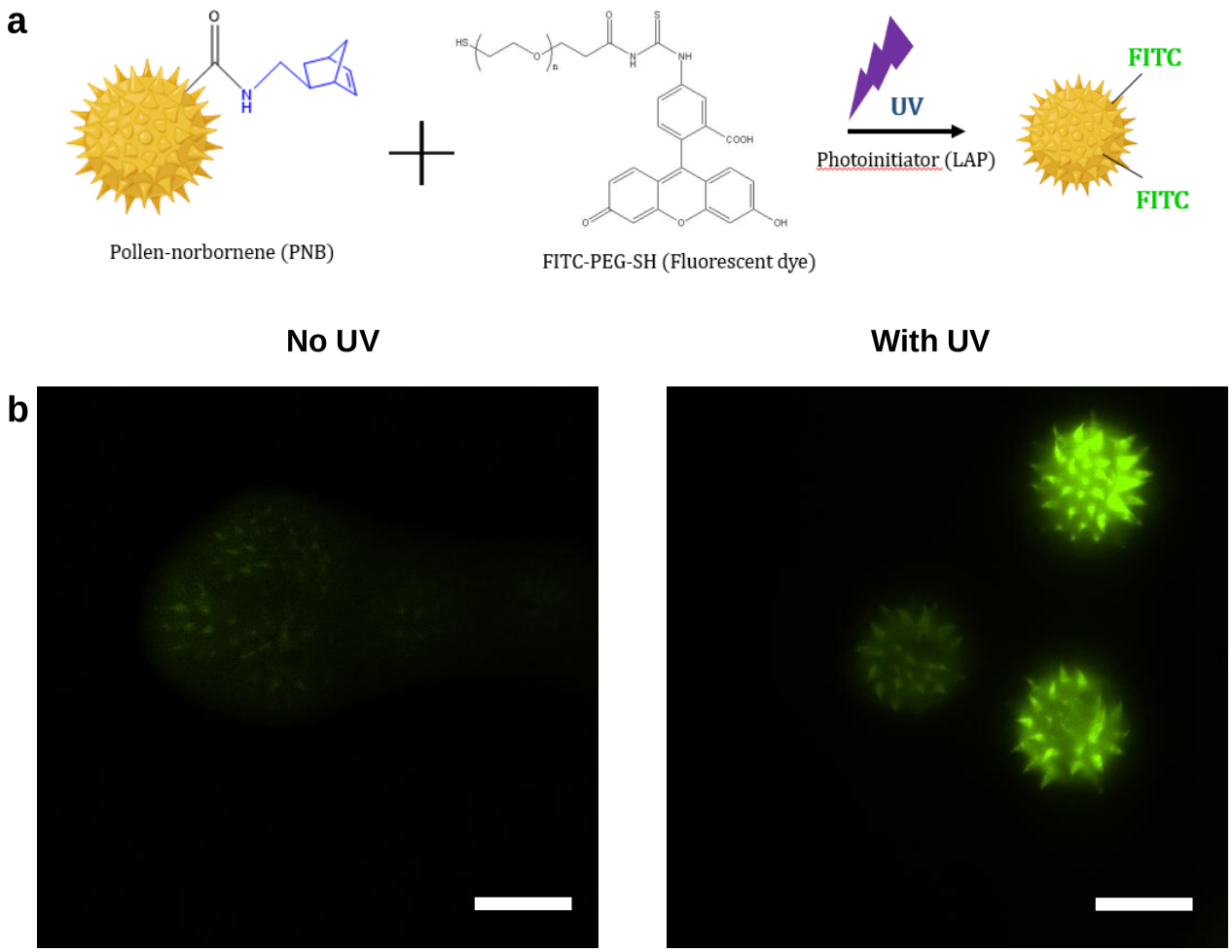

Appendix 4.1. a) Schematic of labelling of pollen-norbonene with FITC via photopolymerization. b) Pollen microgels labelled with FITC indicates presence of norbonene tethered on the surface of pollen microgels. Scale bar: 25 µm

Bibliography

1 Faegri & Van Der Pijl. *Principles of pollination ecology*. (Elsevier, 2013).

2 Tylianakis. The global plight of pollinators. *Science* **339**, 1532-1533 (2013).

3 Erdtman. *Pollen morphology and plant taxonomy: angiosperms*. Vol. 1 (Brill Archive, 1986).

4 Mackenzie, Boa, Diego-Taboada, Atkin & Sathyapalan. Sporopollenin, the least known yet toughest natural biopolymer. *Frontiers in Materials* **2**, 66 (2015).

5 Rojas, Hotton & Dumais. Chemically mediated mechanical expansion of the pollen tube cell wall. *Biophysical journal* **101**, 1844-1853 (2011).

6 Heslop-Harrison & Heslop-Harrison. The microfibrillar component of the pollen intine some structural features. *Annals of Botany* **50**, 831-842 (1982).

7 Birks, Birks & Ammann. The fourth dimension of vegetation. *Science* **354**, 412-413 (2016).

8 de Miranda Chaves. Pollen Grains, Landscapes, and Paleoenvironments. *Foundations of Paleoparasitology*, 205.

9 Martin & Sharrock. Pollen analysis of prehistoric human feces: a new approach to ethnobotany. *American Antiquity* **30**, 168-180 (1964).

10 Blackmore, Wortley, Skvarla & Rowley. Pollen wall development in flowering plants. *New Phytologist* **174**, 483-498 (2007).

11 Katifori, Alben, Cerda, Nelson & Dumais. Foldable structures and the natural design of pollen grains. *Proceedings of the National Academy of Sciences* **107**, 7635-7639 (2010).

12 Couturier, Dumais, Cerda & Katifori. Folding of an opened spherical shell. *Soft Matter* **9**, 8359-8367 (2013).

13 Heslop-Harrison. in *International review of cytology* Vol. 107 1-78 (Elsevier, 1987).

14 Bosch & Hepler. Pectin methylesterases and pectin dynamics in pollen tubes. *The Plant Cell* **17**, 3219-3226 (2005).

15 Wolf, Hématy & Höfte. Growth control and cell wall signaling in plants. *Annual review of plant biology* **63**, 381-407 (2012).

16 Vieira & Feijó. Hydrogel control of water uptake by pectins during in vitro pollen hydration of Eucalyptus globulus. *American Journal of Botany* **103**, 437-451 (2016).

17 Bosch, Cheung & Hepler. Pectin methylesterase, a regulator of pollen tube growth. *Plant physiology* **138**, 1334-1346 (2005).

18 Place, Evans & Stevens. Complexity in biomaterials for tissue engineering. *Nature materials* **8**, 457 (2009).

19 Wang, Kim, Vunjak-Novakovic & Kaplan. Stem cell-based tissue engineering with silk biomaterials. *Biomaterials* **27**, 6064-6082 (2006).

20 Ebrahimi, Tokareva, Rim, Wong, Kaplan & Buehler. Silk–its mysteries, how it is made, and how it is used. *ACS biomaterials science & engineering* **1**, 864-876 (2015).

21 Gupta, Lorentz, Haskett, Cunnane, Ramaswamy, Weinbaum, Vorp & Mandal. Bioresorbable silk grafts for small diameter vascular tissue engineering applications: In vitro and in vivo functional analysis. *Acta Biomaterialia* (2020).

22 Li, Li, Chen, He, Han, Wang & Kaplan. Silk-based biomaterials in biomedical textiles and fiber-based implants. *Advanced healthcare materials* **4**, 1134-1151 (2015).

23 Li, Xu, Xu, Mao, Xu, Zhong, Zhang, Wang & Sui. Cellulose sponge supported palladium nanoparticles as recyclable cross-coupling catalysts. *ACS applied materials & interfaces* **9**, 17155-17162 (2017).

24 Wang, He, Wang, Zhang, Yu, Peng, Wu, Ren, Zeng & Xue. A cellulose sponge with robust superhydrophilicity and under-water superoleophobicity for highly effective oil/water separation. *Green Chemistry* **17**, 3093-3099 (2015).

25 Wang, Gunasekara, Reed, DiSalvo, Bultman, Sims, Magness & Allbritton. A microengineered collagen scaffold for generating a polarized crypt-villus architecture of human small intestinal epithelium. *Biomaterials* **128**, 44-55 (2017).

26 Tozzi, Laurent, Di Buduo, Mu, Massaro, Bretherton, Stoppel, Kaplan & Balduini. Multi-channel silk sponge mimicking bone marrow vascular niche for platelet production. *Biomaterials* **178**, 122-133 (2018).

27 Somsesta, Sricharoenchaikul & Aht-Ong. Adsorption removal of methylene blue onto activated carbon/cellulose biocomposite films: equilibrium and kinetic studies. *Materials Chemistry and Physics* **240**, 122221 (2020).

28 Lu, Xu, Zhang, Pan, Wang, Alshehri, Ahamad, Kim, Na & Hossain. High-Performance Capacitive Deionization by Lignocellulose-Derived Eco-Friendly Porous Carbon Materials. *Bulletin of the Chemical Society of Japan* **93**, 1014-1019 (2020).

29 Guo, Lu, Zhao, Zhou, Shi & Yu. Biomass-Derived Hybrid Hydrogel Evaporators for Cost-Effective Solar Water Purification. *Advanced Materials* **32**, 1907061 (2020).

30 Vining & Mooney. Mechanical forces direct stem cell behaviour in development and regeneration. *Nature Reviews Molecular Cell Biology* **18**, 728 (2017).

31 Ladoux & Mège. Mechanobiology of collective cell behaviours. *Nature Reviews Molecular Cell Biology* **18**, 743 (2017).

32 Sheridan, Shea, Peters & Mooney. Bioabsorbable polymer scaffolds for tissue engineering capable of sustained growth factor delivery. *Journal of controlled release* **64**, 91-102 (2000).

33 Sill & von Recum. Electrospinning: applications in drug delivery and tissue engineering. *Biomaterials* **29**, 1989-2006 (2008).

34 Biondi, Ungaro, Quaglia & Netti. Controlled drug delivery in tissue engineering. *Advanced drug delivery reviews* **60**, 229-242 (2008).

35 Zhao, Zou, Tang & Mulcahy. Recent developments in forward osmosis: opportunities and challenges. *Journal of membrane science* **396**, 1-21 (2012).

36 Klaysom, Cath, Depuydt & Vankelecom. Forward and pressure retarded osmosis: potential solutions for global challenges in energy and water supply. *Chemical society reviews* **42**, 6959-6989 (2013).

37 Gray, McCutcheon & Elimelech. Internal concentration polarization in forward osmosis: role of membrane orientation. *Desalination* **197**, 1-8, doi:https://doi.org/10.1016/j.desal.2006.02.003 (2006).

38 Pham & Dickerson. Superhydrophobic Silanized Melamine Sponges as High Efficiency Oil Absorbent Materials. *ACS Applied Materials & Interfaces* **6**, 14181-14188, doi:10.1021/am503503m (2014).

39 Zhu, Chu, Wang, Chen, Lin, Liu & Pan. Robust superhydrophobic polyurethane sponge as a highly reusable oil-absorption material. *Journal of Materials Chemistry A* **1**, 5386-5393, doi:10.1039/C3TA00125C (2013).

40 Chu & Pan. Three-Dimensionally Macroporous Fe/C Nanocomposites As Highly Selective Oil-Absorption Materials. *ACS Applied Materials & Interfaces* **4**, 2420-2425, doi:10.1021/am3000825 (2012).

41 Lim & Huang. Evaluation of kapok (Ceiba pentandra (L.) Gaertn.) as a natural hollow hydrophobic–oleophilic fibrous sorbent for oil spill cleanup. *Chemosphere* **66**, 955-963 (2007).

42 Zhang, Sèbe, Rentsch, Zimmermann & Tingaut. Ultralightweight and Flexible Silylated Nanocellulose Sponges for the Selective Removal of Oil from Water. *Chemistry of Materials* **26**, 2659-2668, doi:10.1021/cm5004164 (2014).

43 Quilichini, Grienenberger & Douglas. The biosynthesis, composition and assembly of the outer pollen wall: A tough case to crack. *Phytochemistry* **113**, 170-182 (2015).

44 Gonzalez-Cruz, Uddin, Atwe, Abidi & Gill. Chemical treatment method for obtaining clean and intact pollen shells of different species. *ACS biomaterials science & engineering* **4**, 2319-2329 (2018).

45 Bernard, Benzerara, Beyssac, Balan & Brown Jr. Evolution of the macromolecular structure of sporopollenin during thermal degradation. *Heliyon* **1**, e00034 (2015).

46 Bağcıoğlu, Zimmermann & Kohler. A multiscale vibrational spectroscopic approach for identification and biochemical characterization of pollen. *PLoS One* **10**, e0137899 (2015).

47 Liu & Zhang. Mechanical properties of desiccated ragweed pollen grains determined by micromanipulation and theoretical modelling. *Biotechnology and bioengineering* **85**, 770-775 (2004).

48 Xia, Li, Gao, Fu, Fang, Zhang & Zhang. Tissue repair and regeneration with endogenous stem cells. *Nature Reviews Materials* **3**, 174 (2018).

49 Mikhael, Jurcic, Schneider, Karr, Fisher, Fridgen, Diego-Taboada, Georghiou, Mackenzie & Banoub. Demystifying and Unravelling the Molecular Structure of the Biopolymer Sporopollenin. *Rapid Communications in Mass Spectrometry* (2020).

50 Saxena, Hansen & Lyon. Microgel mechanics in biomaterial design. *Accounts of chemical research* **47**, 2426-2434 (2014).

51 Li, Lu & Walz. Freeze casting of porous materials: review of critical factors in microstructure evolution. *International materials reviews* **57**, 37-60 (2012).

52 Wu, Zhu, He, Xue, Fan, Song, Francisco, Zeng & Wang. Ion-specific ice recrystallization provides a facile approach for the fabrication of porous materials. *Nature communications* **8**, 15154 (2017).

53 Balaji, Pakalapati, Khalid, Walvekar & Siddiqui. Natural and synthetic biocompatible and biodegradable polymers. *Navinchandra Gopal Shimpi. Biodegradable and biocompatible polymer composites. Oxford: Elsevier*, 3-32 (2018).

54 Asghari, Samiei, Adibkia, Akbarzadeh & Davaran. Biodegradable and biocompatible polymers for tissue engineering application: a review. *Artificial cells, nanomedicine, and biotechnology* **45**, 185-192 (2017).

55 Joyce, Fabra, Bozkurt & Pandit. Bioactive potential of natural biomaterials: identification, retention and assessment of biological properties. *Signal transduction and targeted therapy* **6**, 1-28 (2021).

56 Sbrodov. in *IOP Conference Series: Materials Science and Engineering.* 012016 (IOP Publishing).

57 Malujda & Wilczyński. Mechanical properties investigation of natural polymers. *Procedia engineering* **136**, 263-268 (2016).

58 Ghalia & Abdelrasoul. in *Mechanical and physical testing of biocomposites, fibre-reinforced composites and hybrid composites* 123-140 (Elsevier, 2019).

59 Ardalan, Emamzadeh, Rasekh, Joshaghani & Samali. Physical and mechanical properties of polymer modified self-compacting concrete (SCC) using natural and recycled aggregates. *Journal of Sustainable Cement-Based Materials* **9**, 1-16 (2020).

60 Terlikowski, Sobczyńska, Gregoriou-Szczepaniak & Wasilewski. in *IOP Conference Series: Materials Science and Engineering.* 012135 (IOP Publishing).

61 Pintea & Manea. Influence of natural organic polymers upon plaster mortar workability. *Procedia Manufacturing* **46**, 158-164 (2020).

62 Ngwuluka, Ochekpe & Aruoma. Naturapolyceutics: the science of utilizing natural polymers for drug delivery. *polymers* **6**, 1312-1332 (2014).

63 George, Shah & Shrivastav. Guar gum: Versatile natural polymer for drug delivery applications. *European Polymer Journal* **112**, 722-735 (2019).

64 Anwunobi & Emeje. Recent applications of natural polymers in nanodrug delivery. *J Nanomedic Nanotechnol S* **4** (2011).

65 Gavasane & Pawar. Synthetic biodegradable polymers used in controlled drug delivery system: an overview. *Clin Pharmacol Biopharm* **3**, 1-7 (2014).

66 Patel & Goyal. Applications of natural polymer gum arabic: a review. *International Journal of Food Properties* **18**, 986-998 (2015).

67 Celli, Gandini, Gioia, Lacerda, Vannini & Colonna. Polymers from pristine and modified natural monomers. *Chemicals and Fuels from Bio-Based Building Blocks* **1** (2016).

68 Caillol. (Multidisciplinary Digital Publishing Institute, 2021).

69 Mallakpour & Dinari. Progress in synthetic polymers based on natural amino acids. *Journal of Macromolecular Science, Part A* **48**, 644-679 (2011).

70 Namazi. Polymers in our daily life. *BioImpacts: BI* **7**, 73 (2017).

71 Kulkarni Vishakha, Butte Kishor & Rathod Sudha. Natural polymers–A comprehensive review. *International journal of research in pharmaceutical and biomedical sciences* **3**, 1597-1613 (2012).

72 Abedini, Ebrahimi, Roozbehani, Domb & Hosseinkhani. Overview on natural hydrophilic polysaccharide polymers in drug delivery. *Polymers for Advanced Technologies* **29**, 2564-2573 (2018).

73 Schmidt. Hydrophilic Polymers. *Polymers* **11**, 693 (2019).

74 Rajeswari, Prasanthi, Sudha, Swain, Panda & Goka. Natural polymers: a recent review. *World J. Pharm. Pharm. Sci* **6**, 472-494 (2017).

75 Ceglia, Merlin, Viot, Schmitt & Mondain-Monval. Porous materials with tunable mechanical properties. *Journal of Porous Materials* **21**, 903-912 (2014).

76 Li, Huang, Gao, Zhong, Cao, Chen, Zhang & Cai. Reinforced mechanical properties and tunable biodegradability in nanoporous cellulose gels: poly (l-lactide-co-caprolactone) nanocomposites. *Biomacromolecules* **17**, 1506-1515 (2016).

77 Abid, Khan & Iqbal. A study on optical and thermal properties of natural polymer-based hemicellulose compounds. *Journal of Biomaterials Science, Polymer Edition*, 1-14 (2021).

78 Birajdar, Joo, Koh & Park. Natural bio-based monomers for biomedical applications: a review. *Biomaterials Research* **25**, 1-14 (2021).

79 de Moraes Porto. Polymer biocompatibility. *Polymerization. Croatia: InTech* **2012**, 47-63 (2012).

80 Bhatia. in *Natural Polymer Drug Delivery Systems* 95-118 (Springer, 2016).

81 Cao & Uhrich. Biodegradable and biocompatible polymers for electronic applications: A review. *Journal of Bioactive and Compatible Polymers* **34**, 3-15 (2019).

82 Altuntaş, Özkan & Yener. in *Nanobiomaterials Science, Development and Evaluation* 27-59 (Elsevier, 2017).

83 Samadian, Maleki, Allahyari & Jaymand. Natural polymers-based light-induced hydrogels: Promising biomaterials for biomedical applications. *Coordination Chemistry Reviews* **420**, 213432 (2020).

84 Albuquerque, Coelho, Teixeira & Carneiro-da-Cunha. Approaches in biotechnological applications of natural polymers. (2016).

85 Torres, Troncoso, Pisani, Gatto & Bardi. Natural polysaccharide nanomaterials: an overview of their immunological properties. *International journal of molecular sciences* **20**, 5092 (2019).

86 Banwell, Pollard, Liu & Connal. Exploiting Nature's Most Abundant Polymers: Developing New Pathways for the Conversion of Cellulose, Hemicellulose, Lignin and Chitin into Platform Molecules (and Beyond). *Chemistry–An Asian Journal* **16**, 604-620 (2021).

87 Acquavia, Pascale, Martelli, Bondoni & Bianco. Natural polymeric materials: A solution to plastic pollution from the agro-food sector. *Polymers* **13**, 158 (2021).

88 Liu, Holzwarth & Ma. Functionalized synthetic biodegradable polymer scaffolds for tissue engineering. *Macromolecular bioscience* **12**, 911-919 (2012).

89 Oh & Lee. Hydrophilization of synthetic biodegradable polymer scaffolds for improved cell/tissue compatibility. *Biomedical materials* **8**, 014101 (2013).

90 Bou-Gharios, Abraham & de Crombrugghe. in *Principles of bone biology* 295-337 (Elsevier, 2020).

91 Abedinia, Mohammadi Nafchi, Sharifi, Ghalambor, Oladzadabbasabadi, Ariffin & Huda. Poultry gelatin: Characteristics, developments, challenges, and future outlooks as a sustainable alternative for mammalian gelatin. *Trends in Food Science & Technology* **104**, 14-26, doi:https://doi.org/10.1016/j.tifs.2020.08.001 (2020).

92 Cao, Wang, Hao, Zhang & Zhou. Antihypertensive Effects in Vitro and in Vivo of Novel Angiotensin-Converting Enzyme Inhibitory Peptides from Bovine Bone Gelatin Hydrolysate. *Journal of Agricultural and Food Chemistry* **68**, 759-768, doi:10.1021/acs.jafc.9b05618 (2020).

93 Mony, Shenoy, Raj, Geetha, Pratheesh, Nair, Purnima & Anilkumar. Gelatin-Modified Cholecyst-Derived Scaffold Promotes Angiogenesis and Faster Healing of Diabetic Wounds. *ACS Applied Bio Materials* **4**, 3320-3331, doi:10.1021/acsabm.0c01648 (2021).

94 Alipal, Mohd Pu'ad, Lee, Nayan, Sahari, Basri, Idris & Abdullah. A review of gelatin: Properties, sources, process, applications, and commercialisation. *Materials Today: Proceedings* **42**, 240-250, doi:https://doi.org/10.1016/j.matpr.2020.12.922 (2021).

95 Wang, Ao, Tian, Fan, Tong, Hou & Bai. Gelatin-based hydrogels for organ 3D bioprinting. *Polymers* **9**, 401 (2017).

96 Lin, Regenstein, Lv, Lu & Jiang. An overview of gelatin derived from aquatic animals: Properties and modification. *Trends in Food Science & Technology* **68**, 102-112, doi:https://doi.org/10.1016/j.tifs.2017.08.012 (2017).

97 Wilson, Amirkhani & Taylor. Evaluation of Gelatin as a Biostimulant Seed Treatment to Improve Plant Performance. *Frontiers in Plant Science* **9**, doi:10.3389/fpls.2018.01006 (2018).

98 Karim & Bhat. Fish gelatin: properties, challenges, and prospects as an alternative to mammalian gelatins. *Food Hydrocolloids* **23**, 563-576, doi:https://doi.org/10.1016/j.foodhyd.2008.07.002 (2009).

99 Jongjareonrak, Rawdkuen, Chaijan, Benjakul, Osako & Tanaka. Chemical compositions and characterisation of skin gelatin from farmed giant catfish (Pangasianodon gigas). *LWT - Food Science and Technology* **43**, 161-165, doi:https://doi.org/10.1016/j.lwt.2009.06.012 (2010).

100 Roy & Rhim. Preparation of Gelatin/Carrageenan-Based Color-Indicator Film Integrated with Shikonin and Propolis for Smart Food Packaging Applications. *ACS Applied Bio Materials* **4**, 770-779, doi:10.1021/acsabm.0c01353 (2021).

101 Campiglio, Contessi Negrini, Farè & Draghi. Cross-Linking Strategies for Electrospun Gelatin Scaffolds. *Materials* **12**, doi:10.3390/ma12152476 (2019).

102 Tytgat, Van Damme, Van Hoorick, Declercq, Thienpont, Ottevaere, Blondeel, Dubruel & Van Vlierberghe. Additive manufacturing of photo-crosslinked gelatin scaffolds for adipose tissue engineering. *Acta Biomaterialia* **94**, 340-350, doi:https://doi.org/10.1016/j.actbio.2019.05.062 (2019).

103 Soltan, Ning, Mohabatpour, Papagerakis & Chen. Printability and Cell Viability in Bioprinting Alginate Dialdehyde-Gelatin Scaffolds. *ACS Biomaterials Science & Engineering* **5**, 2976-2987, doi:10.1021/acsbiomaterials.9b00167 (2019).

104 Ferracci, Zhu, Ibrahim, Ma, Fan, Lee & Cho. Photocurable Albumin Methacryloyl Hydrogels as a Versatile Platform for Tissue Engineering. *ACS Applied Bio Materials* **3**, 920-934 (2020).

105 Fox, Li, Xu & Edgar. Regioselective Esterification and Etherification of Cellulose: A Review. *Biomacromolecules* **12**, 1956-1972, doi:10.1021/bm200260d (2011).

106 Zhao, Kwak, Wang, Franz, White & Holladay. Effects of Crystallinity on Dilute Acid Hydrolysis of Cellulose by Cellulose Ball-Milling Study. *Energy & Fuels* **20**, 807-811, doi:10.1021/ef050319a (2006).

107 Thakur & Thakur. Processing and characterization of natural cellulose fibers/thermoset polymer composites. *Carbohydrate polymers* **109**, 102-117 (2014).

108 Liu, Du, Zhang, Liu, Liu, Xie, Zhang & Si. Bacterial Cellulose-Based Composite Scaffolds for Biomedical Applications: A Review. *ACS Sustainable Chemistry & Engineering* **8**, 7536-7562, doi:10.1021/acssuschemeng.0c00125 (2020).

109 Dugan, Gough & Eichhorn. Bacterial cellulose scaffolds and cellulose nanowhiskers for tissue engineering. *Nanomedicine* **8**, 287-298, doi:10.2217/nnm.12.211 (2013).

110 Modulevsky, Lefebvre, Haase, Al-Rekabi & Pelling. Apple derived cellulose scaffolds for 3D mammalian cell culture. *PloS one* **9**, e97835 (2014).

111 Courtenay, Johns, Galembeck, Deneke, Lanzoni, Costa, Scott & Sharma. Surface modified cellulose scaffolds for tissue engineering. *Cellulose* **24**, 253-267 (2017).

112 Abitbol, Rivkin, Cao, Nevo, Abraham, Ben-Shalom, Lapidot & Shoseyov. Nanocellulose, a tiny fiber with huge applications. *Current Opinion in Biotechnology* **39**, 76-88, doi:https://doi.org/10.1016/j.copbio.2016.01.002 (2016).

113 Dufresne. Nanocellulose: a new ageless bionanomaterial. *Materials today* **16**, 220-227 (2013).

114 Kyle, Jessop, Al-Sabah, Hawkins, Lewis, Maffeis, Charbonneau, Gazze, Francis, Iakovlev, Nelson, Eichhorn & Whitaker. Characterization of pulp derived nanocellulose hydrogels using AVAP® technology. *Carbohydrate Polymers* **198**, 270-280, doi:https://doi.org/10.1016/j.carbpol.2018.06.091 (2018).

115 Kim, Shim, Kim, Lee, Min, Jang, Abas & Kim. Review of nanocellulose for sustainable future materials. *International Journal of Precision Engineering and Manufacturing-Green Technology* **2**, 197-213 (2015).

116 Auad, Contos, Nutt, Aranguren & Marcovich. Characterization of nanocellulose-reinforced shape memory polyurethanes. *Polymer International* **57**, 651-659, doi:https://doi.org/10.1002/pi.2394 (2008).

117 Thomas, Raj, B, H, Joy, Moores, Drisko & Sanchez. Nanocellulose, a Versatile Green Platform: From Biosources to Materials and Their Applications. *Chemical Reviews* **118**, 11575-11625, doi:10.1021/acs.chemrev.7b00627 (2018).

118 Frey, Widner, Segmehl, Casdorff, Keplinger & Burgert. Delignified and Densified Cellulose Bulk Materials with Excellent Tensile Properties for Sustainable Engineering. *ACS Applied Materials & Interfaces* **10**, 5030-5037, doi:10.1021/acsami.7b18646 (2018).

119 Khan & Khan. Use of collagen as a biomaterial: An update. *Journal of Indian Society of Periodontology* **17**, 539 (2013).

120 Brodsky & Ramshaw. The collagen triple-helix structure. *Matrix biology* **15**, 545-554 (1997).

121 Brodsky & Persikov. Molecular structure of the collagen triple helix. *Advances in protein chemistry* **70**, 301-339 (2005).

122 Egli, Schnitzer, Dietschreit, Ochsenfeld & Wennemers. Why proline? Influence of ring-size on the collagen triple helix. *Organic letters* **22**, 348-351 (2019).

123 Zhang, Gopalakrishnan, Li, Wang, Han & Rotello. Fabrication of Collagen Films with Enhanced Mechanical and Enzymatic Stability through Thermal Treatment in Fluorous Media. *ACS Applied Materials & Interfaces* **12**, 6590-6597, doi:10.1021/acsami.9b18256 (2020).

124 Kim, Yun & Kim. An innovative cell-laden α-TCP/collagen scaffold fabricated using a two-step printing process for potential application in regenerating hard tissues. *Scientific Reports* **7**, 3181, doi:10.1038/s41598-017-03455-9 (2017).

125 Zarei, Samimi, Khorram, Abdi & Golestaneh. Fabrication and characterization of conductive polypyrrole/chitosan/collagen electrospun nanofiber scaffold for tissue engineering application. *International Journal of Biological Macromolecules* **168**, 175-186, doi:https://doi.org/10.1016/j.ijbiomac.2020.12.031 (2021).

126 Seong, Kang, Song, Kim & Jeong. Calcium Phosphate–Collagen Scaffold with Aligned Pore Channels for Enhanced Osteochondral Regeneration. *Advanced Healthcare Materials* **6**, 1700966, doi:https://doi.org/10.1002/adhm.201700966 (2017).

127 Yang, Ding, Tang, Deng, Yang, Wu, Chen, Ni, Huang & Zhang. Novel modification of collagen: Realizing desired water solubility and thermostability in a conflict-free way. *ACS omega* **5**, 5772-5780 (2020).

128 Avila Rodríguez, Rodriguez Barroso & Sánchez. Collagen: A review on its sources and potential cosmetic applications. *Journal of cosmetic dermatology* **17**, 20-26 (2018).

129 Rapson, Christley-Balcomb, Jackson & Sutherland. Enhancement of metallomacrocycle-based oxygen reduction catalysis through immobilization in a tunable silk-protein scaffold. *Journal of inorganic biochemistry* **204**, 110960 (2020).

130 Belda Marín, Fitzpatrick, Kaplan, Landoulsi, Guénin & Egles. Silk Polymers and Nanoparticles: A Powerful Combination for the Design of Versatile Biomaterials. *Frontiers in chemistry* **8**, 604398-604398, doi:10.3389/fchem.2020.604398 (2020).

131 Marín, Fitzpatrick, Kaplan, Landoulsi, Guénin & Egles. Silk polymers and nanoparticles: a powerful combination for the design of versatile biomaterials. *Frontiers in Chemistry* **8** (2020).

132 Zhang, Zhang, Hu, Fei, Liu, Huang, Wang, Ruan, Heng, Chen & Shen. Systematic Review of Silk Scaffolds in Musculoskeletal Tissue Engineering Applications in the Recent Decade. *ACS Biomaterials Science & Engineering* **7**, 817-840, doi:10.1021/acsbiomaterials.0c01716 (2021).

133 Gu, Jiang & Hu. Scalable Spider-Silk-Like Supertough Fibers using a Pseudoprotein Polymer. *Advanced Materials* **31**, 1904311 (2019).

134 Mu, Wang, Guo, Li, Ling, Huang, Cebe, Hsu, De Ferrari & Jiang. 3D Printing of Silk Protein Structures by Aqueous Solvent-Directed Molecular Assembly. *Macromolecular bioscience* **20**, 1900191 (2020).

135 Agostinacchio, Mu, Dirè, Motta & Kaplan. In situ 3D printing: opportunities with silk inks. *Trends in Biotechnology* (2020).

136 Huang, Yuan, Hong, Fan, Yao, Ren, Song, Yang & Zhang. 3D printed hydrogels with oxidized cellulose nanofibers and silk fibroin for the proliferation of lung epithelial stem cells. *Cellulose* **28**, 241-257 (2021).

137 Gore, Naebe, Wang & Kandasubramanian. Progress in silk materials for integrated water treatments: Fabrication, modification and applications. *Chemical Engineering Journal* **374**, 437-470, doi:https://doi.org/10.1016/j.cej.2019.05.163 (2019).

138 Lu, Hu, Wang, Kluge, Lu, Cebe & Kaplan. Water-insoluble silk films with silk I structure. *Acta Biomaterialia* **6**, 1380-1387, doi:https://doi.org/10.1016/j.actbio.2009.10.041 (2010).

139 Zheng, Zhong, Qi, Ling & Kaplan. Isolation of Silk Mesostructures for Electronic and Environmental Applications. *Advanced Functional Materials* **28**, 1806380, doi:https://doi.org/10.1002/adfm.201806380 (2018).

140 Rinaudo. Chitin and chitosan: Properties and applications. *Progress in Polymer Science* **31**, 603-632, doi:https://doi.org/10.1016/j.progpolymsci.2006.06.001 (2006).

141 Ravi Kumar. A review of chitin and chitosan applications. *Reactive and Functional Polymers* **46**, 1-27, doi:https://doi.org/10.1016/S1381-5148(00)00038-9 (2000).

142 Croisier & Jérôme. Chitosan-based biomaterials for tissue engineering. *European polymer journal* **49**, 780-792 (2013).

143 Jayakumar, Menon, Manzoor, Nair & Tamura. Biomedical applications of chitin and chitosan based nanomaterials—A short review. *Carbohydrate Polymers* **82**, 227-232, doi:https://doi.org/10.1016/j.carbpol.2010.04.074 (2010).

144 Jayakumar, Chennazhi, Srinivasan, Nair, Furuike & Tamura. Chitin Scaffolds in Tissue Engineering. *International Journal of Molecular Sciences* **12**, doi:10.3390/ijms12031876 (2011).

145 Shamshina, Berton & Rogers. Advances in Functional Chitin Materials: A Review. *ACS Sustainable Chemistry & Engineering* **7**, 6444-6457, doi:10.1021/acssuschemeng.8b06372 (2019).

146 Madhumathi, Kumar, Abhilash, Sreeja, Tamura, Manzoor, Nair & Jayakumar. Development of novel chitin/nanosilver composite scaffolds for wound dressing applications. *Journal of Materials Science: Materials in Medicine* **21**, 807-813 (2010).

147 Yoon, Kim, Wang, Fang, Hsiao & Chu. High flux ultrafiltration membranes based on electrospun nanofibrous PAN scaffolds and chitosan coating. *Polymer* **47**, 2434-2441 (2006).

148 Zhao, Zheng, Wang, Zhang & Han. High performance ultrafiltration membrane based on modified chitosan coating and electrospun nanofibrous PVDF scaffolds. *Journal of membrane science* **394**, 209-217 (2012).

149 Goetz, Jalvo, Rosal & Mathew. Superhydrophilic anti-fouling electrospun cellulose acetate membranes coated with chitin nanocrystals for water filtration. *Journal of Membrane Science* **510**, 238-248 (2016).

150 Asghar & Henrickson. Chemical, biochemical, functional, and nutritional characteristics of collagen in food systems. *Advances in food research* **28**, 231-372 (1982).

151 Gómez-Guillén, Giménez, López-Caballero & Montero. Functional and bioactive properties of collagen and gelatin from alternative sources: A review. *Food Hydrocolloids* **25**, 1813-1827, doi:https://doi.org/10.1016/j.foodhyd.2011.02.007 (2011).

152 Bello, Kim, Kim, Park & Lee. Engineering and functionalization of gelatin biomaterials: From cell culture to medical applications. *Tissue Engineering Part B: Reviews* **26**, 164-180 (2020).

153 Xing, Yates, Vogt, Qian, Frost & Zhao. Increasing mechanical strength of gelatin hydrogels by divalent metal ion removal. *Scientific reports* **4**, 1-10 (2014).

154 Shoulders & Raines. Collagen structure and stability. *Annual review of biochemistry* **78**, 929-958 (2009).

155 Tanaka, Inoue & Mizuno. Hydrophobic interaction of P25, containing Asn-linked oligosaccharide chains, with the HL complex of silk fibroin produced by Bombyx mori. *Insect biochemistry and molecular biology* **29**, 269-276 (1999).

156 Zhou, Confalonieri, Jacquet, Perasso, Li & Janin. Silk fibroin: structural implications of a remarkable amino acid sequence. *Proteins: Structure, Function, and Bioinformatics* **44**, 119-122 (2001).

157 Asakura, Ito, Okudaira & Kameda. Structure of Alanine and Glycine Residues of Samia c ynthia r icini Silk Fibers Studied with Solid-State 15N and 13C NMR. *Macromolecules* **32**, 4940-4946 (1999).

158 Gage & Manning. Internal structure of the silk fibroin gene of Bombyx mori. I The fibroin gene consists of a homogeneous alternating array of repetitious crystalline and amorphous coding sequences. *Journal of Biological Chemistry* **255**, 9444-9450 (1980).

159 Fedic, Zˇurovec & Sehnal. Correlation between fibroin amino acid sequence and physical silk properties. *Journal of Biological Chemistry* **278**, 35255-35264 (2003).

160 Huang, Ling, Li, Omenetto & Kaplan. Silkworm silk-based materials and devices generated using bio-nanotechnology. *Chemical Society Reviews* **47**, 6486-6504 (2018).

161 Husmann, Pawelec, Burdett, Best & Cameron. Numerical simulations to determine the influence of mould design on ice-templated scaffold structures. *genesis* **6**, 8 (2015).

162 Asuncion, Goh & Toh. Anisotropic silk fibroin/gelatin scaffolds from unidirectional freezing. *Materials Science and Engineering: C* **67**, 646-656 (2016).

163 Pawelec, Husmann, Best & Cameron. A design protocol for tailoring ice-templated scaffold structure. *Journal of the Royal Society Interface* **11**, 20130958 (2014).

164 Shao, Hanaor, Shen & Gurlo. Freeze Casting: From Low-Dimensional Building Blocks to Aligned Porous Structures—A Review of Novel Materials, Methods, and Applications. *Advanced Materials* **32**, 1907176, doi:https://doi.org/10.1002/adma.201907176 (2020).

165 Martoïa, Cochereau, Dumont, Orgéas, Terrien & Belgacem. Cellulose nanofibril foams: Links between ice-templating conditions, microstructures and mechanical properties. *Materials & Design* **104**, 376-391 (2016).

166 Deville, Viazzi & Guizard. Ice-structuring mechanism for zirconium acetate. *Langmuir* **28**, 14892-14898 (2012).

167 Wu, Li, Xue, Liu, Fan, Bai & Wang. Size Controllable, Transparent, and Flexible 2D Silver Meshes Using Recrystallized Ice Crystals as Templates. *ACS Nano* **11**, 9898-9905, doi:10.1021/acsnano.7b03821 (2017).

168 Zhang, Li, Lv, Zhao & Qu. Vertically Aligned Graphene Sheets Membrane for Highly Efficient Solar Thermal Generation of Clean Water. *ACS Nano* **11**, 5087-5093, doi:10.1021/acsnano.7b01965 (2017).

169 Wu, Zhu, He, Xue, Fan, Song, Francisco, Zeng & Wang. Ion-specific ice recrystallization provides a facile approach for the fabrication of porous materials. *Nature communications* **8**, 1-8 (2017).

170 Baheti, Kumar & Bansal. Excipients used in lyophilization of small molecules. *Journal of Excipients and Food Chemicals* **1**, 1135 (2016).

171 Whang, Thomas, Healy & Nuber. A novel method to fabricate bioabsorbable scaffolds. *Polymer* **36**, 837-842 (1995).

172 Owen, Sherborne, Evans, Reilly & Claeyssens. Combined porogen leaching and emulsion templating to produce bone tissue engineering scaffolds. *International Journal of Bioprinting* **6** (2020).

173 Yıldırım, Demirtaş, Dinçer, Yıldız & Karakeçili. Preparation of polycaprolactone/graphene oxide scaffolds: A green route combining supercritial CO2 technology and porogen leaching. *The Journal of Supercritical Fluids* **133**, 156-162 (2018).

174 Yin, Qian, Zhang, Lin, Li, Xu & Li. Engineering porous poly (lactic acid) scaffolds with high mechanical performance via a solid state extrusion/porogen leaching approach. *Polymers* **8**, 213 (2016).

175 Chen & Ma. Nano-fibrous poly(l-lactic acid) scaffolds with interconnected spherical macropores. *Biomaterials* **25**, 2065-2073, doi:https://doi.org/10.1016/j.biomaterials.2003.08.058 (2004).

176 Salerno, Fernández-Gutiérrez, del Barrio & Domingo. Bio-safe fabrication of PLA scaffolds for bone tissue engineering by combining phase separation, porogen leaching and scCO2 drying. *The Journal of Supercritical Fluids* **97**, 238-246 (2015).

177 Janik & Marzec. A review: Fabrication of porous polyurethane scaffolds. *Materials Science and Engineering: C* **48**, 586-591, doi:https://doi.org/10.1016/j.msec.2014.12.037 (2015).

178 Yu, Hua, Yang, Fu, Teng, Niu, Zhao & Yi. Fabrication and characterization of electrospinning/3D printing bone tissue engineering scaffold. *RSC advances* **6**, 110557-110565 (2016).

179 Do, Khorsand, Geary & Salem. 3D printing of scaffolds for tissue regeneration applications. *Advanced healthcare materials* **4**, 1742-1762 (2015).

180 Maroulakos, Kamperos, Tayebi, Halazonetis & Ren. Applications of 3D printing on craniofacial bone repair: A systematic review. *Journal of Dentistry* **80**, 1-14 (2019).

181 Ventola. Medical applications for 3D printing: current and projected uses. *Pharmacy and Therapeutics* **39**, 704 (2014).

182 Ko, Pan, Grigoropoulos, Luscombe, Fréchet & Poulikakos. All-inkjet-printed flexible electronics fabrication on a polymer substrate by low-temperature high-resolution selective laser sintering of metal nanoparticles. *Nanotechnology* **18**, 345202 (2007).

183 Costantini & Barbetta. in *Functional 3D Tissue Engineering Scaffolds* 127-149 (Elsevier, 2018).

184 Chen, Zhou, Tang, Weir, Bao & Xu. Gas-foaming calcium phosphate cement scaffold encapsulating human umbilical cord stem cells. *Tissue Engineering Part A* **18**, 816-827 (2012).

185 Song, Zhou, Fan, Zhang, Pei, Fan, Jiang, Bao, Yang & Dong. Novel 3D porous biocomposite scaffolds fabricated by fused deposition modeling and gas foaming combined technology. *Composites Part B: Engineering* **152**, 151-159 (2018).

186 Gorna & Gogolewski. Preparation, degradation, and calcification of biodegradable polyurethane foams for bone graft substitutes. *Journal of Biomedical Materials Research Part A: An Official Journal of The Society for Biomaterials, The Japanese Society for Biomaterials, and The Australian Society for Biomaterials and the Korean Society for Biomaterials* **67**, 813-827 (2003).

187 Kim & Hollinger. Recombinant human bone morphogenetic protein-2 released from polyurethane-based scaffolds promotes early osteogenic differentiation of human mesenchymal stem cells. *Biomedical materials* **7**, 045008 (2012).

188 Kim, Park, Kim, Cho & Kim. Gas foaming fabrication of porous biphasic calcium phosphate for bone regeneration. *Tissue Engineering and Regenerative Medicine* **9**, 63-68 (2012).

189 Quirk, France, Shakesheff & Howdle. Supercritical fluid technologies and tissue engineering scaffolds. *Current Opinion in Solid State and Materials Science* **8**, 313-321 (2004).

190 Ramakrishna, Fujihara, Teo, Yong, Ma & Ramaseshan. Electrospun nanofibers: solving global issues. *Materials today* **9**, 40-50 (2006).

191 Dror, Salalha, Khalfin, Cohen, Yarin & Zussman. Carbon nanotubes embedded in oriented polymer nanofibers by electrospinning. *Langmuir* **19**, 7012-7020 (2003).

192 Kanani & Bahrami. Review on electrospun nanofibers scaffold and biomedical applications. *Trends Biomater Artif Organs* **24**, 93-115 (2010).

193 Yang, Chen, Wang, Zhu, Xu, Chen, Ma & Li. A facile electrospinning method to fabricate polylactide/graphene/MWCNTs nanofiber membrane for tissues scaffold. *Applied Surface Science* **362**, 163-168 (2016).

194 Liang, Zhang, Huang, Xu & Fong. Superhydrophobic and elastic 3D conductive sponge made from electrospun nanofibers and reduced graphene oxide for sweatproof wearable tactile pressure sensor. *Polymer*, 124025, doi:https://doi.org/10.1016/j.polymer.2021.124025 (2021).

195 Karki, Kafle, Ojha, Song & Kim. Three-dimensional nanoporous polyacrylonitrile-based carbon scaffold for effective separation of oil from oil/water emulsion. *Polymer* **153**, 597-606, doi:https://doi.org/10.1016/j.polymer.2018.08.069 (2018).

196 Desai, Kit, Li & Zivanovic. Morphological and surface properties of electrospun chitosan nanofibers. *Biomacromolecules* **9**, 1000-1006 (2008).

197 Makaremi, De Silva & Pasbakhsh. Electrospun nanofibrous membranes of polyacrylonitrile/halloysite with superior water filtration ability. *The Journal of Physical Chemistry C* **119**, 7949-7958 (2015).

198 Xu, Zheng, Chen, Ding, Liang, Liu, Zhu & Fong. Halloysite nanotubes sponges with skeletons made of electrospun nanofibers as innovative dye adsorbent and catalyst support. *Chemical Engineering Journal* **360**, 280-288 (2019).

199 Xu, Miszuk, Zhao, Sun & Fong. Electrospun polycaprolactone 3D nanofibrous scaffold with interconnected and hierarchically structured pores for bone tissue engineering. *Advanced healthcare materials* **4**, 2238-2246 (2015).

200 Nam, Huang, Agarwal & Lannutti. Materials selection and residual solvent retention in biodegradable electrospun fibers. *Journal of Applied Polymer Science* **107**, 1547-1554, doi:https://doi.org/10.1002/app.27063 (2008).

201 Lannutti, Reneker, Ma, Tomasko & Farson. Electrospinning for tissue engineering scaffolds. *Materials Science and Engineering: C* **27**, 504-509, doi:https://doi.org/10.1016/j.msec.2006.05.019 (2007).

202 Zhang, Feng & Zhang. Emulsion electrospinning: Fundamentals, food applications and prospects. *Trends in Food Science & Technology* **80**, 175-186, doi:https://doi.org/10.1016/j.tifs.2018.08.005 (2018).

203 Al-Handarish, Omisore, Duan, Chen, Zebang, Akinyemi, Du, Li & Wang. Facile Fabrication of 3D Porous Sponges Coated with Synergistic Carbon Black/Multiwalled Carbon Nanotubes for Tactile Sensing Applications. *Nanomaterials* **10**, 1941 (2020).

204 Gu, Jeong, Na, Seon, Lee & Kang. Application of semi-permeable membrane for a scaffold in a nature-mimicking vascular system. *Journal of Membrane Science* **611**, 118384, doi:https://doi.org/10.1016/j.memsci.2020.118384 (2020).

205 Mazio, Casale, Imparato, Urciuolo, Attanasio, De Gregorio, Rescigno & Netti. Pre-vascularized dermis model for fast and functional anastomosis with host vasculature. *Biomaterials* **192**, 159-170, doi:https://doi.org/10.1016/j.biomaterials.2018.11.018 (2019).

206 Quintanilla, Casas, Miranzo, Osendi & Belmonte. 3D-Printed Fe-doped silicon carbide monolithic catalysts for wet peroxide oxidation processes. *Applied Catalysis B: Environmental* **235**, 246-255, doi:https://doi.org/10.1016/j.apcatb.2018.04.066 (2018).

207 Sinha, Cha & Kim. Three-dimensional macroporous alginate scaffolds embedded with akaganeite nanorods for the filter-based high-speed preparation of arsenic-free drinking water. *ACS Applied Nano Materials* **1**, 1940-1948 (2018).

208 Fan, Liu, Quan & Chen. Highly permeable thin-film composite forward osmosis membrane based on carbon nanotube hollow fiber scaffold with electrically enhanced fouling resistance. *Environmental science & technology* **52**, 1444-1452 (2018).

209 Cheng. Porous graphene sponge additives for lithium ion batteries with excellent rate capability. *Scientific reports* **7**, 1-11 (2017).

210 Ma, Wang, Zeng & Fang. Amorphous Ge/C Composite Sponges: Synthesis and Application in a High-Rate Anode for Lithium Ion Batteries. *Langmuir* **33**, 2141-2147, doi:10.1021/acs.langmuir.6b04444 (2017).

211 Sengupta, Patra, Mitra, Jena, Das, Majumder & Das. Melt impregnation as a post processing treatment for performance enhancement in high capacity 3D microporous tin-copper-nickel intermetallic anode for Li-ion battery supported by electrodeposited nickel scaffold: A structural study. *Applied Surface Science* **441**, 965-977, doi:https://doi.org/10.1016/j.apsusc.2018.01.311 (2018).

212 Jin, Sheng, Luo, Yuan, Fang, Zhang, Huang, Gan, Xia, Liang, Zhang & Tao. 3D lithium metal embedded within lithiophilic porous matrix for stable lithium metal batteries. *Nano Energy* **37**, 177-186, doi:https://doi.org/10.1016/j.nanoen.2017.05.015 (2017).

213 Pereira, Brito-Pereira, Gonçalves, Silva, Costa, Silva, de Zea Bermudez & Lanceros-Méndez. Silk Fibroin Separators: A Step Toward Lithium-Ion Batteries with Enhanced Sustainability. *ACS Applied Materials & Interfaces* **10**, 5385-5394, doi:10.1021/acsami.7b13802 (2018).

214 Liu, Yuan, Cheng, Chen, Titirici, Huang, Yuan & Zhang. A review of naturally derived nanostructured materials for safe lithium metal batteries. *Materials Today Nano* **8**, 100049, doi:https://doi.org/10.1016/j.mtnano.2019.100049 (2019).

215 You, Zhang, Deng, Li, Zheng, Li, Zhou, Huang & Sun. Suppressing Li dendrite by a protective biopolymeric film from tamarind seed polysaccharide for high-performance Li metal anode. *Electrochimica Acta* **299**, 636-644 (2019).

216 Zhang, Gao, Wang, Lu, Deng, You, Li, Zhou, Huang & Zhou. A natural biopolymer film as a robust protective layer to effectively stabilize lithium-metal anodes. *Small* **14**, 1801054 (2018).

217 Chang, Chung & Manthiram. Dendrite-Free Lithium Anode via a Homogenous Li-Ion Distribution Enabled by a Kimwipe Paper. *Advanced Sustainable Systems* **1**, 1600034 (2017).

218 Kim, Kim, Joo, Choi, Cha, Kim, Kwon, Kwak, Kang & Jin. Hierarchical chitin fibers with aligned nanofibrillar architectures: a nonwoven-mat separator for lithium metal batteries. *ACS nano* **11**, 6114-6121 (2017).

219 Ye, Zhong, Xu, Chang, Yang, Wang, Ye & Zhang. Construction of cellulose/nanosilver sponge materials and their antibacterial activities for infected wounds healing. *Cellulose* **23**, 749-763, doi:10.1007/s10570-015-0851-4 (2016).

220 Nguyen, Nguyen & Hsieh. Curcumin-Loaded Chitosan/Gelatin Composite Sponge for Wound Healing Application. *International Journal of Polymer Science* **2013**, 106570, doi:10.1155/2013/106570 (2013).

221 Ramanathan, Seleenmary Sobhanadhas, Sekar Jeyakumar, Devi, Sivagnanam & Fardim. Fabrication of Biohybrid Cellulose Acetate-Collagen Bilayer Matrices as Nanofibrous Spongy Dressing Material for Wound-Healing Application. *Biomacromolecules* **21**, 2512-2524, doi:10.1021/acs.biomac.0c00516 (2020).

222 Hu, Bi, Yan, Zhou, Sun, Cheng & Chen. Preparation of composite hydroxybutyl chitosan sponge and its role in promoting wound healing. *Carbohydrate Polymers* **184**, 154-163, doi:https://doi.org/10.1016/j.carbpol.2017.12.033 (2018).

223 Tolba, Wang, Ackermann, Neufurth, Muñoz-Espí, Schröder & Müller. In Situ Polyphosphate Nanoparticle Formation in Hybrid Poly(vinyl alcohol)/Karaya Gum Hydrogels: A Porous Scaffold Inducing Infiltration of Mesenchymal Stem Cells. *Advanced Science* **6**, 1801452, doi:https://doi.org/10.1002/advs.201801452 (2019).

224 Ballesteros-Cillero, Davison-Kotler, Kohli, Marshall & García-Gareta. Biomimetic In Vitro Model of Cell Infiltration into Skin Scaffolds for Pre-Screening and Testing of Biomaterial-Based Therapies. *Cells* **8**, doi:10.3390/cells8080917 (2019).

225 Huang, Huang, Shao, Hu, Cao, Fan, Song & Zhang. Silk scaffolds with gradient pore structure and improved cell infiltration performance. *Materials Science and Engineering: C* **94**, 179-189, doi:https://doi.org/10.1016/j.msec.2018.09.034 (2019).

226 Pandey, Singh, Momin & Bhavsar. Chitosan: Application in tissue engineering and skin grafting. *Journal of Polymer Research* **24**, 125, doi:10.1007/s10965-017-1286-4 (2017).

227 Kim, Kim, Ki, Kim & Park. Fabrication of bi-layer scaffold of keratin nanofiber and gelatin-methacrylate hydrogel: Implications for skin graft. *International Journal of Biological Macromolecules* **105**, 541-548, doi:https://doi.org/10.1016/j.ijbiomac.2017.07.067 (2017).

228 Shan, Li, Wu, Li & Liao. Hybrid cellulose nanocrystal/alginate/gelatin scaffold with improved mechanical properties and guided wound healing. *RSC advances* **9**, 22966-22979 (2019).

229 Bouhlouli, Pourhadi, Karami, Talebi, Ranjbari & Khojasteh. Applications of Bacterial Cellulose as a Natural Polymer in Tissue Engineering. *ASAIO Journal* **67** (2021).

230 Hsu, Whu, Hsieh, Tsai, Chen & Tan. Evaluation of chitosan-alginate-hyaluronate complexes modified by an RGD-containing protein as tissue-engineering scaffolds for cartilage regeneration. *Artificial organs* **28**, 693-703 (2004).

231 Poupart, Grande, Carbonnier & Le Droumaguet. Porous polymers and metallic nanoparticles: A hybrid wedding as a robust method toward efficient supported catalytic

systems. *Progress in Polymer Science* **96**, 21-42, doi:https://doi.org/10.1016/j.progpolymsci.2019.05.003 (2019).

232 Guo, Warnicke, Griffa, Müller, Chen, Schaeublin, Zhang & Luković. Hierarchical Porous Wood Cellulose Scaffold with Atomically Dispersed Pt Catalysts for Low-Temperature Ethylene Decomposition. *ACS Nano* **13**, 14337-14347, doi:10.1021/acsnano.9b07801 (2019).

233 Kamal. Aminophenols formation from nitrophenols using agar biopolymer hydrogel supported CuO nanoparticles catalyst. *Polymer Testing* **77**, 105896, doi:https://doi.org/10.1016/j.polymertesting.2019.105896 (2019).

234 Chtchigrovsky, Primo, Gonzalez, Molvinger, Robitzer, Quignard & Taran. Functionalized Chitosan as a Green, Recyclable, Biopolymer-Supported Catalyst for the [3+2] Huisgen Cycloaddition. *Angewandte Chemie International Edition* **48**, 5916-5920, doi:https://doi.org/10.1002/anie.200901309 (2009).

235 Wang, Gao, Yao, Liu, Wu, Li, Liu, Sun & Pan. A nanoconfined-LiBH4 system using a unique multifunctional porous scaffold of carbon wrapped ultrafine Fe3O4 skeleton for reversible hydrogen storage with high capacity. *Chemical Engineering Journal* **428**, 131056, doi:https://doi.org/10.1016/j.cej.2021.131056 (2022).

236 Zhu, Wang, Mei & Wu. Highly sensitive and flexible tactile sensor based on porous graphene sponges for distributed tactile sensing in monitoring human motions. *Journal of Microelectromechanical Systems* **28**, 154-163 (2018).

237 Cheng, Du, Wang, Mao, Xu, Zhang, Zhong, Jiang, Wang & Sui. Flexible cellulose-based thermoelectric sponge towards wearable pressure sensor and energy harvesting. *Chemical Engineering Journal* **338**, 1-7 (2018).

238 Gullapalli, Vemuru, Kumar, Botello-Mendez, Vajtai, Terrones, Nagarajaiah & Ajayan. Flexible piezoelectric ZnO–paper nanocomposite strain sensor. *small* **6**, 1641-1646 (2010).

239 Wang, Zhang, Wu & Lu. Tailoring percolating conductive networks of natural rubber composites for flexible strain sensors via a cellulose nanocrystal templated assembly. *Soft Matter* **12**, 845-852 (2016).

240 Wang, Jian, Wang & Zhang. Carbonized silk nanofiber membrane for transparent and sensitive electronic skin. *Advanced Functional Materials* **27**, 1605657 (2017).

241 Wang, Peng, Yu, Chen, Ge & Uyama. Hierarchically porous sponge for oily water treatment: Facile fabrication by combination of particulate templates and thermally induced phase separation method. *Journal of Industrial and Engineering Chemistry* **62**, 192-196, doi:https://doi.org/10.1016/j.jiec.2017.12.057 (2018).

242 Filina, Yousefi, Okshevsky & Tufenkji. Antimicrobial Hierarchically Porous Graphene Oxide Sponges for Water Treatment. *ACS Applied Bio Materials* **2**, 1578-1590, doi:10.1021/acsabm.9b00008 (2019).

243 Wang, Chen, Yoon, Fang, Hsiao & Chu. High Flux Filtration Medium Based on Nanofibrous Substrate with Hydrophilic Nanocomposite Coating. *Environmental Science & Technology* **39**, 7684-7691, doi:10.1021/es050512j (2005).

244 Ismail, Salleh, Ismail, Hasbullah, Yusof, Aziz & Jaafar. Hydrophilic polymer-based membrane for oily wastewater treatment: A review. *Separation and Purification Technology* **233**, 116007, doi:https://doi.org/10.1016/j.seppur.2019.116007 (2020).

245 Li, Li, Zhou, Xian, Shui, Wu & Yao. Super-hydrophilic electrospun PVDF/PVA-blended nanofiber membrane for microfiltration with ultrahigh water flux. *Journal of Applied Polymer Science* **137**, 48416, doi:https://doi.org/10.1002/app.48416 (2020).

246 Hu, Chen, Lu, Fan, Li, Li, Zeng & Liu. A self-supported gel filter membrane for dye removal with high anti-fouling and water flux performance. *Polymer* **201**, 122531, doi:https://doi.org/10.1016/j.polymer.2020.122531 (2020).

247 Chen, Su, Peng, Zhao, Jiang, Dong, Zhang, Liang & Liu. Efficient Wastewater Treatment by Membranes through Constructing Tunable Antifouling Membrane Surfaces. *Environmental Science & Technology* **45**, 6545-6552, doi:10.1021/es200994n (2011).

248 Zhou, Lin & Wu. Electrospinning ultrathin continuous cellulose acetate fibers for high-flux water filtration. *Colloids and Surfaces A: Physicochemical and Engineering Aspects* **494**, 21-29, doi:https://doi.org/10.1016/j.colsurfa.2015.11.074 (2016).

249 Chu & Seeger. Multifunctional Hybrid Porous Micro-/Nanocomposite Materials. *Advanced Materials* **27**, 7775-7781, doi:https://doi.org/10.1002/adma.201503502 (2015).

250 Yu, Yu, Cui, Song, Zhao, Ma & Jiang. Facile Preparation of the Porous PDMS Oil-Absorbent for Oil/Water Separation. *Advanced Materials Interfaces* **4**, 1600862 (2017).

251 Guan, Cheng & Pan. Superwetting Polymeric Three Dimensional (3D) Porous Materials for Oil/Water Separation: A Review. *Polymers* **11**, doi:10.3390/polym11050806 (2019).

252 El-Samak, Ponnamma, Hassan, Ammar, Adham, Al-Maadeed & Karim. Designing flexible and porous fibrous membranes for oil water separation—A review of recent developments. *Polymer Reviews* **60**, 671-716 (2020).

253 Yang, Yin, Zhang, Zhu & Zhang. Fabrication of emulsion-templated macroporous poly(ε-caprolactone) towards highly effective and sustainable oil/water separation. *Polymer* **204**, 122852, doi:https://doi.org/10.1016/j.polymer.2020.122852 (2020).

254 Cheng, Guan, Meng & Wang. Dual-Functional Porous Wood Filter for Simultaneous Oil/Water Separation and Organic Pollutant Removal. *ACS Omega* **5**, 14096-14103, doi:10.1021/acsomega.0c01606 (2020).

255 Shen, Huang, Gan, Liu, Gong & Long. Rational design of Si@ SiO2/C composites using sustainable cellulose as a carbon resource for anodes in lithium-ion batteries. *ACS applied materials & interfaces* **10**, 7946-7954 (2018).

256 Zhao, Wang, Chong, Yu, Wang & Shi. An electrospun lignin/polyacrylonitrile nonwoven composite separator with high porosity and thermal stability for lithium-ion batteries. *Rsc Advances* **5**, 101115-101120 (2015).

257 Song, Li, Shi, Qian, Feric, Fu, Zhang, Li, Wang & Li. Thermally stable, nano-porous and eco-friendly sodium alginate/attapulgite separator for lithium-ion batteries. *Energy Storage Materials* **22**, 48-56 (2019).

258 Keck, Haluza, Selig, Jahl, Lumenta, Kamolz & Frey. Adipose tissue engineering: three different approaches to seed preadipocytes on a collagen-elastin matrix. *Annals of plastic surgery* **67**, 484-488 (2011).

259 Pekşen, Üzelakçil, Güneş, Malay & Bayraktar. A novel silk fibroin-supported iron catalyst for hydroxylation of phenol. *Journal of Chemical Technology & Biotechnology: International Research in Process, Environmental & Clean Technology* **81**, 1218-1224 (2006).

260 Mahadeva, Yun & Kim. Flexible humidity and temperature sensor based on cellulose–polypyrrole nanocomposite. *Sensors and Actuators A: Physical* **165**, 194-199 (2011).

261 Xie, Zheng, Wang & Lee Kaplan. Low-Density Silk Nanofibrous Aerogels: Fabrication and Applications in Air Filtration and Oil/Water Purification. *ACS Nano* **15**, 1048-1058, doi:10.1021/acsnano.0c07896 (2021).

262 Yan, Li, Zhou, Wang, Fan, Chen, Fang & Liu. Shrimp Shell-Inspired Antifouling Chitin Nanofibrous Membrane for Efficient Oil/Water Emulsion Separation with In Situ Removal of Heavy Metal Ions. *ACS Sustainable Chemistry & Engineering* **7**, 2064-2072, doi:10.1021/acssuschemeng.8b04511 (2019).

263 Duan, Gao, He & Zhang. Hydrophobic Modification on Surface of Chitin Sponges for Highly Effective Separation of Oil. *ACS Applied Materials & Interfaces* **6**, 19933-19942, doi:10.1021/am505414y (2014).

264 Faegri & Van der Pijl. Principles of pollination ecology. (2013).

265 Ferreira, Reinhard & Araújo. *Foundations of paleoparasitology*. (Editora Fiocruz, 2014).

266 Radja, Horsley, Lavrentovich & Sweeney. Pollen cell wall patterns form from modulated phases. *Cell* **176**, 856-868. e810 (2019).

267 Prabhakar. *Pine pollen for molecular encapsulation and oral delivery applications*, (2018).

268 Brooks & Shaw. Chemical structure of the exine of pollen walls and a new function for carotenoids in nature. *Nature* **219**, 532-533 (1968).

269 Ariizumi & Toriyama. Genetic Regulation of Sporopollenin Synthesis and Pollen Exine Development. *Annual Review of Plant Biology* **62**, 437-460, doi:10.1146/annurev-arplant-042809-112312 (2011).

270 Fan, Park, Shi, Zhang, Liu, Song, Chin, Ibrahim, Mokrzecka & Yang. Transformation of hard pollen into soft matter. *Nature communications* **11**, 1-10 (2020).

271 Heslop-Harrison. Pollen germination and pollen-tube growth. *International review of cytology* **107**, 1-78 (1987).

272 Thomas. The effect of supplementary cementing materials on alkali-silica reaction: A review. *Cement and Concrete Research* **41**, 1224-1231, doi:https://doi.org/10.1016/j.cemconres.2010.11.003 (2011).

273 Jardine, Abernethy, Lomax, Gosling & Fraser. Shedding light on sporopollenin chemistry, with reference to UV reconstructions. *Review of Palaeobotany and Palynology* **238**, 1-6 (2017).

274 Clausen, Willats & Knox. Synthetic methyl hexagalacturonate hapten inhibitors of anti-homogalacturonan monoclonal antibodies LM7, JIM5 and JIM7. *Carbohydrate Research* **338**, 1797-1800 (2003).

275 Parre & Geitmann. More than a leak sealant. The mechanical properties of callose in pollen tubes. *Plant Physiology* **137**, 274-286 (2005).

276 Qu & Meredith. The atypically high modulus of pollen exine. *Journal of The Royal Society Interface* **15**, 20180533 (2018).

277 Zeng & Tan. AFM nanoindentation to quantify mechanical properties of nano-and micron-sized crystals of a metal–organic framework material. *ACS applied materials & interfaces* **9**, 39839-39854 (2017).

278 Hutter & Bechhoefer. Calibration of atomic-force microscope tips. *Review of scientific instruments* **64**, 1868-1873 (1993).

279 Neumann. Determining the elastic modulus of biological samples using atomic force microscopy. *JPK Instruments Application Report*, 1-9 (2008).

280 Fan, Hwang, Ibrahim, Ferracci & Cho. Influence of Chemical and Physical Change of Pollen Microgels on Swelling/De-Swelling Behavior. *Macromolecular Rapid Communications* **41**, 2000155, doi:https://doi.org/10.1002/marc.202000155 (2020).

281 Saunders, Laajam, Daly, Teow, Hu & Stepto. Microgels: From responsive polymer colloids to biomaterials. *Advances in colloid and interface science* **147**, 251-262 (2009).

282 Knox, Linstead, King, Cooper & Roberts. Pectin esterification is spatially regulated both within cell walls and between developing tissues of root apices. *Planta* **181**, 512-521 (1990).

283 Parre & Geitmann. Pectin and the role of the physical properties of the cell wall in pollen tube growth of Solanum chacoense. *Planta* **220**, 582-592 (2005).

284 Gnanasambandam & Proctor. Determination of pectin degree of esterification by diffuse reflectance Fourier transform infrared spectroscopy. *Food chemistry* **68**, 327-332 (2000).

285 Balaria & Schiewer. Assessment of biosorption mechanism for Pb binding by citrus pectin. *Separation and Purification Technology* **63**, 577-581 (2008).

286 Diaz, Anthon & Barrett. Nonenzymatic degradation of citrus pectin and pectate during prolonged heating: effects of pH, temperature, and degree of methyl esterification. *Journal of agricultural and food chemistry* **55**, 5131-5136 (2007).

287 Yule, Roberts & Marshall. The thermal evolution of sporopollenin. *Organic Geochemistry* **31**, 859-870, doi:https://doi.org/10.1016/S0146-6380(00)00058-9 (2000).

288 Sułkowski, Pentak, Nowak & Sułkowska. The influence of temperature, cholesterol content and pH on liposome stability. *Journal of molecular structure* **744**, 737-747 (2005).

289 Renard & Thibault. Degradation of pectins in alkaline conditions: kinetics of demethylation. *Carbohydrate Research* **286**, 139-150 (1996).

290 Wehr, Menzies & Blamey. Alkali hydroxide-induced gelation of pectin. *Food Hydrocolloids* **18**, 375-378 (2004).

291 Maciel, Yoshida & Franco. Chitosan/pectin polyelectrolyte complex as a pH indicator. *Carbohydrate polymers* **132**, 537-545 (2015).

292 Kiser, Wilson & Needham. A synthetic mimic of the secretory granule for drug delivery. *Nature* **394**, 459-462 (1998).

293 Zhao & Moore. Fast pH-and ionic strength-responsive hydrogels in microchannels. *Langmuir* **17**, 4758-4763 (2001).

294 BeMiller. An introduction to pectins: structure and properties. (1986).

295 Michard, Simon, Tavares, Wudick & Feijó. Signaling with ions: the keystone for apical cell growth and morphogenesis in pollen tubes. *Plant Physiology* **173**, 91-111 (2017).

296 Zhang. *Ice templating and freeze-drying for porous materials and their applications*. (John Wiley & Sons, 2018).

297 MacKenzie. Factors affecting the mechanism of transformation of ice into water vapor in the freeze-drying process. *NYASA* **125**, 522-547 (1965).

298 Oetjen & Haseley. *Freeze-drying*. (John Wiley & Sons, 2004).

299 Franks & Auffret. *Freeze-drying of Pharmaceuticals and Biopharmaceuticals*. (royal Society of Chemistry, 2008).

300 Ohtake, Izutsu & Lechuga-Ballesteros. *Drying Technologies for Biotechnology and Pharmaceutical Applications*. (Wiley Online Library, 2020).

301 Rey. *Freeze-drying/lyophilization of pharmaceutical and biological products*. (CRC Press, 2016).

302 Zheng, Winnubst, Velianti, Fang & Salamon. Manipulation of Sintering Behavior by Initial Freeze Pressing an Aqueous Alumina Suspension. *Advanced Engineering Materials* **13**, 77-81, doi:https://doi.org/10.1002/adem.201000199 (2011).

303 Vidovskii. Experimental determination of pressure during ice expansion. *Hydrotechnical Construction* **6**, 791-792, doi:10.1007/BF02377294 (1972).

304 Hwang, Ibrahim, Deng, Jackman & Cho. Colloid-Mediated Fabrication of a 3D Pollen Sponge for Oil Remediation Applications. *Advanced Functional Materials*, 2101091 (2021).

305 Zhao, Hwang, Yang, Fan, Song, Suresh & Cho. Actuation and locomotion driven by moisture in paper made with natural pollen. *Proceedings of the National Academy of Sciences* **117**, 8711-8718 (2020).

306 Xie, Zhou, Bi, Yin, Wan & Sun. Large-range control of the microstructures and properties of three-dimensional porous graphene. *Scientific reports* **3**, 1-6 (2013).

307 Chen, Huang, Li, Yu & Yan. Preparation of a macroporous flexible three dimensional graphene sponge using an ice-template as the anode material for microbial fuel cells. *Rsc Advances* **4**, 21619-21624 (2014).

308 Hobbs. *Ice physics*. (Oxford university press, 2010).

309 O'Brien, Harley, Yannas & Gibson. The effect of pore size on cell adhesion in collagen-GAG scaffolds. *Biomaterials* **26**, 433-441, doi:https://doi.org/10.1016/j.biomaterials.2004.02.052 (2005).

310 Wu, Li, Zhang, Zhong, Xu, Mao, Wang & Sui. Thiol–ene click reaction on cellulose sponge and its application for oil/water separation. *Rsc Advances* **7**, 20147-20151 (2017).

311 Guo, Chen, Lyu, Fu & Wang. Highly flexible cross-linked cellulose nanofibril sponge-like aerogels with improved mechanical property and enhanced flame retardancy. *Carbohydrate polymers* **179**, 333-340 (2018).

312 Zhang, Wang, Eghtedari, Motamedi & Kotov. Inverted-colloidal-crystal hydrogel matrices as three-dimensional cell scaffolds. *Advanced Functional Materials* **15**, 725-731 (2005).

313 Antonini, Wu, Zimmermann, Kherbeche, Thoraval, Nyström & Geiger. Ultra-porous nanocellulose foams: A facile and scalable fabrication approach. *Nanomaterials* **9**, 1142 (2019).

314 Meryman. Review of biological freezing. *Cryobiology* **1**, 114 (1966).

315 Kuprianoff. in *Conference on Fundamental aspects of the Dehydration of Foodstuffs.* 14-23.

316 Caurie. Bound water: its definition, estimation and characteristics. *International Journal of Food Science & Technology* **46**, 930-934, doi:https://doi.org/10.1111/j.1365-2621.2011.02581.x (2011).

317 Chhetry, Sharma, Yoon, Ko & Park. Enhanced sensitivity of capacitive pressure and strain sensor based on CaCu3Ti4O12 wrapped hybrid sponge for wearable applications. *Advanced Functional Materials* **30**, 1910020 (2020).

318 Fan, Li, Zhang, Zhao, Cao, Yin, Xing, Wang, Guo & Li. A dual-salt gel polymer electrolyte with 3D cross-linked polymer network for dendrite-free lithium metal batteries. *Advanced Science* **5**, 1800559 (2018).

319 Wang, Zhang, Tang, Zhang, Ning, Tian, Li, Zhang, Mao & Liang. Single-electrode triboelectric nanogenerators based on sponge-like porous PTFE thin films for mechanical

energy harvesting and self-powered electronics. *Journal of Materials Chemistry A* **5**, 12252-12257 (2017).

320 Giorgianni, Vicario, Shalaby, Tenuzzo, Marcelli, Zhang, Zhao, Chen, Hauri & Lupi. High-Efficiency and Low Distortion Photoacoustic Effect in 3D Graphene Sponge. *Advanced Functional Materials* **28**, 1702652 (2018).

321 Cherukupally, Sun, Wong, Williams, Ozin, Bilton & Park. Surface-engineered sponges for recovery of crude oil microdroplets from wastewater. *Nature Sustainability* **3**, 136-143 (2020).

322 Zhang, Liu, Yang, Shi, Zhang, Shan, Mi, Liu, Shen & Guo. Ultrasensitive and highly compressible piezoresistive sensor based on polyurethane sponge coated with a cracked cellulose nanofibril/silver nanowire layer. *ACS applied materials & interfaces* **11**, 10922-10932 (2019).

323 Zhao & Zhu. High sensitivity and broad range flexible pressure sensor using multilayered porous PDMS/AgNP sponge. *Advanced Materials Technologies* **4**, 1900414 (2019).

324 Zhou, Yang, Zhu, Zheng, Handschuh-Wang, Zhou, Zhang, Liu, Liu & He. Hydrophilic Sponges for Leaf-Inspired Continuous Pumping of Liquids. *Advanced Science* **4**, 1700028 (2017).

325 Qi, Miao, Chi, Zhang, Zhang, Du, An, Ma & Zhang. Ultralight PEDOT: PSS/graphene oxide composite aerogel sponges for electric power harvesting from thermal fluctuations and moist environment. *Nano Energy* **77**, 105096 (2020).

326 Li, Hu, Yang, Zou, Yang, Yu, Wang, Qu, Tan & Wang. Elastic Cu@ PPy sponge for hybrid device with energy conversion and storage. *Nano Energy* **58**, 852-861 (2019).

327 Ruan, Ai, Li & Lu. A superhydrophobic sponge with excellent absorbency and flame retardancy. *Angewandte Chemie* **126**, 5662-5666 (2014).

328 Zhu, Ji, Liu, Mine, Matsuoka, Zhang & Xing. Designing 3D-MoS2 sponge as excellent cocatalysts in advanced oxidation processes for pollutant control. *Angewandte Chemie International Edition* **59**, 13968-13976 (2020).

329 Jiang, Cheong, Nam, Kim, Agarwal & Greiner. High-density fibrous polyimide sponges with superior mechanical and thermal properties. *ACS applied materials & interfaces* **12**, 19006-19014 (2020).

330 Wu, Li, Li, Zhang & Wang. Magnetic, durable, and superhydrophobic polyurethane@ Fe3O4@ SiO2@ fluoropolymer sponges for selective oil absorption and oil/water separation. *ACS applied materials & interfaces* **7**, 4936-4946 (2015).

331 Song, Chen, Su, Chen, Miao, Zhang, Cheng & Zhang. Highly compressible integrated supercapacitor–piezoresistance-sensor system with CNT–PDMS sponge for health monitoring. *Small* **13**, 1702091 (2017).

332 Zhang, Feng, Qin, Gao, Li, Zhao, Zhang, Lv & Feng. Stress controllability in thermal and electrical conductivity of 3D elastic graphene-crosslinked carbon nanotube sponge/polyimide nanocomposite. *Advanced Functional Materials* **29**, 1901383 (2019).

333 Li, Yang, Li, Wang & Liu. From commercial sponge toward 3D graphene–silicon networks for superior lithium storage. *Advanced Energy Materials* **5**, 1500289 (2015).

334 Li, Phyo, Jacobowitz, Hong & Weng. (2019).

335 Wang, Potroz, Jackman, Khezri, Marić, Cho & Pumera. Bioinspired spiky micromotors based on sporopollenin exine capsules. *Advanced Functional Materials* **27**, 1702338 (2017).

336 Mundargi, Potroz, Park, Shirahama, Lee, Seo & Cho. Natural sunflower pollen as a drug delivery vehicle. *Small* **12**, 1167-1173 (2016).

337 Fang, Wang, Yu, Zhang, Baluška, Šamaj & Lin. Isolation of de-exined pollen and cytological studies of the pollen intines of Pinus bungeana Zucc. Ex Endl. and Picea wilsonii Mast. *Flora-Morphology, Distribution, Functional Ecology of Plants* **203**, 332-340 (2008).

338 Pomelli, D'Andrea, Mezzetta & Guazzelli. Exploiting pollen and sporopollenin for the sustainable production of microstructures. *New Journal of Chemistry* **44**, 647-652 (2020).

339 Chu, Feng & Seeger. Oil/water separation with selective superantiwetting/superwetting surface materials. *Angewandte Chemie International Edition* **54**, 2328-2338 (2015).

340 Gunstone & Harwood. *The lipid handbook with CD-ROM*. (CRC press, 2007).

341 Ralston & Hoerr. The Solubilities of the Normal Saturated Fatty Acids. *The Journal of Organic Chemistry* **07**, 546-555, doi:10.1021/jo01200a013 (1942).

342 Hu, Zen, Gong & Deng. Water resistance improvement of paper by superhydrophobic modification with microsized CaCO3 and fatty acid coating. *Colloids and Surfaces A: Physicochemical and Engineering Aspects* **351**, 65-70 (2009).

343 Dolez, Arfaoui, Dubé & David. Hydrophobic treatments for natural fibers based on metal oxide nanoparticles and fatty acids. *Procedia Engineering* **200**, 81-88, doi:https://doi.org/10.1016/j.proeng.2017.07.013 (2017).

344 Chen, Zhang, Wang, Lv, Zhu & Gao. Fabrication and characterization of novel shape-stabilized stearic acid composite phase change materials with tannic-acid-templated mesoporous silica nanoparticles for thermal energy storage. *RSC advances* **7**, 15625-15631 (2017).

345 Charde, Sonawane, Sonawane & Navin. Influence of functionalized calcium carbonate nanofillers on the properties of melt-extruded polycarbonate composites. *Chemical Engineering Communications* **205**, 492-505 (2018).

346 Fu, Zheng, Liu, Dresselhaus, Dresselhaus, Satcher Jr & Baumann. The Fabrication and Characterization of Carbon Aerogels by Gelation and Supercritical Drying in Isopropanol. *Advanced Functional Materials* **13**, 558-562, doi:https://doi.org/10.1002/adfm.200304289 (2003).

347 Laitinen, Suopajärvi, Österberg & Liimatainen. Hydrophobic, superabsorbing aerogels from choline chloride-based deep eutectic solvent pretreated and silylated cellulose nanofibrils for selective oil removal. *ACS applied materials & interfaces* **9**, 25029-25037 (2017).

348 Tan, Potroz, Ferracci, Jackman, Jung, Wang & Cho. Light-induced surface modification of natural plant microparticles: toward colloidal science and cellular adhesion applications. *Advanced Functional Materials* **28**, 1707568 (2018).

349 Mundargi, Potroz, Park, Seo, Lee & Cho. Extraction of sporopollenin exine capsules from sunflower pollen grains. *RSC advances* **6**, 16533-16539 (2016).

350 Matamoro-Vidal, Raquin, Brisset, Colas, Izac, Albert & Gouyon. Links between morphology and function of the pollen wall: an experimental approach. *Botanical journal of the Linnean Society* **180**, 478-490 (2016).

351 Potroz, Mundargi, Gillissen, Tan, Meker, Park, Jung, Park, Cho & Bang. Plant-based hollow microcapsules for oral delivery applications: toward optimized loading and controlled release. *Advanced Functional Materials* **27**, 1700270 (2017).